

**Amyloid precursor protein (APP) and copper homeostasis in the
human neuroblastoma cell line *SH-SY5Y***

Juliane Klein

B.Sc. Hons. Newcastle University

Thesis submitted for the degree of Doctor of Philosophy
to the University of Newcastle upon Tyne

Institute for Cell- and Molecular Biosciences

24th September 2010

Memorandum

Part of the data presented in this thesis is being prepared for submission to Metallomics.

Statement

No portion of the work referred to in this thesis has been submitted in support of an application for another degree or qualification of this or any other University, or institution of learning.

Acknowledgements

I would like to thank Prof. Nigel Robinson for supervision and advice throughout this project as well as Dr. Steve Tottey. In particular, I thank Dr. Kevin Waldron for his guidance, support, patience and interest. I would also like to thank Dr. David Howlett for inviting me to his laboratory and his supervision and advice during that time. Further I would like to thank the Lightowler group, especially Pierre, for helping me to perform cell fractionation.

Special thanks to all my friends for being so supportive and understanding when I yet again had to turn you down for weekend fun and much needed distraction. Nevertheless, you did not stop asking and for that I am immeasurably grateful and promise that things will change in the future.

A special mention is also deserved by members of my BioTechYES and conference team, who all showed me that science is more than just basic lab work. I had a lot of fun working and winning with you.

Two very important people in the completion of my project are Monica and Shilpa. You were there when things were rough and I needed someone to talk to. Your compassion and encouragement helped me so much. For that I thank you.

I would also like to show my appreciation to Lily and Donal for their constant support and interest in the project. Although you might not have fully understood what I was doing, you were always curious and that made a big difference.

A person without whom I could not have descended onto this path and fulfilled my dream is my mum. You supported me in whatever I wanted to do and without your love, strength and courage I would not be where I am today. You built the foundation on which I could grow and empowered me to achieve this.

I would also like to express my love and appreciation to my dear Shane. Your constant encouragement, kindness and loving words lifted me up when I was down. You saw the good times and more often the bad, but you stood by me and did not run the other way. You gave me strength to face the difficult days and you celebrated my successes. I could not have done this without you.

I dedicate this thesis to both of you.

„Die Endlosigkeit des wissenschaftlichen Ringens sorgt unablässig dafür, daß dem forschenden Menschegeist seine beiden edelsten Antriebe erhalten bleiben und immer wieder von neuem angefacht werden: die Begeisterung und die Ehrfurcht.“

Max Planck (1858-1947)

“The immensity of the scientific struggle constantly makes sure that the inquiring spirit of man will receive his two finest drives and be fanned again and again: the excitement and awe.”

Max Planck (1858-1947)

Abstract

Alzheimer's disease (AD) is characterised by cerebellar accumulation and aggregation of amyloid beta ($A\beta$), a cleavage product of the transmembrane amyloid precursor protein (APP). APP contains a range of functional domains in its large extracellular portion, among which are two copper-binding motifs and one zinc-binding motif. The copper-binding motifs are present in the amino-terminal region of APP and within the $A\beta$ region of the protein and readily reduce Cu(II) to Cu(I), thus APP and its cleavage products are linked to copper metabolism and have been hypothesised to participate in cellular copper homeostasis.

In this project human neuroblastoma cell lines *SH-SY5Y* were utilised to determine the effect of expressing a familial AD mutation on intracellular copper concentrations and possible functional alterations or deficits of enzymes that require copper as a co-factor. The familial AD mutation first found in a Swedish population was previously shown to increase the total amount of released $A\beta$. Direct phenotypic comparison between *SH-SY5Y* APP_{WT} cell lines expressing endogenous levels of APP and APP_{swe} cell lines overexpressing APP carrying the Swedish mutation was performed in standard culture and manipulated copper concentrations.

Coupling native two dimensional liquid chromatography with metal analysis, SDS-PAGE and Principal Component Analysis identified one major copper and zinc containing pool as copper-zinc superoxide dismutase (SOD1) in soluble whole cell protein extracts. Comparative analysis of metal content between APP_{WT} and APP_{swe} cultures indicated a difference in metallation of SOD1 with copper. APP_{swe} cultures displayed reduced metallation of SOD1, whereas SOD1 metallation with zinc remained unaltered. Functional analysis of copper-binding enzymes, such as SOD1 and cytochrome c oxidase (CCO), using standard biochemical approaches, identified lower activities for both enzymes during standard cell culture in APP_{swe} cells. Upon treatment of cultures with increasing concentrations of exogenous copper APP_{WT} enzyme activities remained unaltered but enzyme activities in APP_{swe} cultures increased in direct correlation with increasing copper concentrations. Combined with phenotypic analysis of growth, survival and intracellular metal content it appears that APP_{swe} cultures are copper deficient, but

this can be overcome by copper supplementation. Lower copper accumulation also enables greater survival of APP_{swe} cells in elevated copper.

Overall, these data suggest that APP_{swe} overexpression in *SH-SY5Y* cells results in functional copper deficiency which can be rescued by supplementation of cultures with exogenous copper. APP_{swe} further confers resistance to copper toxicity not only via increased A β release, but also via increased copper delivery to enzymatic target proteins improving cellular antioxidant response and energy metabolism. These data are consistent with a function of APP in copper efflux either in a regulatory capacity or directly contributing to copper egress.

Content

Memorandum	ii
Statement	ii
Acknowledgements	ii
Abstract	v
Contents	vii
Abbreviations	xiii

<u>1 Introduction</u>	1
1.1 Brain anatomy	1
1.2 Alzheimer's disease	2
1.2.1 Hallmarks of Alzheimer's disease	2
1.2.2 Genetic determinants of Alzheimer's disease	4
1.2.2.1 Sporadic Alzheimer's disease	4
1.2.2.2 Familial Alzheimer's disease	5
1.3 The amyloid precursor protein and its enzymatic processing to form beta-amyloid	6
1.3.1 The amyloid precursor protein	6
1.3.2. Expression, translation and maturation of the amyloid precursor protein during progression through the secretory pathway	8
1.3.3 Cleavage and processing pathways of the amyloid precursor protein	14
1.3.4 Protein interactions with the amyloid precursor protein	18
1.3.5 Aggregation of the amyloid beta peptide and formation of plaques	19
1.3.6 Degradation of amyloid aggregates	20
1.4 Beta-amyloid mediated mechanisms of neurotoxicity	22
1.4.1 The amyloid cascade hypothesis	22
1.4.2 Oxidative stress	23
1.4.3 Axonal transport inhibition	27
1.4.4 Other potential causes of A β mediated neurodegeneration	27
1.5 Copper in biology	28
1.5.1 An introduction to metals in biology	28
1.5.1.1 Metal selectivity and biochemical properties of copper	29
1.5.2 Zinc in synaptic transmission	31
1.5.3 Copper homeostasis within the body	32
1.5.4 Copper homeostasis within the cell	33
1.5.5 Copper dependent proteins in the brain	43

1.5.5.1 Superoxides dismutase	43
1.5.5.2 Cytochrome c oxidase	44
1.5.5.3 Dopamine β -hydroxylase and peptidylglycine α -amidating monooxygenase	44
1.5.6 Disorders of copper imbalance	45
1.5.6.1 Menkes disease	45
1.5.6.2 Wilson's disease	45
1.5.6.3 Neurological disorders	46
1.6 Metals and APP	46
1.6.1 Metal-binding properties of amyloid precursor protein and amyloid beta	46
1.6.2 The proposed role for APP in copper homeostasis	49
1.7 Experimental design and challenges for the study of metalloproteins	50
1.7.1 Metalloproteomics	50
1.7.2 Limitations of various biochemical approaches	51
1.7.3 A low resolution native two dimensional liquid chromatography approach coupled to denaturing separation of proteins and Principal Component Analysis	52
1.8 This study	53
1.8.1 Hypothesis	53
1.8.2 Aims	53
<u>2 Materials and Methods</u>	57
2.1 Equipment, chemicals and reagents	57
2.2 Strains, cell lines and plasmids used	57
2.2.1 <i>Saccharomyces cerevisiae</i> strain and maintenance	57
2.2.2 <i>SH-SY5Y</i> APP _{WT} and APP _{swe} mutation	57
2.2.3 Cell culture of <i>SH-SY5Y</i>	58
2.2.3.1 Maintenance	58
2.2.3.2 Harvest	58
2.2.4 Cell culture of <i>HepG2</i>	58
2.2.4.1 Maintenance	58
2.2.4.2 Harvest	61
2.3 Genetic techniques	61
2.3.1 Reverse Transcription Polymerase Chain Reaction (RT-PCR)	61
2.3.1.1 RNA extraction from whole cells	61
2.3.1.2 cDNA synthesis	62

2.3.1.2.1 DNaseI treatment of RNA	62
2.3.1.2.2 RNA and primer denaturation	62
2.3.1.2.3 Reverse transcription	62
2.3.1.3 Polymerase Chain Reaction (PCR)	63
2.3.1.4 DNA separation by agarose gel electrophoresis	63
2.4 Molecular biology techniques	63
2.4.1 Copper and BCS supplementation	63
2.4.1.1 Modified method for copper supplementation	64
2.4.2 Estimation of protein concentration and standardization	64
2.4.2.1 Membranous protein	64
2.4.2.2 Soluble protein	64
2.4.3 Whole cell metal profiling	67
2.4.3.1 Preparation of soluble whole cell extracts by freeze-grinding	67
2.4.3.2 First dimension liquid chromatographic separation by anion exchange	67
2.4.3.3 Second dimension liquid chromatographic separation by size exclusion	67
2.4.3.4 Metal analysis by inductively coupled plasma-mass spectrometry	68
2.4.4 Identification of metal-binding proteins	69
2.4.5 SDS-PAGE analysis for protein analysis	69
2.4.5.1 Preparation of SDS-PAGE gels	69
2.4.5.2 Sample analysis using SDS-PAGE gels	69
2.4.5.3 Protein identification by MALDI-TOF-MS peptide mass fingerprinting	70
2.4.6 Phenotype analysis under metal depletion and supplementation	70
2.4.6.1 Growth curves	70
2.4.6.2 Survival studies using trypan blue exclusion as indication of survival	71
2.4.6.3 Testing for intracellular metal accumulation by whole cell acid digest	71
2.4.7 Enzyme activity assays	72
2.4.7.1 Colorimetric determination of glutathione content	72
2.4.7.2 SOD1 activity assay	72
2.4.7.2.1 Native polyacrylamide gel electrophoresis of SOD1	72

2.4.7.2.2 In-gel activity assay of SOD1 activity	74
2.4.7.2.3 Modified method for soluble whole cell protein extraction	74
2.4.7.2.4 Spectrophotometric analysis of SOD1 activity	76
2.4.7.3 Cytochrome c oxidase activity assay	79
2.4.7.3.1 Preparation of total cellular membrane fraction	79
2.4.7.3.2 Reduction of cytochrome c and dialysis	79
2.4.7.3.3 Demetallation of dialysis tubing	79
2.4.7.3.4 Ascorbic acid reduction of cytochrome c	80
2.4.7.3.5 Removal of ascorbic acid from the cytochrome c stock using dialysis	80
2.4.7.3.6 Spectrophotometric analysis of cytochrome c oxidase activity	80
2.4.8 Subcellular fractionation of rat liver tissue and <i>SH-SY5Y</i> cell cultures	81
2.4.8.1 Extraction of liver tissue from Wistar rats	81
2.4.8.2 Cellular fractionation for mitochondrial extract of rat liver	81
2.4.8.3 Confirmation of rat liver mitochondrial fraction by Western Blot	82
2.4.8.3.1 Sample preparation for Western Blot	82
2.4.8.3.2 Transfer of protein onto blotting membrane	82
2.4.8.3.3 Blocking of membrane with antibodies	82
2.4.8.3.4 Protein detection by chemiluminescence	83
2.4.9 Metal binding analysis of a low molecular copper binding compound	83
2.4.9.1 Preparation of copper (I) stock solution	83
2.4.9.2 Cu(I) titration to biological 2D-LC extracts	84
2.4.9.3 Cu(I) binding assay using the Cu(I)-specific chelator BCS	84
2.4.9.4 Gel filtration analysis of a low molecular weight metal binding compound	84
2.4.9.5 ICP-MS analysis of samples	85
2.4.10 Bioinformatics and statistical analysis	85
2.4.10.1 Quantity one software	85
2.4.10.2 Matlab for Principal Component Analysis (PCA)	85
2.4.10.3 Statistical analysis	86
2.4.10.4 General Bio-informatics	86

<u>3 Results</u>	87
3.1 Low resolution two dimensional liquid chromatographic analysis of soluble metal-complexes in eukaryotic model species	87
3.1.1 Two dimensional liquid chromatographic analysis of <i>Saccharomyces cerevisiae</i> whole cell soluble protein extract	87
3.1.2 Two dimensional liquid chromatographic analysis of rat liver mitochondria soluble protein extract	89
3.1.3 Two dimensional liquid chromatographic analysis of <i>HepG2</i> whole cell soluble protein extract	92
3.1.4 Two dimensional liquid chromatographic analysis of <i>SH-SY5Y</i> APP _{WT} whole cell soluble protein extract	98
3.1.5 Two dimensional liquid chromatographic analysis of <i>SH-SY5Y</i> APP _{swe} whole cell soluble protein extract	98
3.2 Analysis of glutathione content of fractionated <i>Saccharomyces cerevisiae</i> extracts	99
3.3 Two dimensional liquid chromatographic analysis of rat liver mitochondria soluble protein extracts	104
3.3.1 2D-LC analysis of rat liver mitochondria soluble protein extract	104
3.3.2 Identification of p1 _{RLM} as copper-zinc superoxide dismutase from rat mitochondrial extract	107
3.4 Purification and partial characterisation of a low molecular weight copper complex in rat liver mitochondria	113
3.4.1 Protein analysis of the low molecular weight copper-binding complex	113
3.4.2 Analysis of metal binding to the copper – ligand	115
3.4.2.1 Cu(I) competition with BCS	116
3.4.2.2 Copper depletion of low molecular weight copper complex using the monovalent copper specific chelator BCS	121
3.5 Low resolution 2D-LC analysis of metal distribution in <i>SH-SY5Y</i> APP_{WT} and APP_{swe} whole cell extracts	121
3.5.1 Two dimensional liquid chromatographic metal analysis of <i>SH-SY5Y</i> APP _{WT} mitochondrial soluble protein fraction	122
3.5.2 Two dimensional liquid chromatographic metal analysis of <i>SH-SY5Y</i> APP _{WT} and APP _{swe} soluble whole cell protein	126
3.5.3 Identification of SOD1 in <i>SH-SY5Y</i> APP _{WT}	131
3.6 Comparative analysis of enzymatic activity of copper binding enzymes in <i>SH-SY5Y</i> APP_{WT} and APP_{swe}	135
3.6.1 In-gel SOD activity assay	135
3.6.2 Spectrophotometric analysis of SOD1 activity	138
3.6.3 Analysis of cytochrome c oxidase activity	143

3.7 Phenotypic analysis and comparison of <i>SH-SY5Y</i> APP_{WT} and APP_{swe}	150
3.7.1 Survival studies under copper supplementation	150
3.7.2 Growth analysis under copper depletion and supplementation	154
3.7.3 Metal accumulation under copper depletion and supplementation	158
<u>4 Discussion</u>	159
4.1 Analysis of metal content and distribution in mammalian cells	159
3.7 Comparison of functional copper content and distribution in <i>SH-SY5Y</i> APP_{WT} and APP_{swe} cell lines	161
4.3 Future work	185
<u>References</u>	188
<u>5 Appendix</u>	220
5.1 Spectrophotometric analysis of SOD1 activity	220
5.2 Analysis of CCO activity	226
5.3 Survival studies under copper supplementation	233
5.4 Metal content of APP_{WT} and APP_{swe} under copper depletion	236
5.5 Comparison of expression levels of <i>hsod1</i> and <i>hccs</i> genes in <i>SH-SY5Y</i> APP_{WT} and APP_{swe} under copper supplementation and depletion	238

Abbreviations

A	Absorbance
aa	Amino acid
ABAD	A β -binding alcohol dehydrogenase
A β	Amyloid beta peptide
ACE	Angiotensin-converting enzyme
AD	Alzheimer's Disease
ADAM	A disintegrin and metalloproteinase
ADDL	APP-derived diffusible ligand
AICD	APP intracellular domain
ALS	Amyloid lateral sclerosis
APP	Amyloid precursor protein
APS	Ammonium persulfate
BACE1	Beta-site amyloid precursor protein cleaving enzyme 1
BCA	Bicinchoninic acid
BCS	Bathocuproine disulphonate
bp	Base pair
BPB	Bromophenol blue
BSA	Bovine serum albumin
Ca	Calcium
CCO	Cytochrome c oxidase
CCS	Copper chaperone for superoxide dismutase 1
cDNA	Copy deoxyribonucleic acid
CSF	Cerebrospinal fluid
Cu	Copper
Da	Dalton
DBH	Dopamine β -hydroxylase
DEPC	Diethylpyrocarbonate
DMEM	Dulbecco's modified eagle's medium
DMSO	Dimethylsulphoxide
DNA	Deoxyribonucleic acid
D-PBS	Dulbecco's phosphate buffered saline
DTT	Dithiothreitol
ECL	Electrogenerated chemiluminescence
EDTA	Ethylenediaminetetraacetic acid
EGTA	Ethylene glycol tetraacetic acid
EPR	Electron paramagnetic resonance
ER	Endoplasmic reticulum
FCS	Foetal calf serum
xg	Gravity
GIF	Growth inhibitory factor
HNE	4-hydroxy-2-nonenal
HNO ₃	Nitric acid
HPLC	High pressure liquid chromatography
HRP	Horseradish peroxidase
ICP-MS	Inductively coupled plasma mass spectrometry

IDE	Insulin-degrading enzyme
IRE	Iron responsive element
kb	Kilo base
KCl	Potassium chloride
KLC	Kinesin light chain
KPO ₄	Potassium phosphate
LTP	Long-term potentiation
MALDI-TOF-MS	Matrix-assisted laser-desorption ionisation time-of-flight mass spectrometry
Mg	Magnesium
MMP2	Matrix-Metalloproteinase 2
MNK	Menkes disease protein
MSE	Mannitol sucrose EGTA
MW	Molecular weight
NaCl	Sodium chloride
NaHCO ₃	Sodium bicarbonate
NBT	Nitro blue tetrazolium
NEP	Neprilysin
NFT	Neurofibrillary tangles
NMR	Nuclear magnetic resonance
NO	Nitric oxide
NOS	Nitric oxide synthase
OD	Optical density
OST	Oligosaccharyltransferase
PAGE	Polyacrylamide gel electrophoresis
PAM	Peptidylglycine α -amidating monooxygenase
PCA	Principal component analysis
PCC	Proprotein convertase
PCR	Polymerase chain reaction
PD	Parkinson's disease
Pen/Strep	Penicillin/Streptomycin
PKC	Protein kinase C
PMSF	Phenylmethylsulphonyl fluoride
ppb	Parts per billion
ppm	Parts per million
PS1/2	Presenilin1/2
RNA	Ribonucleic acid
ROS	Reactive oxygen species
rpm	revolutions per minute
RT	Reverse Transcription
SDS	Sodium dodecyl sulphate
SDS-PAGE	Sodium dodecyl sulphate polyacrylamide gel electrophoresis
SOD1	Superoxide dismutase 1
SPC	Signal peptidase complex
TACE	Tumor necrosis factor- α -converting enzyme
TBE	Tris-boric acid-EDTA buffer
TBS	Tris-buffered saline
TEMED	<i>N,N,N',N'</i> -tetramethylethylenediamine
TGN	Trans-Golgi network
2D-LC	Two-dimensional liquid chromatography

UTR	Untranslated region
UV	Ultra-violet
V	Volt
WT	Wild type
w/v	Weight/volume
v/v	Volume/volume
XO	Xanthine oxidase
YPD	Yeast peptone dextrose

Chapter 1 – Introduction

1.1 Brain anatomy

The brain weighs approximately 1.5 kg in adults and is roughly subdivided into three areas. The cerebral hemispheres, collectively called cerebrum, account for most of the brain's size and are covered in a highly convoluted cortical layer. The cortex is the center for higher-order thinking, learning and memory, thus also represents the area most affected in neurodegenerative diseases. Beneath lies the brain stem which controls breathing, heart rate, body temperature and other autonomic functions. The cerebellum is located beneath the brain stem and is involved in motor control and cognitive functions such as language, attention and possibly emotions (Strange, 1996). Due to constant functional demands, the brain is the greatest consumer among the organs of the body of oxygen and glucose to fuel its oxidative metabolism. There is extensive blood supply to the cerebral cortex delivered by a large network of blood vessels and capillaries, which are thought to be within a 40-50µm vicinity to each individual nerve cell. Nerve cell function and synaptic transmission depend on specific ionic concentrations in the extracellular space, thus fluctuations in blood composition could easily disrupt this sensitive environment. To avoid this scenario, the brain is surrounded by a compartment containing cerebrospinal fluid (CSF), which links the extracellular nerve cell space with the blood supply, but prevents direct contact (Strange, 1996).

The CSF occupies the space around and between cerebral ventricles and the central canal of the spinal cord. It is produced at a rate of 500ml per day with an approximate turn over of 3 times per day and is in constant motion, thus providing nutrient supply to all areas of the brain and a clearance mechanism for metabolic waste. The CSF is formed from blood mainly by a network of ventricular capillaries, the choroid plexus, but also from capillaries around the brain and represents a low protein ultra-filtrate of blood plasma. Spatial and chemical separation of CSF from blood is achieved by a physical barrier called the blood-brain-barrier (BBB), a layer of specialized epithelial cells lining cerebral capillaries (Saunders et al., 1999). Chemical gradients between blood and CSF are established

by selective active transport of nutrients such as glucose, trace metals, proteins and L-DOPA, a neurotransmitter precursor produced outside the brain. CSF has four major functions. It provides buoyancy for the brain to reduce weight associated pressure and resulting blockage of blood supply. Further it acts as a buffer, preventing physical injury to the brain when hit and facilitates blood reperfusion of swollen brains after head injury by decreasing its volume (Saladin, 2007). However, providing chemical stability by homeostatic regulation of biological molecules is one of the most important functions of CSF.

1.2 Alzheimer's disease

1.2.1 Hallmarks of Alzheimer's disease

Alzheimer's disease (AD) is the most common form of dementia in humans accounting for 50-80% of dementia cases. Late-onset AD is typically diagnosed from the age of 65 and a rough estimate determined the risk of developing AD to double every five years thereafter. In 2006, there were 26.6 million sufferers worldwide and it is predicted that by 2050 1 in 85 people globally will be directly affected by the disease (Brookmeyer et al., 2007).

Attention was first brought to this disorder in 1906 by the psychiatrist Alois Alzheimer, who detected abnormal deposits in the cortex of the post-mortem brain of one of his patients. What Alzheimer described about 100 years ago is now seen as the hallmark structures in the identification of Alzheimer's disease (AD), however, it has not yet been determined whether these characteristic deposits are causative or an effect of pathological events in the brain.

The pathological hallmarks developed by AD patients comprise of extracellular amyloid deposits referred to as plaques and intracellular neurofibrillary tangles (NFT) in brain regions involved in learning and long-term memory. Considerable progress has been made in the identification of proteins involved in the disease and their potential physiological and pathological functions. Amyloid plaques are composed of a hydrophobic fragment derived from a protein known as the amyloid precursor protein (APP). APP has a multitude of proposed functions which are discussed in later sections. NFT are composed of the hyperphosphorylated species of tau, a protein involved in micro-tubule directed neuronal trafficking. Both APP

and tau are at the center of multiple metabolic pathways, thus determining the cause of AD is not a straightforward task. Mis-regulation of vesicular trafficking, metabolic changes in neuronal metal and neurotransmitter homeostasis and oxidative stress resulting in energy loss due to mitochondrial disintegration have all been implicated in the progression of the disease. One common factor, however, is the proteolytic processing of APP to synaptotoxic A β , giving rise to the A β hypothesis (see section 1.4.1).

AD is a form of progressive neurodegeneration in which first physiological changes occur up to 20 years before the first symptoms become apparent. First symptoms at the stage of mild cognitive impairment include short-term memory loss, mood changes, loss of numerical skills and poor judgement. Patients with moderate AD usually display symptoms like confusion, restlessness, difficulties in person and face recognition, whereas patients in the later stages of AD may suffer from seizures, severe weight loss and a complete loss of awareness (Förstl and Kurz, 1999). Comparison of brain volumes of hippocampal and endorhinal cortex in patients with mild cognitive impairment and AD with a control group show a significant reduction in volume of these two regions with AD patients being affected more than patients with cognitive impairment. Reduction in cortex volume starts in the endorhinal region and proceeds to the hippocampal cortex with symptoms closely correlating with the affected brain region (Pennanen et al., 2004). AD is clinically diagnosed through a series of behavioral and cognitive tests and the diagnosis is supported by medical imaging techniques such as computed tomography, magnetic resonance imaging, single photon emission computed tomography or positron emission tomography. However, diagnosis of AD can only be confirmed post-mortem through the identification of extracellular amyloid deposits and intracellular NFT. AD is a terminal illness and patients usually die within seven years of diagnosis, not through AD itself, but the cause of death is typically a secondary infection such as pneumonia.

1.2.2 Genetic determinants of Alzheimer's disease

1.2.2.1 Sporadic Alzheimer's disease

A variety of factors influence the development and occurrence of sporadic AD or late-onset AD, which accounts for 90% of all AD cases. The greatest risk factor is age and the likelihood of developing AD increases drastically past the age of 65. Age-dependent changes in membrane composition in conjunction with hypercholesterolaemia are thought to be involved in the formation of amyloid plaques. Cholesterol is concentrated in membrane lipid rafts and it has been shown that enzymes involved in the processing of APP, such as β and γ -secretase, localise in those rafts, whereas α -secretase localizes outside lipid rafts (Ehehalt et al., 2003).

There is also a correlation between sex and AD. It was demonstrated that testosterone reduces neuronal secretion of amyloid peptides (Gouras et al., 2000b), whereas female transgenic mice displayed increased plaque load due to increased β -secretase activity (Schäfer et al., 2007). Refer to section 1.3.3 for more detail.

Stroke and brain injury greatly contribute to AD development. Ischaemia is characterized by a reduction in cerebral oxygen levels due to restrictions in blood flow. Intracellular energy stores are rapidly depleted of ATP and absence of aerobic metabolism results in changes in metal ion homeostasis. Particularly potassium and calcium transport is interrupted thus increasing the possibility of synaptotoxicity by changes in neurotransmitter release, generation of reactive oxygen species (ROS) and induction of the mitochondrial apoptotic cascade. Reperfusion of the brain can cause additional generation of ROS once the fine chemical balance of the cell is altered. Cerebral reperfusion after brain injury is not a localized event, thus toxic effects are displayed globally and may pre-condition the brain to be more susceptible to AD (Raichle, 1982). It was also shown that under hypoxic conditions gene transcription and expression of β -secretase, an enzyme central to amyloid generation, were elevated thus possibly inducing the production of the first amyloid species which could initiate the amyloid cascade as described section 1.4.1 (Sun et al., 2006).

Among others Apolipoprotein E (APOE) is the major risk gene associated with AD. There are three isoforms of APOE: APOE- ϵ 2, APOE- ϵ 3 and APOE- ϵ 4. It was recently shown that APOE promotes the proteolytic degradation of amyloid thus facilitating its clearance from the brain. The reduction in plaque burden was isoform specific with the greatest plaque reduction observed for mice homozygous for the APOE- ϵ 2 allele. APOE- ϵ 4, the isoform predominantly involved in the predisposition for development of AD, exhibited impaired ability to facilitate A β clearance. APOE enhances the break-down of amyloid indirectly by engaging with and altering the activity of neprilysin and insulin-degrading enzyme, major players involved in amyloid reduction as detailed in section 1.3.6 (Jiang et al., 2008). Heterozygous and homozygous allelic variation involving all three isoforms determines the risk of possible AD development. Although individuals homozygous for APOE- ϵ 4 carry the highest risk of AD predisposition, some never develop AD, whereas 40-65% of AD cases are APOE- ϵ 4 negative. This indicates that environmental factors such as diet, exercise regime, cognitive training and social interaction play a large role and if adjusted appropriately could potentially delay late-onset of AD.

1.2.2.2 Familial Alzheimer's disease

Patients displaying genotypes of inherited or familial AD (FAD) account for less than 5% of all AD cases. Often multiple generations in one family display signs of dementia since patients develop symptoms from the age of 50. Three genes are involved in the autosomal dominant inheritance of early-onset AD and comprise of APP (chromosome 21), Presenilin1 (chromosome 14) and Presenilin2 (chromosome 1). There are at least 38 mutations in the APP, 94 in the Presenilin1 and 12 in the Presenilin2 genes (<http://www.alzforum.org>) most of which lead to increased production of A β , specifically A β ₁₋₄₂, the major component of amyloid plaques (Scheuner et al., 1996). The increase in A β release is achieved in multiple ways. The London mutation in APP decreases the ratio of A β ₁₋₄₀ to A β ₁₋₄₂ (Suzuki et al., 1994) thus increasing amyloid deposition, whereas the Swedish mutation in APP (hereafter referred to as APP_{swe}) enhances overall amyloidogenic APP processing (Citron et al., 1992).

Of particular interest for this thesis is the double point mutation at positions 670 and 671 (as shown in figure 1.1) in the 770 amino acid transcript of APP first discovered by Mullan et. al. (Mullan et al., 1992) in a Swedish family. This mutation just N-terminal of the APP A β sequence enhances APP processing thus increasing amyloid concentrations and its neurodegenerative effects. It is hypothesized that A β influences a variety of physiological pathways causing disruption to synaptic plasticity and function, refer to section 1.4. To study the effects of the Swedish mutation many animal and cell culture models have been created. The most prominent mouse model is Tg2576 containing the human APP_{swe} protein. Expression testing of the human APP_{swe} variant in a rat model demonstrated high expression patterns in the cortex, hippocampus and cerebellum, brain regions most affected in AD (Folkesson et al., 2007). Comparison studies of fibroblasts obtained from symptomatic and pre-symptomatic carriers of the APP_{swe} variant detected elevated A β levels in both groups suggesting that increased A β production is not a secondary event, but likely the cause in the development of AD (Citron et al., 1994). Thus a model organism containing the APP_{swe} variant and displaying an increased APP metabolism is advantageous in studying possible roles of APP, in particular its role in cellular metal homeostasis. The human neuroblastoma cell line *SH-SY5Y* stably transfected with human APP_{swe} is used in this study in order to achieve the aims outlined in section 1.8.2.

1.3 The amyloid precursor protein and its enzymatic processing to form beta-amyloid

1.3.1 The amyloid precursor protein

The amyloid precursor protein (APP) is ubiquitously expressed in human neuronal as well as non-neuronal tissues (Selkoe et al., 1988, Bush et al., 1990, Weidemann et al., 1989) and constitutes a type 1 membrane glycoprotein suggested to resemble a cell-surface receptor (Kang et al., 1987). It is localized to intracellular membranes such as the endoplasmic reticulum and the Golgi as well as to plasma membranes. The secretory trafficking processes involved in APP maturation will be described in detail in section 1.3.2. APP belongs to an evolutionarily conserved protein family (Coulson et al., 2000), which displays high amino acid and domain homology and contains the NPXY – clathrin internalization signal. Individual knock out mutations

of all three members in mice suggest a function to promote neurite outgrowth, neural cell migration and a role in copper homeostasis (Heber et al., 2000, Zheng et al., 1995, Müller et al., 1994, White et al., 1999b, Young-Pearse et al., 2007), whereas mice with the genotype for a triple knock out die *in utero* with symptoms of cranial defects (Herms et al., 2004). Cleavage of APP by the α -secretase complex, comprising of proteases ADAM10 and ADAM17, results in the release of soluble APP α (sAPP α) which is implicated in the regulation of neurite outgrowth and cell survival in developing hippocampal neurons (Milward et al., 1992, Mattson et al., 1993, Mattson, 1994) and adult synaptic plasticity, a term describing the reconnection and reorganization of neurons upon a variation of stimuli. Furthermore APP interacts with several trans-membrane and cytosolic proteins involved in axonal transport and receptor signaling. These interactions and their respective function will be discussed in section 1.3.4.

The gene for APP is located on the human chromosome 21 (Goldgaber et al., 1987). Transcriptional products of the gene are alternatively spliced into three variants with corresponding proteins of 695, 751 and 770 amino acid residues (Kitaguchi et al., 1988) with APP₆₉₅ being the prevalent isoform in the human brain (Tanaka et al., 1989, Kang and Müller-Hill, 1990, Rockenstein et al., 1995). This APP₆₉₅ isoform was used in the transfection of *SH-SY5Y* neuroblastoma cells in the scope of this project due to its relevance to AD. The general protein structure of all three isoforms comprises of a short intracellular portion, a 23 amino acid transmembrane domain and a large extracellular N-terminal tail comprising structural and functional domains. As demonstrated in figure 1.1 the most N-terminal domain is a cysteine-rich heparin binding domain (growth factor domain), which is thought to be the main contributor to the biological functions of APP specified above (Rossjohn et al., 1999). A copper binding site and a zinc binding site are followed by an aspartic and glutamic acid rich part of the protein sequence. The Kunitz-type protease inhibitor domain (KPI) is present in the splice forms APP₇₇₀ and APP₇₅₁ at residue 365, but is absent from the APP₆₉₅ isoform, which attributes to the difference in protein length. The Ox2 domain is followed by a second heparin binding domain, a region of random coil and a second copper binding site within the A β peptide sequence (Botelho et al., 2003). The difference in length between the APP₇₇₀ and APP₇₅₁

isoforms results from splicing of the O_{x2} containing exon from the APP₇₅₁ mRNA transcript.

It has been demonstrated that APP is involved in homodimerisation facilitated by two independent sites in its extracellular portion. It was further shown that mutational modulation of distinctive sites leads to increased dimerisation and A β peptide formation, suggesting that this interaction contributes to the regulation of its proposed signal activity (Scheuermann et al., 2001). Further evidence exists that heparin might be involved in the dimerisation process (Gralle et al., 2006) and that *in vivo* APP forms homo- as well as heterodimer complexes with other APP family members, promoting cell-cell adhesion (Soba et al., 2005).

1.3.2. Expression, translation and maturation of the amyloid precursor protein during progression through the secretory pathway

APP gene expression can be influenced by a variety of factors. It was shown by Bellingham et. al. (Bellingham et al., 2004b) that APP protein levels and gene expression are decreased in copper deplete human fibroblasts overexpressing the Menkes protein (MNK), a major mammalian copper efflux protein. Furthermore Hung et. al. (Hung et al., 1992) demonstrated increased gene expression and levels of protein for APP₆₉₅ *in vivo* during neuronal differentiation in P19 murine embryonal carcinoma cells and increased protein levels of APP₆₉₅ in primary hippocampal neurons during *in vitro* differentiation. Research suggests that the APP cleavage product APP intracellular domain (AICD – as described in more detail in section 1.3.3) indirectly regulates the gene expression of APP, BACE and Tip60 (Cao and Sudhof, 2001). AICD is either restricted to cytosolic membranes by the adaptor protein X11 α or interacts with the adaptor protein Jip1b which aids AICD transport into the nucleus and subsequent interaction with the nuclear histone acetylase Tip60 (von Rotz et al., 2004). In accordance with the hypothesis of APP involvement in neuronal metal homeostasis, Rogers et. al. (Rogers et al., 2002) identified a novel type-II iron responsive element (IRE) in the 5'-untranslated region (5'-UTR) of the APP transcript. Selective down-regulation of APP mRNA translation in *SH-SY5Y* neuroblastoma cells in response to intracellular iron chelation was reversed by iron influx. The variation of stimulatory and inhibitory stimuli and multi-factorial influence on both expression and translation of APP

indicates the complexity of APP based disorders and the difficulties of identifying the exact functions of this multi-faceted protein.

Figure 1.1: Schematic representation of APP domains and sequential differences between *SH-SY5Y* APP_{WT} and APP_{swe} cell lines

a) APP is an integral membrane protein ubiquitously expressed in a variety of tissues. Several splice variants of the protein are known ranging from 695 (APP₆₉₅) to 751 (APP₇₅₁) and 770 (APP₇₇₀) amino acid residues. In the brain APP₆₉₅ is the most common form, whereas APP₇₅₁ and APP₇₇₀ are expressed in other tissues. The difference in length is dependent on the presence (APP₇₅₁ and APP₇₇₀) or absence (APP₆₉₅) of the Kunitz protease inhibitor domain (KPI). Beginning from the N-terminus other domains include a heparin-binding/growth-factor-like domain (HBD1) and a copper binding domain (CuBD1) followed by a zinc binding domain (ZnBD). An aspartic and glutamic acid rich part of the sequence (DE) is followed by a Kunitz protease inhibitor domain (KPI) for isoforms APP₇₅₁ and APP₇₇₀ and a second heparin-binding domain (HBD2). A region of random coil (RC) precedes the A β peptide sequence (shown in red) which contains a second copper-binding site (CuBD2) (Botelho et al., 2003).

b) The A β region (shown in red) of the APP protein is shown in more detail. The difference in peptide sequence between APP_{WT} and APP_{swe} is represented by a two amino acid residue change just N-terminal of the A β sequence. Lysine (K) and methionine (M) at positions 595/596 have been mutated to asparagine (N) and leucine (L). Cleavage sites are indicated by arrows and the appropriate secretase responsible for proteolytic processing at any particular site. The β -secretase cleavage site is located most N-terminal of the peptide at amino acid residue 596, followed by the α -secretase cleavage site at amino acid residue 612. The two most common γ -secretase cleavage sites just C-terminal of the A β peptide sequence at residues 636 and 638 result in A β isoforms 40 and 42. Designated amino acid residues are derived from the APP₆₉₅ isoform, which is predominant in the brain.

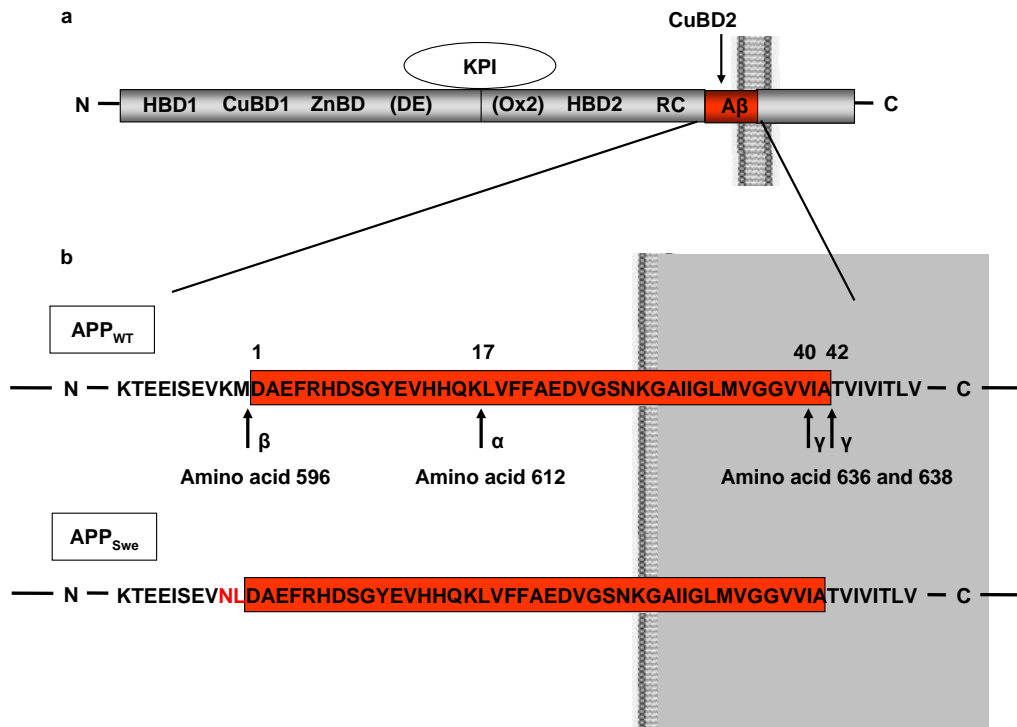
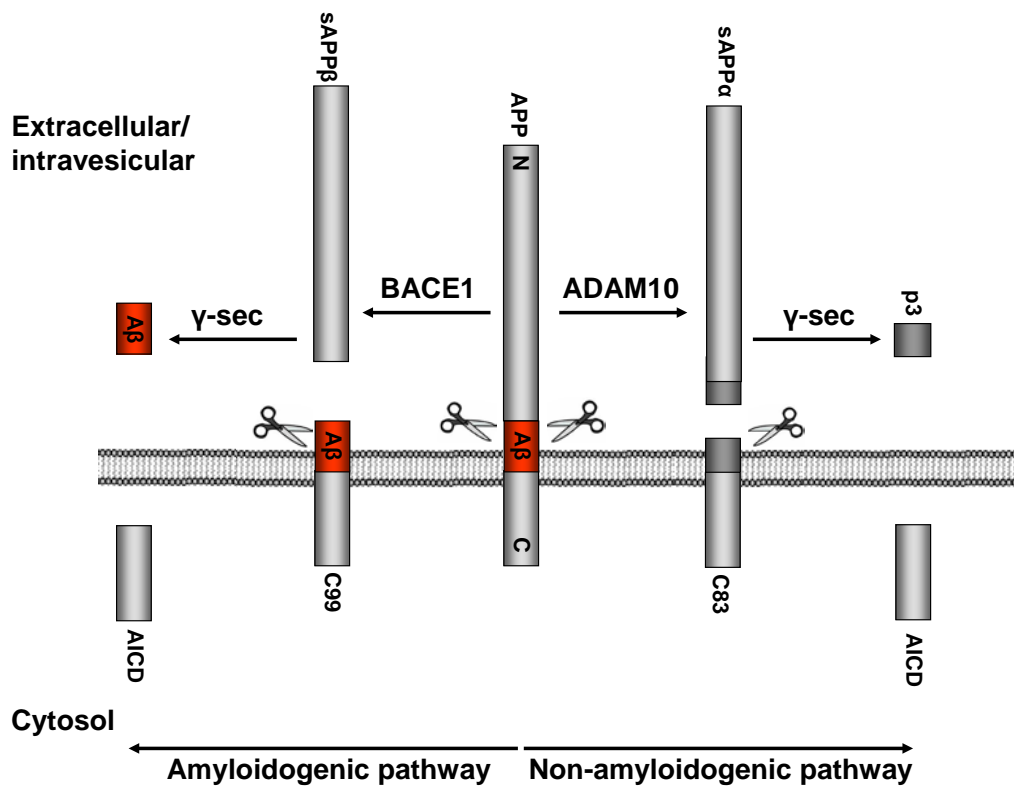


Figure 1.2: Metabolic derivatives of APP in non-amyloidogenic and amyloidogenic proteolysis

The membrane bound APP protein can be processed in two ways leading to a pathogenic and non-pathogenic phenotype. APP is proteolytically processed by a complex of α -secretases mainly comprising of ADAM10 within the A β peptide releasing a soluble ectodomain (designated sAPP α), and membrane bound fragment C83, which is subsequently cleaved by γ -secretase to generate the p3 fragment and the intracellular domain (AICD).

The amyloidogenic processing of APP is initiated by β -secretase (BACE1) cleavage of APP just N-terminal of the A β peptide sequence resulting in the extracellular release of a peptide fragment designated sAPP β . Subsequent heterogeneous cleavage of the membrane bound fragment C99 just C-terminal of the A β sequence by γ -secretase results in extracellular A β peptide and intracellular AICD generation. The most commonly generated forms of the A β peptide vary in length from 40-42 amino acid residues with the majority being of the more soluble 40 amino acid residue nature.



Translation of APP mRNA occurs simultaneously to insertion of the newly synthesised polypeptide chain into the rough endoplasmic reticulum (ER). A 17-amino acid signal recognition particle at the N-terminus of the APP nascent chain directs trafficking into the ER via the Sec61 translocon, mediating APP integration into the lipid bilayer via interactions with Sec61 α and Sec61 β subunits (Alder and Johnson, 2004). Following translocation a number of accessory components such as the signal peptidase (SPC) complex and the oligosaccharyltransferase (OST) complex facilitate processing of the unfolded protein (Alder and Johnson, 2004) and initiate O-linked N-glycosylation (Griffith et al., 1995). Experiments in Cos-7 cells further identified facilitation of APP transfer from the translocon into the membrane bilayer by interaction with Ribophorin 1, a translocon associated subunit of the OST, and SPC25 (Wilson et al., 2005). Ribophorin is implicated in co-localisation of the N-glycosylating subunit STT3 of the OST with APP (Wilson and High, 2007). APP is subsequently transported to the trans-Golgi network (TGN) via Sec23 and Sec24 in a COPII dependent manner (Huttunen et al., 2007). Phosphorylation of the APP ectodomain occurs at two distinct cellular locations. Regardless of familial mutations APP undergoes phosphorylation in a post-TGN compartment and also at the cell surface mediated by an ectoprotein kinase (Walter et al., 1997). Furthermore phosphorylation of APP at a site different to usual phosphorylation sites (namely at S655) increases the vesicular exit from the TGN and secretory cleavage of APP to produce the non-amyloidogenic sAPP α fragment, which is described in detail in section 1.3.3 (Vieira et al., 2009). Thus posttranslational modifications are imperative for APP processing and secretion (Caporaso et al., 1992).

Global cellular studies of APP localization patterns reveal a dynamic process of APP secretion and internalization. Apart from being localized to intracellular membrane such as ER and the TGN it is also observed at the plasma membrane (Caporaso et al., 1994, Tomimoto et al., 1995). Evidence exists that APP is re-internalised and processed in lysosomes (Haass et al., 1992a). However, proteolytic processing of APP mainly occurs in the ER, TGN and in endosomes (Grbovic et al., 2003, Yan et al., 2001). Using immunofluorescent antibodies Yamazaki et al (Yamazaki et al., 1996) showed rapid internalization of APP via coated pits into

endosomes, prelysosomes and lysosomes contributing to the constitutive processing of this protein. In the brain APP has been detected in the membranes of synaptic extracts (Kirazov et al., 2001) and has been localized to postsynaptic moieties, axons and dendrites (Schubert et al., 1991, Shigematsu et al., 1992) as well as cholesterol enriched membranes (Hayashi et al., 2000) and cell adhesion patches (Storey et al., 1996). There is evidence that APP might be involved in axonal transport acting as kinesin-1 receptor, thus facilitating vesicular trafficking and APP fragment secretion. Deletion of the kinesin-binding region in the APP C-terminal disrupted vesicular trafficking along the axon (Gunawardena and Goldstein, 2001) and *in vitro* studies detected direct interactions of APP with the TPR domain of the kinesin light chain (Kamal et al., 2000). Recent research identifies a novel interaction of the APP cytosolic tail sequence YKFFE with the adaptor protein AP-4, which is thought to reduce the amyloidogenic processing of APP by redirection of membrane vesicles from TGN to endosomes, thus eliminating the post-TGN cleavage of APP by γ -secretase (Burgos et al., 2010).

1.3.3 Cleavage and processing pathways of the amyloid precursor protein

Upon maturation APP undergoes processing by three individual proteases at two extracellular and one transmembrane site. Figure 1.1 shows a schematic representation of the APP protein and its cleavage sites termed α , β and γ according to their respective protease. APP processing at α - and β - cleavage sites is a mutually exclusive event and results in the release of large extracellular domains sAPP α (Esch et al., 1990) and sAPP β of the protein. Membrane tethered C-terminal fragments, C83 for α - and C99 for β -secretase generated products, are further processed by the transmembrane γ -secretase complex, which generates the p3 and A β ₁₋₄₀/A β ₁₋₄₂ fragments, respectively. The APP intracellular domain (AICD) is released into the cytosol after γ -secretase cleavage of both fragments (see figure 1.2).

The α -secretase complex has not been characterised in very much detail. The complex has both constitutive and inducible components with the inducible activity being controlled by protein kinase C (PKC) (Nitsch et al., 1997), which in turn is stimulated by glutamate signaling (Lee et al., 1995). The constitutive activity, however, has not yet been identified. The complex mainly consists of two

disintegrin metalloproteinases ADAM 10 and ADAM17 or TACE. It was shown that mice lacking TACE show decreased levels of sAPP α and die *in utero* indicating a vital role for sAPP α in embryonic development (Buxbaum et al., 1998a, Peschon et al., 1998). Overexpression of ADAM10 increased α -secretase activity, whereas a point mutation in its zinc-binding site inhibited enzyme activity, but did not abolish all sAPP α production (Lammich et al., 1999) indicating that α -secretase activity might be governed by more than two proteinases. Further ADAM10 activity has been demonstrated *in vitro* using the A β peptide 11-28 fragment as substrate (Lammich et al., 1999). Both ADAM10 and ADAM17 are synthesised as proproteins and require prodomain cleavage by proprotein convertases (PCC) to be activated (Anders et al., 2001), a process which readily occurs in the late TGN (Schlondorff et al., 2000).

BACE1 (beta-site amyloid precursor protein cleaving enzyme 1) was first identified in 1999 as a membrane-anchored aspartyl protease with homology to the pepsin family (Vassar et al., 1999, Hussain et al., 1999, Yan et al., 1999). It cleaves APP after residue 596 (APP₆₉₅ isoform) releasing the sAPP β and C99 fragments. BACE1 contains a single membrane-spanning region near its carboxy-terminus, a signal sequence and a propeptide sequence close to its amino-terminal and two aspartate residues at positions 93 and 289, which are vital for enzyme activity (reviewed in (Suh and Checler, 2002). Upon BACE maturation by propeptide cleavage and N-glycosylation of its ectodomain in the ER, it is relocated to the TGN and endosomes, a process catalysed by the phosphorylation of serine 498 in the cytosolic tail of the protein (Walter et al., 2001). BACE1 is highly expressed in neuronal tissues with a particularly high distribution to cholesterol-specific lipid rafts (Marlow et al., 2003), but is also detected in a variety of other human tissues (Vassar et al., 1999, Yan et al., 1999). Knock out mice lacking both alleles for the enzyme are phenotypically normal and show reduced secretion of A β , indicating that inhibition of BACE1 might be a potent therapeutic for AD (Luo et al., 2001, Cai et al., 2001). Further it has been reported that APP_{swe} (as depicted in figure 1.1) is cleaved more readily to produce larger quantities of the potentially neurotoxic A β peptide (Yan et al., 1999, Perez et al., 1996, Cai et al., 1993). The reasons for increased processing of APP_{swe} need to be established. One cause may be increased approximation of APP and BACE1 through interactions facilitated by the mutation

or possible increased enzyme activity. Angeletti et al. (Angeletti et al., 2005) discovered that BACE1 contains a 24 residue cytosolic domain with high affinity for Cu(I). Intricate studies showed that BACE1 interacts with the copper chaperone for superoxide dismutase (CCS) (see section 1.8.1) thus potentially redirecting copper away from the cellular antioxidant defence system and ultimately linking superoxide dismutase activity, cytosolic copper and ectodomain cleavage (Dingwall, 2007).

A second aspartyl protease, BACE2, was also identified in the brain (Farzan et al., 2000). However, it is expressed at much lower levels than BACE1 (Bennett et al., 2000a) and thought to be of more importance in vascular tissues such as placenta, heart and kidney (Farzan et al., 2000).

The γ -secretase is a multi-subunit complex that cleaves the transmembrane APP fragments C83 and C99 into p3 and A β _{1-40/1-42} at the carboxy-terminus of the A β sequence, respectively, releasing AICD into the cytosol. It was reported that GXXXG motifs within the transmembrane region determine the etiology of A β depending on the dimerisation strength of the motif. Mutations in GXXXG cause a shift to the generation of shorter A β species (Munter et al., 2007). There are opposing views with regards to the main components of this complex. Presenilin 1 (PS1) and presenilin 2 (PS2) are thought to be the major catalytic enzymes in the secondary APP cleavage step. Both are integral membrane proteins containing eight transmembrane domains. Inactive full-length proteins undergo cleavage between domains 6 and 7 to produce two fragments which associate in a hetero-dimer complex (Capell et al., 1998). Evidence in support of the theory that presenilins are the catalytic cleavage subunits of the γ -secretase complex, includes reduced γ -secretase activity in PS1 knockout mice resulting in reduced secretion of the A β and p3 fragments and cellular accumulation of the C83 and C99 fragments (De Strooper et al., 1998). However, another line of evidence demonstrating no changes in A β production in fibroblasts derived from presenilin knockout mice (Armogida et al., 2001) suggests that presenilins may act as mediators facilitating the trafficking of APP C-terminal fragments to their cleavage specific site (Sisodia et al., 2001, Xia et al., 2000, Cai et al., 2003). Ponting et al. (Ponting et al., 2002) discovered an evolutionarily conserved presenilin homologue gene family coding for proteins with

multiple transmembrane domains and two predicted catalytic aspartyl residues, as were previously detected in presenilins and thought to mediate endoproteolysis and γ -secretase activity (Wolfe et al., 1999). These other family members might account for the compensatory catalytic cleavage in fibroblasts from PS1 knockout mice. A second component of the γ -secretase complex is nicastrin, a transmembrane protein, which interacts with the C-terminal fragments of APP and presenilins (Esler et al., 2002). It was shown by Yu et al. (Yu et al., 2000) that mutational modifications in conserved regions of the protein resulted in increased A β production, whereas deletion of the same region resulted in complete abrogation of A β secretion. Post-translational modifications such as glycosylation and nicastrin trafficking were abolished in presenilin double knockout mice strengthening the arguments of a potential role for presenilins in the assembly and maturation of the γ -secretase complex rather than enzyme activity itself (Leem et al., 2002).

Similarities between APP cleavage and Notch cleavage have been detected. Notch is a type-I transmembrane receptor that is catalytically processed by TACE (Brou et al., 2000) or ADAM10 (Hartmann et al., 2002) upon ligand binding and thought to be involved in fate decisions during embryonal development. Subsequent intramembrane cleavage (De Strooper et al., 1999) is reminiscent of APP C-terminal cleavage by γ -secretase with the resulting cytosolic fragment engaging in transcriptional activation. Both proteins interact with presenilins during γ -secretase cleavage, indicating that due to binding competition this might be the rate limiting step in A β production.

Not only post-translational modifications and exogenous stimuli determine the fate of APP cleavage. One important factor is the putative localization of its processing enzymes. After translation in the rough ER, APP is transported through the TGN to the plasma membrane, where partial re-internalisation of full-length and transmembrane carboxy-terminal fragments via endosomes occurs (Yamazaki et al., 1996). Endosomal vesicles are either redirected to the TGN for recycling or to the lysosomal compartment for degradation. α -secretase activity is found in compartments of the anterograde transport system, namely the ER, the TGN and secretory vesicles, whereas β - and γ -secretases act on APP and its proteolytic

products in all anterograde and retrograde compartments, ie. the ER, the TGN, secretory vesicles, endosomes and lysosomes.

1.3.4 Protein interactions with the amyloid precursor protein

Continuous production of APP during embryogenesis and adulthood suggests a permanent role for the protein in neuronal development and implications in synaptic plasticity implying effects on memory and cognition. In addition to its involvement in neurite growth and neuronal maintenance via sAPP α it was suggested that APP may play a part in G-protein coupled signaling in the brain. APP displays a structural configuration reminiscent of a membrane anchored receptor. In fact, it was shown that APP is coupled to trimeric G₀ proteins via its intracellular tail (Nishimoto et al., 1993). Downstream signaling cascades may include adenylyl cyclase, phospholipase C, voltage-dependent calcium channels and pathways for apoptosis (Nishimoto et al., 1993). However, the downstream effects of APP mediated G-protein signaling are not known.

APP has also been implicated in cell adhesion and motility due to its ability to bind specific proteins involved in these processes. The large extracellular portion of APP contains several domains that provide binding motifs for heparin (Mok et al., 1997), collagen (Behr et al., 1996), laminin (Kibbey et al., 1993), beta-1-integrin (Yamazaki et al., 1997) and telencephalin. It was observed that PS1 binds both APP and telencephalin providing a possible spatial link between the two proteins (Annaert et al., 2001).

APP is also involved in the formation of actin filaments. The adaptor protein Fe65 binds to the intracellular domain of APP and interacts with mammalian homologue of drosophila enabled (MENA), which binds to profilin and enhances actin filament formation. This interaction provides a link between a potential receptor protein and the cytoskeleton other than APP binding to micro-tubules via JIP1. Overexpression of APP and Fe65 demonstrated increased cell motility and growth cone dynamics (Sabo et al., 2001).

The same binding motif responsible for interactions of Fe65 and JIP1 with APP (YENPTY), which is conserved in cytoplasmic domains of several tyrosine kinase

receptors, also facilitates the interaction of APP with the adaptor protein family X11 (Borg et al., 1998). X11 α and X11 β are the two neuronal isoforms, however, most research to date was performed to elucidate the function of X11 α . X11 α binds to APP via its phospho-tyrosine-binding (PTB) domain preventing APP processing and production of amyloidogenic as well as non-amyloidogenic soluble fragments (Borg et al., 1998) and a decrease in amyloid plaque deposition was detected *in vivo* in APP_{swe} transgenic mice (Lee et al., 2003). The inhibition of A β production is thought to be due to attenuated γ -secretase processing of APP upon interaction with X11 α (Xie et al., 2005). It was further demonstrated that X11 α binds to PS1, thus direct competition between APP and X11 α for PS1 binding might account for decreased APP processing. Direct inhibition of APP and PS1 interaction was demonstrated for X11 β bound to caldein resulting in the retardation of intracellular protein maturation (Araki et al., 2003). The X11 protein family might also have a role in the regulation of protein trafficking since they are localized throughout the neuron and co-purification of caldein and X11 β with the kinesin heavy chain was demonstrated (Araki et al., 2003). It was shown by Vassar et. al. (Vassar, 2005) that the optimal pH for BACE activity is slightly acidic, conditions attributed to the late Golgi, endosomes and lysosomes. Thus enzyme activity is prominent in those compartments. Due to X11 interactions with the transport system and reduced processing of APP, it was suggested that X11 proteins retain APP or direct APP trafficking to compartments unsuitable for α , β , or γ -secretase activity. A further function attributed to X11 proteins is involvement in cellular copper homeostasis by providing a connective link between APP and the copper chaperone for superoxide dismutase (CCS) (McLoughlin et al., 2001), which in turn interacts with the cytosolic domain of BACE (Angeletti et al., 2005). There is a large body of evidence that AD can be correlated with copper imbalance and that APP is one of the major players in this metabolic disruption (reviewed in (Bush, 2003)). Since the involvement of copper in the pathology of AD is the major focus of this thesis, detailed analysis of copper transport, metabolism and its role in neurodegeneration will be provided in sections 1.5 and 1.6.

1.3.5 Aggregation of the amyloid beta peptide and formation of plaques

A β is produced in small amounts by a variety of cell types and under physiological conditions in the CSF of AD and non-AD patients suggesting physiological relevance for the peptide and its participation in neurotoxic events as an effect of misregulation (Busciglio et al., 1993, Shoji et al., 1992, Haass et al., 1992b). It was suggested that A β might have a physiological role as neuronal modulator of A-type K⁺ currents (Plant et al., 2006). BACE1 processes approximately 10% of all APP protein with the resulting species of A β peptides varying in length from 39-42 amino acids. The major two species are A β ₁₋₄₀ (90%) and A β ₁₋₄₂ (10%) and represent an indicative means of measuring the advance of AD as their relative ratio decreases with disease progression. Studies suggest that most A β species are produced in the late secretory and endocytic compartments (Buxbaum et al., 1998b, Wirths et al., 2004), however, an extensive line of research suggests that the more hydrophobic form A β ₁₋₄₂ is mainly produced in the ER, whereas A β ₁₋₄₀ is produced in the TGN (Cook et al., 1997, Greenfield et al., 1999, Hartmann et al., 1997, Haass et al., 1993, Wilson et al., 2002). Studies in canine kidney epithelial (MDCK) cells determine the main cleavage event of APP to occur intracellularly rather than on the cell surface (Haass et al., 1995). The A β peptide exists as monomer, dimer and in oligomeric form, before it forms protofibrils and ultimately fibrils, which aggregate to plaques characteristic for AD (Bitan et al., 2003). Although large β -sheet aggregates of amyloid remain mainly extracellular, pools of intracellular small, soluble, non-fibrillar oligomers known as A β -derived diffusible ligands (ADDLs) (Lambert et al., 1998) have been determined. The discovery of intracellular A β suggests either the re-internalisation of soluble oligomers or the formation of oligomers in vesicular compartments, and identify the intracellular soluble pool of A β as causative for the extracellular plaque formation (Oddo et al., 2006). *In vitro* experiments demonstrate a dependence of fibril aggregation on time and concentration, characteristics of two major risk factors determined for FAD-linked AD patients, age and the shift of soluble to insoluble amyloid species production in mutations linked to APP, PS1 and PS2 (as explained in section 1.2.2.2).

1.3.6 Degradation of amyloid aggregates

The steady state levels of A β in the brain are finely controlled by maintaining a balance between anabolism and catabolism of the peptide (Saido, 1998).

Accumulation of A β and subsequent aggregation into fibrils and plaques in sporadic cases of AD can mainly be accounted for due to a reduction in catabolism. No single protease has been identified as potential A β degrading enzyme. However, candidate enzymes include cathepsin D and E, gelatinase A and B, trypsin or chymotrypsin-like endopeptidases, aminopeptidase, neprilysin (NEP), serine protease complexed with α -2 macroglobulin and insulin degrading enzyme (IDE) (Saido and Iwata, 2006). During aggregation A β undergoes structural changes from an α -helical to a β -sheet conformation which reduces the accessibility for proteases at particular cleavage sites and renders the peptide more resistant for cerebral clearance via the CSF. Thus a range of proteases might be involved in distinct A β clearance depending on its aggregation state.

Special focus has so far been placed on IDE, NEP and matrix metalloproteinase 2 (MMP2) as potential A β proteases. IDE exists in soluble form in the cytoplasm and extracellularly in the CSF of the nervous system. *In vivo* and *in vitro* studies demonstrate that the motif recognized by IDE is not the β -sheet, but conformations of the monomeric form in a pre-amyloid state (Bennett et al., 2000b, Qiu et al., 1998). Recent studies on PS1 V97L mutant cell cultures revealed an increased level of A β ₁₋₄₂ accompanied by the decrease of expression and activity of IDE (Qin and Jia, 2008) indicating that the severity of disease progression due to reduced A β clearance not only exists in sporadic AD cases, but potentially has a major influence on FAD patients. NEP was detected in the brain almost exclusively in form of a membrane-bound protein. Using inhibitors to IDE and NEP it was shown that IDE preferably degrades soluble forms of A β , whereas NEP degrades membrane bound forms of the peptide. Further NEP knockout mice showed distinct A β deposition in the order of hippocampus, cortex, thalamus/striatum and cerebellum, areas especially affected by A β deposition in AD patients (Iwata et al., 2001) and a reduction in neprilysin levels with increasing age in human brains is thought to contribute to higher amyloid levels (Hersh and Rodgers, 2008). It was reported that Angiotensin-converting enzyme (ACE) is involved in the regulation of the ratio of hydrophobic and more hydrophilic amyloid species in Tg2576 mice. Reduction of A β ₁₋₄₂ concentrations and increases A β ₁₋₄₀ was observed, an effect which was blocked by ACE inhibitor captopril suggesting ACE involvement in the promotion of soluble A β (Zou et al., 2007). Gelatinase A, or MMP2, was also found to play a

role in A β degradation (Roher et al., 1994). It was shown that increased A β hydrophobicity, interactions with zinc or copper resulting in increased aggregation and specific FAD mutations prevented MMP2 activity dependent clearance of amyloid (Crouch et al., 2009). However, this effect was reversed by addition of zinc and copper together with the chelating agent clioquinol (White et al., 2006, Crouch et al., 2009) indicating that metal induced aggregation of A β is one of the major challenges in finding a cure to AD. However, before therapeutic agents can be developed it is important to determine the severity of neurotoxicity of monomeric, oligomeric and fibrillar species of A β . For a comprehensive review of APP processing and A β clearance refer to Makarova et. al. (Makarova et al., 2004).

1.4 Beta-amyloid mediated mechanisms of neurotoxicity

1.4.1 The amyloid cascade hypothesis

The amyloid hypothesis is based on the theory that gradually changing steady-state levels of A β initiate a pathological cascade that ultimately results in the formation of amyloid plaques and neurodegeneration in the brain (Hardy and Higgins, 1992). A quick overview of various stages of the process is shown in figure 1.3. However, this hypothesis is somewhat controversial as several groups discovered a discrepancy between disease severity and plaque burden. It has been shown that the soluble pool of A β oligomers is characteristic for disease severity (McLean et al., 1999) and that fibrillar aggregates are less toxic than their soluble counterpart (Hartley et al., 1999, Lambert et al., 2001, Gong et al., 2003, Lacor et al., 2007, Crouch et al., 2005). ADDLs, as mentioned before, have been implicated in the inhibition of hippocampal long-term potentiation (LTP) in rats *in vivo* when present at concentrations comparable to those in human AD brain and CSF (Walsh et al., 2002) and were found to be 70 fold more concentrated in AD patients compared to non-AD patients (Gong et al., 2003). Further studies of cerebral distributions of soluble and fibrillar amyloid (Kayed et al., 2003) imply a close correlation between distribution and concentration of ADDLs with AD toxicity. An alternative to the traditional amyloid hypothesis discusses the possible interaction of A β oligomers with the PrP protein, which resembles an A β receptor in neuronal membranes and might be facilitating the induction of down-stream neurodegenerative processes (Lauren et al., 2009).

Behavioral studies in rat implicate A β oligomers in cognitive dysfunction (Cleary et al., 2005), however, the exact biochemical interactions are not yet fully understood. Lacor et. al. (Lacor et al., 2007) recently demonstrated that ADDLs alter dendritic spine composition, morphology and density by binding specifically to excitatory pyramidal neurons and reducing the expression of NMDA and EphB2 receptors. Both receptors are functionally related to synaptic plasticity with the NMDA receptor playing a central role in LTP and EphB2 exerting control over NMDA-dependent LTP (Lacor et al., 2007). Although, recent developments attribute toxic characteristics to soluble oligomeric forms of A β , an insoluble pool of intraneuronal A β was detected in NT2N cultures, which accumulated in a time dependent manner in the ER and intermediate compartment (Skovronsky et al., 1998). This accumulation of A β_{1-42} precedes the formation of NFT and plaque deposition suggesting that intracellular aggregation occurs in the early stages of AD (Gouras et al., 2000a, Wirths et al., 2004).

No single major function or target of the amyloid peptide has been determined, which leaves room for speculation about the physiological significance of naturally produced base levels of A β . As alteration or addition to the traditional amyloid hypothesis, Haass et. al. (Haass and Selkoe, 2007) suggest a role for large insoluble A β deposits as a source for oligomeric and monomeric species, thus implying a constant equilibrium between the two aggregation forms.

1.4.2 Oxidative stress

Oxidative stress has been identified as a major contributor to neuronal impairment in a number of degenerative diseases such as AD, Amyloid Lateral Sclerosis (ALS) and Parkinson's disease (PD).

In the resting state the brain consumes around 20% of total systemic oxygen indicating the need for a tight control of oxidative balance and regulation of antioxidant status (Smith et al., 2007). Apart from being produced via the oxidative phosphorylation pathway, highly reactive oxygen species (ROS) such as hydrogen peroxide, hydroxyl radicals, superoxides and nitric oxide (NO) are generated through interactions of molecular oxygen with biological compounds. This can be in the form of metal-catalysed Haber-Weiss or Fenton reactions or by calcium

mediated phospholipase activation, xanthine oxidase (XO) and nitric oxidase synthase (NOS) activity (Lewen et al., 2000). A β has been implicated in stimulating the influx of excess synaptic Ca²⁺, thus causing the synthesis of nitric oxide by NOS upon glutamate release from NMDA receptors (Parks et al., 2001). A β generated ROS was also shown to cause cell death in AD brains by increasing intracellular Ca²⁺ levels (Mattson and Goodman, 1995, Yamamoto et al., 1998). Further it was demonstrated that A β increases ROS concentrations (Hensley et al., 1994, Harris et al., 1995), which lead to apoptotic cell death in differentiated neuronal cell culture (Tamagno et al., 2003). However, the apoptotic cascade was inhibited upon cell exposure to antioxidants (Keller et al., 1997a).

A variety of biomarkers has been determined to measure the degree of oxidative damage with respect to DNA damage (Dizdaroglu, 1992) including mitochondrial DNA (Mecocci et al., 1994), peroxidation of lipids and altered gene expression as a result of ROS generation (Allen and Tresini, 2000). Increased nuclear DNA damage in AD brain has been reported (Gabbita et al., 1998) as well as extensive protein carbonylation (Vitek et al., 1994). A high correlation between fibrillar A β and protein and lipid peroxidation stress markers (3-nitro-tyrosine and 4-hydroxy-2-nonenal – HNE, respectively) has been observed (Matsuoka et al., 2001) indicating that, although ROS is produced intra and extracellularly (Schippling et al., 2000), the species responsible for oxidative damage is the aggregated form of A β .

Removal of extracellular synaptic glutamate by high-affinity glutamate receptors is crucial in the prevention of neuronal excitotoxicity. HNE, an aldehydic product of membrane lipid peroxidation, mediates oxidation-induced impairment of glutamate (Keller et al., 1997b) and glucose transporters (Mark et al., 1997) leading to a decrease in cellular ATP levels, synaptic degeneration and cell death. HNE further inhibits Na⁺/K⁺ ATPases (Mark et al., 1995) and promotes protofibril formation of A β via covalent modifications (Siegel et al., 2007).

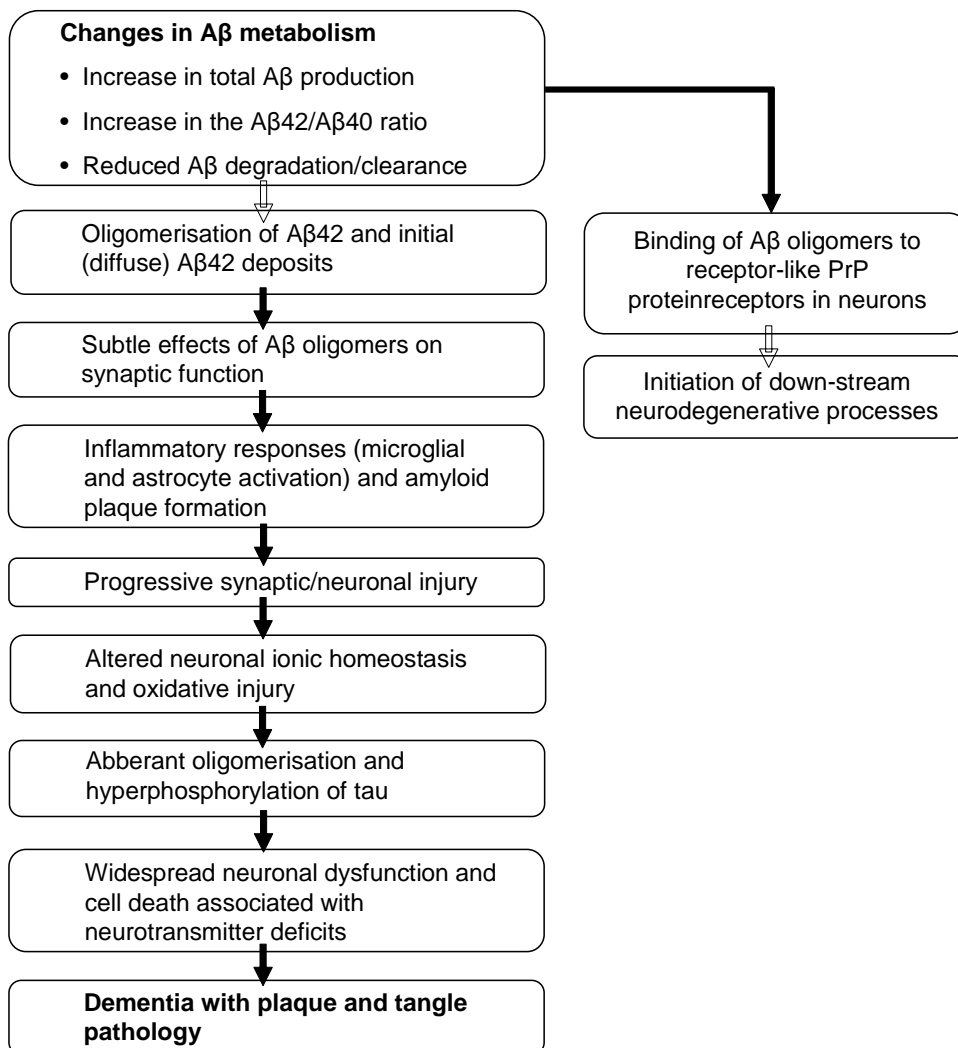
As a metallo-protein A β is directly involved in the generation of ROS by Fenton-type reactions. Details about metal-binding specificity of amyloid and APP will be discussed in section 1.6.1. Upon metal binding A β aggregates and in a mode of catalytic recycling reduces bound Cu(II) and Fe(III) to Cu(I) and Fe(II) releasing H₂O₂ and hydroxyl radicals (Huang et al., 1999). Synaptically released zinc is also

involved in A β aggregation supporting the oxidative properties and plaque formation of amyloid. Peptide aggregation was reversed *in vitro* upon treatment of brain slices with metal chelators and production of H₂O₂ was only detectable in

Figure 1.3: Amyloid cascade hypothesis

The schematic describing the amyloid hypothesis has been directly taken from Haass et. al. (Haass and Selkoe, 2007) and explains the biological steps for accumulative A β toxicity. Gradual changes in A β metabolism leads to increased levels of the peptide and its oligomerisation into higher aggregation states. Oligomeric toxicity results in inflammatory responses, synaptic disruption and changes in metal ion homeostasis. Finally oligomers aggregate to form plaques characteristic for AD.

A recent alternative hypothesis is based on A β binding to PrP which presents a receptor-like structure in neuronal membranes potentially leading to down-stream neurodegenerative processes (Lauren et al., 2009).



aggregated species of A β (Curtain et al., 2001). Barnham et. al. (Barnham et al., 2003a) reported that spontaneous oxidation of methionine 35 in the A β peptide inhibits membrane penetrating abilities, thus increasing extracellular amyloid burden. Further it was observed that this oxidation facilitated the binding of redox active Cu(II) and its reduction to produce H₂O₂.

1.4.3 Axonal transport inhibition

Fast anterograde axonal transport of APP has been reported (Koo et al., 1990). This active transport is facilitated by kinesin motor proteins, which interact with microtubule associated tau protein. Pathologic hyperphosphorylated tau aggregates to form NFT, thus compromising anterograde and retrograde kinesin-dependent transport of Golgi-derived vesicles, neurofilaments and peroxisomes, a process which enhances ROS production and neurotoxicity (Stamer et al., 2002). It was thought that APP binds to kinesin via the kinesin light chain-1 (KLC) subunit (Kamal et al., 2000), however, it now emerged that APP indirectly interacts with kinesin via c-Jun N-terminal kinase-interacting protein 1 (JIP1) (Sisodia, 2002). Hyperphosphorylated tau also binds JIP1, thus directly competing for physiological binding of JIP1 to KLC (Ittner et al., 2009). Mice carrying a double delete mutation for the KLC1 subunit displayed cytoskeletal disorganization, abnormal cargo accumulation, axonal and dendritic swelling and axonopathies (Falzone et al., 2009), symptoms which were also detected in AD transgenic mice with an increased amyloid deposit burden (Stokin et al., 2005). The direct link, if one exists, between amyloid burden and the hyperphosphorylation of tau needs to be established.

1.4.4 Other potential causes of A β mediated neurodegeneration

There is a variety of mechanisms by which A β exerts toxicity such as protein aggregation, oxidative stress, biometal dyshomeostasis and mitochondrial failure (Crouch et al., 2008). A recent and comprehensive review discussed these major neurodegenerative pathways.

The promotion of increased synaptic Ca^{2+} influx and cellular Ca^{2+} imbalance, which causes consistent synaptic neurotransmitter release, is facilitated by amyloid penetration into the membrane bilayer forming an ion channel pore which supports the selective current of cations additional to Ca^{2+} across the membrane (Arispe, 2004). Increased cellular Ca^{2+} levels have been associated with the release of mitochondrial cytochrome c culminating in the initiation of the apoptotic cascade and neuropathology.

Amyloid aggregates have also been detected in mitochondria and are implicated in the reduction of mitochondrial respiration by impairing cytochrome oxidase, α -ketoglutarate dehydrogenase and pyruvate dehydrogenase enzyme activity. Increased levels in NO, as detected in post-mortem AD brains, exacerbated enzyme impairment resulting in major loss of energy production (Casley et al., 2002). Neuronal mitochondrial alcohol dehydrogenase readily binds $\text{A}\beta$ (ABAD), which results in distortion of enzyme structure, loss of function and promotes the generation of free radicals. Double transgenic mice displayed increased ABAD concentrations in $\text{A}\beta$ -rich environments and an accelerated decline in spatial learning ability and memory (Lustbader et al., 2004).

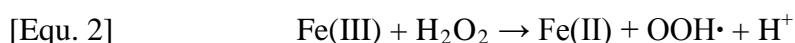
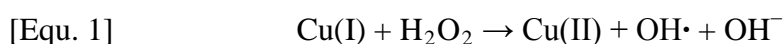
Recently extracellular metallated amyloid plaques have been described as exhibiting type-3 copper oxidase activity by catalyzing the oxidation of dopamine, catecholamine and indoleamine, thus interfering with the re-uptake of neurotransmitters and directly contributing to a decrease in excitatory potential (da Silva and Ming, 2007).

Additional effects of $\text{A}\beta$ accumulation are the increased endocytosis of NMDA receptors thus decreasing the potential for neurotransmission (Snyder et al., 2005), stimulation of actin polymerisation and interference with neuronal transport (Mendoza-Naranjo et al., 2007), downregulation of IDE (Qin and Jia, 2008) and initiation of immune responses.

1.5 Copper in biology

1.5.1 An introduction to metals in biology

Metals are essential for the survival of all organisms. Current estimates suggest that around 50% of all enzymes require metals as a co-factor (Andreini et al., 2008) either to maintain structural integrity or as catalytic facilitator. However, these essential metals can have toxic effects when accumulated in excess or bound by the wrong protein species. Some metals are redox-active, thus can participate in Fenton or Haber-Weiss type reactions and generate ROS. Metals involved in Fenton reactions are mainly Cu(I) and Fe(II) which, upon oxidation with biologically produced hydrogen peroxide, generate hydroxyl radicals. Haber-Weiss reactions contribute to oxidative stress burden by iron catalysed generation of hydroxyl radicals from hydrogen peroxide.



Freely available and excess metal could potentially prevent the binding of metals to their respective binding-site, thus interfering with the biological function of particular metalloproteins.

To avoid these detrimental effects metal ion availability needs to be tightly controlled. An intricate cellular system comprised of regulatory and sensory elements has evolved to ensure the adaption of the cell's metabolism to environmental stimuli. Intracellular metal homeostasis is maintained by active influx, efflux and storage of ions depending on their cellular concentration (Rutherford and Bird, 2004), thus preventing excess cellular metal and cellular deficiency. Metal-regulated changes in metallothionein storage, importers or exporters are mainly attained by metal-activated transcription factors or repressors, thus adjusting the homeostatic properties of the cell to systemic fluctuations in metal concentrations (O'Halloran, 1993). Additionally, upon sensing excess metal, cells may also switch their metabolism to a set of proteins which binds the particular excess metal, thus providing alternative ligands.

1.5.1.1 Metal selectivity and biochemical properties of copper

It is traditionally assumed that upon folding in the ER or as apo-protein in the cytosol, proteins acquire their metal co-factor(s) from a readily available pool of

metals simply by distinction of the ion's thermodynamic properties. Such properties are fairly unique to each metal ion. Ligands chemically distinguish between different metals by size, charge, hydration status and the metal's affinity for different binding-sites and ligands. It is not unusual that, upon metal binding, the structure of both the protein ligand and the metal ion are slightly altered to accommodate a change in bond angles and lengths (Frausto da Silva and Williams, 2001). The coordination geometry of a metal is also a discerning factor in metal-binding specificity. Each metal ion has preferential coordination geometries within a biological molecule. Cu(II) can be coordinated in a tetragonal or tetrahedral geometry, whereas Cu(I) prefers trigonal, linear or tetrahedral coordination (Crichton and Pierre, 2001). Enzymes binding more than one metal ion species developed different metal sites that are specific for a certain coordination geometry. Copper-zinc containing superoxide dismutase binds zinc in a conformation close to tetrahedral, whereas copper is bound in a distorted tetragonal way. The provision of different binding pockets for different metals ensures the correct insertion of the correct metal. Metal ion specificity can further be established by selective control of oxidation state (ie, the reduction of Cu(II) to Cu(I) by importer associated reductase FRE1 in yeast) and by adjustment of cellular concentrations and availability of both metals and ligands (Frausto da Silva and Williams, 2001).

However, in the past decade it was observed that some proteins have a higher affinity for metal ions other than their proposed biological binding-partner. A model has been established, which describes the order of affinity of organic ligands for divalent cations and the stability of metal-ligand complexes.



The Irving-Williams stability order (as shown above) implies that organic ligands bind to monovalent and divalent copper ions with a higher affinity than to any of the other divalent transition metals in the series (Frausto da Silva and Williams, 2001). Thus it is vital for the assembly of metalloproteins other than copper-binding proteins, that copper is maintained in a protein-bound state at all times to avoid binding and replacement of metal ions essential for particular enzyme function. Elaborate cellular mechanisms have evolved that ensure that copper and other metal ions remain in a protein-bound or ligand-bound state. Trafficking of copper ions is

monitored and facilitated by metal-specific importers that transfer the copper ion to metallochaperones via direct protein-protein interaction. Metallochaperones in turn deliver and at times insert copper directly into target protein again via direct interaction, thus eliminating the possibility of free copper existing anywhere in the cell (Rae et al., 1999). For detailed analysis of cellular copper transport refer to section 1.5.4. The direct protein-protein interaction during metal ion transfer allows for additional specificity, not only governed by chemical properties of the metal ion, but also through physical inhibition or mediation of protein binding and interaction.

Copper is an essential trace element and plays a role in a number of metabolic reactions. A list of copper-dependent enzymes and their functions is outlined in table 1.1 together with a list of copper handling proteins. Copper exists in two oxidation states as mentioned above, thus represent a valuable element in biological reduction and oxidation reactions. However, the cycling between oxidised and reduced state may also contribute to the generation of ROS, leading to chemical alterations of lipid membranes, proteins and DNA molecules as described in section 1.4.2.

1.5.2 Zinc in synaptic transmission

Zinc is a ubiquitous element in all tissues of the human body and it is estimated that as much as 10% of all human genes encode zinc-binding proteins (Andreini et al., 2006). Zinc is used mainly as a structural co-factor (eg. In zinc-fingers) by all groups of enzymes namely hydrolases, ligases, transferases, oxidoreductases, lyases and isomerases, but also as redox-active agent when bound to thiolate ligands (Maret and Vallee, 1998), indicating the importance of maintaining systemic zinc levels.

Zinc involvement in neuronal signaling was first described in 1984 (Howell et al., 1984) with an estimation that 10% of all cerebral zinc is found in pre-synaptic vesicles (Howell and Frederickson, 1990). Pre-synaptic vesicular zinc concentrations were found to be 300-350 μ M (Frederickson et al., 1983), whereas the average zinc concentration across the brain is 100-150 μ M. Further it was demonstrated that in neuronal cells intracellular amounts of zinc are in the pM range, whereas zinc levels in the extracellular fluid of the synaptic cleft can reach

μM concentrations (Bozym et al., 2006), indicating tight active control and transport of the ion. The divalent zinc transporter ZnT-3 is highly expressed in brain regions that contain zinc-containing glutamatergic neurons, where it serves to transport cytosolic zinc into vesicles (Palmiter et al., 1996) and in the clearance of synaptic zinc (zinc transport is reviewed in (Sekler et al., 2007)). Increased calcium-dependent vesicular zinc release was demonstrated following electrical stimulation of hippocampal brain slices (Crichton and Pierre, 2001) or stimulation with high concentrations of K^+ (Assaf and Chung, 1984).

Zinc is co-released with the neurotransmitters glutamate and GABA and acts as a neuromodulator of inhibitory and excitatory amino acid receptor ion channels (Smart et al., 1994). It was hypothesized that another form of zinc signaling is intracellular zinc signaling analogous but distinct in response to that of calcium (Rink and Haase, 2009). Calcium is stored in the sarcoplasmic or smooth endoplasmic reticulum, however no cellular storage for pools of intracellular zinc or mechanism of zinc release have been identified, apart from metallothioneins and possibly synaptic vesicles. A neurotransmitter like signaling process via the synaptic cleft has been observed in which zinc enters postsynaptic dendrites and somata through gated, zinc-permeable channels (Li et al., 2001). Recent studies identified a selective postsynaptic Zn(II)-sensing receptor in the hippocampus, which upon activation, stimulated intracellular calcium release, thus actively participating in transduction of neuronal signaling (Besser et al., 2009).

1.5.3 Copper homeostasis within the body

Copper is used as enzymatic co-factor in a number of biological reactions and pathways. The major mammalian copper-binding proteins are summarized in table 1.1. Absorption of dietary copper mainly occurs in the lumen of the small intestine and is to some extent regulated by systemic copper demands. Most of the absorbed copper is directed towards the liver via portal circulation where it is either incorporated into cytosolic proteins, ceruloplasmin for further transport via the circulatory system or to the bile for excretion.

Two genes involved in systemic and cellular copper transport are the Menkes (Vulpe et al., 1993) and Wilson (Bull et al., 1993) disease genes. Both were first

identified due to abnormal copper phenotypes of either severe copper deficiency or copper overload. Both ATP7A and ATP7B (Menkes and Wilsons disease proteins, respectively) are copper efflux pumps of the P-type ATPase family of cation transporters (Vulpe et al., 1993) and display 70% homology. ATP7A and ATP7B contain eight transmembrane domains and six copper-binding domains with a canonical sequence of GMXCXXC in their intracellular N-terminal domain. These six domains are thought to be involved in receiving copper from cytosolic trafficking molecules and regulating the transport of the ion out of the cell or into organelles such as the TGN, where copper is inserted into secreted proteins. Since both proteins perform the same function yet mutations in either contribute to vastly different systemic copper status, it has been hypothesized that there is a distinct pattern of tissue expression facilitating the secretion from or uptake of copper into the body. Indeed, it was demonstrated by Mercer et. al. (Mercer et al., 2003) that ATP7A is expressed in most tissues with minimal expression in the liver, whereas ATP7B is expressed in small amounts in mammary glands, placenta, ovaries and mainly in the liver (Llanos and Mercer, 2002), thus promoting excretion of excess copper into bile. A schematic representation of systemic copper transport is shown in figure 1.4. It was first reported by Petris et. al. (Petris et al., 1996) and subsequently confirmed by Strausak et. al. (Strausak et al., 1999) that ATP7A and ATP7B undergo copper-induced trafficking to maintain stable cellular copper levels. Deletions or mutations in the metal binding sites closer to the membrane (binding site 5 or 6) result in ATP7A retention in the TGN rather than trafficking to the plasma membrane upon copper supplementation (Strausak et al., 1999). Thus ATP7A is not simply a copper exporter, but also provides some sort of copper sensing mechanism.

1.5.4 Copper homeostasis within the cell

Regulation of cellular copper homeostasis is as important as controlling systemic copper levels. Copper is in a protein-bound or ligand-bound state at all times when trafficked or transferred from one ligand to another to prevent its participation in the generation of ROS or occupation of metal sites intended for other metal ions. To achieve constant copper binding it was shown that copper transfer can occur through sequential creation and elimination of intermolecular bonds between copper

provider and recipient and/or conformational rearrangement of both (Lamb et al., 2001).

Table 1.1: Examples of copper binding and copper homeostasis proteins

Protein	Function
APP	Protein involved in neuronal development and potentially Cu metabolism; cleavage leads to the generation of A β peptide that aggregates in senile plaques associated with AD
ATOX1	Metallochaperone that delivers Cu to ATP7A and ATP7B Cu(I) transporters
ATP7A	Cu(I)-transporting P-type ATPase expressed in all tissues except the liver
ATP7B	Cu(I)-transporting P-type ATPase expressed primarily in the liver
CCS	Metallochaperone that delivers Cu to Cu/Zn SOD
Ceruloplasmin	Serum ferroxidase that functions in Fe(III) loading onto transferrin
COMMD1	Copper metabolism MURR domain1 involved in hepatic copper efflux
COX11	Involved in copper transfer from COX17 to COX1
COX17	Metallochaperone that transfers Cu to Sco1 and Cox11 for cytochrome oxidase Cu loading in mitochondria
CTR1	High-affinity Cu(I) transporter involved in cellular Cu uptake
CTR2	High-affinity Cu(I) transporter involved in endosomal copper transport

Cytochrome c oxidase (CCO)	Terminal enzyme in the mitochondrial respiratory chain; catalyses the reduction of dioxygen to water
DMT1	Divalent metal transporter involved in Cu(II) and Cu(I) import
Dopamine β -hydroxylase (DBH)	Oxygenase; converts dopamine to noradrenaline
Hephaestin	Transmembrane multi-Cu ferroxidase; involved in iron efflux from enterocytes and macrophages
Laccase	Phenol oxidase involved in melanin production
Lysyl oxidase	Catalyses the formation of aldehydes from lysine in collagen and elastin precursors for connective tissue maturation
Metallothionein	Cysteine-rich small-molecular-weight metal-binding and detoxification protein
Peptidylglycine- α -amidating mono-oxygenase (PAM)	Catalyses the conversion of peptidylglycine substrates into α -amidated products; involved in neuropeptide maturation
Prion protein (Prp)	Protein whose function is unclear, but binds Cu via N-terminal octapeptide repeats
SCO1/2	Involved in copper transfer from COX17 to COX2
SOD1	Antioxidant enzyme; catalyses the disproportionation of superoxide to hydrogen peroxide and dioxygen
Tyrosinase	Mono-phenol mono-oxygenase; involved in melanin synthesis
XIAP	X-linked inhibitor of apoptosis involved in hepatic efflux

Adapted from Kim et. al. (Kim et al., 2008) and Prohaska (Prohaska, 2008).

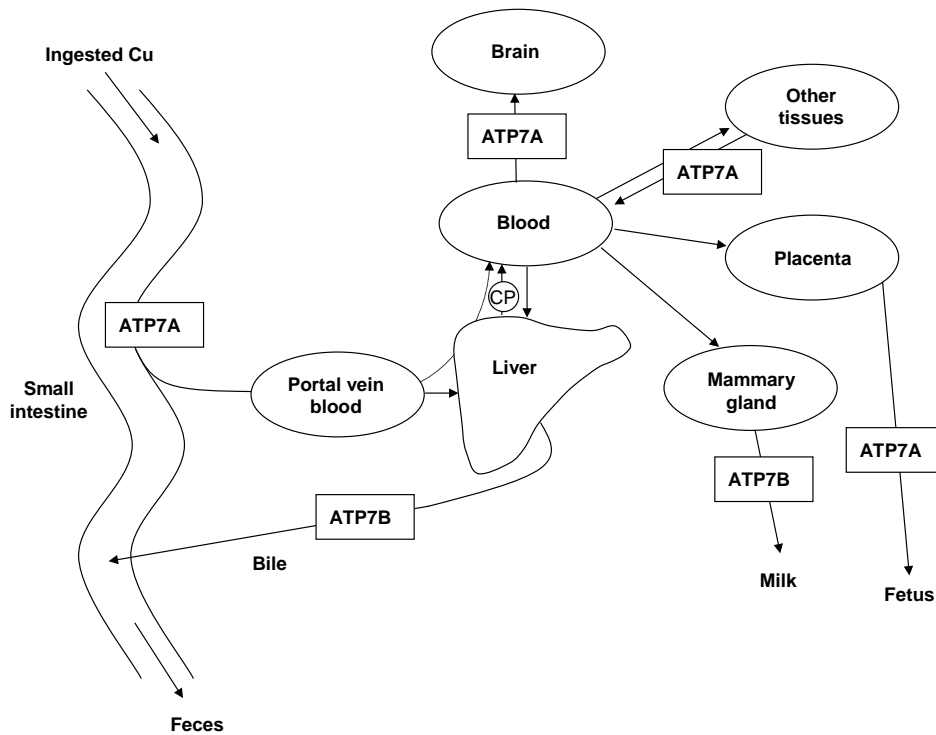


Figure 1.4: Model of systemic copper homeostasis

Copper is absorbed in the small intestine via ATP7A and transported to the liver where it is incorporated into cytosolic enzymes, incorporated into ceruloplasmin (CP) for systemic transport or excreted into bile via ATP7B. Copper is delivered to most tissues and the fetus via ATP7A, whereas copper destined for the placenta and mammary glands is delivered via ATP7B.

Directly taken from Mercer and Llanos (Mercer and Llanos, 2003).

During vascular transport copper is bound to ceruloplasmin, a multi-copper plasma ferroxidase which is essential for mammalian iron homeostasis. The enzyme contains six copper ions in three distinct copper-binding sites, however in the absence or impaired function of ATP7B, holoprotein is released into the blood stream resulting in increased and toxic levels of iron in the brain (Hellman et al., 2002). Copper transfer mechanisms between ceruloplasmin and cellular copper importers have not yet been established.

CTR1 is a highly conserved high-affinity Cu(I) importer containing three transmembrane domains, a methionine-rich N-terminal, a cysteine-histidine cluster in its C-terminal and an MXXXM motif in its second transmembrane domain (Kim et al., 2008). Recent studies provide evidence that CTR1 is present as a homotrimer possibly forming a pore-like structure for copper import between the subunit interfaces (Aller and Unger, 2006). It is not yet known what drives the import of Cu(I) via CTR1 or whether CTR1 is associated to metalloreductases to maintain copper in its reduced state for uptake. However, it has been established that CTR1 expression is not dependent on cellular copper status and experimental evidence suggests that upon elevated levels of copper the importer is trafficked to endosomal compartments in HEK293 cells (Petris et al., 2003). It is suggested by Kim et. al. (Kim et al., 2008) that high and low affinity copper binding sites in the CTR1 transporter or a CTR1 interacting molecule might be directly involved in sensing of extracellular or organellar copper concentrations. A role for CTR1 in copper transport from endosomal compartments to cytosolic copper chaperones was proposed after experiments in CTR1 knockout mice showed elevated levels of copper chaperones and reduced levels in copper-binding enzymes although intracellular copper was hyperaccumulated, thus depleted CTR1 is thought to prevent endosomal copper pools from becoming bioavailable (Nose et al., 2006). Recently a second mechanism of copper sensing by CTR1 via its cytosolic C-terminus was suggested. Wu et. al. (Wu et al., 2009) observed that yeast lacking the entire C-terminus of CTR1 were still functional in high-affinity copper uptake, but also displayed extreme sensitivity to elevated extracellular copper concentrations.

Expression levels or changes in subcellular localization were not observed in the mutant indicating that the C-terminal domain of CTR1 might be involved in trafficking of CTR1 in excess copper and copper sensing.

A copper sensing mechanism for depleted copper levels in yeast includes MAC1, a transcriptional regulator of *ctr1* and *fre1* genes. *Fre1* encodes a plasma membrane reductase which provides reduced Cu(I) ions for uptake via Ctr1. Both molecules are co-expressed and display the same palindromic sequence in the 5'-flanking region of their individual promoters. Copper deprivation is transduced via the MAC1 cysteine-rich domains causing direct and specific binding of MAC1 to *ctr1* and *fre1* promoters resulting in upregulation of gene expression (Yamaguchi-Iwai et al., 1997), whereas elevated copper levels lead to intramolecular interactions in Mac1 preventing transcription activation (Jensen and Winge, 1998). Excessive accumulation of copper in yeast is prevented by ACE1, a transcriptional activator of *cup1* and *crs5* genes, which encode copper metallothioneins and sequester surplus copper from the cytoplasm (Thiele, 1988). A third gene activated by ACE1 is that of Cu/Zn superoxide dismutase (Gralla et al., 1991) which is suggested to play a role in the metal ion buffering capacity of yeast and simultaneously decreases the copper-induced production of ROS (Culotta et al., 1995). Copper-dependent activation is achieved through the formation of a tetracopper-thiolate cluster in the copper regulatory domain of ACE1 (Dameron et al., 1991). Both activation of Ace1 and inactivation of MAC1 by copper is executed in the nucleus, however, transport routes for copper to signal copper excess or deficiency have not yet been established. To date no equivalent copper sensing system has been identified in humans.

Excess neuronal copper is sequestered by metallothionein 3 (MT-3) or GIF for growth inhibitory factor, a mammalian brain specific member of the metallothionein family (Palmiter et al., 1992) which is synthesized in axons and dendrites of zinc-containing neurons of the cortex and hippocampus (Masters et al., 1994). MT-3 is a cysteine-rich 68 amino acid residue peptide with a metal-binding cluster of cysteines at the N- and C-terminal which can accommodate monovalent and divalent metal ions and are linked via a flexible region. MT-3 isolation from human brain revealed a mixture of Cu(I) and Zn(II) (Uchida et al., 1991) bound in

homometallic clusters with a predominant metal ion occupation of M(II)(3)(CysS)(9) and a M(II)(4)(CysS)(11) (Meloni et al., 2009). However, due to detection of MT-3 foremost in zinc-containing neurons it was hypothesised that copper-binding represents displacement of zinc from the clusters (Masters et al., 1994), a theory that could be explained with a higher affinity of ligands for copper than any other metal as stated in the Irving-Williams stability order. MT-3 has also been implicated in clearance of zinc from the synaptic cleft due to its extracellular presence and storage of zinc for transfer into synaptic vesicles intracellularly.

After transfer of Cu(I) into the cell it is directed towards three possible targets by a group of proteins that are evolutionarily conserved and act as copper chaperones (see figure 1.5). First identified in *Saccharomyces cerevisiae* as an antioxidant in the prevention of oxidative stress (Hung et al., 1998), ATX1 was shown to bind Cu(I) with high affinity via two conserved cysteine residues (Pufahl et al., 1997). It is trafficked to the TGN where it supplies proteins destined for excretion with copper by interaction with the transmembrane copper transporter CCC2. The human equivalent to ATX1, human ATX1 homologue 1 (HAH1) or ATOX1 (Klomp et al., 1997), which contains the same conserved cysteine residues (Hung et al., 1998), was observed to interact with the N-terminus of the human equivalent for CCC2, the copper transporting ATPases ATP7A and ATP7B (Larin et al., 1999) (see section 1.5.3).

A second target for cellular copper transport is Cu/Zn superoxide dismutase (SOD1), a soluble enzyme involved in the disproportionation of hydroxyl radicals, thus preventing oxidative damage to the cell. Part of the cellular SOD1 and its chaperone have been localized to the mitochondrial inner membrane space (Sturtz et al., 2001), however the highest concentrations of SOD1 and its chaperone can be found in the cytoplasm. SOD1 receives copper from, and is activated by, its copper chaperone for SOD1 (CCS), a process which is eliminated in *lys7* null mutants of yeast (*lys7* being the gene for yeast CCS) and results in an immature version of SOD1 due to the failure of CCS to incorporate copper into the SOD1 active site (Culotta et al., 1997). Provision of CCS restored SOD1 maturation to form an active holoprotein *in vivo*. CCS consists of three functional domains that are structurally distinct. Domain I is the most N-terminal domain and contains the metal-binding

motif MHCXXC resembling that of the Atx1 metallochaperone. Domain II is highly homologous in amino acid sequence and structural folding to SOD1 and involved in heterodimer formation with its target protein (Casareno et al., 1998), however, it does not contain the functional sites present in SOD1, while domain III, the most

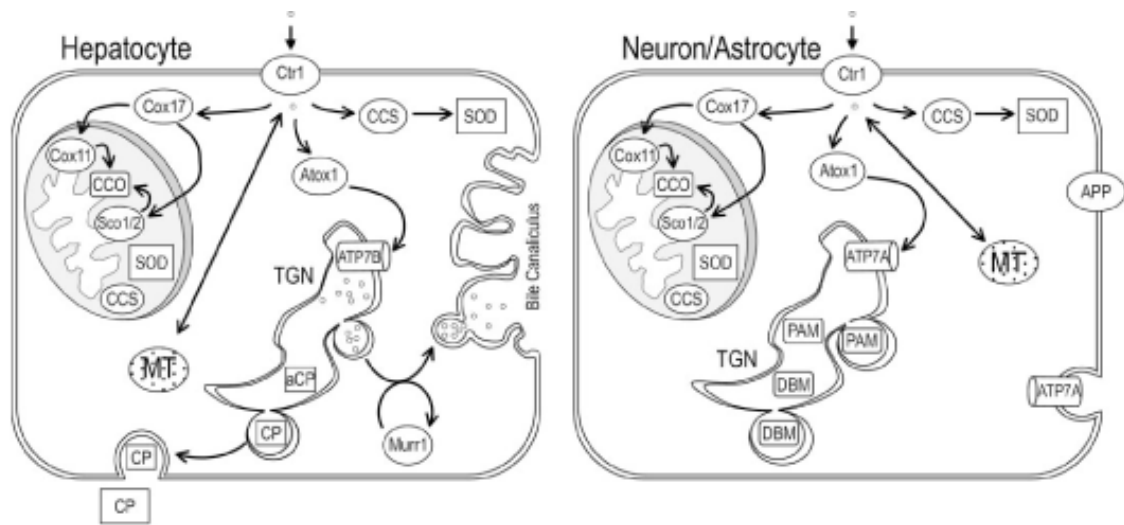


Figure 1.5: Model of cellular copper homeostasis

Copper is imported into the cell via Ctr1 and trafficked towards three cuproenzyme targets (rectangles). Copper chaperones (circles) CCS, ATOX1 and COX17 deliver copper to cytosolic SOD1, TGN ATP7A (neuronal) or TGN ATP7B (hepatic) and CCO, respectively. Excess copper is directed towards metallothionein (MT) for cellular storage. Hepatic TGN copper is inserted into ceruloplasmin or excreted via exocytosis into the bile canaliculus, a process facilitated by COMMD1 (MURR1), whereas neuronal TGN copper is inserted into cupro-enzymes for secretion.

Directly taken from Prohaska and Gybina (Prohaska and Gybina, 2004).

C-terminal of the three domains, contains the metal-binding motif CXC and is vital for CCS function. Upon heterodimer formation structural rearrangement of both proteins is observed with domain III being linked to SOD1 via an intermolecular disulfide bond and in a proximate position to the SOD1 active site to participate in metal ion transfer (Schmidt et al., 1999, Lamb et al., 2001, Rae et al., 2001). It was observed that a pre-existing pool of apo-SOD1 serves as a substrate for CCS in yeast without the need for SOD1 synthesis or protein unfolding (Schmidt et al., 2000).

Although previous experiments demonstrated CCS as a vital factor for SOD1 maturation through copper insertion (Bartnikas and Gitlin, 2003) a second role has been suggested in which CCS deploys an oxygen and disulfide-dependent mechanism of copper transfer. SOD1 contains two cysteine residues on its globular surface, which are not involved in metal-binding in the active site of the enzyme. These cysteine residues are in a reduced state due to SOD1 localisation in the cytosol, which is known for its reducing properties. It is suggested that the copper-loaded form of CCS catalyses SOD1 maturation in four distinct steps. Firstly, the copper-binding motif of CCS domain III interacts with Cys-146 of SOD1 in an oxygen-dependent manner to form a disulfide bridge. This dimerisation process leads to copper transfer from CCS to the active site of SOD1 and the exchange of the intermolecular disulfide to form an intra-molecular disulfide bridge with SOD1 Cys-56 resulting in the release of CCS (Furukawa et al., 2004). It is not clear in which order these two steps occur. Upon intra-molecular disulfide formation SOD1 is more likely to form homodimers which are thought to be the enzymatically active species, whereas reduced and de-metallated SOD1 favors the monomeric state (Arnesano et al., 2004). Thus oxygen-responsive CCS induction of SOD1 maturation might imply a role for CCS in sensing of intracellular oxygen concentrations (Brown et al., 2004).

Contrary to previous findings of CCS being vital for SOD1 maturation, Carroll et al. (Carroll et al., 2004) have demonstrated CCS-independent partial activation and enzymatic function of human SOD1, but not the yeast protein. Glutathione activation of human SOD1 was observed in yeast cells or immortalized fibroblasts indicating differences between the yeast and human enzyme. The dependence of yeast SOD1 for CCS is due to two proline residues near its C-terminal which are missing in the human protein and introduction of which into the human protein renders its activation dependent on CCS. Reconstitution of human SOD1 was observed by Cu(I)-GSH complexes using EPR and optical spectroscopy as well as NMR spectroscopy (Ciriolo et al., 1990).

The third target for copper in the eukaryotic cell is the mitochondrial enzyme cytochrome c oxidase (CCO). The enzyme is located in the inner membrane and functions in the final step of the respiratory electron transfer chain. Copper is required as a co-factor for two individual copper-binding sites. The Cu_A site in subunit COX2 binds three copper ions, whereas the Cu_B site in subunit COX1 binds one. CCO contains thirteen subunits ten of which are encoded by the nuclear genome. The copper-binding subunits however are encoded by the mitochondrial genome indicating copper insertion into CCO within the mitochondrion (Carr and Winge, 2003). The maturation of CCO is complex for three reasons. Firstly for availability of all required subunits, subunit synthesis in two different compartments needs to be synchronized. Secondly the ten nuclear encoded subunits have to be imported into the mitochondrion, a process which involves a multitude of accessory proteins and transporters and needs to bridge two layers of membrane. Finally the assembly of CCO is dependent on a variety of metal co-factors which need to be imported into the mitochondrion. The focus for a role in intracellular copper transport as a metallochaperone to the mitochondrion has been on COX17, since its presence was demonstrated in both the cytosol and the inner-membrane space (Beers et al., 1997). COX17 is a small cysteine-rich protein which binds three Cu(I) ions (Heaton et al., 2000) and when knocked out prevents the formation of a functional CCO complex, a phenotype that is rescued by additions of copper to the growth medium (Glerum et al., 1996a). However, this proposed role was not supported by data showing formation of a functional CCO complex upon tethering of COX17 to the mitochondrial inner membrane (Maxfield et al., 2004). Thus other

mechanisms must exist for the transfer of copper to the mitochondrion. Several accessory proteins have been identified that aid the transfer of copper from COX17 to CCO subunits COX1 and COX2. SCO1 (Nittis et al., 2001) and COX11 (Carr et al., 2002) are Cu(I)-binding membrane-bound proteins and thought to be copper donors to COX2 and COX1, respectively. *In vitro* studies demonstrated COX17 requirement in the metallation of both SCO1 and COX11 (Hornig et al., 2004) and the ability of SCO1 overexpression to compensate for COX17 null mutant phenotypes (Glerum et al., 1996b) emphasizes the intricate interplay of these accessory proteins in the metallation of CCO. The discovery of a large non-proteinaceous low molecular weight copper pool within yeast mitochondrial matrix (Cobine et al., 2004) presents another possible way of metallation of CCO and SOD1 located in the inter-membrane space (Cobine et al., 2006) explaining functional CCO upon COX17 tethering to the mitochondrial inner membrane. In a separate experiment the expression of yeast metallothionein in the mitochondrial matrix attenuated enzyme activities of SOD1 and CCO without decreasing overall mitochondrial copper levels, and possibly resulting in the demetallation of the small matrix ligand, suggesting that the result is demetallation of the small matrix ligand and that copper binding to the low molecular weight ligand is essential for COX17- and CCS-mediated copper transfer within the mitochondria. The factor or chaperone contributing to the mitochondrial copper pool has not yet been identified.

1.5.5 Copper dependent proteins in the brain

1.5.5.1 Superoxide dismutase

SOD1 is localized to the cytoplasm and the mitochondrial intermembrane space (Sturtz et al., 2001) in yeast and mitochondrial matrix in human brain (Vijayvergiya et al., 2005) and is activated by its copper chaperone CCS. Entry to the mitochondria occurs prior to disulfide formation or metallation with zinc and copper (Field et al., 2003). Expression of SOD1 is relatively stable and enzyme activity is considered to be an internal control of SOD1 gene expression (Zelko et al., 2002). SOD1 expression has been shown to be activated by ACE1 in yeast (Gralla et al., 1991) following exposure of cells to copper suggesting a potential role for SOD1 in copper buffering or functional storage. Multiple mutations in SOD1 are associated with forms of familial ALS (Rosen et al., 1993) and aggregation of the protein.

Dysfunction results in increased oxidative damage and accelerated neuronal damage.

1.5.5.2 Cytochrome c oxidase

The multi-component assembly of CCO has been described in section 1.5.4. Since AD is characterised by neurodegeneration likely caused in part by mitochondrial-induced apoptosis attention has been focussed on the mitochondrial respiratory complexes and their potential contribution to neuronal death. Through comparison of CCO activity tested in normal and AD brains a decrease in CCO activity was observed in the latter group. The altered enzyme activity was caused by decreased levels of mRNA of CCO specific subunits 1 and 3 (Chandrasekaran et al., 1994) with subunit 1 representing one of the copper binding sites in the enzyme and altered kinetic properties due to structural changes of the protein (Parker and Parks, 1995). However, there are many more factors that could influence CCO activity, such as alteration in activity or expression of any one of the 13 subunits and numerous accessory proteins that contribute to copper supply and incorporation.

1.5.5.3 Dopamine β -hydroxylase and peptidylglycine α -amidating monooxygenase

Dopamine β -hydroxylase (DBH) is a soluble and membrane-anchored cuproenzyme present in catecholamine releasing vesicles in sympathetic nerves and catalyses the conversion of the neurotransmitter dopamine to noradrenaline. Structural analysis of DBH confirms the presence of two Cu(II) binding sites involved in redox-cycling, thus catalysing the conversion of neurotransmitters (Friedman and Kaufman, 1965). Decreases in enzyme activity, mRNA levels and protein levels were observed in rats deficient in dietary copper (Nelson and Prohaska, 2008) and also in patients with Menkes disease (Kaler et al., 2008).

Peptidylglycine α -amidating monooxygenase (PAM) is an oxidoreductase localised in the secretory pathway which catalyses the α -amidation of glycine extended

peptide precursors, a process essential for the bioactivation of several hormones and neuropeptides (Kulathila et al., 1999). Amidation is a two step reaction performed by the two separate catalytic subunits peptidylglycine alpha-hydroxylating monooxygenase (PHM) and peptidyl-alpha-hydroxyglycine alpha-amidating lyase (PAL). The PHM subunit is a copper-binding domain containing two distinct copper binding sites both of which are essential for enzyme activity (Kolhekar et al., 1997) and requires molecular oxygen and ascorbate as co-factors. As with DBH, dietary or hereditary copper deficiency could potentially result in decreased enzyme activity.

1.5.6 Disorders of copper imbalance

1.5.6.1 Menkes disease

Menkes disease is an X-linked genetic condition caused by mutations in a gene, encoding a highly conserved copper-transporting ATPase (ATP7A). The protein functions in intestinal copper import as well as systemic and cellular distribution of the metal (Danks et al., 1972), a function, which has partly been established due to low serum copper and ceruloplasmin levels in patients carrying mutations. The incidence of Menkes disease is 1 per 298,000 live-born babies (Tønnesen et al., 1991) and development of symptoms occurs within the first few months of life often resulting in death at the age of three. Clinical symptoms include characteristic white kinky hair, hypothermia, seizures, hypo-pigmented skin and focal cerebral and cerebellar degeneration (Danks et al., 1972). Some of the symptoms are indicative for copper deficiency in essential copper-binding enzymes such as PAM, DBH, CCO or tyrosinase. Treatments include copper injections to bypass unresponsive intestinal uptake, however although low hepatic copper stores are replenished quickly, brain copper levels only gradually recover (Danks et al., 1972).

1.5.6.2 Wilson's disease

Wilson's disease is a rare autosomal recessive genetic disorder and characterized by excess hepatic copper accumulation. The mutated gene encodes the highly conserved copper-transporting ATPase (ATP7B), which functions in copper excretion into bile and copper loading into ceruloplasmin with localisation in the liver, placenta and kidneys. Clinical symptoms usually develop between the ages of 6 and 20 years and include chronic hepatitis, tremor, seizures, insomnia,

parkinsonism and signs of depression and psychosis. The disease affects 1 in 100,000 individuals and if detected early can be treated with chelating agents such as dimercaprol or penicillamine and zinc salts to prevent intestinal copper uptake. However, damages incurred to liver and brain are not reversible, thus early detection is essential to prevent liver cirrhosis and mental retardation. In extreme cases treatment includes liver transplants (Aftab et al., 2007).

1.5.6.3 Neurological disorders

Neurological disorders that have been implicated in perturbed metal homeostasis include Parkinson's disease (Wang et al., 2010), Prion disease or Creutzfeldt Jakob disease (Thompsett et al., 2005, Jobling et al., 2001), familial amyotrophic lateral sclerosis (FALS) (Furukawa and O'Halloran, 2005) and AD. All of these disorders display abnormal levels of protein unfolding and/or aggregation in response to increased or decreased metal availability leading to intracellular or extracellular deposits. The metals involved, the toxic protein species and aggregation form are summarized in table 1.2.

1.6 Metals and APP

AD has been described as a disease of perturbed metal regulation and homeostasis. In particular copper, iron and zinc have been implicated in the disease progression and development of detectable symptoms. In the scope of this project special attention is paid to changes in copper homeostasis due to a familial mutation in the APP protein and downstream effects on cellular characteristics and phenotypes. In the following sections the biological link of APP and its cleavage product with copper and potential consequences for copper misregulation with regards to neurodegenerative diseases will be discussed.

1.6.1 Metal-binding properties of amyloid precursor protein and amyloid beta

APP has a zinc-binding and two copper-binding domains, one of which is located next to the N-terminal growth factor like domain; the second one is located within the amyloid beta sequence (see figure 1.1). Processing of APP is positively influenced by dimerisation and increases A β production 6-8 fold (Scheuermann et al., 2001). However, Cu(II) binding to the N-terminal domain is readily reduced to

Cu(I) (White et al., 1999a) and has been proven to reduce A β levels probably due to copper-mediated disruption of APP dimerisation (Kong et al., 2008). No significant conformational changes in APP have been observed upon Cu(II)-binding (Kong et al., 2008), thus this copper-binding site might have a lower affinity for copper than the copper-binding site found within the A β sequence and potentially present a candidate binding-site involved in protein-protein copper transfer. Structural homology of APP to copper chaperones and the location of the copper-binding site on the protein surface support this hypothesis (Barnham et al., 2003b).

Recent research demonstrates a new possible role for APP as iron export ferroxidase. It has been shown by Duce et al. (Duce et al., 2010) that this activity lies within a conserved H-ferritin-like active site, which leaves APP to catalytically oxidize Fe(II) and is inhibited by Zn(II). Upon APP ablation in primary neurons and HEK293T cell lines iron retention was observed and mice carrying the APP null mutation showed increased sensitivity to dietary iron. Further analysis of the expression levels of APP and the iron-storage protein ferritin in high cellular copper levels support a possible role for APP as an iron exporter.

A β is a peptide with high affinity for Cu(II), Fe(III) and Zn(II). The Cu(II) binding site displays attomolar affinity and was found to be stronger in A β ₁₋₄₂ than A β ₁₋₄₀ (Atwood et al., 2000). Coordination of metallated A β into fibrils and plaques is induced by synaptically available Zn(II) at concentrations of 300nM, which are exceeded upon release of synaptic vesicles by 1000 fold (Bush et al., 1994). Lovell et al. (Lovell et al., 1999) demonstrated neuroprotective properties of zinc-mediated amyloid aggregation that were mainly due to enhancement of Na⁺/K⁺ ATPase activity which prevents the disruption of calcium homeostasis and cell death in cultured, primary hippocampal neurons. However, excess zinc and copper concentrations facilitate plaque formation conferring a metalloenzyme-like activity to A β (Opazo et al., 2002) and increasing catalytic oxidation of cholesterol and lipids to form H₂O₂. Concentrated ROS production might overwhelm the local antioxidant defence system and enhance neurodegenerative pathology. Amyloid formation can be reversed by application of chelators to the brains of post-mortem patients (Cherny et al., 1999) and amyloid accumulation is markedly inhibited by

treatment with copper and zinc chelators in AD transgenic mice (Cherny et al., 2001).

Table 1.2: Neurodegenerative diseases and the respective metals involved in protein aggregation

Disease	Protein deposit	Toxic protein	Metal
Alzheimer's disease	Extracellular A β plaques and intracellular neurofibrillary tangles	A β / Hyper-phosphorylated tau, possibly Prp ^c	Cu, Zn, Fe
Creutzfeldt-Jakob disease/Prion disease	Prion plaques	Prp ^c	Mn
Familial ALS	Bunina bodies	SOD1	Cu, loss of Zn
Parkinson's disease	Lewy bodies	A-synuclein	Cu, Fe

Adapted from Bush (Bush, 2003).

1.6.2 The proposed role for APP in copper homeostasis

A role for APP in neuronal copper homeostasis either as a regulator or efflux protein or mediator of such has been suggested (Maynard et al., 2002, Bush et al., 2003). Both A β and APP have high-affinity Cu(II) binding sites which readily promote the reduction to Cu(I) (Multhaup et al., 1996). It has been suggested that A β might be involved in extracellular copper scavenging activities and clearance of excess metal during normal physiology thus reducing the risk of copper-related neurotoxicity and that AD is an apparent phenotype of clearance corruption (Bush, 2003). Analysis of human CSF demonstrated promotion of soluble A β degradation under physiological copper and zinc concentrations, whereas excess zinc and copper induce A β precipitation (Strozyk et al., 2009) contributing to amyloidosis and increased oxidative neurotoxicity.

Overexpression of APP opposes the age-dependent elevation in brain copper thus AD might develop due to increased clearance of copper from brains containing versions of APP FAD mutations promoting functional defects in mitochondrial CCO and antioxidant enzymes due to a functional copper deficiency. The role as a possible efflux mechanism for copper is supported by findings that copper levels are increased in the cerebral cortex and liver of APP and APLP2 knockout mice (White et al., 1999b) and embryonic fibroblasts (Bellingham et al., 2004a). It was also shown that expression of an APP mutation that abolishes copper binding increased intracellular copper concentrations several fold supporting the role of APP as a potential copper exporter (Treiber et al., 2004) especially since the APP copper binding site shows structural homology to copper chaperones and is located at the surface of the protein (Barnham et al., 2003b). Borchardt et. al. (Borchardt et al.,

1999) discovered a dose-dependent window of opportunity in which particular copper concentrations promote non-amyloidogenic processing of APP, whereas higher concentrations, as are detected in the ageing brain, promote A β production. However, opposing analyses of APP function in copper homeostasis identified decreased levels of A β in the CSF of AD-patients (Van Nostrand et al., 1992), increased concentrations of copper, zinc and iron in AD brain (Lovell et al., 1998) and elevated copper content in APP overexpressing HEK293 cells indicating that a possible mechanism of increased APP cleavage might restore intracellular copper levels and reverse functional copper deficiency of CCO, antioxidants and other copper-binding enzymes (Suazo et al., 2009). This finding was supported by observations that intracellular copper deficiency increases A β secretion (Cater et al., 2008) and the occurrence of increased A β and copper complexation with lipid rafts upon cellular copper deficiency (Hung et al., 2009), a mechanism which opposed the suggested role of APP in facilitating efflux of excess copper.

Due to conflicting results of APP overexpressing models with regards to copper distribution and the lack of understanding concerning whether a lack of functional copper or excess copper induces neurotoxicity and pathological phenotypes, no definite statement can be made about the exact role of APP in copper homeostasis. APP clearly is involved in copper metabolism, however whether it plays a regulatory role or functions as a transporter or chaperone remains to be determined.

1.7 Experimental design and challenges for the study of metalloproteins

1.7.1 Metalloproteomics

Bioinformatic approaches to determine metal-binding sites in proteins based on amino acid sequence and folding predictions present a challenge since metal-coordination is not only governed by the individual amino acid residues that coordinate the metal ion (first coordination sphere), but also, among others, by residues adjacent to ligand amino acids which contribute to specific binding geometries (so called second coordination spheres), extra ligands such as water, and post-translational modifications of the protein. Metal-occupancy can only be established with confidence experimentally.

A variety of experiments have been designed to identify metalloproteins and to determine the specificity of the metal bound by proteins. Experiments differ in their approach by focussing on the protein or the metal during purification.

Attempts have been made to identify metalloproteins in *Pyrococcus furiosus* using two levels of chromatography with subsequent analysis of the fractions for metal content by ICP-MS and protein content by high-throughput tandem mass spectrometry. Data obtained was analysed using bioinformatics databases to assign metalloproteins to peptide fragments (Cvetkovic et al., 2010). Remarkably more than half of the identified proteins were not predicted through bioinformatics emphasizing the view that metalloproteomes are largely uncharacterised.

Another study focused on metal-based determination of metalloproteins by targeted labeling of particular trace elements with suitable radioisotopes and native separation of holoproteins by isoelectric focusing combined with blue native acrylamide gel electrophoresis during which the G250 stain binds to and visualizes proteins without denaturation and demetallation. Radiolabelled isotopes in the gel were subsequently visualized using autoradiography and proteins identified by tandem mass spectrometry (Sevcenco et al., 2009).

Ferrer et. al. (Ferrer et al., 2007) performed two-dimensional non-denaturing PAGE followed by visualization of metalloproteins in the gel by treatment with the chemiluminescent substrate luminal. Candidate proteins were subjected to sequential quadrupole TOF-MS and high resolution ICP-MS with a result of over 85% of all identified metalloproteins binding iron in *Ferroplasma acidiphilum*. In contrast to the method described previously this experimental design allows for quantification of the total metalloprotein content of the proteome.

A fourth approach was tested by members of this research group (Kevin Waldron unpublished data) and comprised of comparative diagonal two-dimensional native gel electrophoresis. Proteins were separated by native PAGE in two dimensions in duplicate resulting in diagonal alignment with one set of proteins being subjected to a native gel containing a metal-specific chelator. Direct comparison of both gels allowed detection of demetallated proteins due to differences in separation and resolution away from the diagonal. Proteins of interest were analysed by MALDI-

TOF-mass spectrometry. The reverse experiment in which metal is added to the PAGE gel before second dimension separation is performed.

1.7.2 Limitations of various biochemical approaches

One constant risk during metalloprotein-based experiments is exposure to reducing agents such as DTT or SDS and sample exposure to oxygen. Contact can result in metal dissociation from the protein due to disulfide formation of cysteine ligands or metal oxidation. Thus it is useful to limit purification and analysis steps to a minimum.

A further obstacle is the ubiquitous presence of trace metals in experimental solutions and disposables, which could potentially result in flawed data and misinterpretation of metals and their concentrations actually present in a sample. This is particularly true for metal analysis in PAGE samples, with regards to polyacrylamide itself containing a variety of metals which could potentially displace the original metal in a sample protein or bind to a non-metal-binding protein containing suitable ligands.

To identify proteins by mass spectrometry it is often necessary to purify the particular protein through many handling steps, which could potentially result in metal oxidation and altered migratory properties of the protein.

Immobilised metal affinity chromatography (IMAC), usually used for the purification of His-tagged proteins, is occasionally used to purify metal-binding proteins, which bind to the column and can be eluted with high concentrations of histidine. However this approach has the potential to bind all sample proteins that contain a gratuitous metal-binding site.

1.7.3 A low resolution native 2D-LC approach coupled to denaturing separation of proteins and Principal Component Analysis

A metal-based approach for routine identification of metal binding proteins has been established within this research group (<http://www.natureprotocols.com/2008/11/12/metalloprotein.php>). Low resolution of metalloproteins in soluble protein extracts is achieved by native 2D-LC using anion exchange as first and size exclusion as second dimension and subsequent

analysis of the obtained samples for metal content by ICP-MS to identify the major metalloprotein pools. Fractions containing large amounts of metal are resolved by SDS-PAGE and amounts of protein measured by densitometric analysis. Principal component analysis, PCA, (as described in section 2.4.10.2) is employed to compare the change of abundance of each individual protein with the change in abundance of metal and allows for the selection of a candidate protein which is identified by MALDI-TOF-MS. This method is specifically developed to identify major metalloproteins and their abundance or metal-binding properties in response to environmental stimuli and genetic manipulation. The protocol can be refined by altering anion exchange and size exclusion chromatographic conditions to adjust protein separation and aid PCA analysis, but crucially enables protein identification without the need for vigorous purification through many steps.

1.8 This study

1.8.1 Hypothesis

1. It is hypothesized that APP or its cleavage products make an unspecified contribution to copper homeostasis.
2. Interactions of human CCS with the neuronal adaptor protein X11 α via domain III (McLoughlin et al., 2001) and with BACE1 via domain I (Angeletti et al., 2005) have been demonstrated as well as interactions of X11 α with APP (McLoughlin and Miller, 1996). Together with the findings that BACE1 contains a high affinity Cu(I) binding site in its cytosolic domain (Angeletti et al., 2005) these observations open up the possibility of physiological or pathological copper supply via CCS to proteins other than SOD1. Alternatively CCS could mediate physiological or aberrant BACE1 interactions. Although, direct copper transfer from CCS has only been demonstrated for SOD1 (Rae et al., 2001), the co-localisation of CCS, BACE1 and APP by X11 α may play a significant role in a potentially copper-regulated way of determining APP processing fate and the development of AD. This model would, in addition to possible copper transfer from CCS to APP or BACE1, involve the redirection of copper from the original target protein SOD1 potentially contributing to AD pathology by decreasing the levels of enzymatically active antioxidant. This could potentially result in more pronounced phenotypes related to oxidative stress in

APP_{swe} carriers with a predicted 6-8 fold increase in APP cleavage and A β production (Citron et al., 1992). The hypothesis is outlined in a simplified way in figure 1.6.

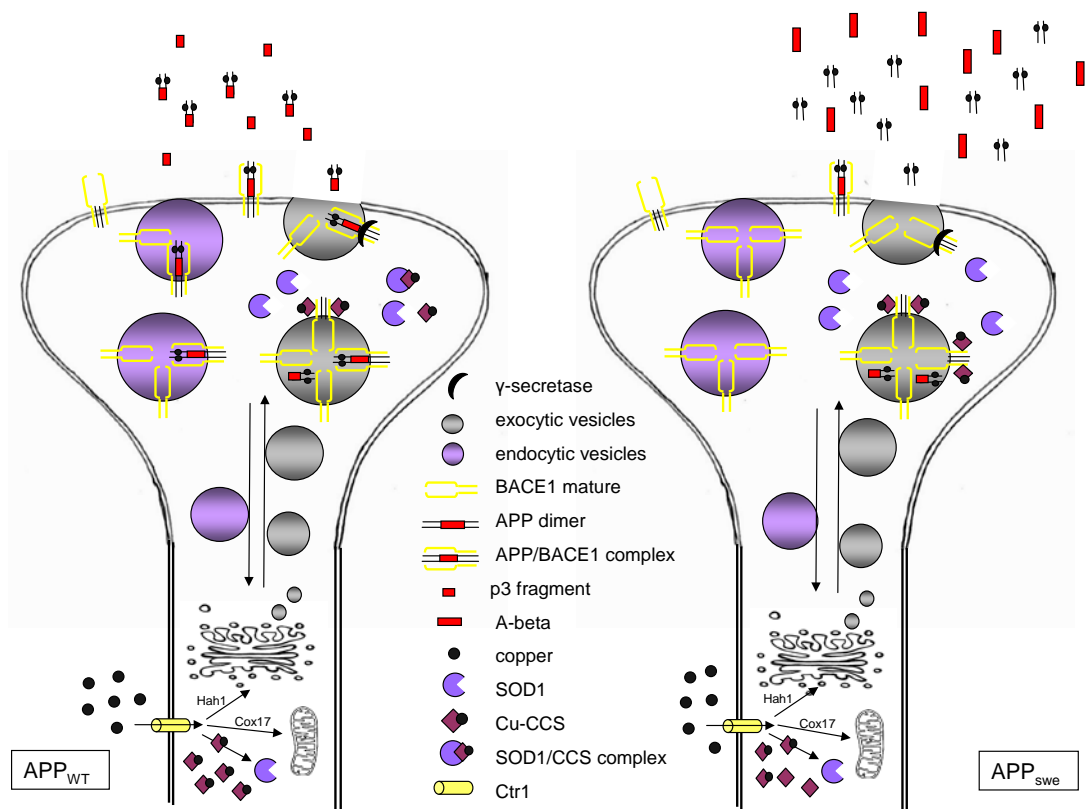
1.8.2 Aims

The aims of this project were three-fold:

1. Identification of major metal-binding pools (especially for copper) in whole cell protein extracts by low resolution chromatography as described in section 1.7.3 in conjunction with statistical analysis by principal component analysis has only been performed in prokaryotic organisms. The method was tested on a variety of eukaryotic organisms.
2. Attempts were made to determine and identify major metal pools (especially for copper) in the *SH-SY5Y* neuroblastoma wild type (APP_{WT}) cell line and a *SH-SY5Y* cell line overexpressing the Swedish mutation in APP (APP_{swe}).
3. Any contribution of APP to neuronal copper homeostasis was explored by assaying a range of copper-related phenotypes in neuronal cells overexpressing APP_{swe} and subsequent comparison with the control APP_{WT} cell line.

Figure 1.6: Hypothesis of alteration in copper homeostasis by the Swedish mutation and its implication in APP processing and antioxidants status in *SH-SY5Y* cells

Copper is imported into the cell by CTR1 and distributed to three distinct pathways. Copper is bound by the copper chaperone for superoxide dismutase (CCS) for metal delivery to SOD1, to COX17 for insertion into mitochondrial cytochrome c oxidase and to HAH1 for incorporation into proteins in the Golgi and exocytosis. Upon trafficking to the cell surface APP is cleaved either by α -secretase (APP_{WT}) or β -secretase (APP_{swe}). It was shown by McLoughlin et. al. (McLoughlin et al., 2001) that CCS binds BACE1 through the adapter protein X11- α . Citron et. al. (Citron et al., 1992) demonstrated that the Swedish mutation causes a 6-8 fold increase in APP cleavage by BACE1. It is thus hypothesised that the ability of CCS to deliver copper to SOD1 and BACE1, or at least interact with both proteins might lead to aberrant copper homeostasis in cells containing the Swedish mutation. This could impact not only on plaque formation and oxidative stress, but also cause an intracellular copper deficit which might manifest itself in the decline of copper specific metalloenzymes such as SOD1, cytochrome oxidase and dopamine-beta-hydroxylase, important for neuronal conductivity. It is noted that there is a continuous base level of α -secretase cleavage in the APP_{swe} cell line and a low level cleavage by β -secretase in APP_{WT} .



Chapter 2 - Materials and methods

2.1 Equipment, chemicals and reagents

All chemicals were purchased from Sigma (Haverhill, UK) unless otherwise stated. All enzymes used for nucleic acid manipulation were purchased from Promega (Southampton, UK) unless otherwise stated.

For trace metal work, all glassware was washed in 4% (v/v) HNO₃ over night to remove traces of residual metal. Glassware was then rinsed with nano-pure water (Millipore Simplicity 185 Filtration System) and used immediately.

Cell culture solutions were purchased from PAA (DMEM, D-PBS, Somerset, UK), Invitrogen (Glutamine, Penicillin/Streptomycin, foetal calf serum, TrypLE Express, Glasgow, UK) and Autogene Bioclear (foetal calf serum, Nottingham, UK).

All plastic consumables were purchased sterile, flasks from TPP (Helena Biosciences, Sunderland, UK) and centrifuge tubes and pipettes from Starlab (Milton Keynes, UK). Non sterile equipment and solutions were autoclaved at 121°C for 20 minutes.

2.2 Strains, cell lines and plasmids used

2.2.1 *Saccharomyces cerevisiae* strain and maintenance

The haploid budding yeast strain *Saccharomyces cerevisiae* W 303 1a was grown in liquid Yeast Peptone Dextrose (YPD) medium (10g/L yeast extract, 20g/L peptone, 20g/L glucose). Cultures were grown at 30°C while agitated. Culture medium was sterilized by autoclaving at 121°C for 20 minutes before inoculation.

2.2.2 *SH-SY5Y* APP_{WT} and APP_{swe} mutation

The original neuroblastoma cell line *SK-N-SH* was created by bone marrow biopsy of a female patient in 1975 (Helson et al., 1975), however, the genetically female and thrice sub-cloned neuroblastoma cell line *SH-SY5Y* was chosen as model cell line for my studies. The wild type *SH-SY5Y* cell line expressing endogenous levels of APP (designated APP_{WT}) and the APP Swedish mutation (APP 695aa) overexpressing *SH-SY5Y* cell line (designated APP_{swe}) were used for experiments (see table 2.1). Mutant cell lines were previously produced by transfection of the high-expression mammalian transfection vector pcDNA3.1 carrying the Swedish APP mutation gene. The structure of the vector is shown in figure 2.1.

2.2.3 Cell culture of *SH-SY5Y*

2.2.3.1 Maintenance

SH-SY5Y cells were cultured as monolayers in Dulbecco's Modified Eagle Medium (DMEM) containing 1.5g/L sodium bicarbonate, 1 mM sodium pyruvate, 0.1 mM nonessential amino acids and supplemented with 10% (v/v) foetal calf serum (FCS), 2mM L-glutamine, 100units/ml Penicillin and 100µg/ml Streptomycin. The cultures were incubated at 37°C in a humidified 5% (v/v) CO₂ atmosphere. Cryo-stocks were produced by resuspension of confluent cells in FCS containing 10% (v/v) DMSO and gradual freezing of 1ml aliquots for cryo-storage in isopropanol.

2.2.3.2 Harvest

Culture medium was aspirated and the monolayer thoroughly washed with D-PBS (without Ca, Mg) before being dissociated from the cell culture flask using the trypsin equivalent TrypLE Express. The flask was then rocked to ensure the coverage of the whole monolayer with TrypLE Express and incubated at 37°C for 2 minutes. Subsequently cells were resuspended in D-PBS and pelleted at 800 rpm for 5 minutes. The pellet was aspirated and either used immediately or stored at -20°C.

The maximum dilution rate used for passaging cells was 1:7. Cells were not used beyond their 30th passage.

2.2.4 Cell culture of *HepG2*

2.2.4.1 Maintenance

HepG2 cells were cultured as monolayers in Roswell Park Memorial Institute medium (RPMI 1640) supplemented with 10% (v/v) foetal calf serum (FCS), 2mM L-glutamine, 100units/ml Penicillin and 100µg/ml Streptomycin. The cultures were incubated at 37°C in a humidified 5% (v/v) CO₂ atmosphere. Cryo-stocks were produced by resuspension of confluent cells in FCS containing 10% (v/v) DMSO and gradual freezing of 1ml aliquots for cryo-storage in isopropanol.

Strain	Description	Expression	Source
<i>SH-SY5Y</i> APP _{WT}	Subclone of <i>SK-N-SH</i> cell line and can be obtained from the ATCC/DSMZ	N/A	David Howlett at GSK
<i>SH-SY5Y</i> APP _{swe}	Cell line transfected with 695 aa APP _{swe} gene using the pcDNA3.1 mammalian transfection vector	stable	David Howlett at GSK

Table 2.1: *SH-SY5Y* cell lines used in experiments

Both cell lines were obtained from GSK. *SH-SY5Y* APP_{WT} represents the experimental control with base level expression of endogenous APP. The *SH-SY5Y* APP_{swe} cell line was established by lipofection of the APP gene carrying the Swedish mutation linked to familial AD into the control cell line using the high-expression mammalian transfection vector pcDNA3.1 (figure 2.1). For future analysis of experimental data it should be noted that the APP_{swe} cell line represents

phenotypes as a function of overexpressing the Swedish mutation in *SH-SY5Y*, not as a function of the Swedish mutation per se.

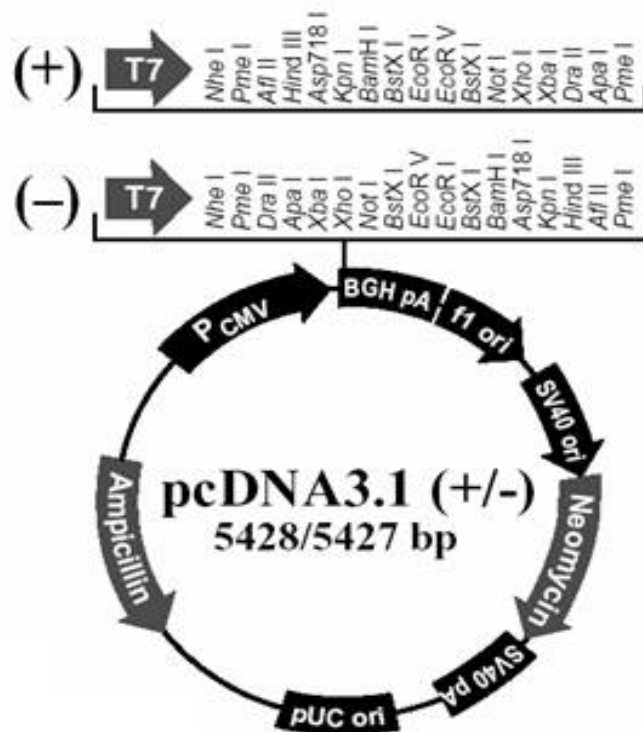


Figure 2.1: Schematic representation of the mammalian transfection vector pcDNA3.1

The high-expression plasmid was utilised as an expression vector for the APP_{swe} mutation gene. The plasmid contains the neomycin resistance gene for mammalian cell selection using geneticin (G418) and the ampicillin resistance gene for selection in *E.coli*. The inserted APP gene is regulated by the CMV promoter giving constitutive high expression.

Directly taken from the Invitrogen vector catalogue ([http://www.liv.ac.uk/physiology/ncs/catalogue/Cloning/pcDNA3.1\(-\).htm](http://www.liv.ac.uk/physiology/ncs/catalogue/Cloning/pcDNA3.1(-).htm)).

2.2.4.2 Harvest

Culture medium was aspirated and the monolayer thoroughly washed with D-PBS (without Ca, Mg) before being dissociated from the cell culture flask using the trypsin equivalent TrypLE Express. The flask was then rocked to ensure the coverage of the whole monolayer with TrypLE Express and incubated at 37°C for 2 minutes. Subsequently cells were resuspended in D-PBS and pelleted at 800 rpm for 5 minutes. The pellet was aspirated and either used immediately or stored at -20°C. The maximum dilution rate used for passaging cells was 1:7. Cells were not used beyond their 30th passage.

2.3 Genetic Techniques

2.3.1 Reverse Transcription Polymerase Chain Reaction (RT-PCR)

2.3.1.1 RNA extraction from whole cells

All solutions used in this procedure were produced in DEPC-treated water, which was prepared by supplementing ddH₂O with DEPC (0.1% v/v), incubation at 37°C for at least 12 hours and subsequent autoclaving at 121°C for 20 minutes. Gloves,

centrifugation tubes, pipettes and benches were treated with RNase AWAY (Molecular BioProducts Inc., San Diego, CA, USA).

Cell pellets were defrosted, resuspended in 10 volumes of pre-warmed RNA lysis buffer (50mM Tris-Cl, pH 8.0, 100mM NaCl, 20mM EDTA, pH 8.0, 2% (w/v) SDS, 60mM β -mercaptoethanol, 10 μ g/ml proteinase K) and incubated at 37°C for 30 minutes. A 5x phenol extraction was performed by adding an equal volume of 5:1 phenol:lysis buffer to the sample, which was then centrifuged at 4,000rpm for 10 minutes using a Beckman J6-HC centrifuge. The aqueous top layer was collected into a new tube, an equal volume of 1:1:1 phenol:chloroform:lysis buffer added and the centrifugation step repeated. The aqueous top layer was collected into corex ultracentrifuge tubes and adjusted to 0.5M ammonium acetate using a 10M stock. RNA was subsequently precipitated by adding 2.5 volumes of 100% ethanol (-20°C) and sample incubation at -20°C for 2 hours or at -80°C over night. Following the incubation the nucleic acid was pelleted by ultracentrifugation at 12,000 rpm (Sorvall RC-5B centrifuge) for 30 minutes at 4°C. The supernatant was discarded, the pellet resuspended in a small volume (2ml) of 70% (v/v) ethanol and the centrifugation step repeated. The pellet was then allowed to air-dry over night and resuspended in 50 μ l DEPC-treated water. The sample was either used immediately or snap-frozen and stored at -20°C. The amount of RNA per sample was estimated using a NanoDrop ND-1000 Spectrophotometer (Labtech, East Sussex, UK) according to manufacturer's instructions.

2.3.1.2 cDNA synthesis

2.3.1.2.1 DNaseI treatment of RNA

DNaseI treatment of all RNA samples was performed to prevent genomic DNA amplification at later stages of the experiment. Fresh reaction tubes were prepared containing 5 μ g of RNA (or less depending on RNA concentration of each individual sample), 10 μ l of DNaseI reaction buffer and 4 μ l (8 units) DNaseI. The sample volume was adjusted to 100 μ l using DEPC-treated water and the sample incubated at 37°C for 3 hours. The reaction was stopped by adjusting the sample to 5mM EDTA using a 50mM EDTA, pH 8.0 stock. The sample was subsequently incubated at 70°C for 10 minutes and used immediately or snap-frozen and stored at -20°C.

2.3.1.2.2 RNA and primer denaturation

For further analysis two samples were prepared for each strain and condition providing a reaction with and without reverse transcriptase, the latter serving as a control. Figures in the appendix section indicate the exact amounts of RNA and cDNA used for each experiment as this may vary and adjustments need to be made. In general samples are prepared containing 1µg RNA template, 1µl Oligo(dT)₁₅ primers from the Im-PromII reverse transcription kit (Promega) and are made up to a total volume of 20 or 30µl depending on RNA concentration. A negative control was set up containing no RNA template. Samples were incubated at 70°C for 5 minutes, cooled on ice for at least 5 minutes and briefly centrifuged before the RT reaction.

2.3.1.2.3 Reverse transcription

For the reverse transcription reaction a master mix of solutions as indicated in table 2.2 has been prepared before samples were supplemented with 15µl of the appropriate mix (with or without RT) to ensure better comparability between the samples. Reaction temperatures were as follows: Primer annealing at 25°C for 5 minutes, primer extension at 42°C for 60 minutes and inactivation at 70°C for 15 minutes.

2.3.1.3 Polymerase Chain Reaction (PCR)

The PCR reactions were produced in a total volume of 100µl per sample. Depending on the effectiveness of reverse transcription, cDNA concentration and band visibility on a gel, the volume of cDNA is adjusted for each reaction as described in the individual figures. In general the volumes of the reaction mix are outlined in table 2.3 and the primers used can be found in table 2.4. The protocol for the reaction is as follows: sample denaturation at 95°C for 5 minutes, 30 cycles of 95°C for 1 minute (denature), 65°C for 1 minute (anneal) and 72°C for 20 seconds (extend). The reaction was finished by a 5 minute extension at 72°C and a sample hold at 4°C. The cycle number and annealing temperature can vary between primers and will be specified in each figure legend.

2.3.1.4 DNA separation by agarose gel electrophoresis

A 2% (w/v) gel was produced by microwaving analytical grade agarose (Promega) in 60ml 1x TBE buffer (45mM Tris-borate, 2mM EDTA), cooling and addition of 5µl of 10mg/ml ethidium bromide solution. The gel was cast by pouring the mix into a BioRad Mini-Sub Cell GT gel apparatus and left to set. The gel was then immersed in 1x TBE buffer and 30µl of sample loaded into each well. Sigma 100kb DNA ladder was used as size standards and the gel run at 100V. Gels were visualised under UV light and photographed using BioRad Quantity One Software.

2.4 Molecular biology techniques

2.4.1 Copper and BCS supplementation

Cells were grown to near confluence, supplemented with increasing concentrations of copper (0µM, 50µM, 150µM, 300µM, 500µM) and incubated for another 24 hours. Copper stocks were tested for copper concentration every two weeks by ICP-MS and stock volumes added to the culture media adjusted accordingly.

Chelator supplemented cells were grown in BCS supplemented DMEM (0µM, 5µM, 10µM, 20µM, 25µM, 50µM, 100µM) for 3 passages with the fourth generation being used for subsequent experiments. All solutions used for passaging were supplemented with the appropriate amount of BCS to avoid introduction of copper during the cell passaging procedure.

2.4.1.1 Modified method for copper supplementation

To have a direct comparison between copper and BCS treated cells (copper treated cells did not undergo as many passages), a batch of each *SH-SY5Y* APP_{WT} and APP_{swe} cells was grown as previously described for BCS supplementation. In brief, both cell lines were grown in copper containing media, passaged three times and the 4th generation was then grown to confluence and used for further experiments. In contrast to the BCS supplementation procedure, all solutions used to split copper treated cells, were not supplemented with the transition metal. It was observed that copper in D-PBS and trypsin would pellet upon centrifugation and accumulatively throughout three passages would increase the copper concentration in the individual samples by three fold.

2.4.2 Estimation of protein concentration and standardisation

2.4.2.1 Membranous protein

Membrane protein concentrations were estimated using the BCA protein assay reagent kit (reagent A and B) provided by Thermo Scientific, Illinois, USA. Reagent A was mixed with reagent B in a ratio of 50:1 and 200 μ l were added to 20 μ l sample or standard in a 96-well plate. The plate was incubated at 37°C for 30 minutes and absorbance was measured on a Thermo Labsystems Multiscan Ascent plate reader at a wavelength of 560nm. Standards were prepared from 2mg/ml BSA stock solution (Pierce, Illinois, USA) and ranged from 20 μ g/ml up to 2mg/ml. Samples and standards were prepared in triplicate to ensure accuracy in protein estimation.

2.4.2.2 Soluble protein

Soluble extracts were subjected to protein estimation using Coomassie Plus (Thermo Scientific). Standards were ranging from 5 μ g/ml to 20 μ g/ml and produced using a 20 μ g/ml stock. Samples were diluted 1:10 several times until within standard range. The sample volume of 100 μ l was made up to 200 μ l using

	For experimental samples and negative control	For experimental samples
nH ₂ O	4.5 μ l	5.5 μ l
5x RTase buffer	4 μ l	4 μ l
MgCl ₂ (25mM)	4 μ l	4 μ l
dNTPs (10mM)	1 μ l	1 μ l
RNasin	0.5 μ l	0.5 μ l
Reverse Transcriptase	1 μ l	-
Total Volume	15 μ l	15 μ l

Table 2.2: Reverse transcription master mix

For reverse transcription a master mix of the above solutions was prepared and then aliquoted before supplementation with 1µg of RNA.

Reactant	Experimental volume
cDNA	1.5µl
nH ₂ O	65.5µl
(go)Taq 5x buffer	20µl
MgCl ₂ (25mM)	8µl
dNTPs (10mM)	2µl
Forward primer	1µl
Reverse primer	1µl
Taq polymerase	1µl

Table 2.3: Polymerase chain reaction master mix

For PCR a master mix of the above solutions was prepared and then aliquoted before supplementation with 1.5µl of cDNA.

Gene	Forward Primer	Reverse Primer	Length
<i>hsod1</i>	5'-tggccgatgtgtctattgaa-3'	5'-gggcctcagactacatccaa-3'	20/20
<i>hccs</i>	5'-ccatcagtacggggaccta-3'	5'-ccaggtcatcttctccctca-3'	20/20
<i>hβ-actin</i>	5'-acactgtgcccatctacgagg-3'	5'-aggggccggactcgtcactact-3'	21/21

Table 2.4: Primers used for reverse transcription – polymerase chain reaction (RT-PCR)

To analyse the effect of overexpressing APP carrying the Swedish mutation on copper homeostasis with regards to metallation of intracellular copper binding proteins, expression levels of human SOD1 and CCS were monitored in APP_{WT} and APP_{swe} cell lines under increasing and depleted copper conditions using RT-PCR. The house keeping gene human β-actin was chosen as expression control. Expected product lengths are 210bp (*hsod1*), 230bp (*hccs*), and 612bp (*hβ-actin*).

Coomassie in a 96-well plate and absorbance was measured at a wavelength of 595nm. Samples and standards were produced in triplicate to ensure accuracy.

2.4.3 Whole cell metal profiling

2.4.3.1 Preparation of soluble whole cell extracts by freeze-grinding

Neuroblastoma cultures were harvested as described in section 2.2.3.2. *Saccharomyces cerevisiae* cultures were harvested as described in section 2.2.1. Rat liver mitochondria were prepared as described in section 2.4.8.1 and 2.4.8.2. The resulting pellet was resuspended in a minimum volume (3ml) of extraction buffer (50mM Tris pH 8.8, 1mM PMSF) and added to a liquid nitrogen containing mortar. The cells were ground to a fine powder using a chilled pestle. To maintain a reducing environment the ground cells were transferred into an anaerobic chamber under liquid nitrogen and defrosted before being transferred to an Eppendorf tube and centrifuged at 4,000 rpm (Beckman J6-HC centrifuge) for 15 minutes at 4°C to remove cell debris. The resulting crude extract was then ultracentrifuged at 150,000xg (Beckman L8-80 Ultracentrifuge) for 40 minutes at 4°C to remove

residual membrane fragments. The amount of protein was estimated as described in section 2.4.2.2.

2.4.3.2 First dimension liquid chromatographic separation by anion exchange

All subsequent experiments were performed in the anaerobic chamber and all solutions were purged with nitrogen for at least 30 minutes depending on volume size. The anion exchange column was prepared by three consecutive 10ml washes using extraction buffer (50mM Tris, pH 8.8, 1mM PMSF) containing 0mM NaCl, 1,000mM NaCl, 0mM NaCl. Soluble protein was then loaded onto a 1ml HiTrap Q HP column at 0.3ml min^{-1} at a maximum total protein of 70mg. The column was washed with extraction buffer and then eluted with 1ml each extraction buffer containing 100mM, 200mM, 300mM, 400mM, 500mM and 1,000mM NaCl. A sample volume of 0.2ml of each protein fraction was used for subsequent size exclusion chromatography, the remaining sample was stored at 4°C .

2.4.3.3 Second dimension liquid chromatographic separation by size exclusion

Aliquots (0.2ml) of each of the previously eluted anion exchange protein fractions were subjected to size exclusion chromatography on a Tosoh TSK SW3000 column fitted with a TSKgel SW guard column. The constant flow was provided by a high performance liquid chromatography (HPLC) pump system. Samples were eluted in 10mM Tris, pH 7.5, 50mM NaCl, 1mM PMSF at 0.5ml min^{-1} with fractions being collected every minute for 30 minutes. The column was washed before and between samples with 0.2ml of buffer containing 10mM Tris pH 7.5, 1M NaCl, 10mM EDTA to remove metals bound to the size exclusion matrix. Samples were used immediately for analysis by inductively coupled plasma - mass spectrometry (ICP-MS), and the rest stored at -20°C .

2.4.3.4 Metal analysis by inductively coupled plasma-mass spectrometry

Metal standard solutions were prepared from stock metal solutions of 10,000ppm and 1,000ppm for copper and cobalt, and iron, zinc and manganese (BDH, VWR International, Leicestershire, UK), respectively. ICP-MS calibration standards were prepared through serial dilution of stock solutions in 2.5% (v/v) HNO_3 to 100ppb with further dilution to the appropriate metal standard concentration (0ppb, 0.5ppb, 1ppb, 5ppb, 10ppb and 30ppb). The final dilution produced the standard in a

mixture of 2.5% (v/v) HNO₃ and size exclusion buffer in a ratio 4:1 to standardize for the final sample solution. ICP-MS samples (1.5ml) were prepared by the addition of 0.3ml size exclusion sample to 1.2ml 2.5% (v/v) HNO₃ and analysed using a Thermo X-series ICP-MS. The machine was maintained and auto-tuned before each run in accordance with manufacturer's instructions and operated under conditions suitable for multi-elemental analysis. Samples and standards were analysed in triplicate and the average used for further data analysis. Results are expressed as μM metal present in the sample using the following calculation as means of conversion from ppb.

$$[\text{Equ. 3}] \quad \text{ppb} \times 5 / \text{MWs} = [\mu\text{M}] \text{ sample metal}$$

ppb: being the average of triplicate ICP-MS readings of metal concentration in any particular sample

5: being the dilution factor of ICP-MS samples

MWs: Molecular weight specific to the analysed metal.

2.4.4 Identification of metal-binding proteins

To identify proteins in the 2D-LC fractions that are possible candidates for metal binding, samples containing metal pools as determined by ICP-MS were resolved on SDS-PAGE gels and analysed for correlation of metal pools to protein pools.

2.4.5 SDS-PAGE analysis for protein analysis

2.4.5.1 Preparation of SDS-PAGE gels

Discontinuous SDS-PAGE gels were prepared at 15% (v/v) acrylamide for the resolving gel and 5% (v/v) for the stacking gel using a 30% acrylamide/*bis*-acrylamide stock solution according to Sambrook & Russell (Sambrook and Russell, 2001). The resolving gel was further composed of 375mM Tris, pH 8.8 (1.5M stock) and 0.1% (w/v) electrophoresis grade SDS (10% (w/v) SDS stock), whereas the stacking gel contained 250mM Tris, pH 6.8 (1M stock) and 0.1% (w/v) SDS. Both gels were polymerized using a 10% (w/v) APS stock (freshly prepared weekly to prevent degradation) and TEMED which was added to the gel solutions at

a final concentration of 0.1% (v/v) and 0.0005% (v/v), acting as a polymerization catalyst. Gels were cast in a BioRad Protean II minigel kit using 15mm glass plates.

2.4.5.2 Sample analysis using SDS-PAGE gels

2D-LC samples were prepared as follows. An aliquot (130µl) of sample was mixed with 50µl of 6x SDS gel loading buffer (80% (v/v) glycerol, 1% (w/v) SDS, 50mM Tris-Cl buffer, pH 6.8, 50mM DTT, 0.05% (w/v) BPB). While the samples were denatured by boiling for 10 minutes at 95°C in a PCR thermocycler the gel was immersed in 1x SDS running buffer (25mM Tris-Cl, pH 8.3, 250mM Glycine, 0.1% (w/v) SDS). Subsequently samples were loaded into the gel wells together with a molecular size marker (Sigma Low Range Markers). The high percentage of glycerol enabled multiple loading of samples into wells to increase the protein signal. Gels were run at 120V for 2 hours and proteins were visualized with fluorescent SYPRO Ruby stain (Molecular Probes). The staining process included the gel being rinsed in deionised water to remove residual running buffer and incubation for up to 1 hour with 50% (v/v) methanol, 7% (v/v) acetic acid until the gel decreased in size. The gel was rinsed in deionised water before being placed in the stain over night. A solution of 10% (v/v) methanol, 7% (v/v) acetic acid was used to destain the gel before it was photographed using BioRad quantity 1 software (described in section 2.4.10.1) and analysed by PCA analysis (described in section 2.4.10.2).

2.4.5.3 Protein identification by MALDI-TOF-MS peptide mass fingerprinting

Protein bands identified as possible metal binding proteins were excised from the SDS gel with a scalpel. Following zip-tip purification the samples were digested with trypsin and analysed by matrix-assisted laser desorption ionization – time of flight – mass spectrometry (MALDI-TOF-MS - Applied Biosystems Voyager DESTRA). The MASCOT search tool was subsequently used to search peptide databases for fragment masses comparable to the peptide fragment masses generated by mass spectrometry. The MALDI-TOF-MS analysis and MASCOT search were performed by the Pinnacle Proteomics and Molecular Biology unit, University of Newcastle upon Tyne.

2.4.6 Phenotype analysis under metal depletion and supplementation

2.4.6.1 Growth curves

SH-SY5Y APP_{WT} and APP_{swe} cell lines were grown to confluence in 2x150cm² flasks per line with supplementations made as described previously in section 2.4.1. Cells were harvested as described in section 2.2.3.2 and the resulting pellets were resuspended in 10ml D-PBS. Aliquots (0.2ml) of the resuspended pellet were used for analysis and diluted adequately for the use in a hemocytometer. Cells were manually counted taking into account the 4 corner and 1 central square in each of the hemocytometer chambers. The cell count was performed in triplicate, the average and total cell count ml⁻¹ sample determined using the following calculation:

$$\text{[Equ. 4]} \quad A \times D \times 10,000 = \text{cells/ml}$$

A: being the average of cells counted in 10 squares (counted in triplicate)

D: being the dilution factor of the original sample into trypan blue solution (usually 5)

10,000: hemocytometer specific factor being composed of the volume of each square comprising 1x10⁻³ml, multiplied by the number of squares counted (10).

6x75cm² flasks each containing 1x10⁶ cells were set up for each cell line and growth condition and harvested at appropriate time intervals. Cells were harvested as previously described (section 2.2.3.2), resuspended in 0.6ml D-PBS and appropriately diluted (1/100 and 1/1000) into filter-sterilised casyton solution (isotonic salt solution) to be analysed in a cell counter (Schaerfe Systems, Casy® Cell Counter and Analyser System, Model TT, Reutlingen, Germany) using a 150µm capillary. Final results are expressed as cells ml⁻¹ of original sample for each of the collection days.

2.4.6.2 Survival studies using trypan blue exclusion as indication of survival

Cell cultures were set up as for growth curves (section 2.4.6.1), however only survival studies for cells supplemented with copper were carried out due to the multiple passaging number for BCS supplemented cultures and the resulting loss of cells between passages. Cell cultures were exposed to increasing amounts of CuSO₄ (0µM, 50µM, 150µM, 300µM, 500µM) 24 hours prior to harvesting. Pellets were prepared as described in section 2.2.3.2 and resuspended in 8ml D-PBS. Aliquots

(0.2ml) of the resuspension were mixed with 0.3ml D-PBS and 0.5ml of 0.4% trypan blue for analysis of cell survival using the trypan blue exclusion method. After 10 minutes of incubation (room temperature) in the stain cells were counted manually in triplicate. Cells excluding trypan blue were recorded as live, whereas stained cells were recorded as dead. The survival rate is represented as % survival and compared to the same cell line without copper supplementation.

2.4.6.3 Testing for intracellular metal accumulation by whole cell acid digest

Supplemented cultures were prepared as described previously (section 2.4.6.1) and harvested. Cell counts ml^{-1} of samples were established as described in section 2.4.6.1. Aliquots of 1.5×10^6 cells for each cell line and condition were pelleted at 800xg for 10 minutes and resuspended in 1ml ultrapure 65% (v/v) HNO_3 . Samples were incubated at room temperature for at least 1 week. Independent triplicates for all samples were set up. The cell digests were then centrifuged for 30 minutes at 15,000xg to remove intact cells and debris. The supernatant was transferred to a fresh tube and centrifuged under the same conditions to further purify the sample. Subsequently the digests were analysed for metal content by ICP-MS. Samples were prepared by addition of 0.5ml of acid digest to 2ml of 2.5% (v/v) HNO_3 . ICP-MS metal standards were prepared from 10,000 and 1,000ppm Cu, Zn, and Fe stocks. A serial dilution in 2.5% (v/v) HNO_3 was performed to create a 1ppm metal standard solution mix, which was then used to produce 5ml of various standards (0ppb, 50ppb, 100ppb, 150ppb, 200ppb, 250ppb, 300ppb, 350ppb, 400ppb, 500ppb) in 2.5% (v/v) HNO_3 . Samples were subsequently subjected to ICP-MS analysis as described in section 2.4.3.4.

2.4.7 Enzyme activity assays

2.4.7.1 Enzymatic determination of Glutathione content

The glutathione content of 100mM NaCl samples obtained from yeast whole cell extract through first anionic liquid column chromatography and subsequent separation by high pressure liquid chromatography (HPLC) was determined using the sigma glutathione assay kit according to manufacturer's instructions. In brief, the glutathione content is assayed using a kinetic assay in which catalytic amounts of glutathione are cycled between reduced and oxidized form to cause a continuous

reduction of 5,5'-dithiobis-(2-nitrobenzoic) acid (DTNB) to TNB. Using NADPH, glutathione reductase converts the oxidized form of glutathione into the reduced form. The product, TNB, is assayed colorimetrically at 412 nm. A schematic representation of the reaction is shown in figure 2.2.

2.4.7.2 SOD1 activity assay

2.4.7.2.1 Native polyacrylamide gel electrophoresis to detect SOD1

To retain SOD1 protein structure and enzymatic activity a native polyacrylamide gel is run prior to activity staining. A discontinuous gel comprising a 15% (v/v) resolving gel and 5% (v/v) stacking gel was prepared as previously described in section 2.4.5.1 according to Sambrook and Russell (Sambrook and Russell, 2001) with slight variations. Gels were cast in a BioRad Protean II minigel kit using 15mm glass plates. Under SDS omission TEMED was used as polymerization catalyst and gels were allowed to set over night at 4°C. Unlike described by Beauchamp and Fridovich (Beauchamp and Fridovich, 1971) no riboflavin was added to the gel mixture. Protein samples obtained through 2D-LC were added to

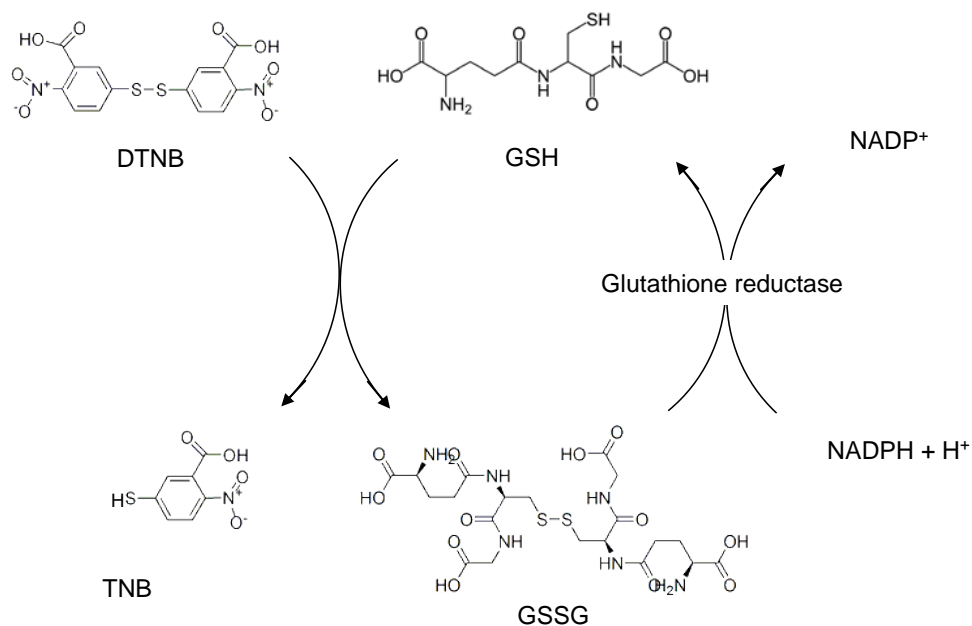


Figure 2.2: Schematic representation of glutathione content assay

The glutathione content of protein extracts is assayed using a kinetic assay in which catalytic amounts of glutathione are cycled between reduced and oxidized form to cause a continuous reduction of 5,5'-dithiobis-(2-nitrobenzoic) acid (DTNB) to TNB. Using NADPH, glutathione reductase converts the oxidized form of glutathione into the reduced form. The product, TNB, is assayed colorimetrically at 412 nm.

Chemical structures were directly taken from chemistry and biology databases (<http://www.chemicalbook.com/CAS%5CGIF%5C70-18-8.gif>, [http://www.bio.davidson.edu/people/kabern/BerndCV/Lab/Website%20\(Summer%202009\)/LSHomepage/Glutathione-skeletal.png](http://www.bio.davidson.edu/people/kabern/BerndCV/Lab/Website%20(Summer%202009)/LSHomepage/Glutathione-skeletal.png)).

2x loading buffer (as described in section 2.4.5.2) lacking SDS and DTT in equal volumes (50 μ l for each sample, 20 μ l for the pure SOD1 control) and transferred into the gel wells. The gel was run in 1x native gel buffer (25mM Tris, 200mM glycine) at 100V for 2 hours. Commercially available human SOD1 extracted from erythrocytes was used as control.

2.4.7.2.2 In-gel activity assay of SOD1 activity

The gel was soaked in 2.45mM NBT for 20 minutes before being immersed in a solution containing 28mM TEMED, 28 μ M riboflavin, 36mM potassium phosphate, pH 7.8 for 15 minutes. Superoxide dismutase activity was initiated by illumination on a Hancock illuminator until the gel changed colour from light yellow to dark purple. Enzyme activity was detected as white bands resulting from the chemical conversion of O₂⁻ radicals generated by photochemically induced riboflavin to H₂O₂, thus preventing the reduction of NBT to formazan and the colour change to purple (Beauchamp and Fridovich, 1971). The exact chemical pathway is displayed in figure 2.3.

2.4.7.2.3 Modified method for soluble whole cell protein extraction

SH-SY5Y monolayer cultures from 150cm² flasks/sample were pelleted at 800xg for 5 minutes and either used immediately or stored at -20°C. Pellets were resuspended in 420µl of 50mM phosphate buffer, pH 7.8 and 120µl of 10% (w/v) SDS. After thorough mixing the samples were incubated at 37°C for 30 minutes with subsequent cooling for 5 minutes on ice. A 60µl addition of 3M KCl was made, the sample vortexed and incubated on ice for a further 30 minutes. Incubation was followed by a 15 minute centrifugation at 13,000xg in a benchtop centrifuge. The supernatant was removed for protein estimation as described in section 2.4.2.2 and the pellet discarded. The extraction process of whole cell soluble protein in this protocol was modified to achieve high protein concentration in a small volume. The extraction process described in section 2.4.2.2 results in a large volume suitable for metal profiling, but not fluorescent spectrophotometry for activity assays.

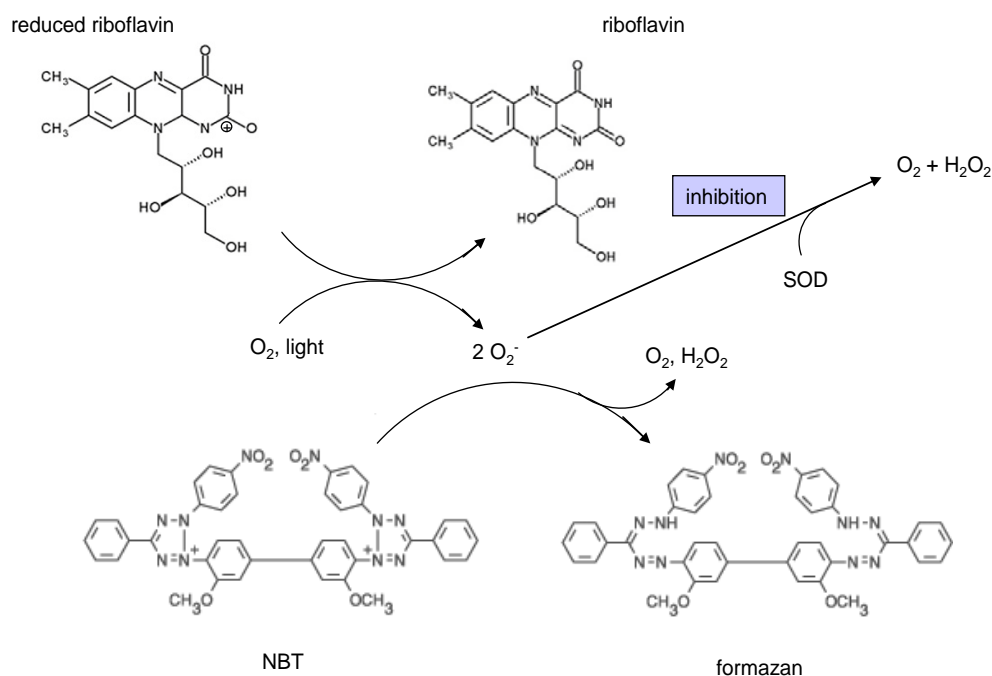


Figure 2.3: Schematic representation of chemical reactions occurring during the in-gel SOD1 activity assay

The in-gel SOD activity staining is a two-step chemical reaction. After resolving protein samples on a native PAGE gel, the gel is soaked in two reaction substrates, which comprise of 2.45mM nitro-tetrazolium blue (NBT) and 28 μ M riboflavin (as described in section 2.4.7.2.2). Subsequently the gel is exposed to O₂ and light to initiate the oxidation of riboflavin during the conversion of O₂ to O₂⁻. This anionic superoxide in turn converts NBT into formazan resulting in a gel colour change from light yellow to purple. Superoxide dismutase prevents the conversion of NBT to formazan by sequestration and dismutation of the O₂⁻ radical to hydrogen peroxide and oxygen. Enzyme activity can be detected as white bands.

Chemical structures were directly taken from chemistry and biology databases (http://www.comberservice.ie/foto/_optional_glovebox_clip_image002.jpg, http://www.invitrogen.com/etc/medialib/en/images/ics_organized/brands/molecular-probes.Par.49619.Image.-1.0.1.gif).

2.4.7.2.4 Spectrophotometric analysis of SOD1 activity

Cells were harvested as described previously (section 2.2.3.2) and whole cell soluble protein extracts obtained using the protocol described in section 2.4.7.2.3.

Total cellular SOD activity was measured as described by McCord and Fridovich (McCord and Fridovich, 1969) by monitoring cytochrome c absorbance intensity using the Varian Cary E4 UV-VIS NIR spectrophotometer at a wavelength of 550nm.

A 100 μ M cytochrome c (bovine heart cytochrome c) stock was prepared in 50mM KPO₄ buffer, pH 7.8 and stored in the dark at 4°C. The working solution for the SOD1 activity assay was prepared fresh on the day of use and was composed of 50 μ M cytochrome c and 0.1mM EDTA in 50mM KPO₄ buffer. A 0.1U addition of xanthine oxidase was made prior to each reaction. SOD1 protein standards using SOD1 protein purified from human erythrocytes (Sigma-Aldrich, UK) were produced by addition of increasing units of active protein to the reaction ranging from 0 to 2.5 units in 0.5 unit increments using a 196.5U/ml, 0.064mg/ml protein stock. Reaction cuvettes for standards were also supplemented with 100 μ g BSA

(50 μ l of 2mg/ml stock) and 60 μ l of the 300mM KCl, 2% (w/v) SDS, 35mM KPO₄ buffer mixture which was used for sample extraction to control for any differences in absorbance arising from reaction components other than cytochrome c. Whole cell protein extracts were added in equal amounts (100 μ g/sample) and the reaction initiated by the addition of 50 μ M xanthine (50 μ l of 10mM stock) and monitored for 30 minutes. The chemical reaction is shown as a schematic representation in figure 2.4.

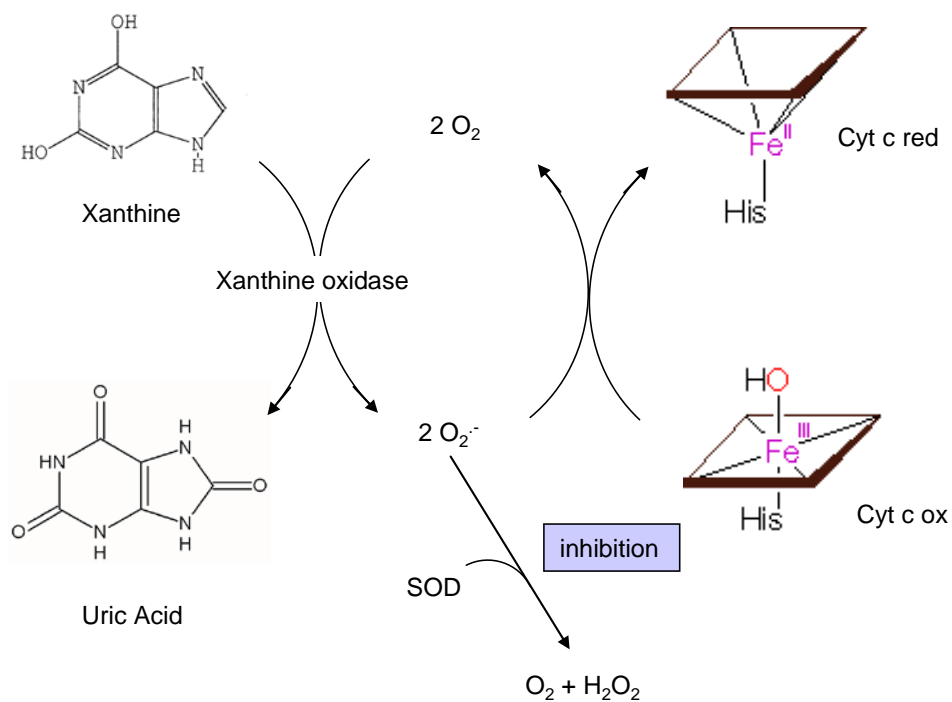


Figure 2.4: Schematic representation of liquid SOD1 activity assay

SOD1 activity is measured spectrophotometrically at a wavelength of 550nm. Under aerobic conditions xanthine is oxidised to uric acid by xanthine oxidase releasing O_2^- . This anionic superoxide in turn reduces oxidised cytochrome c resulting in an increase of absorbance intensity. Superoxide dismutase prevents the reduction of cytochrome c by sequestration and dismutation of the superoxide

radical to hydrogen peroxide and oxygen. Enzyme activity is measured as a function of absorbance intensity quenching.

Chemical structures were directly taken from chemistry and biology databases (<http://www.metallo.scripps.edu/promise/COX.html>, http://www.epa.gov/oppbppd1/biopesticides/ingredients/tech_docs/tech_116900.htm).

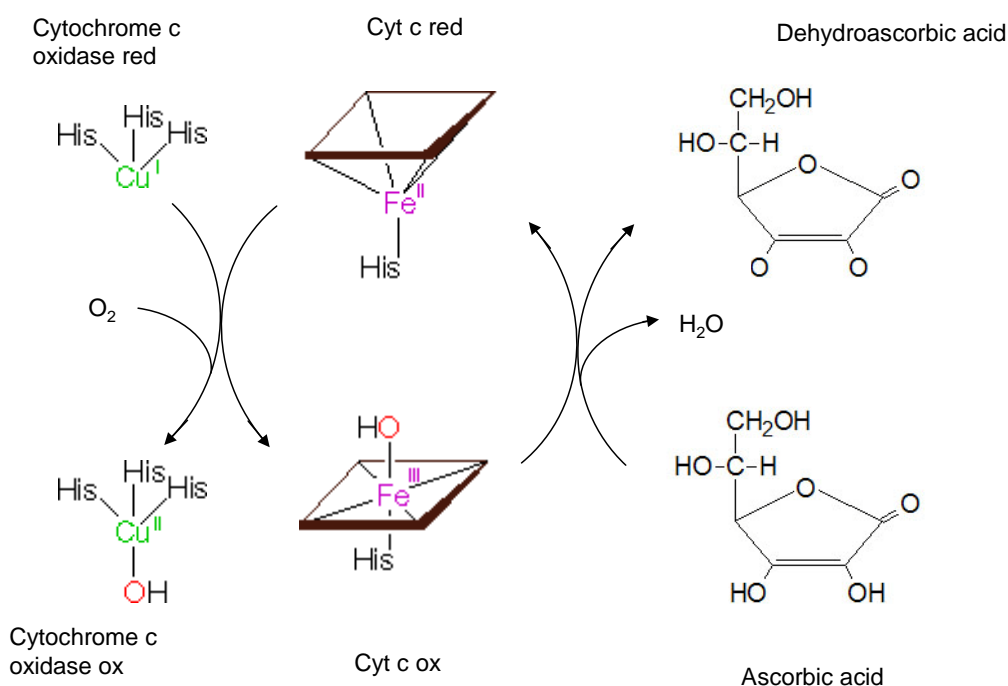


Figure 2.5: Schematic representation of cytochrome c oxidase activity assay

Cytochrome c oxidase activity is measured spectrophotometrically at a wavelength of 550nm. Under aerobic conditions cytochrome c oxidase oxidises the fully reduced form of cytochrome c resulting in a decrease of absorbance intensity. Cytochrome c was fully reduced using molar excess concentrations of ascorbic acid (see section 2.4.7.3.4), which was subsequently removed from the reaction by dialysis (see section 2.4.7.3.5) to prevent cyclic reduction of cytochrome c and reaction inconsistencies.

Chemical structures were directly taken from chemistry and biology databases (<http://www.metallo.scripps.edu/promise/COX.html>, <http://www.themedicalbiochemistrypage.org/vitamins.html>).

2.4.7.3 Cytochrome c oxidase activity assay

Cultures (150cm² flask/sample) of APP_{WT} and APP_{swe} neuroblastoma cell lines were grown to 80% confluence, supplemented as previously described in section 2.4.1 and harvested as described in section 2.2.3.2. The assay was performed as described by Horecker and Heppel (Horecker and Heppel, 1949).

2.4.7.3.1 Preparation of total cellular membrane fraction

Pellets were resuspended in 1ml of 20mM KPO₄ buffer (pH 7.8) and lysed by sonication in a water bath for 3 x 3 minute intervals with 5 minute intervals on ice. To remove undisrupted cells and organelles samples were centrifuged at 800xg (Microcentaur benchtop centrifuge) for 10 minutes and the supernatant transferred to corex tubes for ultracentrifugation. Samples were centrifuged at 150,000xg (Beckman L8-80 ultracentrifuge) to separate the soluble from the membranous material. Pellets were resuspended in 12ml of 20mM KPO₄ buffer (pH 7.8) and the ultracentrifugation step repeated. Pellets were then resuspended in 0.5ml of the same buffer and the protein content was determined by the BCA method as previously described in section 2.4.2.1. Samples were adjusted to the same protein concentration of 120µg/ml in 20mM KPO₄ buffer to reduce variability between different samples during the activity assay with regards to volume and concentration. Samples were used on the same day or the day following extraction.

2.4.7.3.2 Reduction of cytochrome c and dialysis

Since the cytochrome c oxidase assay is measuring the oxidation of reduced cytochrome c (see figure 2.5 for schematic representation of cytochrome oxidase activity assay) it is important to fully reduce the cytochrome c stock in advance of the assay. However, excess reducing agent needs to be removed ahead of the

experiment to avoid competition between the oxidation reaction and residual reducing agent, in this case ascorbic acid.

2.4.7.3.3 Demetallation of dialysis tubing

The dialysis tubing was prepared according to Sambrook & Russell (Sambrook and Russell, 2001). Several pieces (20cm in length) of dialysis membrane (Medicell Int. Ltd., UK) with a molecular-weight cut-off of 3,500 Daltons were boiled over a Bunsen for 10 minutes in 500ml 2% (w/v) sodium bicarbonate (NaHCO_3) and 1mM EDTA, pH 8.0 while being stirred continuously. Following cooling, the tubing was washed repetitively with nH_2O before being boiled for another 10 minutes in 500ml of 1mM EDTA, pH 8.0. The tubing was left to cool and stored in a screw-top Falcon tube at 4°C submerged in nH_2O until further use.

2.4.7.3.4 Ascorbic acid reduction of cytochrome c

A 50 μM cytochrome c (bovine heart cytochrome c) stock was prepared in 20mM KPO_4 buffer, pH 7.8 and stored in the dark at 4°C. The working solution for the cytochrome c oxidase activity assay was prepared fresh on the day of use and consisted of 3 μM cytochrome c in 20mM KPO_4 buffer. Absorbance scans were taken on a Varian Cary E4 UV-VIS NIR spectrophotometer. A quartz cuvette containing 0.9ml of working solution was titrated with increasing amounts of 50mM ascorbic acid (50 μM intervals up to 400 μM final concentration) and UV/visible spectra obtained after each ascorbic acid addition between wavelengths 200-800nm (see appendix 2 figure 5.5). An increase in absorbance (reduction of cytochrome c) was observed at $A_{550\text{nm}}$. Saturation of reduction was observed at 350 μM ascorbic acid addition. It was calculated that 64.8mM ascorbic acid were needed to fully reduce the 50 μM cytochrome c stock. 10ml of stock were reduced by an addition of 100mM (400 μl of 2.5M stock) ascorbic acid.

2.4.7.3.5 Removal of ascorbic acid from the cytochrome c stock using dialysis

Reduced cytochrome c stock was transferred into the dialysis tubing, which was sealed off at both ends. The sample was placed into 2L of 20mM KPO_4 buffer and stirred at 4°C for 1 hour. Subsequently it was transferred to 5L of KPO_4 buffer and stirred at 4°C over night to allow osmosis of ascorbic acid to complete. The reduced

cytochrome c was removed from the dialysis tubing and stored at 4°C until further use.

2.4.7.3.6 Spectrophotometric analysis of cytochrome c oxidase activity

Cytochrome c oxidase activity was measured spectrophotometrically. Aliquots (0.9ml) of above mentioned working solution containing 3 μ M of fully reduced cytochrome c were transferred into a quartz cuvette and scans comprising wavelengths 200-800nm were taken to control for full reduction of cytochrome c at 550nm. Reactions were initiated by addition of 8 μ g protein and analysed for 30 minutes. The rate of cytochrome c oxidation was determined by using $\epsilon_{550\text{nm}} = 29,500 \text{ M}^{-1} \text{ cm}^{-1}$.

2.4.8 Subcellular fractionation of Rat Liver Tissue and *SH-SY5Y* cell cultures

2.4.8.1 Extraction of liver tissue from Wistar rats

Ex-breeder male Wistar rats with a weight of 300g and over were anaesthetised by a low dose of CO₂ in an airtight chamber and their life terminated either by increasing the CO₂ to a lethal dose for 5 minutes or by breaking of the neck. The liver was then removed and immediately used for mitochondrial extraction.

2.4.8.2 Cellular fractionation for mitochondrial extract of rat liver

The protocol was obtained from Mattiazzi et. al. (Mattiazzi et al., 2002) and slightly adjusted.

Rat liver was cut into fine pieces and major veins and obstructions removed. Subsequently the tissue was transferred to an Elvehjem homogenizer and submerged in mannitol sucrose EGTA (MSE) buffer (220mM mannitol, 70mM sucrose, 10mM Hepes, pH 7.4, 1mM MgCl₂, 1mM EGTA) freshly supplemented with 1% (w/v) BSA (functions as protease inhibitor and antioxidant). The mixture was homogenized using a Bosch drill for 4x15 second intervals. The homogenate was transferred into chilled centrifuge tubes and the volume maximised with MSE buffer. The samples were subsequently subjected to 2 low intensity centrifugations at 400xg and 2 high intensity centrifugations at 8,600xg at 4°C in a Sorvall RC-5B centrifuge for 10 minutes/cycle. Supernatant from the low intensity spins and pellets from the high intensity spins were collected and the final pellet resuspended in 4ml

MSE buffer without BSA. The suspension was aliquoted into 1.5ml Eppendorf tubes and pelleted by centrifugation at 8,600xg for 10 minutes. The supernatant was aspirated, the mitochondrial extracts snap-frozen in liquid nitrogen and stored at -20°C.

For mitochondrial extracts of *SH-SY5Y* cells a slight variation in protocol is used. 30x150cm² flasks of 80% confluent monolayer culture were harvested as described in section 2.2.3.2 and the pellet resuspended in 5ml of MSE buffer supplemented with 1% (w/v) BSA. Cells were homogenized with 30 up-and-down strokes of an Elvehjem homogenizer and the homogenate centrifuged as described above for rat liver tissue. Centrifugation speeds were 800xg for the low intensity spin and 8,600xg for the high intensity spin. Pelleted mitochondria were resuspended in MSE buffer without BSA and centrifuged at 800xg for 10 minutes at 4°C. The sample was aspirated and snap-frozen.

2.4.8.3 Confirmation of rat liver mitochondrial fraction by Western Blot

2.4.8.3.1 Sample preparation for Western Blot

Rat liver mitochondria were prepared as described in section 2.4.8.1 and 2.4.8.2. The resulting pellet was resuspended in a minimum volume (3ml) of extraction buffer (50mM Tris pH 8.8, 1mM PMSF) ground to a fine powder in liquid nitrogen as described in section 2.4.3.1. Upon defrosting an aliquot of the crude extract was preserved for later analysis, the remaining sample was centrifuged at 4,000 rpm (Beckman J6-HC centrifuge) for 15 minutes at 4°C to remove cell debris. Both extracts were diluted 1/5 and 1/10 and subjected to Tris-glycine SDS-PAGE as described before (section 2.4.5.1 and 2.4.5.2). Transferable markers were used for protein size determination.

2.4.8.3.2 Transfer of protein onto blotting membrane

Protein was transferred from the SDS-PAGE to a PVDF membrane (Millipore, Bedford, MA) using a half dry blotting machine for 1 hour at 20V. The gel was placed onto the membrane and between filter paper soaked in 1x transfer buffer, pH 8.3 (50mM Tris base, pH 8.3, 40mM glycine, 4% (w/v) SDS, 20% (v/v) methanol).

Before the transfer the PVDF membrane was immersed in 100% methanol followed by nanopure water and soaked in transfer buffer for at least 2 minutes.

2.4.8.3.3 Blocking of membrane with antibodies

The gel was stained with Panceau for a few seconds and rinsed with nanopure water. It was subsequently blocked with blocking solution (5% (w/v) non-fat dry milk powder, 10% (v/v) of 10x TBS buffer, 0.5% (v/v) Tween) for 1 hour before being incubated with a 1/1,000 dilution of primary antibodies in blocking solution over night. Rabbit polyclonal primary antibodies specific to human and rat (Abcam, Cambridge, UK) were directed against the mitochondrial marker protein prohibitin. Following over night incubation, the membrane was washed three times for 5 minutes with blocking solution and incubated with a 1/2,000 dilution of HRP-conjugated goat anti-rabbit secondary antibodies (Abcam) for 2 hours. Excess antibodies were washed from the membrane as before using 1x TBS buffer (50mM NaCl, 20mM Tris, pH 7.5).

2.4.8.3.4 Protein detection by chemiluminescence

Chemiluminescence is induced by the addition of 6.4 μ l H₂O₂ to 10ml of ECL solution (1.25mM luminol, 0.2mM coumaric acid, 100mM Tris, pH 8.5, 0.72% DMSO). The mix was evenly distributed across the membrane and films were developed at various time intervals.

2.4.9 Metal binding analysis of a low molecular copper binding compound

2.4.9.1 Preparation of copper (I) stock solution

Due to the rapid disproportionation characteristics of Cu(I) the titration stock solution was prepared anaerobically and transferred to the rubber sealed sample cuvette using a gas-tight Hamilton syringe. Upon introduction into the anaerobic chamber all solutions were purged with nitrogen to remove residual dissolved oxygen with the exception of ultrapure 30% (w/v) concentrated HCl. 10ml of final working solution (1M NaCl, 0.1M HCl, diluted in nanopure H₂O) were added to 0.05g of solid cuprous chloride and the mixture shaken until all solid material had dissolved. An aliquot (1ml) of this cuprous buffer solution was diluted to the final

working concentration of 2mM Cu(I), 40mM NaCl, 4mM HCl in 24ml of 100mMTris, pH7.5, 150mM NaCl buffer. The quality and accuracy of the Cu(I) stock was measured by ICP-MS using control values of 40ppb and 80ppb. A 1/10 dilution of the 2mM Cu(I) stock was produced in 100mMTris, pH7.5, 150mM NaCl buffer. Aliquots of 31.5 μ l and 62 μ l of the 0.2mM copper stock were added to 968.5 μ l and 937 μ l of buffer to generate the 400 and 800ppb samples, respectively. ICP-MS calibration standards were prepared as previously described in section 2.4.3.4 using final standard concentrations of 0ppb, 1ppb, 5ppb, 30ppb, 50ppb and 100ppb. The final dilution produced the standard in a mixture of 2.5% (v/v) HNO₃ and 100mMTris, pH7.5, 150mM NaCl buffer in a ratio 4:1 to standardize for the final sample solution. ICP-MS samples (1.5ml) were prepared by the addition of 0.3ml of the copper stock sample to 1.2ml 2.5% (v/v) HNO₃ and analysed using a Thermo X-series ICP-MS. The copper stock concentration was recalculated on the basis of ICP-MS results and the μ M additions to the titration reaction adjusted.

2.4.9.2 Cu(I) titration to biological 2D-LC extracts

A 0.5ml (1.2 μ M copper) low molecular weight 2D-LC sample, supposedly containing the low molecular weight copper complex, was anaerobically transferred into an acid-washed 1ml quartz cuvette (Hellma) fitted with a double septum anaerobic seal. Fluorescence spectra were taken between wavelengths of 800-200nm on a Cary Eclipse Fluorescence Spectrometer using second dimension elution buffer as reference point. A 2mM Cu(I) stock was used for additions of molar excess copper increasing in 0.6 μ M increments using a gas-tight Hamilton syringe fitted with an automated dispenser. Spectra were taken after each addition.

2.4.9.3 Cu(I) binding assay using the Cu(I)-specific chelator BCS

A 50mM stock solution of BCS was prepared under anaerobic conditions and serially diluted. BCS was titrated into the same sample with increasing molar excess using a 2mM working solution and increments of 0.6 μ M. Spectra were taken after each addition. The subsequent standardization of the BCS/Cu spectra to the buffer-only spectrum revealed BCS-dependent spectral features.

2.4.9.4 Gel filtration analysis of a low molecular weight metal binding compound

A 0.5ml aliquot of previously eluted 2D-LC sample displaying a low molecular copper peak during ICP-MS analysis was resolved anaerobically on a Sephadex G-25 size exclusion column (PD-10 desalting column, GE Healthcare) to determine the binding of metals to protein. The column was washed with 2ml of second dimension elution buffer (10mM Tris pH 7.5, 50mM NaCl, 1mM PMSF) and residual metal traces removed by washing with 0.2ml buffer containing 10mM Tris pH 7.5, 1M NaCl, 10mM EDTA. Subsequently the column was washed with 3 column volumes of buffer and samples were eluted in 10mM Tris pH 7.5, 50mM NaCl, 1mM PMSF. Eluant fractions (0.5ml) were analysed for protein content by Bradford assay as described in section 2.4.2.2 or metal content for zinc, copper and manganese as described in section 2.4.3.4.

2.4.9.5 ICP-MS analysis of samples

Metal standards for zinc and copper were produced as described in section 2.4.3.4. Protein samples were diluted 1:5 and analysed by ICP-MS. Final results are shown as μM concentrations.

2.4.10 Bioinformatics and statistical analysis

2.4.10.1 Quantity one software

BioRad Quantity 1 software was used to analyse SDS-PAGE and agarose gels and to produce densitometric analyses of individual protein bands for comparison with the according 2 dimensional metal pools by Principal Component Analysis.

2.4.10.2 Matlab for Principal Component Analysis (PCA)

To process data of great variability the statistical software package Matlab is used as basis for Principal Component Analysis. PCA is a mathematical tool to combine and correlate metal content data obtained from metal profiling and ICP-MS analysis of biological extracts and protein data obtained through SDS-PAGE gels across the metal containing fractions of the 2D-LC extract. An example of the use of PCA is given in Nature Protocols for identification of proteins associated with specific periplasmic metal pools of *Synechocystis* PCC 6803 (<http://www.natureprotocols.com/2008/11/12/metalloprotein.php>). PCA works on

the basis of compressing a set of data with high variability to a set of data with lower variability, revealing a way to best indicate variance within the data set. This is achieved by converting a number of correlated variables into a smaller number of uncorrelated variables, which are referred to as principal components. Each principal component removes as much variability as possible, with the most emphasis being placed on the first principal component, then the second and so forth.

2.4.10.3 Statistical analysis

Statistical analysis was performed on data sets that were established by triplicate measurements. BCS or CuSO₄ treated samples were compared to the control using the 1-Way ANOVA (analysis of variance) test provided in Sigma Plot software. The null-hypothesis, which states that differences in enzyme activity, cell growth or survival between control and BCS or CuSO₄ treated cultures is due to random chance, is rejected when the P-value is below the significance level of 5% ($p < 0.05$). The majority of experimental data sets displayed a P-value below the significance level of 1%. Exact statistical significance is specified in all relevant figures.

2.4.10.4 General Bio-informatics

Protein, RNA and DNA sequences were obtained through BLAST searches using PubMed.

Chapter 3 – Results

3.1 Low resolution 2D-LC analysis of soluble metal-complexes in eukaryotic model species

Since 47 % (Andreini et al., 2008) of all proteins require metal as a co-factor to maintain their enzymatic and structural properties, it is of importance to establish methods that enable the study of metalloproteins under physiological conditions. A method has recently been developed by Dr. Kevin Waldron and Dr. Steven Tottey, which comprises of the liquid separation of protein extracts first by charge using anion exchange chromatography followed by size exclusion chromatography under native conditions. Through subsequent analysis of each of the fractions obtained for metal content by inductively coupled plasma – mass spectrometry (ICP-MS) and protein analysis by SDS-PAGE it is possible to establish links between proteins and a possible metal co-factor. By using mathematical methods to create the links it is possible to avoid elaborate purification of proteins to homogeneity under native conditions. This method has been successful in the identification of futA2 as a putative iron-binding protein in periplasmic extracts of *Synechocystis* PCC 6803 (Waldron et al., 2007). More-over, in the course of this work a more elaborate methodology was used to identify the maganese and copper proteins MncA and CucA, respectively (Tottey et al., 2008).

Two dimensional liquid chromatography (2D-LC) is not only useful for detecting previously unknown interactions of metals and proteins, but also in the investigation of changes in metal distribution due to genetic variation and/or environmental stimuli.

To extend the use of this method with respects to differences between prokaryotic systems, eukaryotes and higher mammalian species, a number of model organisms were subjected to 2D-LC and subsequent analysis for copper, zinc, iron, manganese and cobalt.

3.1.1 2D-LC analysis of *Saccharomyces cerevisiae* whole cell soluble protein extract

Saccharomyces cerevisiae is a well understood organism that is often used as the simplest possible model organism for eukaryotic systems. The wild type strain W303 1a was grown in 1L of standard YPD media to $OD_{600nm}=0.4$ and subjected to successive washes in 100 μ M EDTA and nH₂O to remove residual metal from the cell surface before being subjected to 2D-LC. Lysis of cells by freeze grinding in liquid nitrogen as described in section 2.4.3.1 and transfer into an anaerobic environment was intended to minimise the oxidation of any proteinaceous thiol groups, which would otherwise result in metal ions being released from their binding partner rendering the two dimensional separation unsuitable for metal analysis by ICP-MS. The cell lysate was centrifuged to remove intact cells and cell debris as described in section 2.4.3.1 and following estimation of protein content was concentrated on a 1ml anion exchange HiTrap Q HP column at pH 8.8 in buffer containing 50mM Tris, 1mM PMSF. A maximum of 70mg of total soluble whole cell protein extract was loaded onto the column. Protein fractions (1ml) were eluted in elution buffer containing increasing concentrations of NaCl (0mM, 100mM, 200mM, 300mM, 400mM, 500mM, 1,000mM) and aliquots (0.2ml) were transferred to a Tosoh TSK SW3000 size exclusion chromatography column where the anion exchange protein fractions were separated according to their molecular weight (MW). The size exclusion column was coupled with a high performance (HP) peristaltic pump ensuring samples were eluted at a flow rate of 0.5ml min⁻¹ for 30 minutes in 10mM Tris, pH 7.5, 50mM NaCl, 1mM PMSF. Prior to protein loading, the size exclusion column was washed with a solution containing 10mM Tris, pH 7.5, 1M NaCl, 10mM EDTA to remove any residual metals bound to the matrix from previous samples. Of the 35 size exclusion fractions collected the first 5 were discarded since they represent the eluant preceding the void volume of the column and will not contain any molecules derived from the extract. Multi-elemental analysis of each HPLC sample for each anion exchange salt fraction was

performed by ICP-MS as described in section 2.4.3.4 and the data plotted as 3-dimensional contour plot in figure 3.1.

In this analysis the metals, copper (a), zinc (b), manganese (c), and iron (d) but not cobalt (e) show pools that are associated with high molecular weight species; cobalt displays association with only low molecular weight protein species. Each of the divalent metals shows large metal pools in the low molecular weight regions of the contour plot, which could result either from metal relocation from larger metalloproteins to smaller species including non-proteinaceous small molecules during the extraction process or free metal, released during size exclusion chromatography. It seems that for all metals there is a trend in which the high molecular weight metal-binding species elute at a lower salt concentration (ie. 100, 200, 300mM for copper, zinc and manganese) whereas the low molecular weight species are eluted throughout all salt concentrations. Iron seems to be the only metal that is present in all size exclusion fractions in high and low molecular weight species.

Interestingly, a high molecular weight copper pool in the 100mM anion exchange fractions is observed which seemingly co-migrates with a zinc pool at 11.5ml size exclusion volume. Both graphs for copper and zinc are overlaid in figure 3.1 (f) to illustrate co-migration.

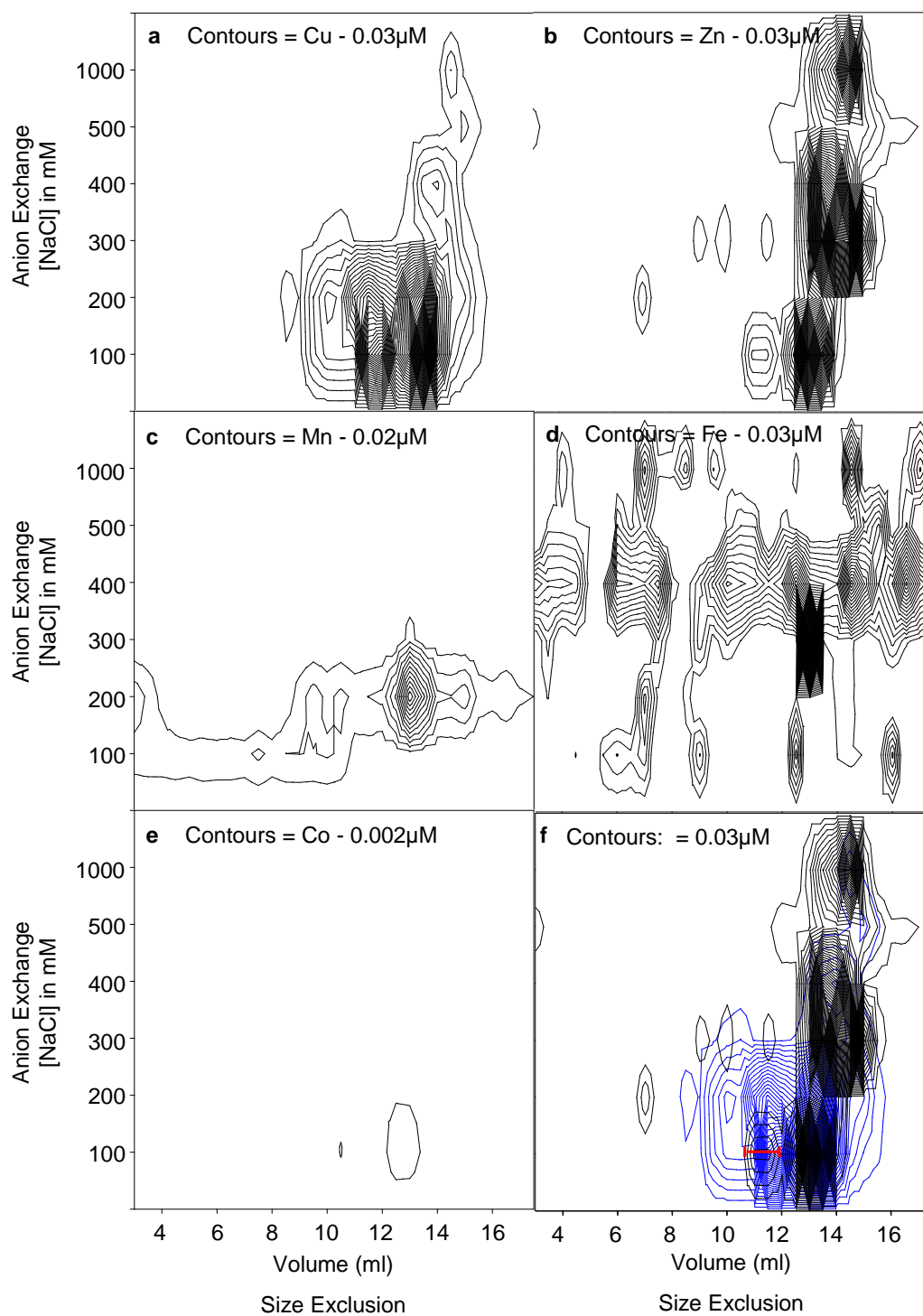
3.1.2 2D-LC analysis of rat liver mitochondria soluble protein extract

Figure 3.1 suggests that such crude 2D-LC in conjunction with metal analysis by ICP-MS could be adequate to identify some of the major metal pools in whole cell extracts of simple eukaryotes. Thus the soluble protein extract an organ of a higher eukaryotic organism, which is know for its high metal content (especially iron) was used. Rat liver is easily accessible and provides a useful sample for such analysis. However, to reduce protein complexity in the sample, fractionation of rat liver for the mitochondrial fraction is attempted. This should provide a 3-dimensional metal profile that focuses on the major metal pools rather than showing every single pool that might be created by binding partners with low abundance, which are anticipated to otherwise generate problems for further analysis if individual proteins are below detection level of the SYPRO Ruby gel stain.

Rat liver was extracted as described in section 2.4.8.1 and the mitochondrial fraction purified by differential centrifugation as described in section 2.4.8.2. Mitochondrial fractionation was tested using Western Blot analysis (data not shown) as described in section 2.4.8.3 using rabbit polyclonal primary antibodies specific to human and rat directed against the mitochondrial marker protein prohibitin and a HRP-conjugated goat anti-rabbit secondary antibody. Mitochondrial soluble extracts were subjected to 2D-LC under anaerobic conditions as described previously for

Figure 3.1: 2D-LC fractionation of metal pools in *Saccharomyces cerevisiae* soluble whole cell protein extract

Soluble whole cell protein extract was prepared from 1L of culture grown to an OD_{600nm} of 0.4. Cells were washed in 100 μ M EDTA and subsequently deionised water to remove residual metal from the culture media and prevent contamination of the extract with EDTA before being lysed by freeze grinding as described in section 2.4.3.1. Subsequent to sequential centrifugation the protein content was estimated by BSA-calibrated Coomassie assay and the extract subjected to 2D-LC (see sections 2.4.3.2 and 2.4.3.3). First the sample was concentrated on a 1ml HiTrap Q HP anion exchange column. Fractions were eluted in extraction buffer (50mM Tris, pH 8.8, 1mM PMSF) containing increasing concentrations of NaCl (0mM, 100mM, 200mM, 300mM, 400mM, 500mM, 1,000mM). Aliquots (0.2ml) of each anion exchange fractions was subjected to high performance liquid chromatography on a Tosoh TSK SW3000 size exclusion column in 10mM Tris, pH 7.5, 50mM NaCl, 1mM PMSF at a flow rate of 0.5ml min⁻¹. Samples were collected every minute for 30 minutes and analysed for metals by inductively coupled plasma-mass spectrometry standardised to standard metal solutions as described in section 2.4.3.4. Results are shown for (a) copper (contours represent 0.03 μ M increments), (b) zinc (contours represent 0.03 μ M increments), (c) manganese (contours represent 0.02 μ M increments), (d) iron (contours represent 0.03 μ M increments), (e) cobalt (contours represent 0.002 μ M increments), and (f) copper (blue) and zinc (black) (contours represent 0.03 μ M increments). Fractions containing both copper and zinc pools are indicated by the red bar and will subsequently be referred to as p1_{yeast}.



Saccharomyces cerevisiae and subjected to multi-elemental analysis by ICP-MS. Figure 3.2 displays contour plots for copper (a), zinc (b), manganese (c), iron (d), and cobalt (e). All contour plots show similarity to the equivalent metal plot for *Saccharomyces cerevisiae*. It is apparent that there are fewer metal pools in the rat mitochondrial extract reducing the complexity of the plot especially for iron (see figure 3.1 (d)). However, those pools are more discernable due to higher micromolar concentration of metal being present in fewer fractions with regards to distribution across anion exchange salt fractions and also size exclusion fractions. Major metal pools are observed in the 200mM and 100mM anion exchange fractions with less metal being distributed throughout the whole extract. Several metal pools for copper (300mM fraction) and zinc (200mM, 300mM fractions) are more resolved in the rat liver mitochondrial extract, which aids the further analysis of distinct metal pools to determine the binding partner for any particular metal pool. Furthermore, the manganese contour plot shows a major manganese pool in the 200mM salt fraction at a size exclusion volume of 9ml.

Co-migrating zinc and copper pools putatively similar to those previously identified in *Saccharomyces cerevisiae* are shown for rat liver mitochondria in figure 3.2 (f). Both metals were eluted in the 100mM anion exchange fraction and migrate at a similar apparent molecular weight eluting at 10.5ml size exclusion volume. The size exclusion volumes at which copper and zinc co-migrate for this particular metal pool vary by 2 fractions (equivalent to 1ml of size exclusion eluant) between *Saccharomyces cerevisiae* and rat liver mitochondrial extracts, it remains possible that the same protein is responsible for copper and zinc binding in both extracts. To assess which protein might be the binding partner to copper and zinc the respective 2D-LC fractions were resolved on a SDS-PAGE gel as described at a later stage in section 3.3.

3.1.3 2D-LC analysis of *HepG2* whole cell soluble protein extract

Advancing to even higher eukaryotes, a human liver carcinoma cell line - *HepG2* – was grown in RPMI media as monolayer cultures to 80% confluency, harvested as described in section 2.2.4.2 and washed with D-PBS several times to remove residual metal contained in the medium. Cell pellets were subjected to lysis and centrifugation as described previously (section 2.4.3.1). Soluble whole cell extracts were subjected to 2D-LC as described for rat liver mitochondria and fractions analysed for metal content by ICP-MS. Figure 3.3 displays 2-dimensional contour plots for copper (a), zinc (b), manganese (c), iron (d), and cobalt (e). In comparison to rat liver mitochondrial metal contour plots, *HepG2* extracts show a significantly different distribution of copper according to charge and size. The copper analysis detects a number of high molecular weight species in the 100mM, 200mM and 1,000mM salt fractions with only a small amount of low molecular copper pools being present in the 100mM and 1,000mM salt fractions, whereas the rat liver mitochondrial extract displayed copper pools that were rather restricted to low molecular weight species. In contrast, the zinc pools are remarkably similar to rat liver mitochondria zinc pools, however they display reduced amounts of zinc in the low molecular weight species and increased amounts of zinc in the high molecular weight species with regards to the 300mM and 400mM salt fractions at a size exclusion volume of 6-8ml. This indicates that a protein present in both cytoplasm and mitochondria might be responsible for these zinc pools or that zinc might have been lost during the rat liver mitochondrial extract and localised to low molecular weight species. Another possibility is that these zinc peaks are caused by proteins too large to enter the column, but releasing zinc into the matrix (causing low molecular weight metal pools) or that protein-specific properties only allow for a slow migration through the column close to the void volume (causing higher molecular weight metal pools). A major difference to contour plots shown for previous species is observed for manganese pools. Only two manganese pools are detected in the 100mM anion exchange fractions, whereas previously manganese was detectable throughout the lower molecular weight range in all salt fractions for rat liver mitochondrial extracts. These findings suggest the existence of a large mitochondria specific manganese pool, which has previously been detected by Luk et al. (Luk et al., 2005) and is thought to be involved in metallation and activation of mitochondrial matrix manganese superoxide dismutase SOD2p in yeast. It is likely that the same manganese pools exist in *HepG2*, APP_{WT} and APP_{swe} cells, but

remain below the limit of metal detection due to the extracts being composed of cytosolic and organelle soluble proteins rather than just mitochondrial proteins. Again, the contour plot for iron is very complex with metal

Figure 3.2: 2D-LC representation of metal pools in rat liver mitochondria soluble protein extract

Rat liver mitochondria were extracted from rat liver by differential centrifugation as described in section 2.4.8.2. Soluble protein extract was prepared by freeze grinding and sequential centrifugation as described in sections 2.4.3.1. Subsequent to sequential centrifugation the protein content was estimated by BSA-calibrated Coomassie assay and the extract subjected to 2D-LC (see sections 2.4.3.2 and 2.4.3.3). First the sample was concentrated on a 1ml HiTrap Q HP anion exchange column. Fractions were eluted in extraction buffer (50mM Tris, pH 8.8, 1mM PMSF) containing increasing concentrations of NaCl (0mM, 100mM, 200mM, 300mM, 400mM, 500mM, 1,000mM). Aliquots (0.2ml) of each anion exchange fractions was subjected to high performance liquid chromatography on a Tosoh TSK SW3000 size exclusion column in 10mM Tris, pH 7.5, 50mM NaCl, 1mM PMSF at a flow rate of 0.5ml min⁻¹. Samples were collected every minute for 30 minutes and analysed for metals by inductively coupled plasma-mass spectrometry standardised to standard metal solutions as described in section 2.4.3.4. Results are shown for (a) copper (contours represent 0.03µM increments), (b) zinc (contours represent 0.03µM increments), (c) manganese (contours represent 0.02µM increments), (d) iron (contours represent 0.03µM increments), (e) cobalt (contours represent 0.002µM increments), and (f) copper (blue) and zinc (black) (contours represent 0.03µM increments). Fractions containing both copper and zinc pools are indicated by the red bar and will be subsequently referred to as p1_{RLM}.

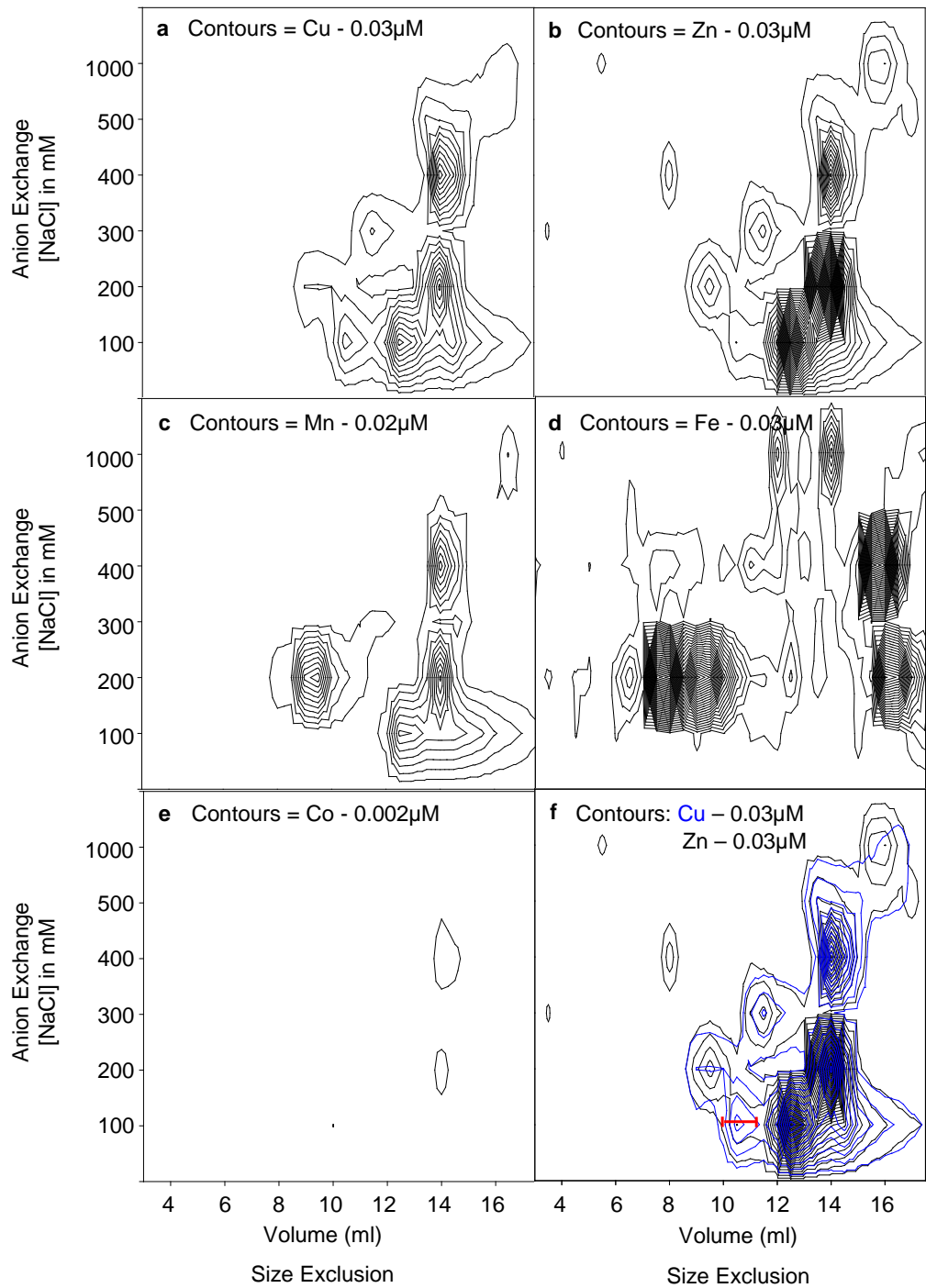
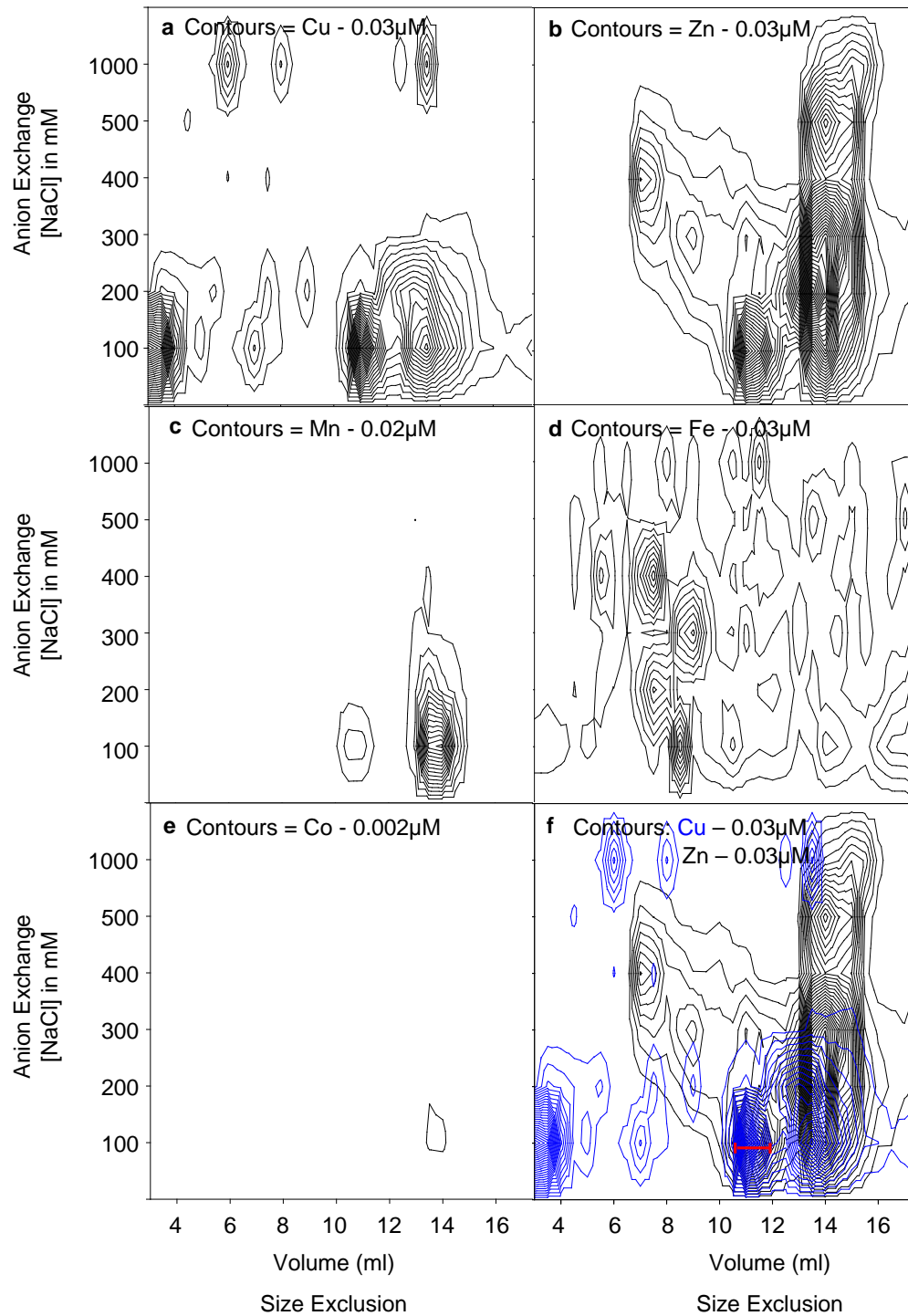


Figure 3.3: 2D-LC representation of metal pools in *HepG2* soluble whole cell protein extract

Soluble whole cell protein extract was prepared from 30x150cm² flasks of 80% confluent *HepG2* monolayer culture and extracted by freeze grinding and sequential centrifugation as described in sections 2.4.3.1. Subsequent to BSA-calibrated protein estimation the extract was subjected to 2D-LC (see sections 2.4.3.2 and 2.4.3.3). First the sample was concentrated on a 1ml HiTrap Q HP anion exchange column. Fractions were eluted in extraction buffer (50mM Tris, pH 8.8, 1mM PMSF) containing increasing concentrations of NaCl (0mM, 100mM, 200mM, 300mM, 400mM, 500mM, 1,000mM). Aliquots (0.2ml) of each anion exchange fractions was subjected to high performance liquid chromatography on a Tosoh TSK SW3000 size exclusion column in 10mM Tris, pH 7.5, 50mM NaCl, 1mM PMSF at a flow rate of 0.5ml min⁻¹. Samples were collected every minute for 30 minutes and analysed for metals by inductively coupled plasma-mass spectrometry standardised to standard metal solutions as described in section 2.4.3.4. Results are shown for (a) copper (contours represent 0.03µM increments), (b) zinc (contours represent 0.03µM increments), (c) manganese (contours represent 0.02µM increments), (d) iron (contours represent 0.03µM increments), (e) cobalt (contours represent 0.002µM increments), and (f) copper (blue) and zinc (black) (contours represent 0.03µM increments).



pools showing throughout both dimensions of the separation with major iron pools being present in the high molecular weight samples of the 100mM - 400mM anion exchange fractions. As for both previous organisms that were tested for metal distribution, *HepG2* cells also display a co-migrating copper and zinc pool within the 100mM salt fraction. Figure 3.3 (f) displays overlaying copper (blue) and zinc (black) metal analyses with a clear overlap of both metals in the region marked by the red bar for $p1_{HepG2}$.

3.1.4 2D-LC analysis of *SH-SY5Y* APP_{WT} whole cell soluble protein extract

An experimental model that is often chosen for studies related to neuronal cell function is the human neuroblastoma cell line *SH-SY5Y*. This cell line was established in 1970 by subcloning the original cell line *SK-N-SH* which was created by bone marrow biopsy of a female patient. *SH-SY5Y* readily grows as a monolayer culture in DMEM supplemented with foetal calf serum, antibiotic and glutamate (see section 2.2.3.1) at 37°C in a 5% CO₂ atmosphere. For crude fractionation of major metalloprotein pools cells were grown to 80% confluency and treated as described for *HepG2* cells. Figure 3.4 shows contour plots for copper (a), zinc (b), manganese (c), iron (d), and cobalt (e) distribution throughout the whole cell soluble extract. The copper analysis detects several copper pools within the 100mM, 200mM, 300mM, and 1,000mM salt fractions, however only the 100mM anion exchange fraction copper pool at size exclusion volume 11ml is resolved as a discrete peak suitable for further analysis of potential metal binding partners. Two major zinc pools are observed in the 100mM and 300mM salt fractions. Low molecular weight zinc fractions are visible throughout all salt fractions and thus are probably consistent of free zinc or zinc inclusions. There are no major detectable metal pools for iron. Contours displayed are most likely due to trace contamination. Contour plots of copper (blue) and zinc (black) in figure 3.4 (f) indicate the presence of the same copper and zinc binding entity in the 100mM salt fraction at 11ml volume. No other metal pools of copper and zinc overlap, which places particular interest on the species that is responsible for binding both metals.

3.1.5 2D-LC analysis of *SH-SY5Y* APP_{swe} whole cell soluble protein extract

The *SH-SY5Y* APP_{swe} cell line was previously established by transfection of the mammalian transfection vector pcDNA3.1 into the *SH-SY5Y* APP_{WT} cell line using lipofectamine 2000 as transfection reagent. The vector contained a copy of the 695 amino acid residue version of APP with the familial Swedish mutation comprising an amino acid change of lysine and methionine at positions 595 and 596 to asparagine and leucine (see figure 1.1). Cells were treated as described before for APP_{WT} cells and subjected to 2D-LC with subsequent metal analysis by ICP-MS. Results for copper (a), zinc (b), manganese (c), iron (d), and cobalt (e) are shown in figure 3.5. A smaller number of copper pools were detectable with the only major copper pool present in the 100mM salt fractions with a size exclusion volume of 10.5ml. A metal pool located at the same position as this copper pool (figure 3.5 (f)) indicates the presence of a copper and zinc binding protein in APP_{swe} cells. No other copper and zinc pools co-migrate so closely, thus further analysis of this metal pool and its binding partner is crucial. It appears that the copper pool in the cell line overexpressing the APP_{swe} is smaller than the corresponding copper pool in the APP_{WT} cell line. However, this needs to be investigated further since the APP_{WT} and APP_{swe} metal profiles shown are not average representations of triplicate experiments, but replicates that best represent the metal distribution across the whole cell extracts.

3.2 Analysis of glutathione content of fractionated *Saccharomyces cerevisiae* extracts

Figure 3.1 (f) shows overlaying copper and zinc pools in the 100mM salt fraction. To assess the potential of the copper pools for p1_{yeast} being associated with glutathione, a cellular antioxidant of low molecular weight, a glutathione assay was performed across all size exclusion fractions of the 100mM salt fraction. Figure 3.6 (a) shows a 2-dimensional contour plot representing the relative presence of glutathione and copper in the 100mM salt fraction. This result clearly demonstrates that the copper pool associated with the zinc pool is not associated with glutathione, thus there must be a different binding partner to both metals. Protein content across the same fractions that were subjected to the glutathione assay was measured in a BSA-calibrated Coomassie assay as described in section 2.4.2.2 and plotted against copper and glutathione content of the same fractions.

Figure 3.6 (b) shows that a protein peak corresponding to the copper pool might be responsible for binding the metal. Determining the identity of the metal-binding protein is subject of the next section.

Figure 3.4: 2D-LC representation of metal pools in *SH-SY5Y* APP_{WT} soluble whole cell protein extract

Soluble whole cell protein extract was prepared from 30x150cm² flasks of 80% confluent APP_{WT} monolayer culture and extracted by freeze grinding and sequential centrifugation as described in sections 2.4.3.1. Subsequent to BSA-calibrated protein estimation the extract was subjected to 2D-LC (see sections 2.4.3.2 and 2.4.3.3). First the sample was concentrated on a 1ml HiTrap Q HP anion exchange column. Fractions were eluted in extraction buffer (50mM Tris, pH 8.8, 1mM PMSF) containing increasing concentrations of NaCl (0mM, 100mM, 200mM, 300mM, 400mM, 500mM, 1,000mM). Aliquots (0.2ml) of each anion exchange fractions was subjected to high performance liquid chromatography on a Tosoh TSK SW3000 size exclusion column in 10mM Tris, pH 7.5, 50mM NaCl, 1mM PMSF at a flow rate of 0.5ml min⁻¹. Samples were collected every minute for 30 minutes and analysed for metals by inductively coupled plasma-mass spectrometry standardised to standard metal solutions as described in section 2.4.3.4. Results are shown for (a) copper (contours represent 0.03µM increments), (b) zinc (contours represent 0.03µM increments), (c) manganese (contours represent 0.02µM increments), (d) iron (contours represent 0.03µM increments), (e) cobalt (contours represent 0.002µM increments), and (f) copper (blue) and zinc (black) (contours represent 0.03µM increments). Fractions containing both copper and zinc pools are indicated by the red bar and will subsequently be referred to as p1APP_{WT}.

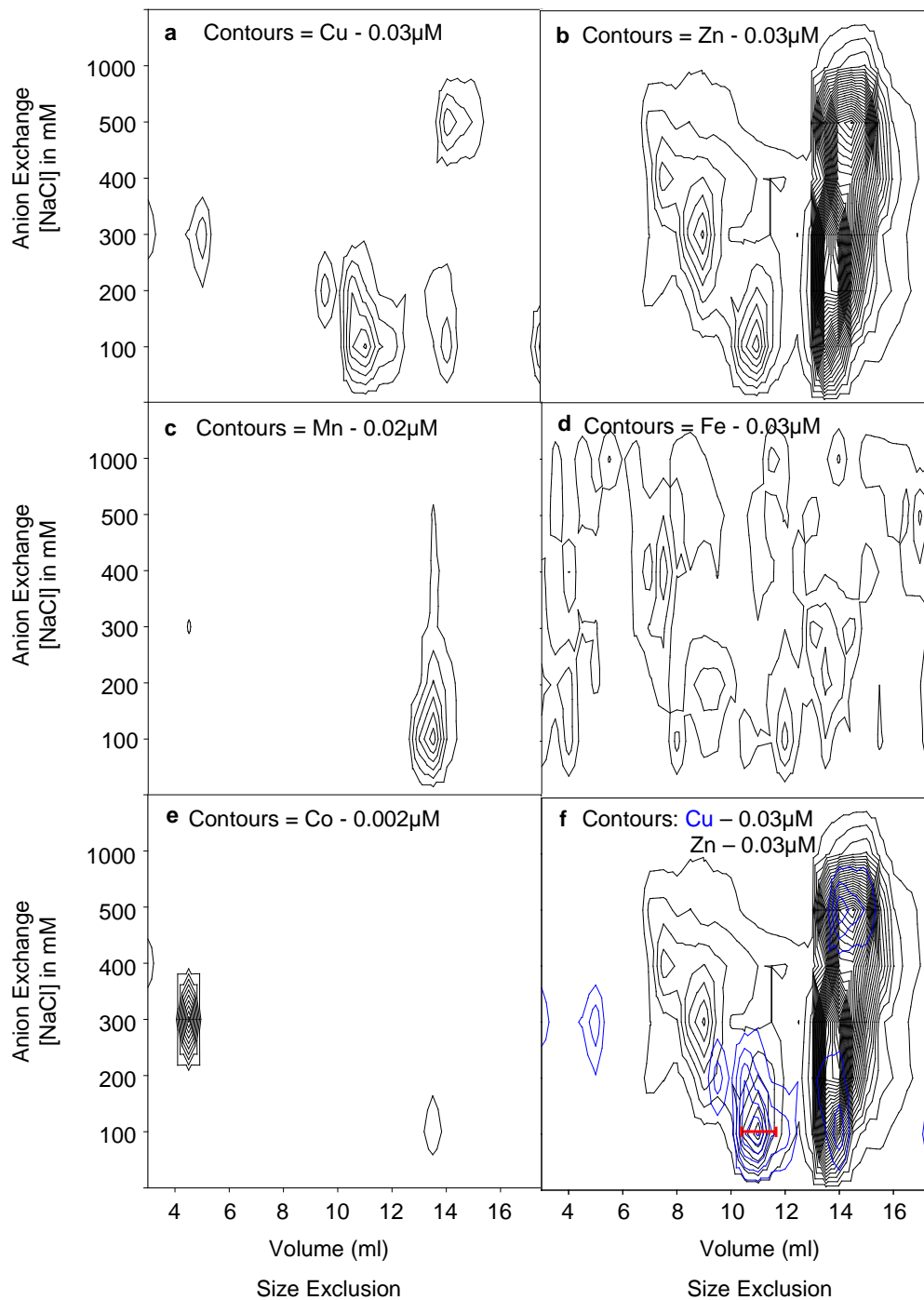
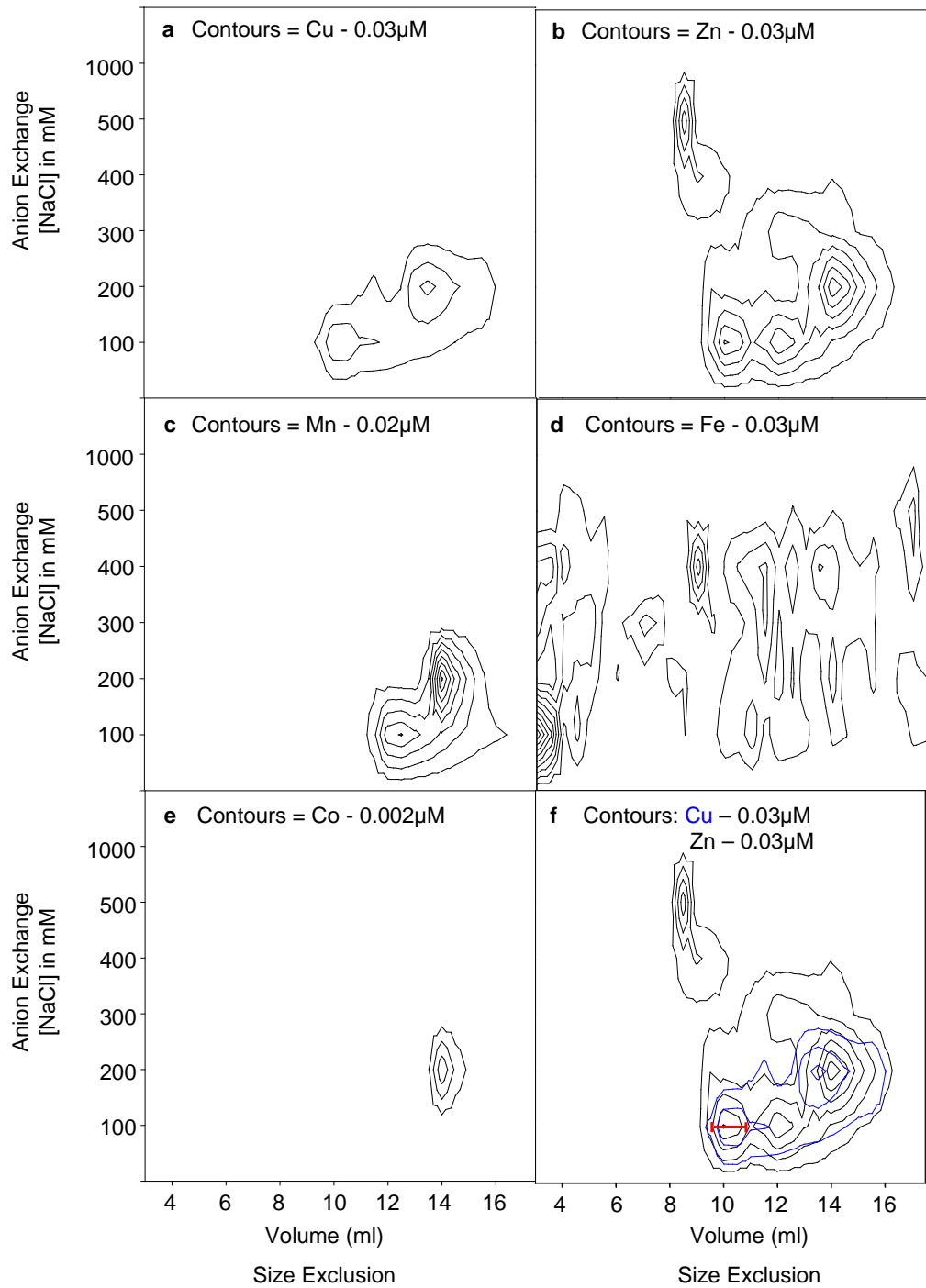


Figure 3.5: 2D-LC representation of metal pools in *SH-SY5Y* APP_{swe} soluble whole cell protein extract

Soluble whole cell protein extract was prepared from 30x150cm² flasks of 80% confluent APP_{swe} monolayer culture and extracted by freeze grinding and sequential centrifugation as described in sections 2.4.3.1. Subsequent to BSA-calibrated protein estimation the extract was subjected to 2D-LC (see sections 2.4.3.2 and 2.4.3.3). First the sample was concentrated on a 1ml HiTrap Q HP anion exchange column. Fractions were eluted in extraction buffer (50mM Tris, pH 8.8, 1mM PMSF) containing increasing concentrations of NaCl (0mM, 100mM, 200mM, 300mM, 400mM, 500mM, 1,000mM). Aliquots (0.2ml) of each anion exchange fractions was subjected to high performance liquid chromatography on a Tosoh TSK SW3000 size exclusion column in 10mM Tris, pH 7.5, 50mM NaCl, 1mM PMSF at a flow rate of 0.5ml min⁻¹. Samples were collected every minute for 30 minutes and analysed for metals by inductively coupled plasma-mass spectrometry standardised to standard metal solutions as described in section 2.4.3.4. Results are shown for (a) copper (contours represent 0.03µM increments), (b) zinc (contours represent 0.03µM increments), (c) manganese (contours represent 0.02µM increments), (d) iron (contours represent 0.03µM increments), (e) cobalt (contours represent 0.002µM increments), and (f) copper (blue) and zinc (black) (contours represent 0.03µM increments). Fractions containing both copper and zinc are indicated by the red bar and will subsequently be referred to as p1APP_{swe}.



3.3 2D-LC analysis of rat liver mitochondria soluble protein extracts

To verify the reproducibility of the two dimensional separation for rat liver mitochondria protein extracts and later for *SH-SY5Y* APP_{WT} and APP_{swe} cell lines (see section 3.5), the experiment was repeated multiple times (n=7). The analyses were performed as described for the rat liver mitochondrial protein extract in section 3.1.2. The resulting contour plots were reproducible with regards to metal distribution as shown in figure 3.2 and figure 3.7, however the total metal measured differed from experiment to experiment. This might be due to metal loss during the experiments at various purification or separation steps, partial sample exposure to air with resulting loss of metal from oxidised metal binding sites or simply due to variation in the metal detection during mass spectrometry. The ICP-MS was calibrated before each experiment. To avoid large errors of standard deviation between replicates due to variation in metal detection during metal analysis, the replicate most representative of the remaining replicates is displayed.

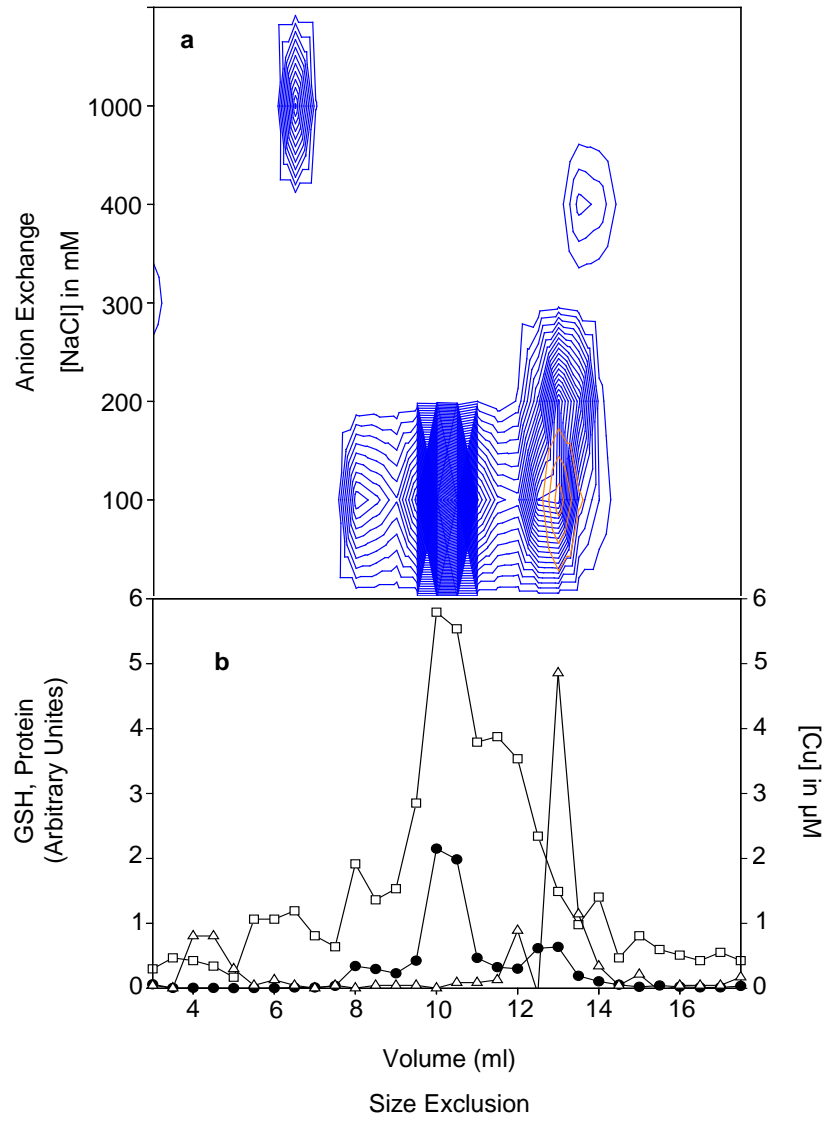
3.3.1 2D-LC analysis of rat liver mitochondria soluble protein extract

A previous replicate of rat liver mitochondrial extract analysed for metal content following 2D-LC as seen in figure 3.2 (f) highlights overlaying metal pools of copper and zinc in the 100mM anion exchange fraction termed p1_{RLM}. These metal pools are reproducible and shown in figure 3.7 (a) for copper and figure 3.7 (b) for zinc and comprise of 0.38 μ M copper and 0.32 μ M zinc, respectively, in the fraction containing the most metal. The metal concentrations thus indicate a possible binding stoichiometry of 1:1 copper:zinc, an observation that might aid further identification of the putative binding partner for both metals. To assess which protein is responsible for the copper and zinc metal pools, fractions across the metal pools were resolved on a SDS-PAGE gel, stained with SYPRO Ruby and analysed for densitometry of each individual band using BioRad Quantity One software. The SDS-PAGE gel is displayed in figure 3.7 (c) with chromatographic representation of copper, zinc and protein content across the fractions of interest in figure 3.7 (d).

Figure 3.6: Copper and glutathione content in *Saccharomyces cerevisiae* whole cell protein extract

a) Whole cell protein extract was prepared from a 1L culture grown to an OD_{600nm} of 0.4 as described in section 2.4.3.1. The extract was concentrated on a 1ml HiTrap Q HP anion exchange column and eluted with increasing concentrations of NaCl (100, 200, 300, 400, 500, 1000mM) in 1ml aliquots. Aliquots (0.2ml) of each salt fraction was resolved on a Tosoh TSK SW3000 size exclusion chromatography column at a flow rate of $0.5ml\ min^{-1}$ and eluted every minute for 30 minutes in buffer containing 10mM Tris pH 7.5, 50mM NaCl, 1mM PMSF. Samples were analysed for copper content by ICP-MS (blue contours) and for glutathione content (orange contours). The 3-D contour plot of whole cell glutathione and copper distribution shows that there is a copper pool in the 100mM salt fraction that is not glutathione bound.

b) Aliquots of anion exchange fractions (100mM NaCl) displaying glutathione content were subjected to size exclusion chromatography on a Tosoh TSK SW3000 HPLC column eluted in 10mM Tris pH 7.5, 50mM NaCl, 1mM PMSF at $0.5ml\ min^{-1}$ with fractions being collected every minute for 30 minutes. Fractions were analysed for copper (filled circles), glutathione (open triangles) and protein content (open squares) by BSA-calibrated Coomassie assay.



3.3.2 Identification of p1_{RLM} as copper-zinc superoxide dismutase from rat mitochondrial extract

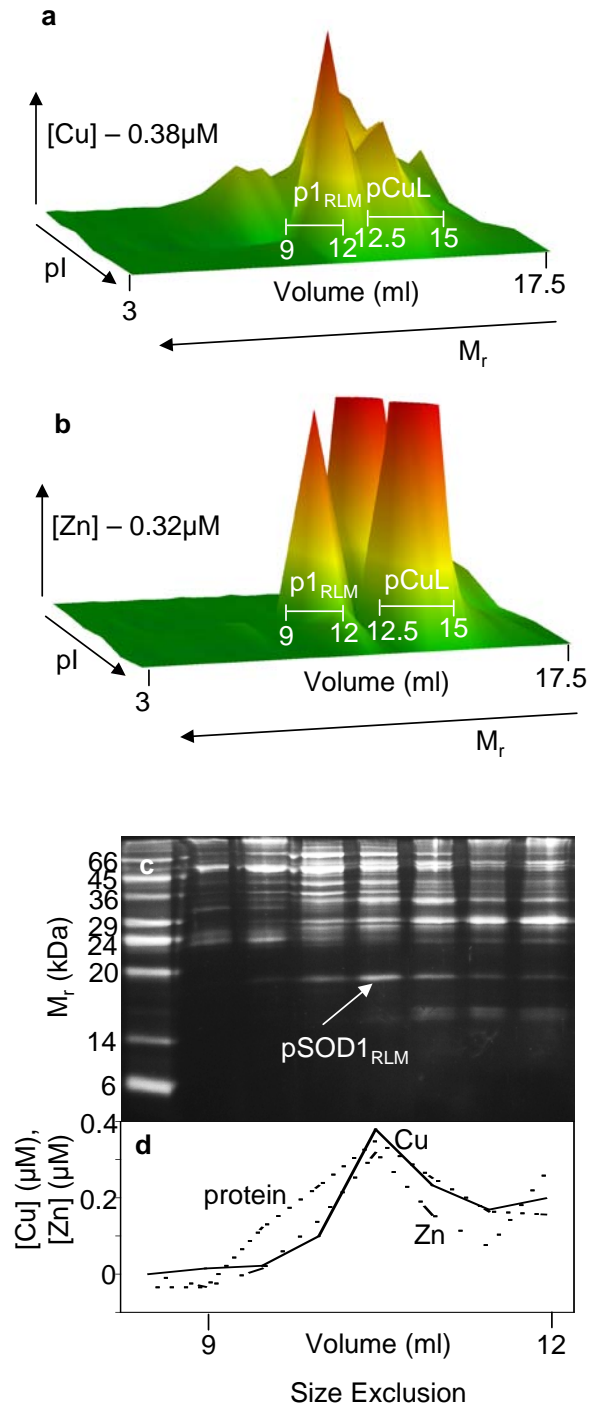
Densitometric data obtained through analysis of bands across copper and zinc containing fractions on SDS-PAGE gels (figure 3.7) was applied to Principal Component Analysis (PCA), a mathematical tool that combines and correlates metal data obtained via ICP-MS analysis and protein data. The statistical analysis is explained in section 2.4.10.2. Figure 3.8 shows the correlation analysis (a) for proteins (grey) with copper and zinc. Protein p1_{RLM SDS-PAGE} correlated best with the distribution and intensity of copper and zinc across the analysed fractions, an observation, which is confirmed in panels (b), (c), and (d). Comparison of various Principal Components generates clustering of p1_{RLM SDS-PAGE} with copper and zinc indicating p1_{RLM SDS-PAGE} as putative binding partner.

The protein band identified as putative metal binding protein was excised from the SDS-PAGE gel and analysed by peptide mass fingerprinting. Following zip-tip purification the sample was restricted by trypsin and analysed by matrix-assisted laser desorption ionisation – time of flight – mass spectrometry (MALDI-TOF-MS). The resulting chromatograph of peptide sizes and sequences were compared to the MASCOT database resulting in the identification of the metal binding protein p1_{RLM SDS-PAGE} as copper – zinc binding superoxide dismutase (hereafter referred to as pSOD1_{RLM}). This analysis was performed by The Pinnacle Proteomics and Molecular Biology unit, Newcastle University. Figure 3.9 (a) shows the Mowse Score analysis which indicates the statistical significance ($p < 0.05$) for any protein with a score above 56 as a random event. The chromatograph in figure 3.9 (b) reveals several experimental peptide fragments (highlighted in red boxes) that match expected MASCOT fragments for rat copper – zinc superoxide dismutase. These data strongly suggest that copper – zinc superoxide dismutase is responsible for the copper and zinc pool observed in the 100mM anion exchange fraction. The protein band corresponding to superoxide dismutase is shown in figure 3.7 (c) designated pSOD1_{RLM} with a molecular weight of 20,000Da. An independent protein identification (data not shown) using a different extract of rat liver mitochondria similarly identified copper – zinc SOD as the prevalent copper and zinc pool in the rat liver mitochondrial extract.

Figure 3.7: 2D-LC representation of metal pools in rat liver mitochondrial extract

Rat liver mitochondria were extracted from rat liver by differential centrifugation as described in section 2.4.8.2. Mitochondria were lysed by freeze grinding in extraction buffer (50mM Tris, pH 8.8, 1mM PMSF) and intact organelles removed by sequential centrifugation. The protein extract was concentrated on a 1ml HiTrap Q HP anion exchange column and eluted in extraction buffer containing increasing concentrations of NaCl (0mM, 100mM, 200mM, 300mM, 400mM, 500mM and 1,000mM). Aliquots (0.2ml) of each anion exchange fraction were subjected to size exclusion chromatography on a Tosoh TSK SW3000 column and analysed for metal content by inductively coupled plasma-mass spectrometry (ICP-MS). Shown are 3-dimensional plots for copper (a) and zinc (b) distribution with emphasis on a particular copper and zinc peak present in the same fractions (p1) and the presence of a putative non-proteinaceous copper binding complex (pCuL) previously identified by Cobine et. al. (Cobine et al., 2004). Bars on panels (a) and (b) depict samples of eluant that were further analysed by SDS-PAGE in figure 3.7 c) or by fluorescent spectroscopy in figure 3.11 b).

Fractions containing the copper and zinc metal pools ($p1_{RLM}$) were resolved on a 15% (w/v) discontinuous SDS-PAGE gel and protein visualised with Sypro Ruby (c). Densitometric analysis of protein bands using BioRad quantity one software indicates pSOD1_{RLM} as possible binding partner to copper and zinc. Corresponding chromatographs (d) of copper (solid line), zinc (long dashed line), and relative abundance of protein (short dashed line) across the resolved fractions implies a metal binding role for pSOD1_{RLM}.



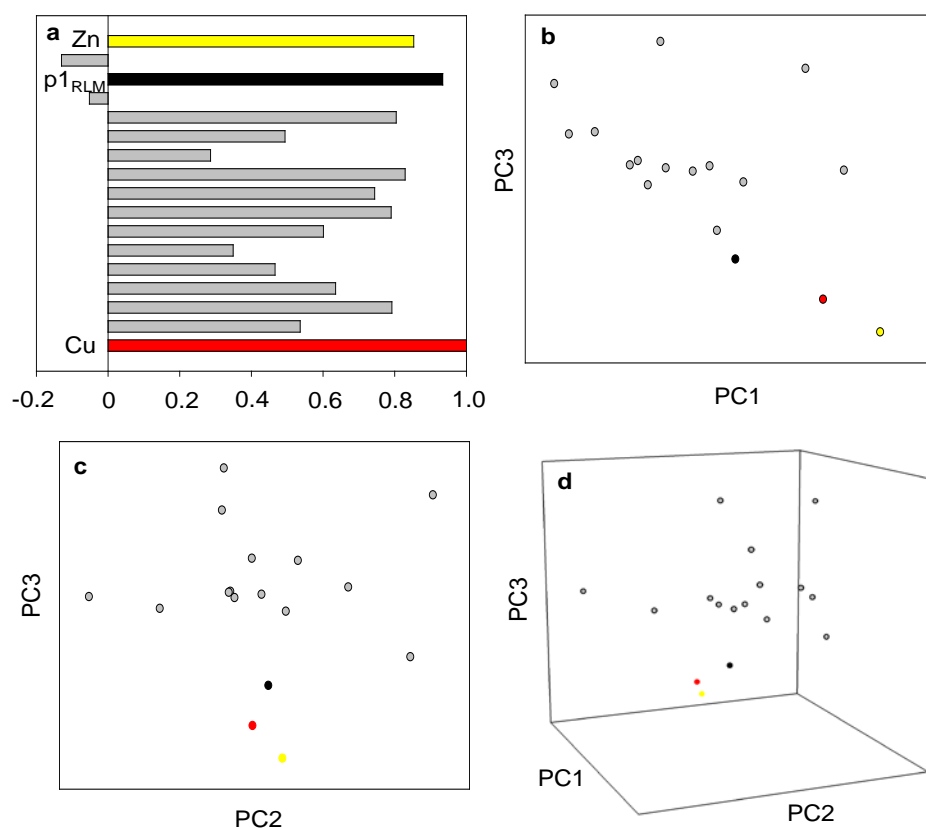


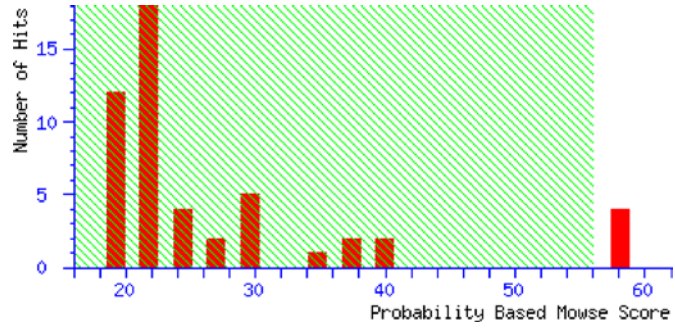
Figure 3.8: Principal component analysis to predict protein binding to copper and zinc in rat mitochondrial protein extract

Aliquots (130 μ l) of 100mM NaCl size exclusion fractions containing copper and zinc (figure 3.7) were resolved on a discontinuous 15% (w/v) SDS-PAGE gel (figure 3.7) and analysed for protein distribution in each fraction using BioRad quantity one software. Data for copper, zinc and protein chromatographs was used to calculate the principal components (see section 2.4.10.2) for this data set. Correlation analysis (a) indicates that p1_{RLM} is the closest match to copper and zinc with regards to distribution across the resolved fractions and comparison of various principal components (b, c and d) shows spatial clustering of copper, zinc and p1_{RLM} suggesting a strong indication of p1_{RLM} being a copper and zinc binding protein.

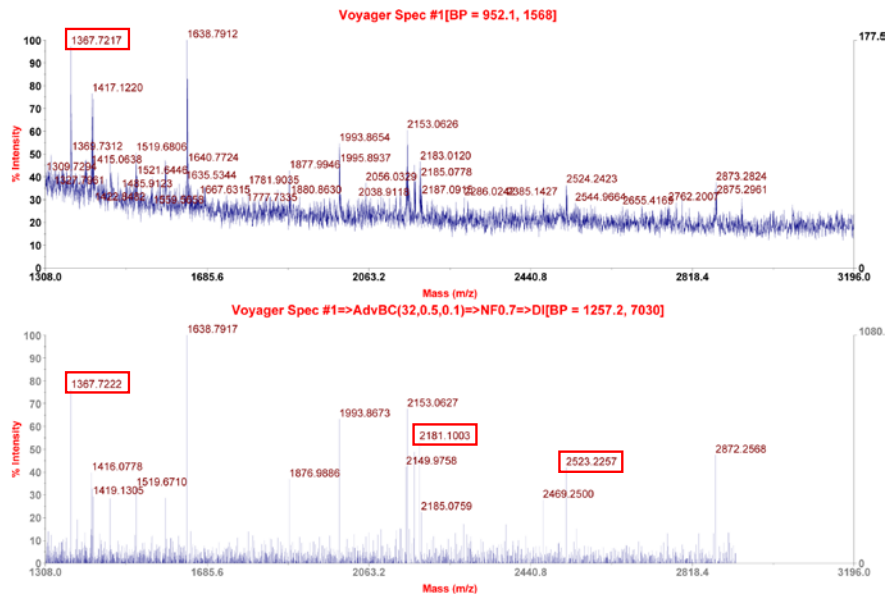
Figure 3.9: Identification of a putative copper and zinc binding protein by matrix-assisted laser desorption-ionisation time-of-flight mass spectrometry (MALDI-TOF-MS)

Rat liver mitochondria were subjected to 2D-LC as previously described, analysed for metal content (figure 3.7) by inductively coupled plasma-mass spectrometry (ICP-MS) and resolved on SDS-PAGE for densitometric analysis (figure 3.7). Principal component analysis identified p1_{RLM} as best protein candidate for the copper and zinc peaks (figure 3.8), thus the band was excised and analysed by MALDI-TOF-MS. The protein analysis involved trypsinisation of the sample for peptide mass fingerprinting and comparison of the generated mass-to-charge chromatograph to the Mascot database. Mowse Score analysis indicates statistical significance ($p < 0.05$) for any protein identified with a score above 56 (a). The chromatograph (b) shows fragments that were generated and compared against the Mascot database, which revealed that several fragments (red boxes) match expected fragments for rat copper/zinc superoxide dismutase.

a



b



3.4 Purification and partial characterisation of a low molecular weight copper complex in rat liver mitochondria

A second large copper pool was detected in the low molecular weight region of the rat liver mitochondrial extract 100mM anion exchange fraction. Previously Cobine et. al. discovered a small non-proteinaceous mitochondrial matrix copper complex (CuL) in yeast (Cobine et al., 2004) thought to be involved in the metallation of cytochrome oxidase and superoxide dismutase (Cobine et al., 2006). Although both extraction protocols vary greatly - Cobine et. al. extracted the copper complex using anion exchange and reverse phase purification in an acetonitrile gradient (Cobine et al., 2006) - the copper pool observed in rat liver mitochondrial extracts may constitute this CuL complex. Figure 3.7 illustrates the intensity and location of the copper pool designated pCuL.

3.4.1 Protein analysis of the low molecular weight copper-binding complex

To further investigate the existence of the CuL complex in rat liver mitochondria, fractions containing the low molecular weight copper pool were resolved anaerobically on a Sephadex G-25 size exclusion column to potentially resolve binding of metal to protein versus non-protein metal complexes. The column was prepared for metal analysis by washing with second dimension elution buffer containing 10mM Tris, pH 7.5, 50mM NaCl, 1mM PMSF before residual metal was removed through washes in buffer containing 10mM Tris, pH 7.5, 1M NaCl and 10mM EDTA. Subsequently the column was washed with three column volumes of elution buffer and sample fractions containing the CuL complex applied. Fractions were eluted with second dimension elution buffer in 0.5ml aliquots and analysed for protein content by BSA-calibrated Coomassie assay and metal content by ICP-MS. Chromatographs shown in figure 3.10 (a) indicate that protein (filled squares) and copper (open triangles) do not co-migrate, thus, in accordance with the findings of Cobine et. al. (Cobine et al., 2004), the entity responsible for the low molecular copper pool (CuL) is not of proteinaceous nature. Metal analyses for manganese and zinc across the copper containing fractions (shown in figure 3.10 b), reveal that both metals are also not protein-bound. However, they do co-migrate with copper, which is an indication for three possible conclusions:

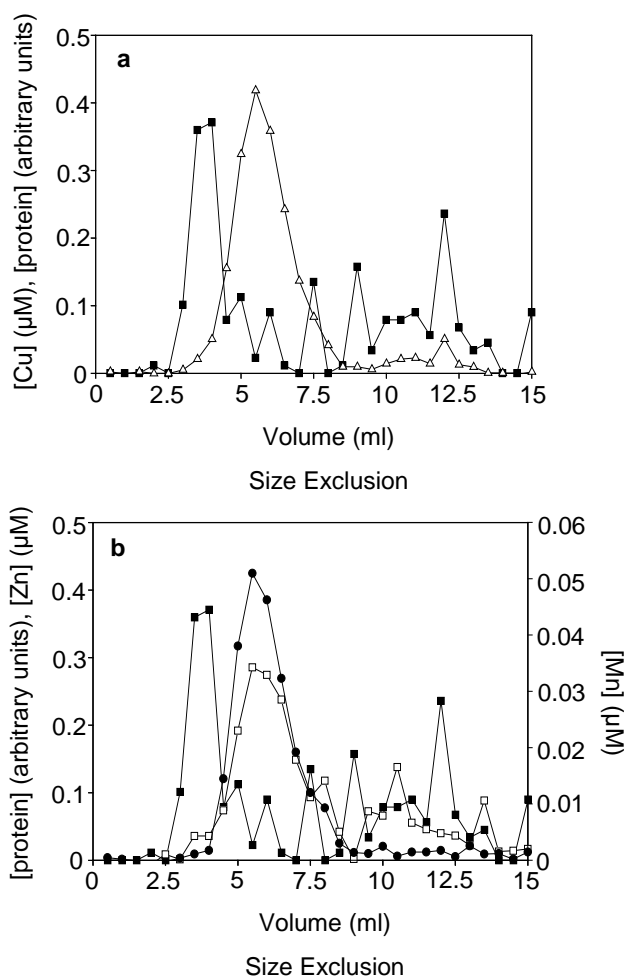


Figure 3.10: Protein analysis of the pCuL copper pool in rat liver mitochondria

Rat liver mitochondria were lysed by freeze grinding, analysed for protein content by BSA-calibrated Coomassie assay, subjected to 2D-LC as previously described and analysed for metal content (figure 3.7) by inductively coupled plasma-mass spectrometry (ICP-MS). The large low molecular weight copper pool designated pCuL (figure 3.7 a) was analysed for protein content and co-migration of protein with copper by chromatographic separation on a sepharose PD-10 size exclusion column with subsequent analysis for metals and protein by ICP-MS and BSA-calibrated Coomassie assay, respectively. Chromatographic separation (a) of copper (open triangles) and protein (filled squares) indicates that copper constituting the low molecular copper peak is not protein-bound. Analysis of metals other than copper (b) shows that neither zinc (open squares), nor manganese (filled circles) binds to protein.

Firstly, it is possible that during the experimental procedure copper, zinc and manganese were released from their protein binding sites with consequent binding to EDTA resulting in a low molecular metal – chelate complex. Secondly, the possibility exists that the CuL complex not only binds copper, but can also accommodate other metal ions. This would, however, pose the problem of providing binding sites to metals with different affinities to different metal sites, different conformations and different valencies. The third conclusion is that the CuL complex binds only copper with the elution of a manganese – EDTA - complex and a zinc - EDTA – complex at the same volume being coincidental and involving different co-migrating complexes. Besides EDTA, other organic or inorganic compounds may contribute to binding of free metal ions. Culotta et. al. (2005) report that in the yeast vacuole toxic levels of manganese are possibly chelated by phosphate groups. Thus, although copper might be bound to the CuL complex, zinc and manganese might be complexed to other low molecular weight compounds.

3.4.2 Analysis of metal binding to the copper - ligand

Cobine et. al. (Cobine et al., 2004) report fluorescence emission of yeast fractions containing the low molecular weight copper pool at 360nm upon sample excitation at 220nm. The rat liver mitochondrial fractions containing low molecular weight copper were pooled and anaerobically transferred to an acid washed Quartz cuvette fitted with a double septum anaerobic seal. Fluorescence spectra were taken on a Cary Eclipse Fluorescence Spectrometer between wavelengths 200nm-800nm. Sample measurements were controlled for by using second dimension elution buffer as blank. Figure 3.12 (a) shows sample fluorescence at 360nm (see inset for more detail) when corrected against the blank.

The metallation status (the extent of metal – saturation) of the CuL complex is unknown. It is anticipated that the low molecular weight copper pool is composed of apo- and holo – ligand and binds Cu(I) rather than Cu(II) as result of the reducing environment present in the cell. PCuL was titrated with Cu(I) using a gas – tight Hamilton syringe fitted with an automated dispenser. Refer to section 2.4.9.1 for Cu(I) stock preparation from cuprous chloride. Due to rapid disproportionation of Cu(I) to Cu(II) stocks were prepared under anaerobic conditions and all solutions purged with nitrogen before the experiment. Scans were taken after each titration,

graphs of which are shown in figure 3.12 (a). As expected, at 360nm spectra decreased in fluorescence with increasing concentrations of Cu(I). Spectral quenching was also observed by Cobine et. al. (Cobine et al., 2004) and indicates that this copper binding ligand might be the same species that was previously detected in yeast and also that it is not fully metallated. Whether this is the physiological status quo or the result of experimental displacement of metal from the ligand cannot be determined at this point. However, only small changes in fluorescence intensity were detectable, suggesting that the majority of the CuL might be metallated.

3.4.2.1 Cu(I) competition with BCS

To investigate the cause of the spectral feature at 400nm a second dimension elution buffer sample (previously representing the blank) was subjected to anaerobic titration with BCS in 2 μ M increments. The results are shown in figure 3.11 (a). As expected, increasing concentrations of BCS cause the increase in fluorescence intensity. It should be noted that the BCS spectra are at their maximum intensity at a wavelength of 420nm. The spectral feature observed at 400nm in the sample containing biological CuL extract, Cu(I) and BCS suggests that the shift of the 420nm BCS spectrum to the lower wavelength is possibly due to BCS interaction with Cu(I), rather than the CuL sample. To investigate the possibility of Cu(I) and BCS interacting without the involvement of the CuL complex, a titration of equimolar concentrations of BCS:Cu(I) in a stoichiometry of 2:1 was performed to an aliquot of second dimension elution buffer. These concentrations were chosen on the basis that BCS binds monovalent copper in a ratio of 2 molecules to 1 atom. Titrations were made simultaneously and spectra taken after thorough mixing by inversion. Spectra are shown in figure 3.11 (b). Data clearly suggest that the spectral feature observed at a wavelength of 400nm is an effect of a BCS - Cu(I) complex as opposed to solely BCS, indicating that free Cu(I) is neutralised by BCS prior to incorporation into the apo-ligand. Even at high μ M concentrations of BCS the signal at 400nm would overcome the signal released from the CuL complex and thus render it undetectable. No further analysis was performed on this copper-binding ligand.

Figure 3.11: Characterisation of putative BCS-related spectral features

Rat liver mitochondrial fractions containing low molecular copper were subjected to fluorescence spectroscopy and CuL complex-like features were observed at 360nm (figure 3.12). To investigate the fluorescence shift from 360nm to 400nm as a BCS-related spectral feature, increasing concentrations of BCS were titrated to sample buffer without sample present (a). Absorbance at 420nm is detected when excited at 220nm indicating that the shift in absorbance is caused by BCS titrations. Copper titrations coupled with BCS titrations to sample buffer without sample present (b) at a stoichiometry of 1:2 shifts the absorbance to 400nm, but does not abolish any features emitted by BCS, but does quench the absorbance intensity slightly.

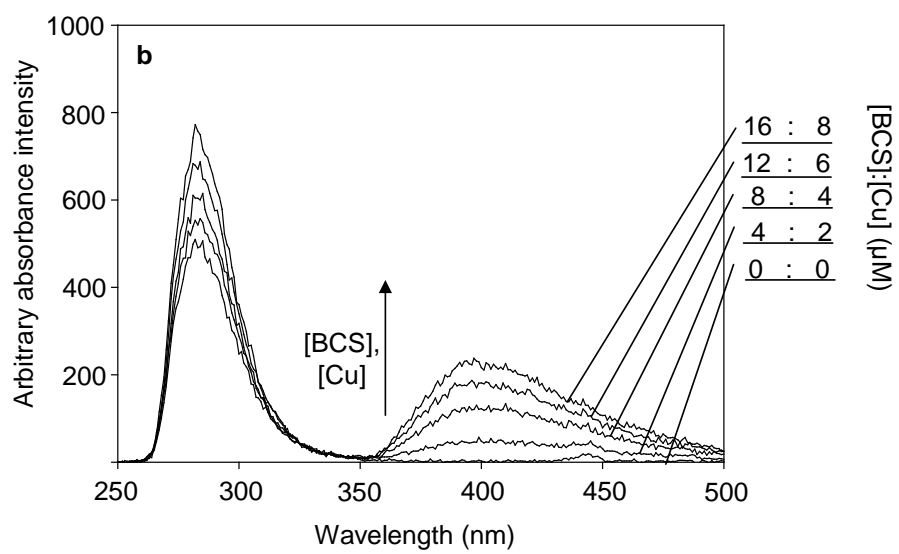
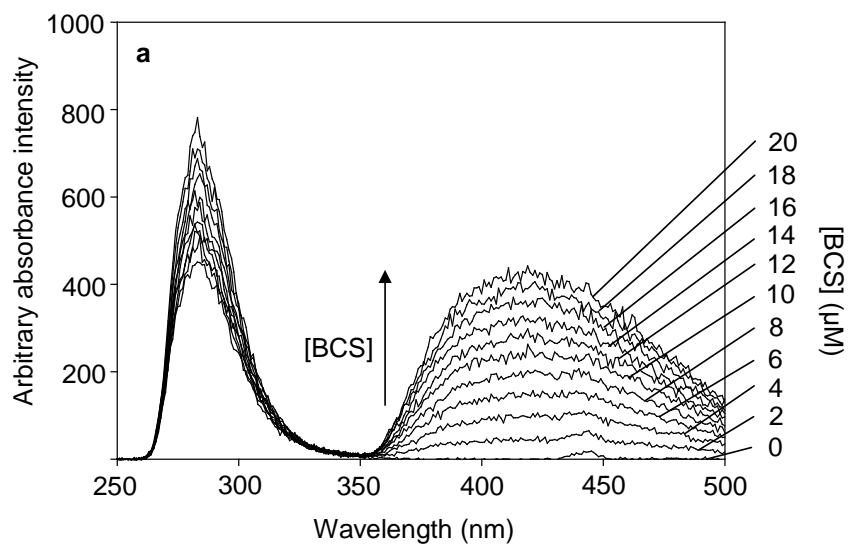
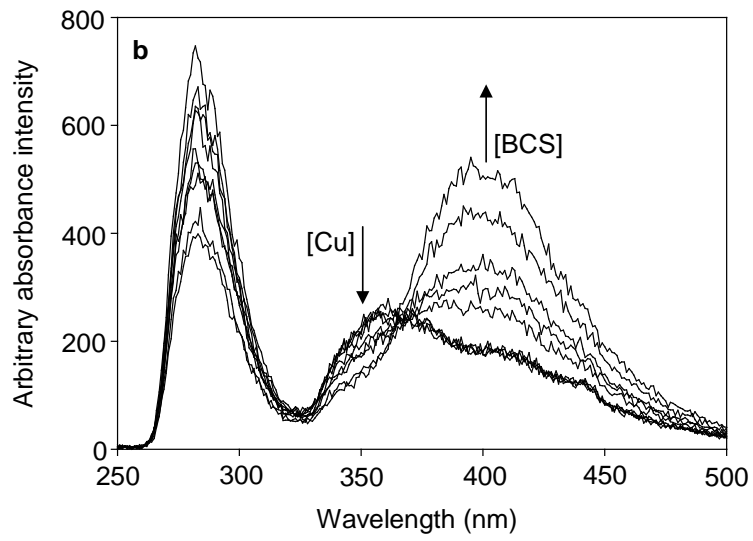
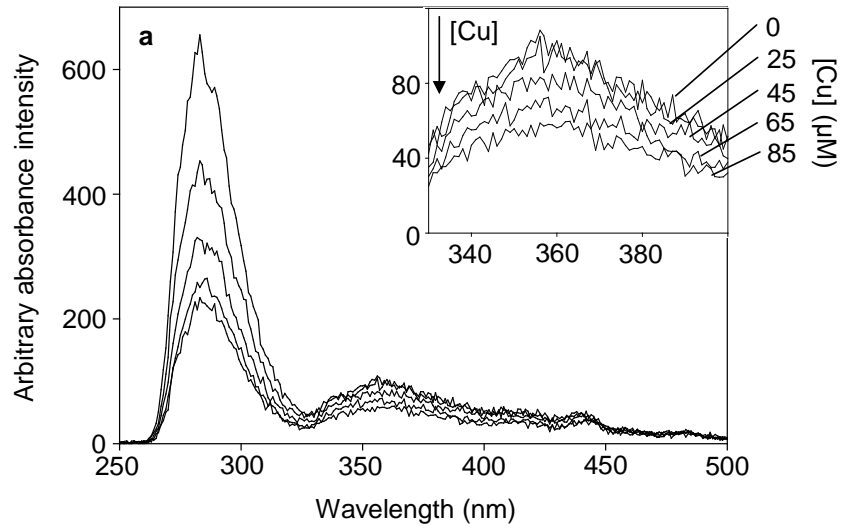


Figure 3.12: Copper binding properties of the putative low molecular copper compound pCuL

Rat liver mitochondrial protein extract was subjected to 2D-LC with subsequent analysis for copper content by ICP-MS (figure 3.7). Size exclusion fractions containing low molecular weight copper, but not protein, in the 100mM NaCl anion exchange fraction were pooled and fluorescence spectra obtained between wavelengths $\lambda_{200\text{nm}-800\text{nm}}$. The copper binding complex emits at 360nm when excited at 220nm (a). Addition of Cu(I) under anaerobic conditions quenches the spectral features (see inset for clearer representation) as previously observed by Cobine et. al. (Cobine et al., 2004). The same fractions of a duplicate mitochondrial protein extract were pooled and Cu(I) and BCS were titrated to the sample (b) resulting in a spectral shift from 360nm to 400nm. With increasing Cu(I) titrations slight quenching is visible until BCS concentrations exceed those of Cu(I).



3.4.2.2 Copper depletion of low molecular weight copper complex using the monovalent copper specific chelator BCS

To determine whether minor changes in fluorescence quenching at 360nm are a result of a high metallation status of the copper-binding ligand or rather due to the low abundance of CuL in the sample, the Cu(I) specific chelator BCS was titrated to a fresh sample of pooled CuL. As previously the sample was first titrated with increasing concentrations of Cu(I) as shown in figure 3.12 (b) at 360nm. However, when titrated with increasing concentrations of Cu(I) the sample shows hardly any quenching in fluorescence intensity. This leads to the conclusion that the ligand might be fully saturated with copper. To counteract saturation, μM concentrations of BCS were titrated to the sample. Contrary to the expected increase in fluorescence absorbance with increasing concentrations of BCS, the spectra remained unchanged at 360nm. However, a significant spectral feature appeared at 400nm which increased in fluorescence intensity upon continued titration with BCS. The appearance of this feature interfered with signal detection at 360nm rendering further analysis of the CuL copper status impossible.

3.5 Low resolution 2D-LC analysis of metal distribution in *SH-SY5Y* APP_{WT} and APP_{swe} whole cell extracts

It was reported by Arciello et. al. (Arciello et al., 2005), that *SH-SY5Y* cells cultured in increasing concentrations of CuSO_4 exhibit phenotypes of copper toxicity. Effects of high cellular copper concentrations included functional impairment and decreased protein levels of several mitochondrial dehydrogenases. It was hypothesised that toxic levels of copper mediate oxidative stress and trigger mitochondrial damage, which could possibly lead to neurodegenerative diseases (Arciello et al., 2005).

Previous analysis of rat liver mitochondrial soluble protein fraction by 2D-LC detected at least the predominant metal pools for copper, zinc, iron and manganese (see figure 3.2). Although, apart from the higher molecular weight copper association to SOD1, none of these metal pools could be attributed to a specific binding partner, the data clearly indicate the possibility of protein identification from mitochondrial fractions rather than whole cell extracts. Subsequent efforts were concentrated on mitochondrial soluble protein two dimensional separation of *SH-SY5Y* extracts of APP_{WT} and APP_{swe} cell lines to investigate changes in metal

distribution and/or binding to proteins as a result of normal cellular copper status (APP_{WT} cell line) and depleted cellular copper status (APP_{swe} cell line).

3.5.1 2D-LC metal analysis of *SH-SY5Y* APP_{WT} mitochondrial soluble protein fraction

Mitochondrial fractionation was performed on 30x150cm² flasks of 80% confluent monolayer cultures of the *SH-SY5Y* APP_{WT} cell line as described in section 2.4.8.2. Small changes to the cell lysis method were applied to compensate for the small volume of cells compared with rat liver mitochondrial extracts. Pellets were resuspended in 5ml MSE buffer supplemented with 1% (w/v) BSA and lysed by 30 strokes in a glass Elvejhem homogeniser. The homogenate was differentially centrifuged as described before for rat liver mitochondrial extracts in section 2.4.8.2. Pelleted mitochondria were resuspended in MSE buffer without BSA before centrifugation and final aspiration. Mitochondrial extracts were subjected to 2D-LC under anaerobic conditions as described previously in sections 2.4.3.2 and 2.4.3. Subsequent multi-elemental analysis by ICP-MS is shown in figure 3.14. displayed as 2-dimensional contour plots for copper (a), zinc (b), manganese (c), iron (d), and cobalt (e).

When compared to the metal analysis for the whole cell soluble protein extract shown in figure 3.4, it becomes apparent, that most of the higher molecular weight metal pools disappeared, while the low molecular weight metal pools remain nearly unchanged (figure 3.14). This can be best observed for copper with the disappearance of the metal pools previously present in the 100mM and 200mM anion exchange fractions and for zinc in the 100mM, 300mM and 400mM anion exchange fractions. It must be noted, however, that the previously observed trace contamination in the iron analysis has diminished and instead a very abundant iron pool can be detected in the 200mM anion exchange fraction.

The most remarkable change in metal distribution between APP_{WT} whole cell and APP_{WT} mitochondrial soluble protein extracts is the elimination of the co-migrating copper and zinc pools in the 100mM exchange fraction which was previously identified as SOD1 from rat liver mitochondrial extracts. This change in copper and zinc pools might be attributed to localisation differences of SOD1 to the mitochondria in rat liver or the cytoplasm in *SH-SY5Y* cells due species variation.

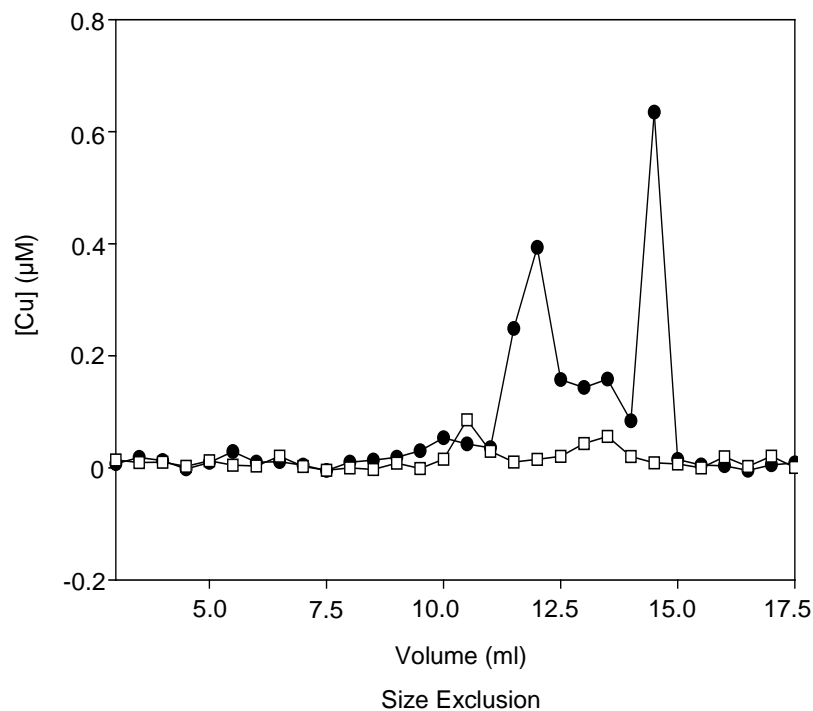
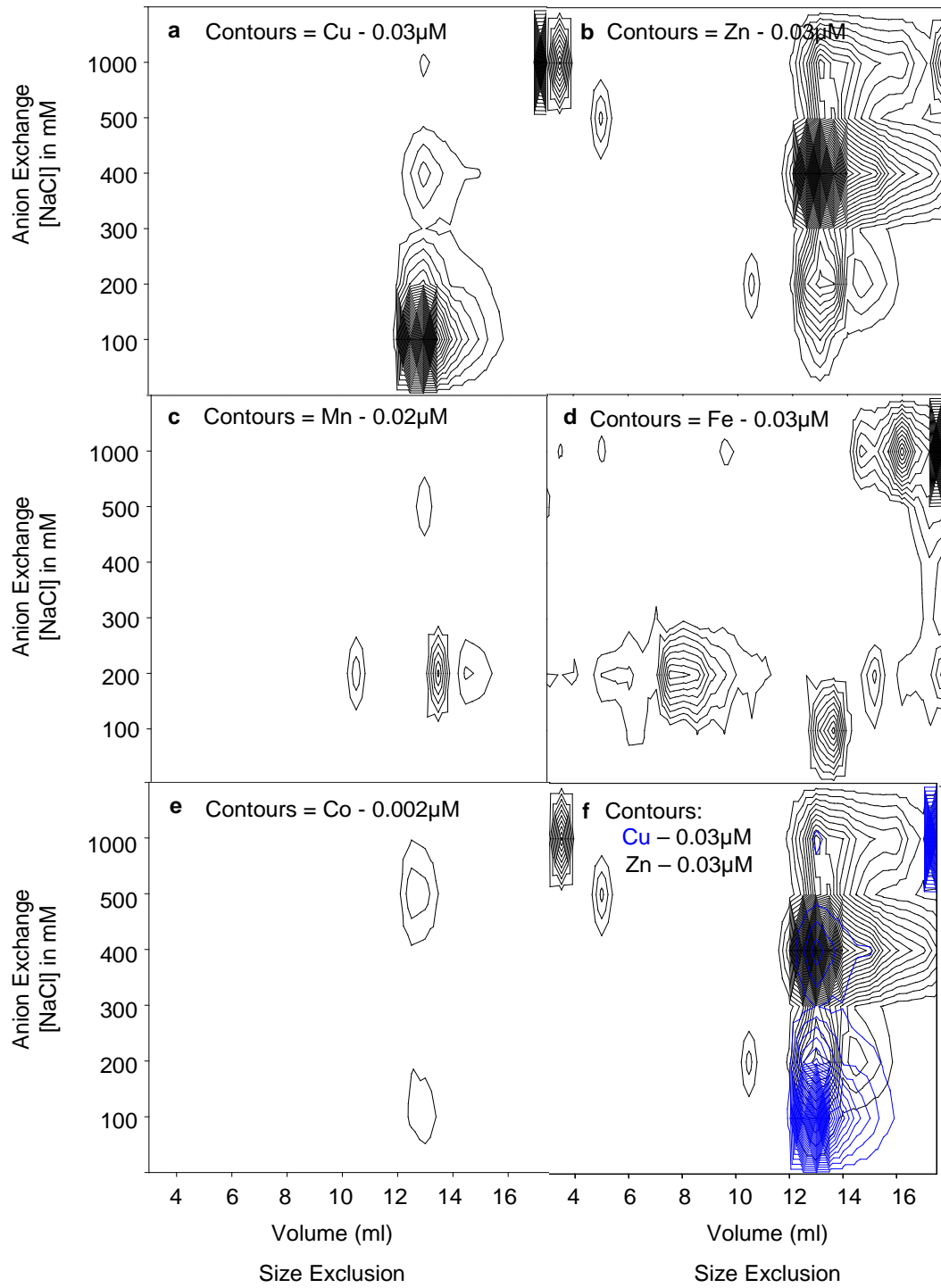


Figure 3.13: Comparison of metal elution upon loading of different protein concentrations on an anion exchange column performed on rat liver mitochondrial protein extracts

Rat liver mitochondria were extracted as described in section 2.4.8.2. Aliquots containing 4mg (open squares) and 40mg (filled circles) of mitochondrial protein extract were loaded onto HiTrap Q HP anion exchange columns at 0.3ml min^{-1} and eluted in 1ml of 50mM Tris, pH 8.8, 1mM PMSF buffer containing 100mM NaCl. Aliquots (0.2ml) of each eluant were resolved by size exclusion chromatography on a Tosoh TSK SW3000 HPLC column and eluted in 10mM Tris pH 7.5, 50mM NaCl, 1mM PMSF at 0.5ml min^{-1} . Fractions were collected every minute for 30 minutes and analysed for copper by ICP-MS.

Figure 3.14: 2D-LC fractionation of metal pools in *SH-SY5Y* APP_{WT} soluble mitochondrial protein extract

Soluble mitochondrial protein extract was prepared from 30x150cm² flasks of 80% confluent APP_{WT} monolayer culture using an adjusted extraction method described in section 2.4.8.2. The soluble protein fraction was extracted by freeze grinding and sequential centrifugation as described in sections 2.4.3.1 and after BSA-calibrated protein estimation subjected to 2D-LC (see sections 2.4.3.2 and 2.4.3.3). First the sample was concentrated on a 1ml HiTrap Q HP anion exchange column. Fractions were eluted in extraction buffer (50mM Tris, pH 8.8, 1mM PMSF) containing increasing concentrations of NaCl (0mM, 100mM, 200mM, 300mM, 400mM, 500mM, 1,000mM). Aliquots (0.2ml) of each anion exchange fractions was subjected to high performance liquid chromatography on a Tosoh TSK SW3000 size exclusion column in 10mM Tris, pH 7.5, 50mM NaCl, 1mM PMSF at a flow rate of 0.5ml min⁻¹. Samples were collected every minute for 30 minutes and analysed for metals by inductively coupled plasma-mass spectrometry standardised to standard metal solutions as described in section 2.4.3.4. Results are shown for (a) copper (contours represent 0.03µM increments), (b) zinc (contours represent 0.03µM increments), (c) manganese (contours represent 0.02µM increments), (d) iron (contours represent 0.03µM increments), (e) cobalt (contours represent 0.002µM increments), and (f) copper (blue) and zinc (black) (contours represent 0.03µM increments).



However, it is very likely to be an artefact of experimental variation between the two dimensional separations. It has to be noted that 70mg of rat liver mitochondrial and whole cell *SH-SY5Y* soluble protein were concentrated onto the first dimension anion exchange column, whereas the accessible soluble protein content of *SH-SY5Y* mitochondria was merely 4mg. The relevance of the amount of protein subjected to the 2D-LC procedure is measured by comparing metal analyses of a protein separation using 4mg and 40mg of the exact same rat liver mitochondrial extract. Figure 3.13 shows the results of copper analysis of the size exclusion fractions obtained from the 100mM anion exchange fraction. The metal pool for SOD1 previously resolved at a volume of 10ml, which coincides with a 0.1 μ M copper peak at 10ml for the 40mg protein separation (filled circles) and 10.5ml for the 4mg protein separation (open squares). Discrepancies in co-localisation of both copper peaks are a result of the second dimension chromatography. Although, the abundance of copper is nearly identical in the fractions containing SOD1 for both extracts, later experiments were performed with whole cell soluble protein extracts for *SH-SY5Y* cell lines to guarantee meaningful metal analysis across all anion exchange fractions.

Comparison of zinc and copper abundance in the individual metal pools identified to bind SOD1 and shown in figure 3.2 and figure 3.4 indicates that upon resolution of the same amount of protein on the first dimension column the abundances of copper and zinc between the two species vary by more than two-fold. The abundance of metal in the putative *SH-SY5Y* SOD1 pool is higher than those in rat liver mitochondria for both metals.

3.5.2 2D-LC metal analysis of *SH-SY5Y* APP_{WT} and APP_{swe} soluble whole cell protein

Previous studies (Treiber et al., 2004) imply that APP might be involved in cellular copper homeostasis by supporting copper efflux from the cell. However, the role of APP in copper transport and direction of transport or in fact its influence on efflux or influx due to it binding copper in the extracellular domain is still unknown and further studies are necessary to assess APP-dependent cellular copper status. To assess the role of APP in copper homeostasis *SH-SY5Y* APP_{WT} and APP_{swe} cell lines were compared to detect any changes in copper abundance in whole cell

extracts that were subjected to 2D-LC and possible changes in copper distribution due to increased or decreased copper availability to protein species. It is noted that the APP_{WT} cell line has endogenous APP levels, whereas the APP_{swe} cell line overexpresses the Swedish mutation in the APP_{WT} cell line. Thus any contribution of APP to, for example, copper efflux could be altered in the APP_{swe} cells due to enhanced production of A β due to increased cleavage and APP expression (Citron et al., 1992).

APP_{WT} and APP_{swe} cell lines were subjected to 2D-LC in triplicate experiments. Both cell lines were grown simultaneously and growth conditions monitored to enable direct comparison between extracts. Due to the large number of cells used for the extraction process (30x150cm² flasks per extract) cell culture medium from different bottles, but the same production batch were used. Supplementation was performed with standard volumes of foetal calf serum, antibiotics and glutamate. However, the possibility of slight substrate variation from bottle to bottle remains. Cultures were harvested and washed several times in D-PBS to remove residual metals from the cell surface. Cell lysis was performed and protein extracts prepared as described in section 2.4.3.1. Following BSA-calibrated protein content analysis of each extract, 70mg of protein were resolved on a HiTrap Q HP anion exchange column under anaerobic conditions and eluted in buffer containing 50mM Tris, pH 8.8, 1mM PMSF and increasing concentrations of NaCl. The effectiveness of first dimension separation of protein is portrayed in figure 3.15, showing different amounts of protein being eluted in different salt concentrations. An aliquot (0.2ml) of each anion exchange eluant was transferred to a high pressure liquid chromatography column further separating proteins on the basis of their molecular weight with high molecular weight species being eluted after the column void volume and low molecular weight species before total column volume. Samples were eluted in 10mM Tris, pH 7.5, 50mM NaCl and 1mM PMSF for 30 minutes at a flow rate of 0.5ml min⁻¹. Samples were analysed for copper and zinc by ICP-MS. Metal content of fractions post gel filtration chromatography of anion exchange fractions is shown in figure 3.16; only the most representative replicate for each cell line is shown. Copper and zinc pools are observed in the 100mM anion exchange fractions in APP_{WT} and APP_{swe} cell lines which have similar chromatographic properties to SOD1 in rat liver mitochondria, volume 9-12ml (see figure 3.7).

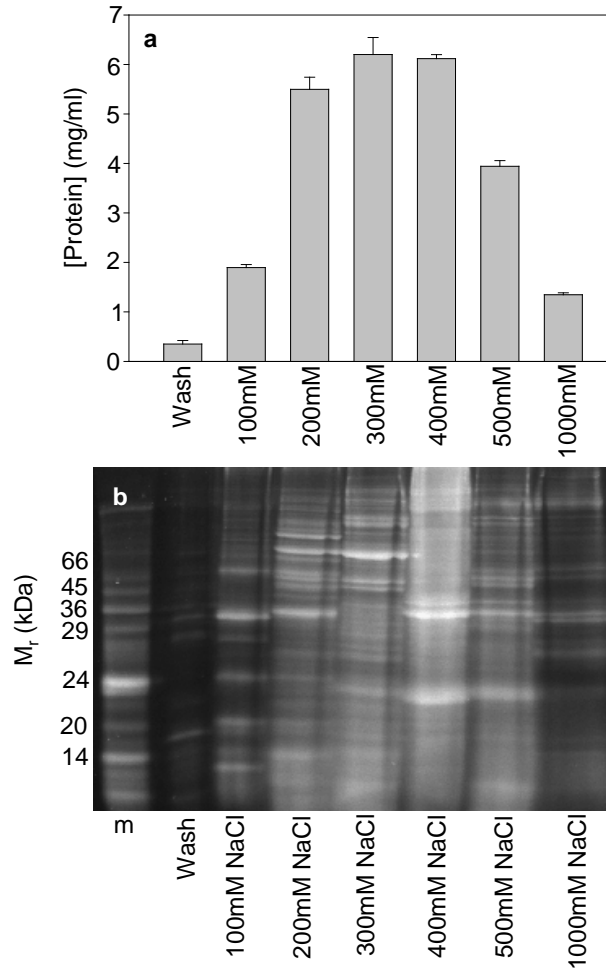


Figure 3.15: Protein content of *SH-SY5Y* APP_{WT} whole cell extract after first dimension liquid chromatography

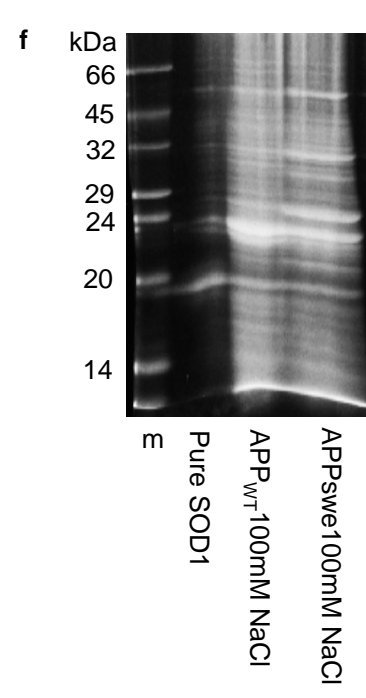
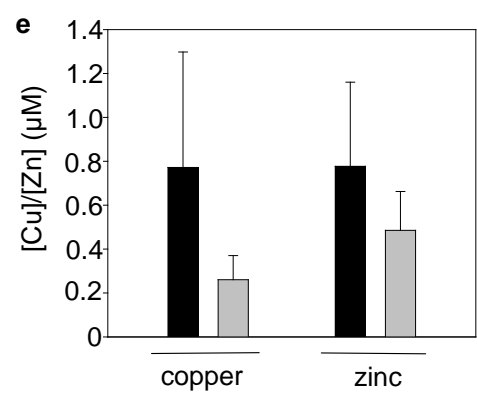
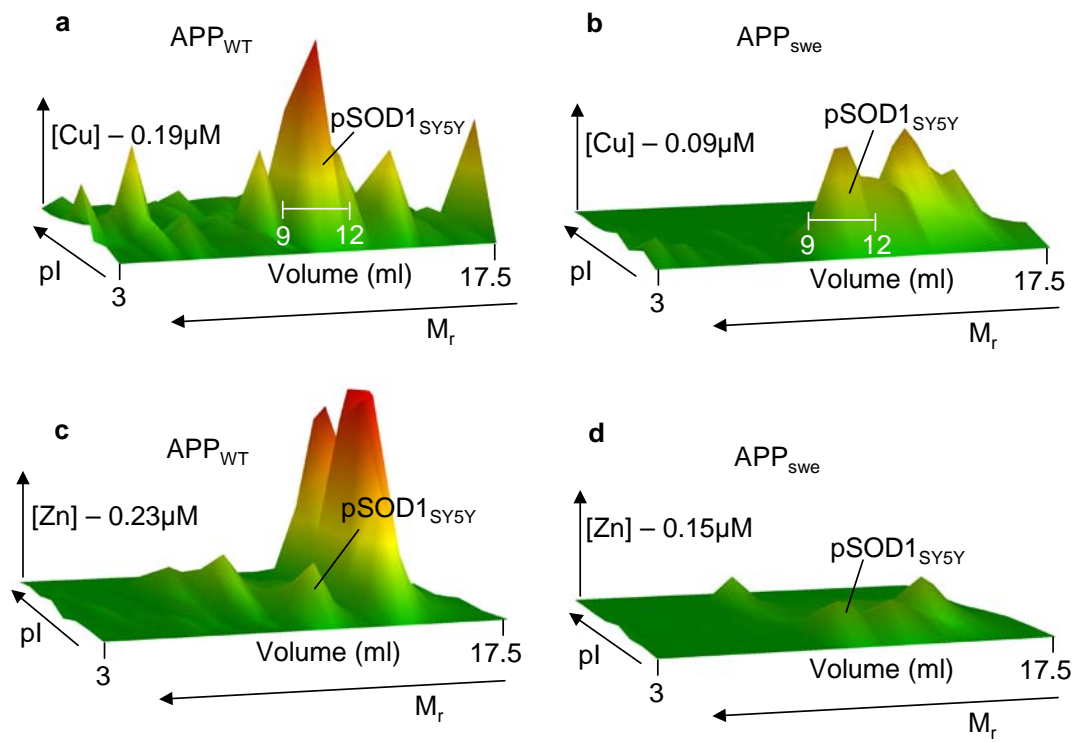
Whole cell extracts of *SH-SY5Y* APP_{WT} (30x150cm² flasks of 80% confluent monolayer culture) were prepared for 2D-LC as described in section 2.3.4.1 and concentrated on a 1ml HiTrap Q HP anion exchange column. Samples were eluted with 1ml buffer (50mM Tris, pH 8.8, 1mM PMSF) containing increasing concentrations of NaCl (0mM, 100mM, 200mM, 300mM, 400mM, 500mM, 1,000mM). Protein content of each sample (a) was determined by BSA-calibrated Coomassie assay. Error bars represent standard deviation from triplicate measurements. Aliquots (50μl) of the anion exchange samples were resolved on a 15% (w/v) SDS-PAGE gel (b) and stained with Sypro Ruby. Individual pools of protein are detectable in the various salt concentrations suggesting that anion exchange is representative for a first dimensional separation step.

Figure 3.16: Comparison of copper and zinc pools in whole cell extracts of *SH-SY5Y* APP_{WT} and APP_{swe}

Whole cell protein extracts were prepared from 30x150cm² flasks of 80% confluent monolayer cultures as described in section 2.4.3.1. After BSA-calibrated protein estimation of each extract equal amount of protein were concentrated on a 1ml HiTrap Q HP anion exchange column and eluted with 1ml buffer (50mM Tris, pH 8.8, 1mM PMSF) containing increasing concentrations of NaCl (100, 200, 300, 400, 500 and 1,000mM). Aliquots (0.2ml) of each salt fraction were resolved on a Tosoh TSK SW3000 high performance size exclusion chromatography column at 0.5ml min⁻¹. Samples were collected every minute for 30 minutes and analysed for copper and zinc content by inductively coupled plasma-mass spectrometry (ICP-MS). 2D-LC was performed in independent triplicate for both APP_{WT} and APP_{swe} and the most representative replicate shown. Whole cell metal pools are visualised on 3-dimensional plots representing the relative metal content for (a) APP_{WT} copper, (b) APP_{swe} copper, (c) APP_{WT} zinc and (d) APP_{swe} zinc. All plots are on the same scale (z-axis showing metal concentration) for one particular metal to allow for direct comparison. pSOD1_{SY5Y} is presumed to be SOD1. Bars on panels (a) and (b) depict sample eluants that were further analysed by SDS-PAGE in figure 3.17. Metal content analysis indicates that there is less copper and zinc in the putative SOD1 peak in the *SH-SY5Y* APP_{swe} cell line.

e) Copper and zinc peaks represented in a) and c) and presumed to contribute to SOD1 activity were compared for metal concentration. Total metal content for zinc and copper was determined by integration of all values under the peak labelled pSOD1_{SY5Y}. *SH-SY5Y* APP_{WT} (black) and *SH-SY5Y* APP_{swe} (grey) are shown. Error bars represent standard deviations from triplicate measurements of three independent whole cell protein extracts.

f) Aliquots (100µl) of 100mM NaCl anion exchange eluant were resolved on a 15% (w/v) SDS-PAGE gel and stained with Sypro Ruby. Anion exchange chromatography was performed with the same amount of protein (70mg) for both cell lines. An equal amount of pure SOD1 was loaded as control.



This metal pool, designated pSOD1_{SY5Y} was further analysed to identify the binding partner for both metals. Metal concentrations are displayed on the same scale to allow for direct comparison for each individual metal. Phenotypic differences in metal content in the pSOD1_{SY5Y} peak for copper and zinc are detectable. The APP_{swe} cell line contains half the amount of copper compared to the APP_{WT} cell line and roughly a third less zinc in this particular replicate. Figure 3.16 (e) shows data for metal analysis of both cell lines across the pSOD1_{SY5Y} peak produced by integrating the concentrations of copper and zinc for all three replicates and calculating the average. Results indicate that the protein species responsible for the pSOD1_{SY5Y} peak is less metallated with copper (50%) and zinc (30%) in the APP_{swe} cell line. Copper – zinc superoxide dismutase acquires a zinc ion before accepting copper metallation by its metallochaperone CCS (Field et al., 2003), thus in accordance with the data the reduced copper status in APP_{swe} cells follows a reduced level of metallation with zinc. To further test the possibility of differences in metallation, an aliquot (100µl) of 100mM anion exchange fraction of APP_{WT} and APP_{swe} was resolved on an SDS-PAGE gel. Bands co-migrating with the control of pure SOD1 at a molecular weight of 20kDa show the same intensity after staining with SYPRO Ruby, indicating that following initial protein estimation of whole cell soluble extracts the same amount of protein was subjected to resolution on anion exchange column. However, the identity of the ligand binding copper and zinc in fractions across 9-12ml of size exclusion elution remains to be established.

3.5.3 Identification of SOD1 in *SH-SY5Y* APP_{WT}

To identify the protein species binding copper and zinc in the pSOD1_{SY5Y} peak, fractions spanning these metal pools were resolved on SDS-PAGE and band intensity determined by densitometric analysis using BioRad Quantity One software. The SDS-PAGE gel for samples being subjected to one size exclusion column is shown in figure 3.17 (a). The corresponding chromatograph (figure 3.17 b) suggests that the relative intensity of one particular protein species correlates with the distribution of copper and zinc across the analysed fractions. Principal Component Analysis reveals pSOD1_{SY5Y} as potential copper and zinc ligand, which is indicated by clustering of the protein with copper and zinc (figure 3.18 a and b). To increase sample resolution in the second dimension size exclusion

chromatography was repeated with two size exclusion columns fitted in sequence generating a larger number of eluted fractions. However, sequential resolution on two size exclusion column decreases copper, zinc and protein concentrations in each individual sample. This might cause protein levels to fall below the detection limit of the SYPRO Ruby gel stain on subsequent SDS-PAGE. Samples subjected to resolution on two size exclusion columns fitted in sequence were analysed for copper and zinc by ICP-MS and SDS-PAGE gel for protein. The gel and chromatograph are shown in figure 3.17 (c) and (d) and again indicate one protein species correlating with the metal peaks. Principal Component Analysis identifies one protein as best candidate to match the distribution and intensity of copper and zinc across the analysed fractions. The relevant protein band was excised and analysed by MALDI - TOF - MS as was previously done with the band identified as best candidate to bind copper and zinc in rat liver mitochondria. However, after several attempts no identification could be achieved due to low abundance of the protein. Comparing the rat liver mitochondrial SDS-PAGE gel (figure 3.7) showing a protein band which was clearly identified as SOD1 at a molecular weight of 20kDa with the gels generated from APP_{WT} samples that were resolved on single - and double size exclusion columns, it is highly likely that the copper and zinc pools in APP_{WT} are also generated by SOD1. Both protein species migrate at the same molecular weight, both co-migrate with copper and zinc and there is the indication of diminished metallation in the same metal pools in APP_{swe} cells.

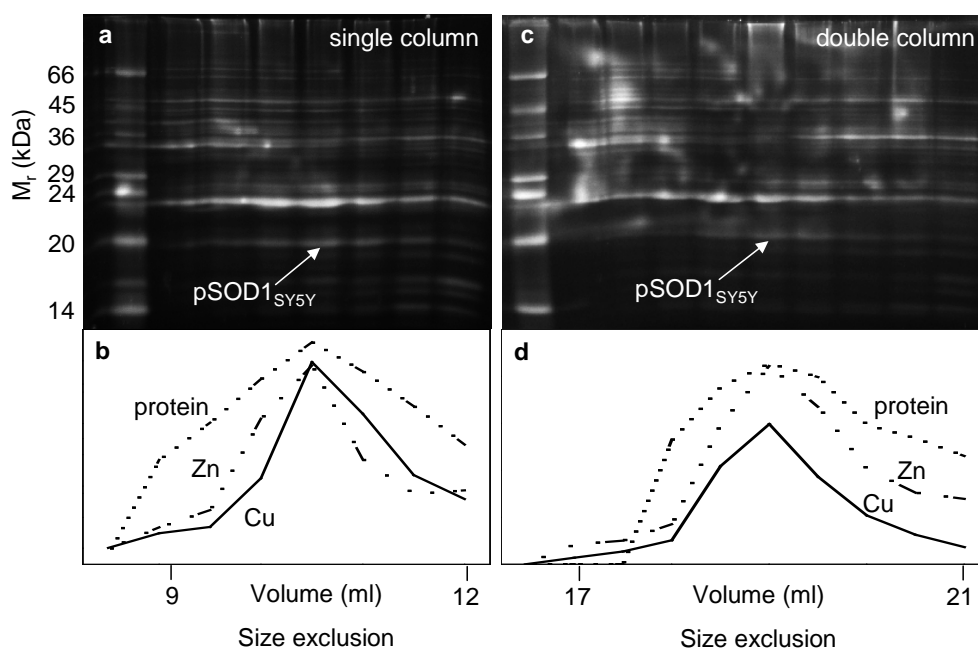


Figure 3.17: SDS-PAGE analysis of *SH-SY5Y* APP_{WT} 2D-LC fractions

Whole cell protein extracts were subjected to 2D-LC and analysed for metals by ICP-MS (figure 3.16). Aliquots (130 μ l) of 100mM NaCl size exclusion fractions containing copper and zinc (figure 3.16) were resolved on a discontinuous 15% (w/v) SDS-PAGE gel (a and c) and analysed for protein distribution in each fraction using BioRad quantity one software. Due to high gel complexity size exclusion of the 100mM NaCl anion exchange fraction was performed using one HPLC Tosoh TSK SW3000 size exclusion column (a) and two SW3000 columns (c) in sequence to allow for better protein resolution. The corresponding chromatographs of copper (solid line), zinc (long dashed line) and relative protein density (short dashed line) obtained from densitometric analysis of protein staining are shown for single column size exclusion (b) and sequential column size exclusion (d). The protein referred to as pSOD1 was identified from the SDS-PAGE gel as best possible match for the copper and zinc pools obtained through ICP-MS by using PCA to correlate the distribution and concentration of zinc and copper to the proteins resolved on the gel.

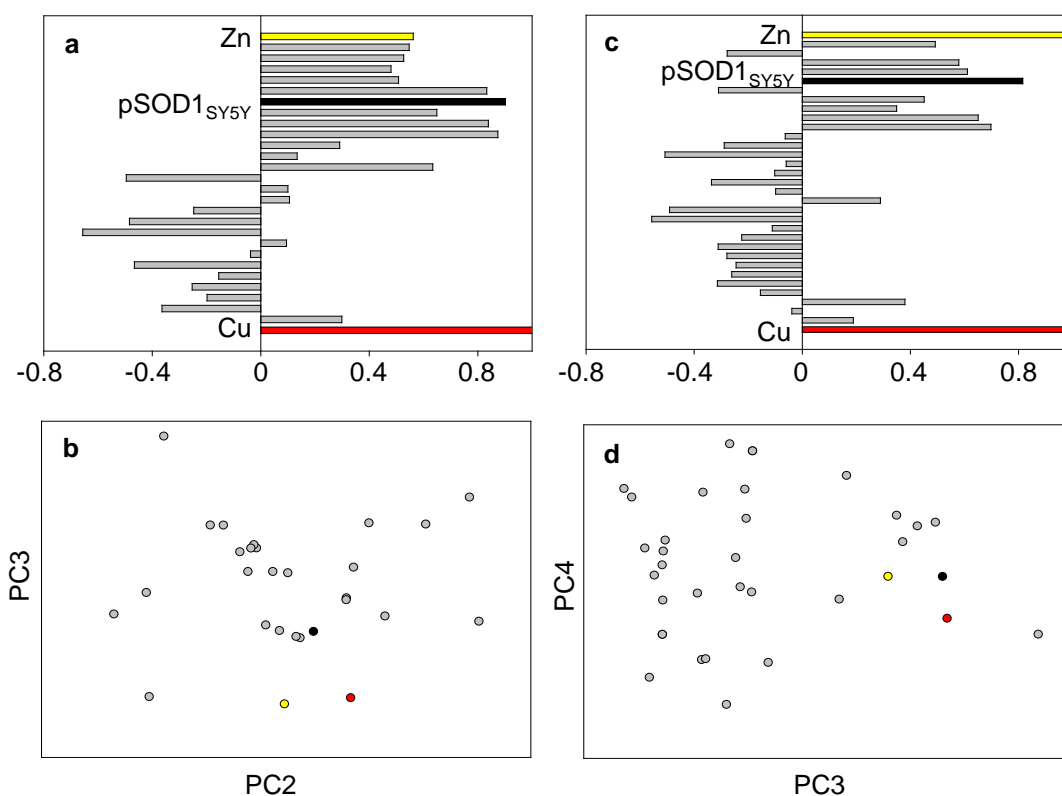


Figure 3.18: Principal component analysis to predict protein binding to copper and zinc

Aliquots (130 μ l) of 100mM NaCl size exclusion fractions containing copper and zinc (figure 3.16) were resolved on a discontinuous 15% (w/v) SDS-PAGE gel (a and c) and analysed for protein distribution in each fraction using BioRad quantity one software. SDS-PAGE gels were prepared for samples subjected to single and sequential size exclusion columns (figure 3.17). Data for copper, zinc and protein chromatographs was used to calculate the principal components (see section 2.4.10.2) for this data set. Correlation analysis for single column (a) and double column (c) indicate protein pSOD1_{SY5Y} as best match with regards to copper, zinc and protein distribution across the size exclusion fractions analysed by SDS-PAGE. Comparing various principal components (b and d) the putative SOD1 protein clusters closely with copper and zinc indicating that this protein is likely to bind both metals.

3.6 Comparative analysis of enzymatic activity of copper binding enzymes in *SH-SY5Y* APP_{WT} and APP_{swe}

Several studies have shown that the Swedish mutation of APP is processed more readily by BACE1 rather than α – secretase (Citron et al., 1992, Scheuner et al., 1996), thus not only generating increased levels of extracellular plaques due to increased release of A β , but also an intracellular copper deficiency which has been correlated with aiding the efflux of copper out of the cell (Maynard et al., 2002, Bush et al., 2003). To clarify whether limitations in intracellular copper availability affect enzymatic activity of copper – dependent enzymes, activity assays were performed for the major cytosolic antioxidant enzyme SOD1 and cytochrome c oxidase. Both are crucial to cell survival with regards to defence against oxidative stress inducing oxygen species and provision of energy as well as generation of mitochondrial membrane gradients involved in energy production. It was reasoned that results of activity assays would provide an insight to the differences in enzyme activity between APP_{WT} and APP_{swe} cell lines under normal culture conditions. Additional experiments also investigated the effect of surplus extracellular copper and intracellular copper limitation by addition of increasing concentrations of copper to the cell culture medium of both strains or by chelation of copper from the medium using the copper specific chelator BCS, respectively. Again it must be noted that data for the APP_{swe} cell line might in part reflect the effects of basic endogenous levels of APP_{WT}.

3.6.1 In-gel SOD activity assay

To test the prediction that the copper and zinc pools in the APP_{WT} 100mM anion exchange fraction are ligands to SOD1, an in-gel SOD1 activity assay was performed. Equal volumes of duplicate samples of the 100mM anion exchange fraction of both APP_{WT} and APP_{swe} cell lines were resolved on a discontinuous 15% (v/v) native PAGE gel under omission of SDS from the gel and the running buffer. In contrast with the method described by Beauchamps and Fridovich (Beauchamp and Fridovich, 1971) riboflavin was omitted from the gel and only introduced during the process of soaking the gel with the substrates required for the activity assay. Including riboflavin in the native gel previously resulted in a colour change from light yellow to purple, too vivid to detect any SOD1 related features.

Figure 3.19: Comparison of whole cell SOD1 activity in *SH-SY5Y* APP_{WT} and APP_{swe} using an in-gel activity assay

Whole cell protein extracts for *SH-SY5Y* APP_{WT} and APP_{swe} were prepared as described in section 2.4.3.1 and concentrated on a HiTrap Q HP anion exchange column at 0.3ml, min⁻¹. Samples were eluted in 1ml of 50mM Tris, pH 8.8, 1mM PMSF buffer containing 100mM NaCl. Aliquots (0.2ml) of each 100mM fraction were further resolved on a Tosoh TSK SW3000 size exclusion chromatography column at 0.5ml min⁻¹. Samples were collected every minute for 30 minutes and analysed for copper and zinc by ICP-MS.

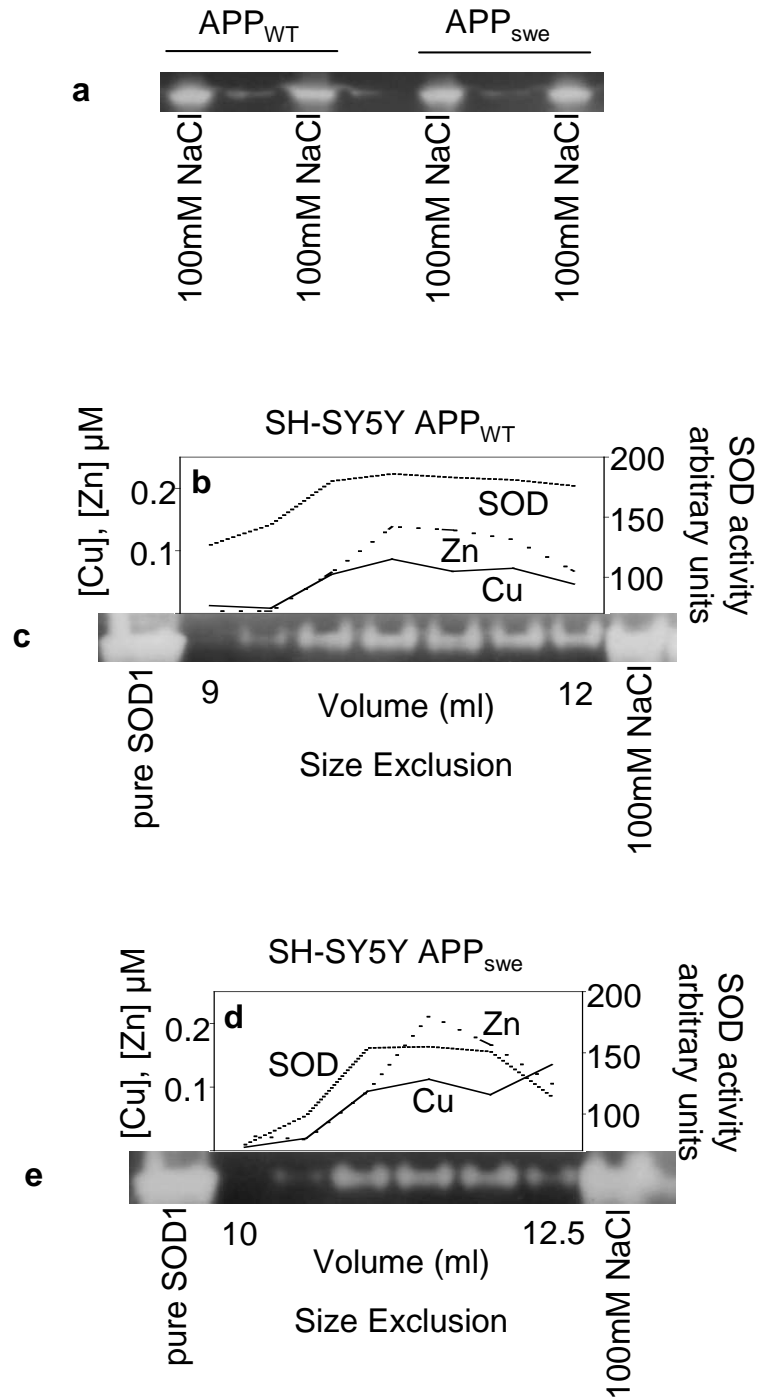
a) Equal aliquots of the 100mM NaCl anion exchange fractions and 2x native loading dye (50µl) were loaded onto a discontinuous 15% (w/v) native polyacrylamide gel and resolved for 2 hours at 100V. Subsequently the gel was prepared for the activity assay as described in section 2.4.7.2.2. *SH-SY5Y* APP_{WT} and APP_{swe} were analysed for SOD1 activity in duplicate. The comparison of AP_{WT} and APP_{swe} samples does not indicate any difference in SOD1 activity between the cell lines.

b) Aliquots of *SH-SY5Y* APP_{WT} samples obtained through 2D-LC as described in sections 2.4.3.2 and 2.4.3.3 were analysed for copper and zinc by ICP-MS. The graph shows matching distributions of copper and zinc across sample fractions and with the relative SOD1 activity, which was analysed by densitometric measurements and is displayed as arbitrary units of SOD1 activity.

c) Aliquots (50µl) of *SH-SY5Y* APP_{WT} samples obtained through anion exchange chromatography followed by size exclusion chromatography were resolved on a discontinuous 15% (w/v) native polyacrylamide gel and treated as described above. Pure SOD1 (20µl) and a sample the 100mM anion exchange fraction were used as a loading control.

d) ICP-MS analysis of *SH-SY5Y* APP_{swe} for copper and zinc indicates that both metals match the distribution of SOD1 activity across protein fractions.

e) The same procedure as described above was applied to *SH-SY5Y* APP_{swe}. The activity gel shows SOD1 activity across fractions obtained through 2D-LC.



Following electrophoresis the gel was soaked in 2.45mM NBT and a solution containing 28mM TEMED, 28 μ M riboflavin and 36mM potassium phosphate. The exact procedure is described in section 2.4.7.2.2 and a schematic representation of chemical processes is shown in figure 2.3. The two – step chemical reaction was initiated by illumination of the gel and SOD1 activity was observed as white bands on a purple background. SOD1 activity in APP_{WT} and APP_{swe} cell lines is depicted in figure 3.19 (a) suggesting that SOD1 is present in the 100mM salt fraction of both cell lines. Due to signal saturation it is not possible to determine any differences in enzyme activity. The assay was repeated with the second dimension size exclusion fractions which contained the copper and zinc pools proposed to bind SOD1, at volume 9-12ml. Figure 3.19 (c) and (e) illustrate activity gels for APP_{WT} and APP_{swe}, respectively. Data obtained by densitometric analysis of relative band intensity across the resolved fractions was compared to copper and zinc chromatographs and indicates a strong co-migration pattern. The data clearly suggest that the metal pool is generated by SOD1. Densitometric data for SOD1 activity suggests that there is slightly more activity in the APP_{WT} cell, line although the chromatograph shows signs of saturation.

3.6.2 Spectrophotometric analysis of SOD1 activity

In order to obtain absolute rather than relative data for SOD1 activity, liquid assays using the xanthine/xanthine oxidase system were performed. The assay works on the basis of xanthine being oxidised to uric acid by xanthine oxidase under aerobic conditions resulting in the release of anionic superoxide. Superoxide in turn reduces oxidised cytochrome c triggering an increase in absorbance intensity when measured at a wavelength of 550nm in a spectrophotometer. Superoxide dismutase prevents this cytochrome c reduction by sequestration of superoxide radicals and dismutation to hydrogen peroxide. Thus enzyme activity is measured as the lack of increasing absorbance intensity.

Whole cell soluble protein extracts of APP_{WT} and APP_{swe} were prepared using a modified extraction method as specified in section 2.4.7.2.3. Cultures were supplemented with increasing concentrations of copper and grown for another 24 hours before being harvested at 80% confluency. BCS supplemented cells were grown at respective BCS concentrations of 5 μ M, 10 μ M, 20 μ M, 25 μ M, 50 μ M and

100 μ M for four generations to limit intracellular copper. All solutions used to passage BCS supplemented cultures were supplemented with BCS at the appropriate concentrations to prevent introduction of copper throughout the passaging procedure. Attempts were made to culture copper supplemented cells for four generations as was done with BCS supplemented cultures to control for the unequal number of passages, which might result in increased antioxidant status due to stress during the passaging process. All cell culture solutions were supplemented with copper. However, during the first passage it was observed that cells and copper pelleted during centrifugation, thus increasing the copper concentrations from generation to generation until toxic levels of copper were achieved. No direct comparison of SOD1 activity in control cultures (not supplemented with either copper or BCS) of APP_{WT} and APP_{swe} cell lines is possible. Therefore data are shown as individual replicates and not as the average of triplicate experiments. Further replicates are shown in appendix 1 figures 5.1 and 5.3 for copper supplemented cultures and appendix 1 figures 5.2 and 5.4 for BCS supplemented cultures.

Cell pellets were obtained from one 150cm² flask per sample and resuspended in 420 μ l of 50mM phosphate buffer, pH 7.8 and 120 μ l of 10% (w/v) SDS. Following incubation at 37°C for 30 minutes the sample was cooled and 60 μ l of 3M KCl added. After further incubation intact cells were pelleted and the supernatant analysed for protein content by BSA – calibrated Coomassie assay. A fresh SOD1 standard curve was prepared on the day of the experiment to control for differences in absorbance readings that arise from mechanical variation and prolonged use of the spectrophotometer. Pure SOD1 extracted from human erythrocytes was added to the working solution in 0.5 unit increments up to 3 units SOD activity. Reactions for the standard curve were also supplemented with 60 μ l of the 300mM KCl, 2% (w/v) SDS, 35mM phosphate buffer mixture, which was used for sample extraction, to control for any differences in absorbance arising from reaction components other than cytochrome c. Spectra for both cell lines, whether supplemented with copper or BCS, were taken for half an hour using 100 μ g of protein per measurement and the reaction initiated by addition of 50 μ M xanthine. Data displayed in figure 3.20 shows SOD1 activity in copper supplemented APP_{WT} (a) and APP_{swe} (b) cell lines. Direct comparison of control samples is not possible due to different standard

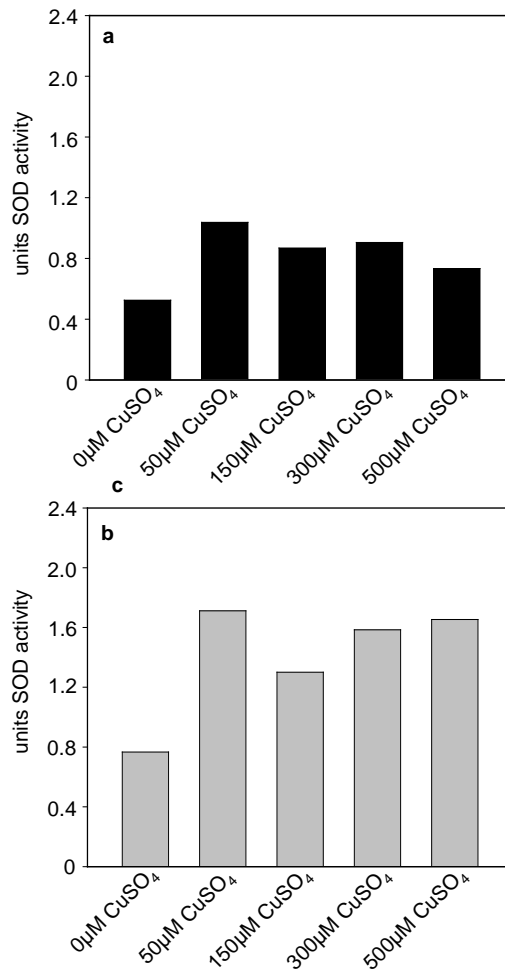
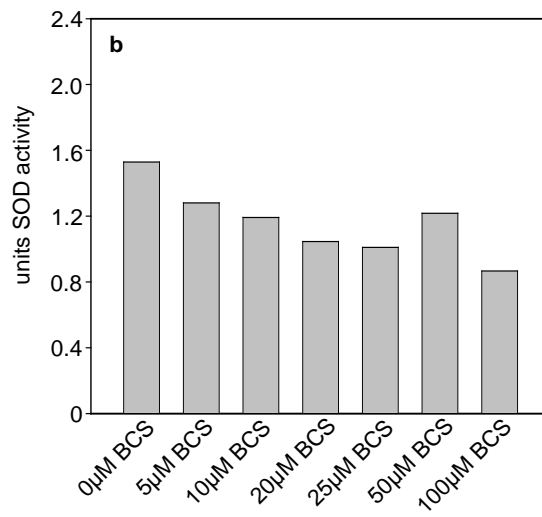
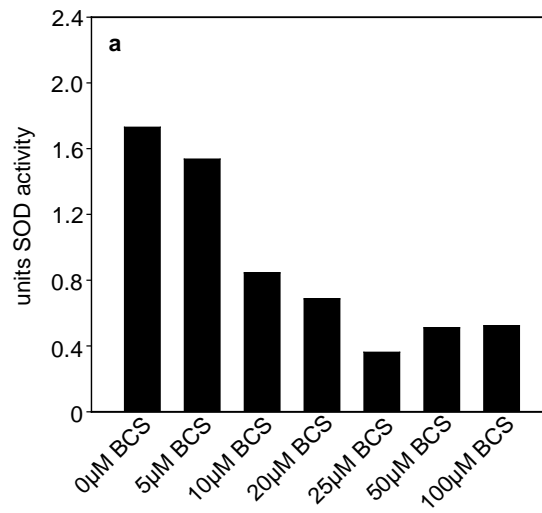


Figure 3.20: SOD1 activity in *SH-SY5Y* APP_{WT} and APP_{swe} under copper supplementation

Whole cell protein extracts were prepared from 1x150cm² flask per sample of 80% confluent monolayer culture as described in section 2.4.7.2.3. Three independent extracts were produced (see appendix 1 figures 5.1 and 5.3 for two further replicates). The protein content was estimated by BSA-calibrated Coomassie assay and all three extracts diluted to the same protein concentration to minimise experimental variation. On the day of the experiment a fresh standard curve using pure SOD1 was prepared. Samples could not be analysed in triplicate due to the duration of individual measurements. SOD1 activity was measured spectrophotometrically at a wavelength of 550nm as described in section 2.4.7.2.4. Histograms represent enzyme activity in units SOD for APP_{WT} (a) and APP_{swe} (b).

Figure 3.21: SOD1 activity in *SH-SY5Y* APP_{WT} and APP_{swe} under copper depletion

APP_{WT} and APP_{swe} cells were cultured in increasing concentrations of BCS for four generations and seeded for the final analysis. Cultures were harvested when 80% confluent and cell numbers determined as described in section 2.4.6.1 using a Coulter Cell Counter system. Whole cell protein extracts were prepared from 1x150cm² flask per sample of monolayer culture as described in section 2.4.7.2.3. Three independent extracts were produced (see appendix 1 figures 5.2 and 5.4 for further two replicates). The protein content was estimated by BSA-calibrated Coomassie assay and all three extracts diluted to the same protein concentration to minimise experimental variation. On the day of experiment a fresh standard curve using pure SOD1 was prepared. Samples could not be analysed in triplicate due to the duration of individual analyses. SOD1 activity was measured spectrophotometrically at a wavelength of 550nm as described in section 2.4.8.2.4. Histograms represent enzyme activity in units SOD for APP_{WT} (a) and APP_{swe} (b). The copper(I) specific chelator BCS was used to culture *SH-SY5Y* for 4 generations to remove all copper.



curves for each replicate. However, the control samples suggest the base levels of SOD activity to be the same in both cell lines. In APP_{WT} cells increasing copper concentration triggers a slight increase in SOD1 activity, although the data are inconclusive with regards to major differences between lower copper concentrations at 50µM and 500µM copper. High copper concentrations do not result in an elevation of SOD1 activity, thus it is expected that cell cultures do not experience oxidative insult. Contrary, in APP_{swe} cells supplemented with increasing concentrations of copper a clear increase in SOD1 activity is detectable. This leads to the conclusion that more copper is available to activate SOD despite the continued increased secretion of Aβ. These data may reflect a mechanism for the APP_{swe} cell line to detoxify excess levels of copper by increased binding, thus enhancing the reduction of copper-mediated ROS generation.

Cell cultures supplemented with BCS and thus deprived of copper for several generations show a drastic decrease in SOD1 activity (see figure 3.21). Both APP_{WT} and APP_{swe} cell lines display decreases in SOD1 activity which seem to be greater in the earlier stages of copper limitation (at 5µM BCS to 20µM BCS) and then trail off, suggesting possible adaptation of the cellular machinery to low level antioxidant defense. Although both cell lines show diminished SOD1 activity with increasing BCS concentrations, the APP_{WT} cell line seems more susceptible to low levels of copper showing a greater decrease in activity than the APP_{swe} cell line. In fact, although levels of activity are lower in the APP_{swe} control sample, activity remains higher in the high BCS concentrations as compared to APP_{WT}. Whether this is due to experimental conditions such as the use of the spectrometer and preparation of standard curves on different days or actual events can not be concluded from this data set.

3.6.3 Analysis of cytochrome c oxidase activity

Cytochrome c oxidase activity was measured spectrophotometrically at a wavelength of 550nm. The assay is based on the same principles as the liquid SOD1 activity assay. The rate of oxidation of reduced cytochrome c by cytochrome c oxidase is measured by observing the level of quenching of absorbance intensity at this particular wavelength. It is necessary for this activity assay that prior to the experiment cytochrome c is fully reduced. Maximum reduction of cytochrome c

was achieved by supplementation of the stock solution with ascorbic acid. Excess reducing agent was subsequently removed by dialysis in 20mM phosphate buffer, pH 7.8 using dialysis membrane with a molecular weight cut - off of 3,500 Daltons. Multiple additions of ascorbic acid stock to a diluted sample of cytochrome c stock determined the minimum concentrations required to fully reduce cytochrome c. The chromatograph of this experiment is shown in appendix 2 figure 5.5.

Whole cell membraneous protein extract was prepared from one 150cm² flask per sample for both cell lines and pellets resuspended in 1ml of 20mM phosphate buffer, pH 7.8 before lysis in a waterbath. Intact cells were removed by low speed centrifugation and the supernatant subjected to ultracentrifugation. Resulting pellets were resuspended in 0.5ml of phosphate buffer and protein content determined by BCA protein assay. Samples for both cell lines and all copper depletion or supplementation conditions were adjusted to the same protein concentration to minimise errors in absorbance measurements due to variations in protein content or sample volume. To control for full cytochrome c reduction before each individual measurement, aliquots (0.9ml) of fully reduced 3 μ M working solution were scanned between wavelengths 200 and 800nm to compare absorbance at 550nm and reactions initiated by addition of 8 μ g of sample protein. The rate of cytochrome c oxidation was determined by using $\epsilon_{550\text{nm}} = 29,500\text{M}^{-1} \text{cm}^{-1}$. Triplicate measurements were taken of each sample. Three individual extracts of APP_{WT} and APP_{swe} cell lines were subjected to analysis of cytochrome c oxidase activity. Further replicates are shown in appendix 2 figures 5.6 and 5.8 for copper supplemented cultures and appendix 2 figures 5.7 and 5.9 for BCS supplemented cultures. Direct comparison of base levels of APP_{WT} and APP_{swe} (figure 3.22) shows that under physiological conditions the cell line overexpressing the Swedish mutation exhibits 50% less enzyme activity. This finding has potential implications for patients carrying the Swedish mutation who are more prone to neurodegeneration than patients carrying the wild type allele of APP. Even small changes in cytochrome c oxidase activity and thus energy production within the brain can cause a multitude of biochemical alterations which can lead to loss of mitochondrial gradients resulting in initiation of the ischaemic cascade and loss of active import of nutrients into the brain.

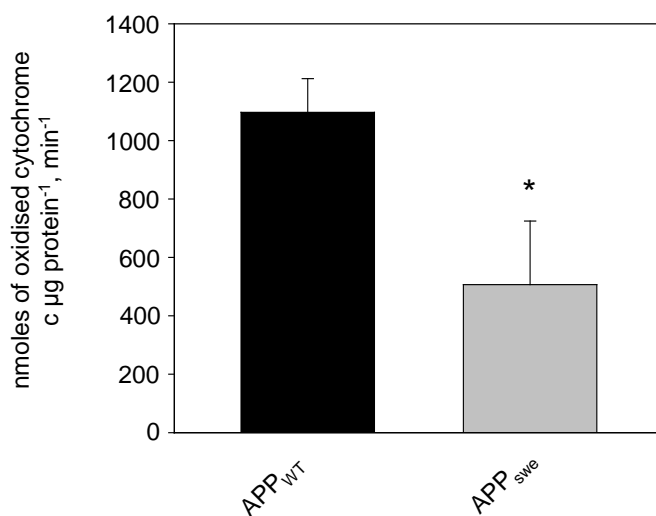


Figure 3.22: Comparison of cytochrome c oxidase activity in *SH-SY5Y* APP_{WT} and APP_{swe} cell lines

Membraneous protein extracts were prepared from 1x150cm² flask per sample of 80% confluent monolayer culture for each cell line as described in section 2.4.7.3.1. Cells pellets were lysed in 1ml of 20mM KPO4 buffer (pH 7.8) by sonication in a water bath followed by centrifugation to remove intact cells. The protein content was estimated using the BCA assay for membraneous protein and both extracts adjusted to the same protein concentration to minimise experimental variation. Prior to the activity assay cytochrome c was fully reduced with molar excess of ascorbic acid, which was subsequently removed by dialysis. Cytochrome oxidase activity was measured spectrophotometrically at a wavelength of 550nm as described in section 2.4.8.3.6. Histograms show enzyme activity as calculated using the extinction coefficient, $\epsilon_{550\text{nm}} = 29,500 \text{ M}^{-1} \text{ cm}^{-1}$ for APP_{WT} (black bar) and APP_{swe} (grey bar). Error bars represent standard deviation for triplicate measurements. Results indicate a higher level of endogenous cytochrome c oxidase activity in the APP_{WT} cell line, compared to the APP_{swe} cell line. Error bars represent standard deviation for triplicate measurements. Symbols represent statistical significance as follows: *: p<0.05 compared to the control, #: p<0.01 compared to the control, **: p<0.05 compared to previous treatment, ###: p< 0.01 compared to previous treatment.

Figure 3.23: Cytochrome c oxidase activity in *SH-SY5Y* APP_{WT} and APP_{swe} under copper supplementation

Membraneous protein extracts were prepared from 1x150cm² flask per sample of 80% confluent monolayer culture as described in section 2.4.7.3.1. Three independent extracts were produced (see appendix 2 figures 5.6 and 5.8 for 2 further replicates). The protein content was estimated using the BCA assay for membraneous protein and all three extracts diluted to the same protein concentration to minimise experimental variation. Prior to the activity assay cytochrome c was fully reduced with molar excess of ascorbic acid, which was subsequently removed by dialysis. Cytochrome oxidase activity was measured spectrophotometrically at a wavelength of 550nm as described in section 2.4.7.3.6. Histograms show enzyme activity as calculated using $\epsilon_{550\text{nm}} = 29,500 \text{ M}^{-1}\text{cm}^{-1}$ for APP_{WT} (a) and APP_{swe} (b). Error bars represent standard deviation for triplicate measurements. Results indicate no changes in cytochrome oxidase activity in APP_{WT} and increased cytochrome oxidase activity in APP_{swe} cell lines. Error bars represent standard deviation for triplicate measurements. Symbols represent statistical significance as follows: *: p<0.05 compared to the control, #: p<0.01 compared to the control, **: p<0.05 compared to previous treatment, ##: p< 0.01 compared to previous treatment.

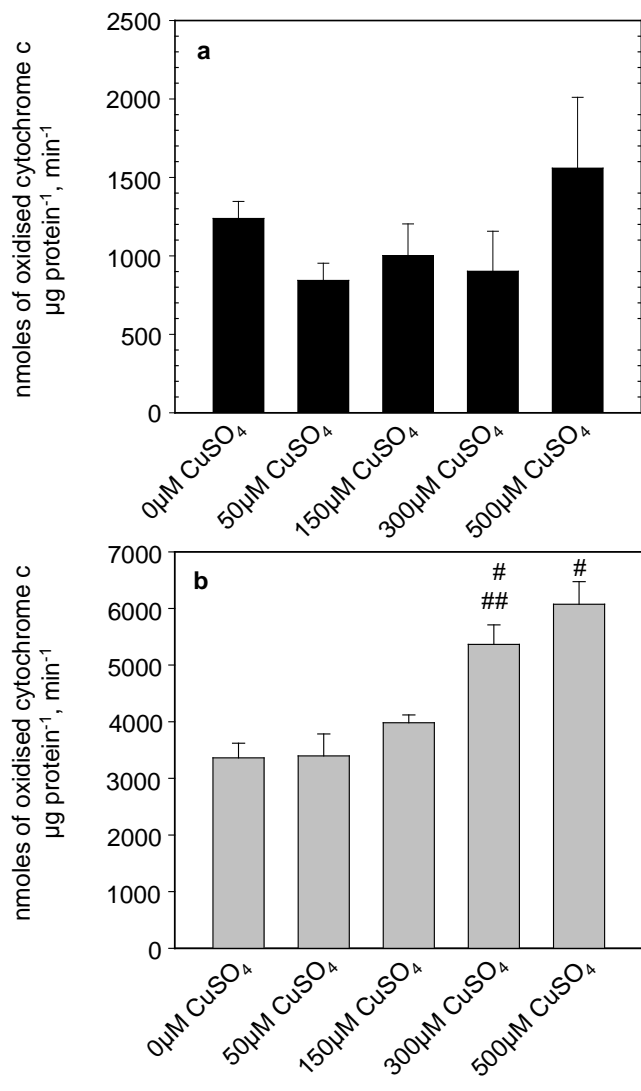
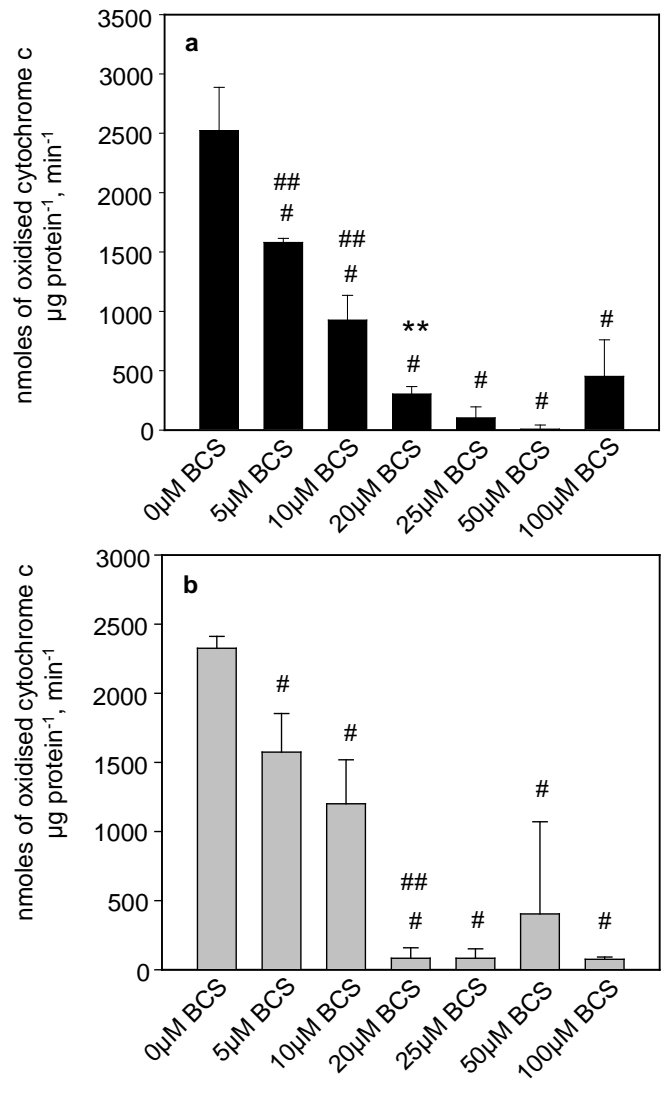


Figure 3.24: Cytochrome c oxidase activity in *SH-SY5Y* APP_{WT} and APP_{swe} under copper depletion

APP_{WT} and APP_{swe} cells were cultured in increasing concentrations of BCS for four generations and seeded for the final analysis. Cultures were harvested when 80% confluent and cell numbers determined as described in section 2.4.6.1 using a Coulter Cell Counter system. Membraneous protein extracts were prepared from one 150cm² flask per sample of monolayer culture as described in section 2.4.7.3.1. Three independent extracts were produced (see appendix 2 figures 5.7 and 5.9 for further two replicates). The protein content was estimated using the BCA assay for membraneous protein and all three extracts diluted to the same protein concentration to minimise experimental variation. Prior to the activity assay cytochrome c was fully reduced with molar excess of ascorbic acid, which was subsequently removed by dialysis. Cytochrome oxidase activity was measured spectrophotometrically at a wavelength of 550nm as described in section 2.4.7.3.6. Histograms show enzyme activity as calculated using $\epsilon_{550\text{nm}} = 29,500 \text{ M}^{-1}\text{cm}^{-1}$ for APP_{WT} (a) and APP_{swe} (b). Error bars represent standard deviation for triplicate measurements. Results indicate a decrease in cytochrome oxidase activity in both cell lines. Error bars represent standard deviation for triplicate measurements. Symbols represent statistical significance as follows: *: p<0.05 compared to the control, #: p<0.01 compared to the control, **: p<0.05 compared to previous treatment, ###: p< 0.01 compared to previous treatment.



Increases in extracellular copper concentrations did not have any effect on the APP_{WT} cell line (figure 3.23), whereas cytochrome c oxidase activity seems to be restored to a certain extent in the APP_{swe} cell line. These data are consistent with a decreased base level of enzyme activity under normal physiological conditions and suggest that cytochrome c oxidase activity is at its maximum in APP_{WT} cells. In cell lines depleted of copper for four generations sharp decreases in cytochrome c oxidase activity were observed (figure 3.24). There is no apparent difference between the two cell lines with regards to intensity of activity reduction upon increasing BCS concentrations or the level to which enzymatic activity is reduced. This observation implies that the naturally increased cleavage of APP in the APP_{swe} cell line does not affect intracellular copper content to a level that prevents or favours cytochrome c oxidase metallation compared to the APP_{WT} cell line.

3.7 Phenotypic analysis and comparison of *SH-SY5Y* APP_{WT} and APP_{swe}

3.7.1 Survival studies under copper supplementation

Since differences with respect to copper sensitivity and activity of copper - binding enzymes had been rescued, survival was monitored for APP_{WT} and APP_{swe} cell lines under increasing copper concentrations. Cultures were supplemented with the appropriate concentration of copper and grown for a further 24 hours. Ratios of live to dead cells were established by counting cells in a hemocytometer following trypan blue staining with cells excluding the stain being counted as live and cells penetrated by the stain as dead. Figure 3.25 shows data represented as % survival. It is clear that toxic levels of copper drastically decrease the survival of APP_{WT} cells, whereas the same concentration of copper rescues survival in APP_{swe} cultures. Findings suggest that APP_{swe} cultures under normal conditions experience intracellular copper deficiency, which results in the loss of vital functions for cell survival. These data are consistent with decreased cytochrome c oxidase activity shown under normal conditions in APP_{swe} cultures. Survival studies could not be performed on cultures supplemented with BCS, due to consecutive passaging to eliminate intracellular copper resulting in dead cells being lost in the process. However, further replicates of survival studies in copper supplemented cultures are shown in appendix 3 figures 5.10 and 5.11 for APP_{WT} and APP_{swe}, respectively.

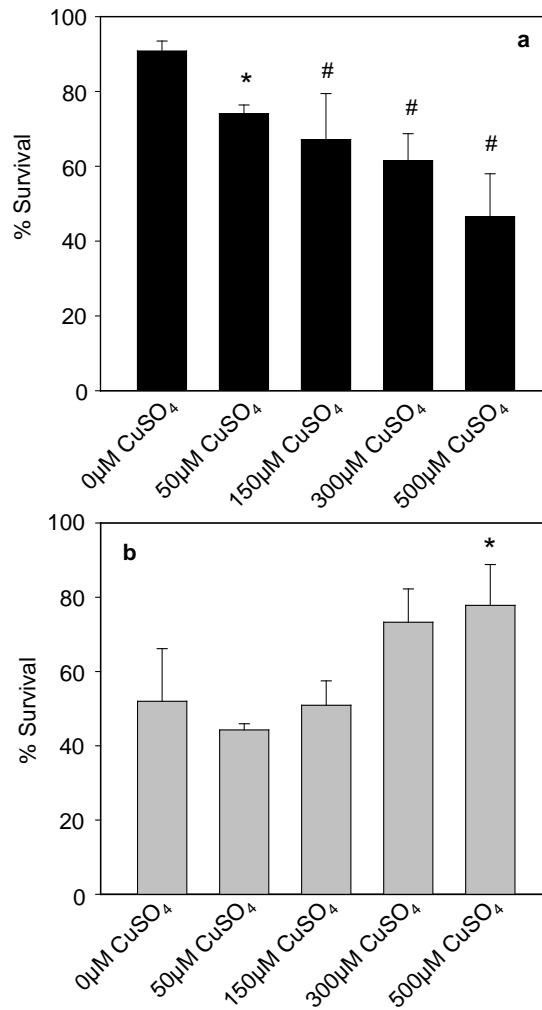


Figure 3.25: Survival of *SH-SY5Y* APP_{WT} and APP_{swe} under increasing copper concentrations

Cell cultures of 1×10^6 cells were prepared for both cell lines and grown for several days before being supplemented with the appropriate concentration of copper and grown for another 24 hours. Cultures were harvested as described in section 2.2.3.2 and analysed for life and dead cells by the trypan blue exclusion method using a hemocytometer. Survival rates are shown for APP_{WT} (a) and for APP_{swe} (b). Error bars represent standard deviation of triplicate measurements. Symbols represent statistical significance as follows: *: $p < 0.05$ compared to the control, #: $p < 0.01$ compared to the control, **: $p < 0.05$ compared to previous treatment, ##: $p < 0.01$ compared to previous treatment.

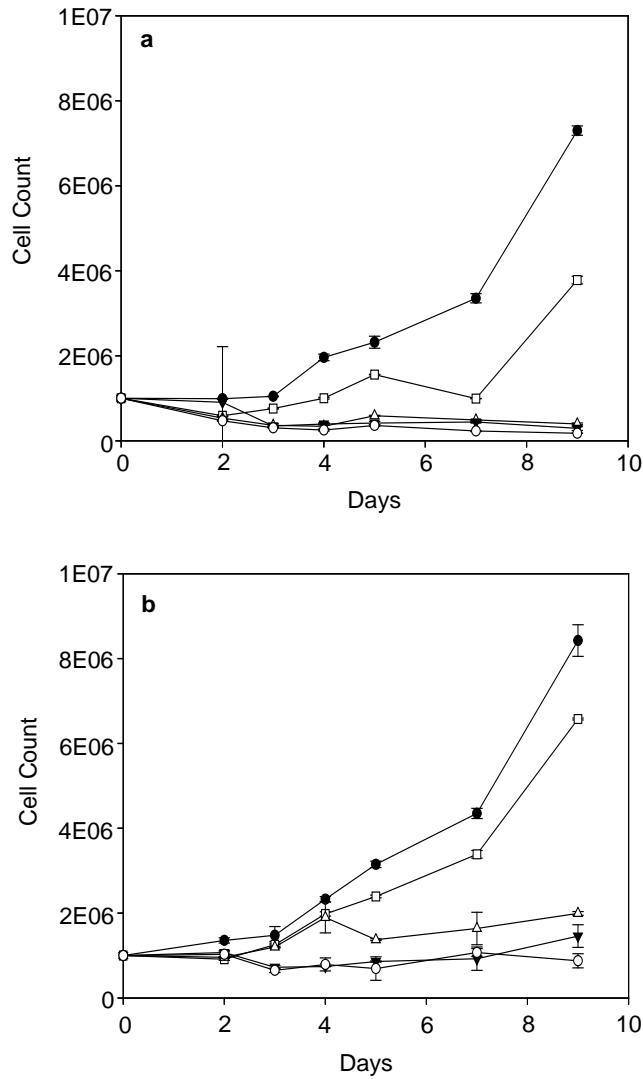


Figure 3.26: Growth of *SH-SY5Y* APP_{WT} and APP_{Swe} under increasing copper concentrations

APP_{WT} (a) and APP_{Swe} (b) cells were seeded at 1×10^6 cells per flask, cultured in increasing concentrations of copper for 10 days and harvested at appropriate time intervals. Cell numbers were determined as described in section 2.4.6.1 using a Coulter Cell Counter system. Copper concentrations were as follows: 0 μM copper (filled circles), 50 μM (open squares), 150 μM (open triangles), 300 μM (filled triangles) and 500 μM (open circles). Error bars represent standard deviation in triplicate measurements.

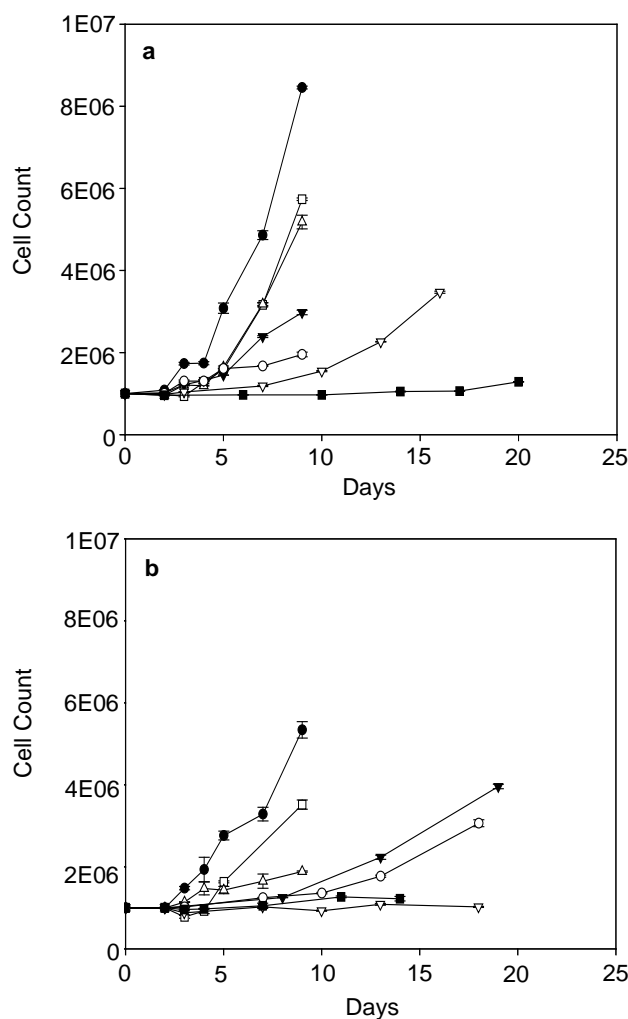


Figure 3.27: Growth of *SH-SY5Y* APP_{WT} and APP_{swe} under copper depletion

APP_{WT} (a) and APP_{swe} (b) cells were cultured in increasing concentrations of BCS for four generations and seeded at 1×10^6 cells per flask for the final analysis. Cultures were harvested at appropriate time intervals and cell numbers determined as described in section 2.4.6.1 using a Coulter Cell Counter system. BCS concentrations were as follows: 0 μM BCS (filled circles), 5 μM BCS (open squares), 10 μM BCS (open triangles up), 20 μM BCS (filled triangles), 25 μM BCS (open circles), 50 μM BCS (open triangles down) and 100 μM BCS (filled square). Error bars represent standard deviation in triplicate measurements.

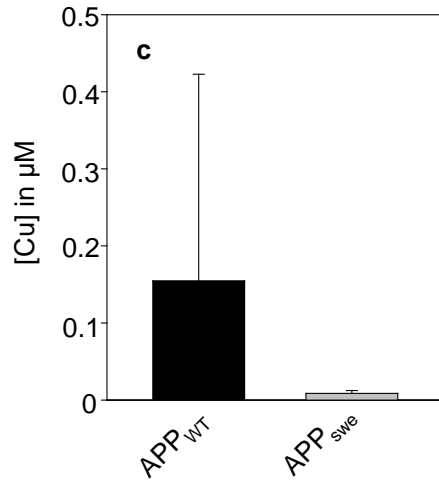
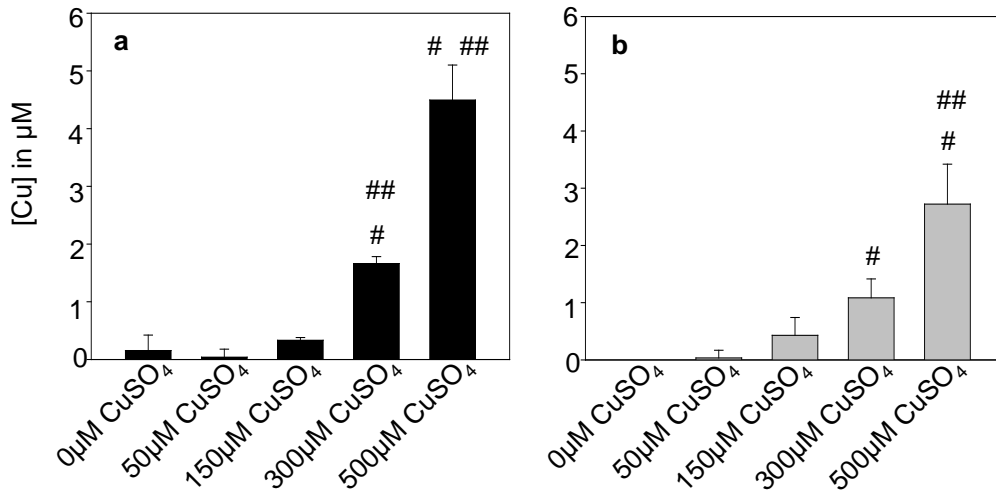
3.7.2 Growth analysis under copper depletion and supplementation

To examine growth characteristics of both cell lines under high copper conditions, cells were seeded at 1×10^6 cells per flask and instantly supplemented with copper. Culture medium was exchanged every two days and cells harvested at various time intervals. Cell numbers were determined using a Coulter Counter. Data shown in figure 3.26 show continued but somewhat decreased growth of APP_{WT} cells in low copper concentrations ($50 \mu\text{M}$). However, toxic concentrations of copper ranging from $150 \mu\text{M}$ to $500 \mu\text{M}$ copper result in complete loss of growth. In contrast, APP_{swe} cells exhibit increased growth in high copper concentrations starting at day 5. At lower copper concentrations of $50 \mu\text{M}$ APP_{swe} cells show slightly decreased growth, however, they are more resistant against copper related insults than APP_{WT} cells. The data imply that the APP_{swe} cell line is more resistant to high copper concentrations on a short term and long term basis.

Cells supplemented with BCS were again cultured for four consecutive passages to deplete intracellular copper levels and seeded at 1×10^6 cells per flask. Culture medium was exchanged every two days and cells harvested at various time intervals. It was observed that in cultures supplemented with higher BCS concentrations longer time intervals were needed between measurements implying reduced growth in both cell lines. Cell numbers were determined using a Coulter Counter. Data shown in figure 3.27 show continued growth for both cell lines. It is noticeable that APP_{swe} cultures supplemented with $20 \mu\text{M}$ and $25 \mu\text{M}$ BCS reach the same levels of growth as APP_{WT} cultures supplemented with the same amount of BCS. However, growth delay results in the APP_{swe} cell line taking nearly twice as much time as APP_{WT} cells to grow to the same level. Further APP_{swe} cultures containing $50 \mu\text{M}$ BCS do not exhibit any signs of growth, whereas APP_{WT} cultures display growth after 7 days of culture in $50 \mu\text{M}$ BCS. Growth of both cell lines is almost abolished at a concentration of $100 \mu\text{M}$ BCS. Special attention needs to be paid to growth behaviour at low BCS concentrations. Although, in comparison with control cultures both cell lines display the same amount of growth for cells supplemented with $5 \mu\text{M}$ BCS, growth delay in the APP_{swe} cell line seems to be initiated at a BCS concentration of $10 \mu\text{M}$. Data suggests that APP_{WT} cultures may be able to compensate for higher BCS concentration by mobilising intracellular

Figure 3.28: Total copper content of whole cell *SH-SY5Y* APP_{WT} and APP_{swe} under copper supplementation

Copper supplemented cultures were prepared as described previously (section 2.4.1), harvested and repeatedly washed in D-PBS. Aliquots of 1.5×10^6 cells for each cell line and copper concentration were resuspended in 1ml of ultrapure 65% (v/v) HNO₃. Samples were incubated at room temperature for at least one week and repeatedly centrifuged to remove cells and cell debris, before being analysed by inductively coupled plasma-mass spectrometry for copper content. Whole cell copper content is shown for APP_{WT} (a) and APP_{swe} (b). Error bars represent standard deviation for triplicate measurements. Symbols represent statistical significance as follows: *: $p < 0.05$ compared to the control, #: $p < 0.01$ compared to the control, **: $p < 0.05$ compared to previous treatment, ##: $p < 0.01$ compared to previous treatment. Panel c represents a direct comparison of whole cell copper content of untreated APP_{WT} and APP_{swe}.



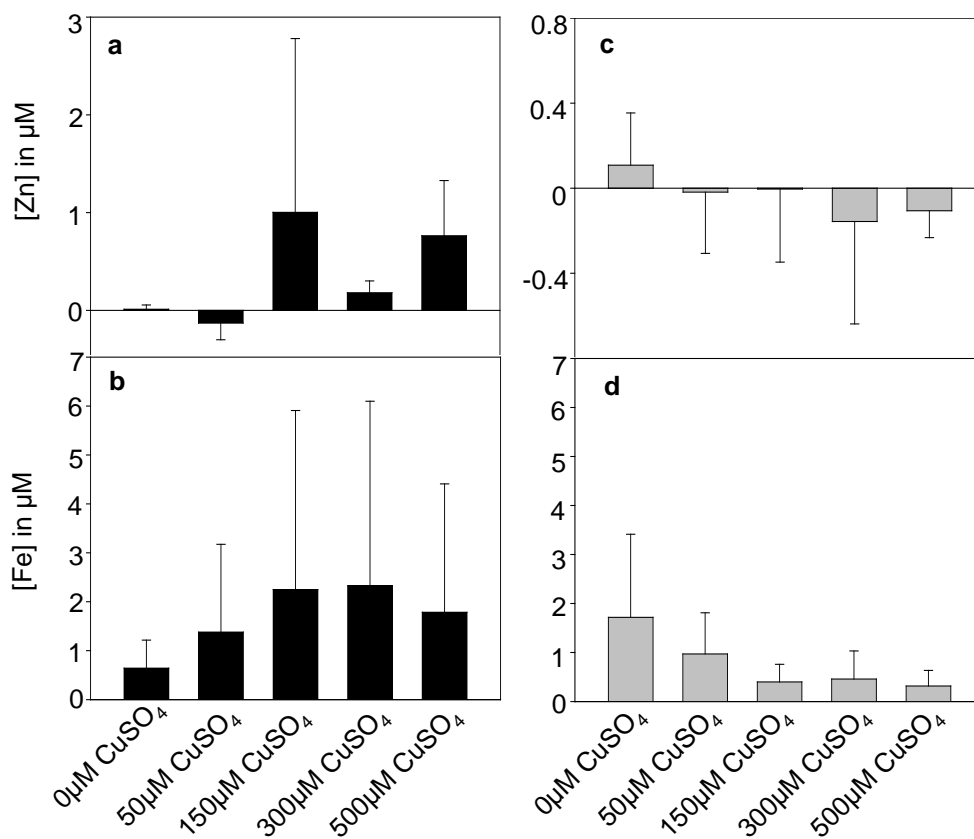


Figure 3.29: Total iron and zinc content of whole cell *SH-SY5Y* APP_{WT} and APP_{swe} under copper supplementation

Copper supplemented culture were prepared as described previously (section 2.4.1), harvested and repeatedly washed in D-PBS. Aliquots of 1.5×10^6 cells for each cell line and copper concentration were resuspended in 1ml of ultrapure 65% (v/v) HNO_3 . Samples were incubated at room temperature for at least one week and repeatedly centrifuged to remove cells and cell debris, before being analysed by inductively coupled plasma-mass spectrometry for iron and zinc content. Whole cell zinc content is shown for APP_{WT} (a), APP_{swe} (c), iron for APP_{WT} (b) and APP_{swe} (d).

copper stores, which are depleted in APP_{swe} cells. This might be due to the total amount of copper being higher in APP_{WT} cells, thus more time is needed relative to the APP_{swe} cell line to fully deplete the culture of copper. Further a metabolic switch might be responsible for the sudden delay in growth in APP_{swe} cells once copper levels fall below a certain level (equivalent to 10 μ M BCS supplementation).

3.7.3 Metal accumulation under copper depletion and supplementation

A simple method of testing for differences in copper efflux between APP_{WT} and APP_{swe} cell lines is to quantify total cellular metal content. Cultures of APP_{WT} and APP_{swe} cell lines were grown in triplicate in high copper concentration or copper depleted conditions, washed thoroughly in D-PBS and after centrifugation resuspended in concentrated nitric acid. Following repeated centrifugation to remove cell debris samples were analysed for metal content by ICP-MS. Results in figure 3.28 for total copper analysis of APP_{WT} and APP_{swe} in increasing copper concentrations show increased intracellular copper content for both cell lines. However, the copper content of APP_{WT} cells is nearly two fold higher than the copper content of APP_{swe} cells, indicating that the latter is more effective in exporting toxic quantities of the metal. This observation is consistent with increased survival of APP_{swe} cells under increasing copper conditions. Metal analyses for zinc and iron are displayed in figure 3.29. The chromatographs for both metals are inconclusive due to large errors and low μ molar abundance. Metal content of acid digests performed on BCS supplemented APP_{WT} and APP_{swe} cell lines are shown in appendix 3 figure 5.12 for copper, zinc and iron.

Chapter 4: Discussion

4.1 Analysis of metal content and distribution in mammalian cells

The development of the 2D-LC method to establish major metal pools in whole cell extracts allows for the analysis, identification and subsequent characterisation of specific and abundant metal-binding proteins without the need for extensive purification steps which might result in the loss of the metal co-factor. This method was previously applied to prokaryotic systems (Waldron et al., 2007, Tottey et al., 2008).

Part of this project was the application and if required further development of the 2D-LC method to eukaryotic organisms. Climbing the evolutionary tree to gain data from increasingly complex organisms analyses were performed on *Saccharomyces cerevisiae*, rat liver mitochondria, *HepG2* and *SH-SY5Y* human cell lines. Rat liver mitochondria were chosen on the basis that the organ contains vast amounts of heme and thus should present major metal pools for iron and be suitable as indicator for the success of the experiment. However, the high abundance of metals in the organ might also lead to saturation of metal detection by ICP-MS resulting in profiles where large amounts of metal, but no individual metal pools are visible. Cell fractionation was performed to obtain liver mitochondria. These organelles are very abundant in the liver and provide solutions to two problems of 2D-LC. The protocol requires large amounts of protein to be present for anion exchange chromatography with the column being able to separate 70mg of protein. This first experimental step also benefits from a large dilution factor of solid protein in buffer. Thus it is important that the starting material for the whole cell protein extracts contains high amounts of protein and is also very easy to grow in high numbers. *Saccharomyces cerevisiae* as well as rat liver mitochondria possess these characteristics and are ideal for first trials.

Shown in figures 3.1 and 3.2 are metal profiles obtained from both organisms, respectively, using the standard 2D-LC protocol as used for *Syneccocystis* and outlined in section 2.4.3. Metal content was analysed for copper, zinc, manganese, iron and cobalt by multi-elemental analysis using ICP-MS. The iron profile for

yeast (figure 3.1 d) shows a variety of individual iron pools mainly in the 100mM, 400mM and 1000mM anion exchange fractions and a wide spread of molecular sizes of individual metal pools indicating successful separation of proteins in the first and also second dimension. It was therefore concluded that protein separation was also successful for protein bound to copper, zinc, manganese and cobalt. Copper and zinc profiles of yeast show major metal pools in the 100mM, 200mM, and 400mM and 100mM, 300mM and 1000mM NaCl fractions, respectively. However, most of the binding partners for both metals are of smaller molecular weight and are eluted towards the total column volume of the HPLC.

Rat liver mitochondria metal profiles (figure 3.2) also show successful separation of metal pools through the first and second dimension and major pools of copper, zinc, manganese and iron can be detected indicating that not only is the 2D-LC protocol suitable for eukaryotic systems, but cell fractionation can be used to determine differences in intracellular metal trafficking between different cell types, environmental stimuli or genetic background of the same organism. Although not tested as part of this project, various organelles such as ER, Golgi, vesicular fractions and nuclei – all known to have some role in metal trafficking or storage - could be subjected to 2D-LC.

Although a slight internal variation between metal profiles of yeast replicates and replicates of all other organisms tested were observed, the major metal pools which were subjected to analysis by SDS-PAGE and subsequent identification by MALDI-TOF-MS were reproducible (data not shown). Slight variations in metal pool concentration or resolution by anion exchange and HPLC column and therefore distribution in the final profile, can be attributed to variations in manual extraction from each column, precision of protein estimations throughout the experiment, slight variation in amounts pipetted for metal content analysis of individual samples and sensitivity of ICP-MS detection.

HepG2 cultured cells – a human liver carcinoma cell line - were the first human cell line to be subjected to 2D-LC in the hope that some resemblance to the metal profiles obtained for rat liver mitochondria would become apparent. The results shown in figure 3.3 indicate the same distribution of several metal pools between *HepG2* and rat liver mitochondria extracts. Low molecular weight zinc pools in the

100mM and 200mM fractions, low molecular weight copper pools in the 100mM fraction, as well as high molecular iron pools in the 200mM and 1000mM fractions with the same distribution are visible in both profiles and are again replicable within different metal profiles of the same cell line.

One final proof of the successful application of the 2D-LC protocol to eukaryotic organisms was the identification of an abundant copper and zinc containing metal pool as SOD1 in rat liver mitochondria which became of particular interest at later stages of the project. All three organisms tested - *Saccharomyces cerevisiae*, rat liver mitochondria and *HepG2* - displayed this replicable co-migrating pool indicated by the red bar in figures 3.1 f, 3.2 f and 3.3 f. Metal concentrations and ratios of 1:1 between copper and zinc remained constant and thus were not an artefact of the experimental procedure. Supported by these findings the 2D-LC protocol was applied to *SH-SY5Y* APP_{WT} and APP_{swe} cell lines to compare copper content and possible differences in copper distribution within both cell lines.

One caveat of 2D-LC is the elimination of the membraneous cell fraction prior to anion exchange chromatography. It is therefore not possible to detect membrane-bound or transmembrane metalloproteins using this method. Western Blot analysis would be required to establish the presence of proteins such as CCO and APP. Metal content analysis of such membraneous proteins is complicated by the fact that membraneous fractions resist resolution on HPLC columns and result in the metal content analysis of all membraneous proteins in one sample without the possibility to differentiate between individual proteins. As a result the 2D-LC profiles obtained from whole cell *SH-SY5Y* cell lines do not contain a metal pool representative for APP and the effect of APP_{WT} or APP_{swe} is purely measuring the balance of copper import and export, the availability of functional copper to soluble copper-binding proteins and the absolute cellular copper content. Additional analyses were performed to verify the data obtained through 2D-LC.

4.2 Comparison of functional copper content and distribution in *SH-SY5Y* APP_{WT} and APP_{swe} cell lines

Several lines of evidence suggest linkage between APP and copper homeostasis and a possible link between APP_{swe} and cellular copper deficiency. These include a

significant decrease in survival of APP_{WT} cells cultured in high concentrations of copper, whereas APP_{swe} cultures display significant increase in survival under the same conditions. Copper is readily accumulated in both cell lines at high exogenous copper supplementation, however APP_{WT} cultures show a higher degree of intracellular copper accumulation than APP_{swe} cells and SOD1 metallation with copper is higher than that detected in APP_{swe} cells. Further copper-dependent enzyme activity assays of cultures grown in high copper concentrations show unchanged and increased SOD1 activity in APP_{WT} and APP_{swe}, respectively and significant decreases and increases in CCO activity in APP_{WT} and APP_{swe} cultures, respectively. SOD1 and CCO enzyme activities were significantly reduced in cultures grown in copper deplete media for both cell lines and a significant difference between APP_{WT} and APP_{swe} basal levels of CCO activity were observed with activity in APP_{WT} being around 50% higher than CCO activity in APP_{swe}. Cell growth is diminished by high levels of copper, whereas slight increases in copper concentration (50µM) result in 25% reduction in growth in APP_{swe} and 50% APP_{WT}. Copper deplete media allows growth of both cell cultures to the same level, although APP_{swe} cultures require twice the amount of time than APP_{WT} cultures and growth of APP_{swe} containing cells is more affected in high BCS concentrations than in APP_{WT}. It needs to be mentioned that the *SH-SY5Y* APP_{swe} cell line contains base levels of endogenous APP as well as an unspecified overexpression of APP_{swe}, whereas the *SH-SY5Y* APP_{WT} cell line contains base levels of endogenous APP only. As part of this project no experiments were performed to estimate the amount of overexpression or expression differences of endogenous APP and APP_{swe} between both cell lines by Western Blot or RT-PCR. Thus the interpretation of all data involving comparisons of both cell lines is limited and effects that could be attributed to the mutation are potentially a consequence of the level of APP expression.

Previously APP was identified to have a role in maintaining cellular copper homeostasis (Strausak et al., 2001) and mutations in APP recognised as major contributors in the development of early onset AD (Citron et al., 1992). In an effort to elucidate the influence of APP on intracellular copper levels the neuroblastoma cell line *SH-SY5Y* was used as a model to compare copper-related phenotypes in an APP_{WT} and APP_{swe} cell line. It was suggested that increased APP cleavage due to

the Swedish mutation might result in detectable differences in copper-dependent phenotypes between the two cell lines, which provide an indication of the possible role of APP in cellular copper homeostasis.

Survival studies (figure 3.25) indicate that even small amounts of exogenous copper (50 μ M) have detrimental effects on APP_{WT} cultures, a feature that is enhanced in cultures that are supplemented with even higher concentrations of copper. This indicates that under normal culture conditions APP_{WT} displays copper sensitivity that can not be rescued by adjustments of cellular mechanisms that prevent toxic copper accumulation and resulting in large scale cell death. It must be noted that cultures were exposed to copper for only 24 hours thus there might be a possibility that gene expression did not adjust according to changes in extracellular conditions. This point raises the question of whether efficient adaptation of the cell's metabolism to excess copper is time-dependent and did not occur within the 24 hour experimental period resulting in induction of apoptosis. It might also be that cellular adjustments were not effective for the chosen copper concentrations, and so cell death was inevitable. Analysis of culture growth in increasing copper concentrations (figure 3.26) supports the view that cell death was not time, but rather concentration-dependent. Cell growth was inhibited upon exposure to copper concentrations including and exceeding 150 μ M and diminished by 50% when supplemented with low amounts of copper. Similar findings were reported in *SH-SY5Y* cells by Arciello et. al. (Arciello et al., 2005), indicating that cellular mechanisms that facilitate excretion of excess copper are either defective or overwhelmed depending on metal concentration. Intracellular copper accumulation (figure 3.28) in APP_{WT} cells further suggests that the equilibrium between copper import and copper efflux is imbalanced resulting in either decreased copper efflux or increased copper import. Cellular defence mechanisms against excess amounts of copper also include metallothioneins, which sequester and store physiological metal ions, thus the increase in intracellular copper levels might represent copper species bound to metallothionein or represent a switch in gene expression to proteins that require copper as co-factor for their physiological function. Copper could also be compartmentalised in the TGN or mitochondrial matrix. Increased exposure to copper potentially causes increased risk of cellular damage due to ROS production in all of these compartments.

To test cellular copper distribution in excess exogenous metal and possible buffering mechanisms, activity assays were performed on the most prevalent copper-dependent enzymes that are vital for cellular energy production (CCO) and antioxidant defence (SOD1). CCO is a mitochondrial membrane bound protein complex that requires a number of accessory proteins for full maturation; in particular the insertion of metal co-factors is a highly co-ordinated process (see section 1.5.4). Total membrane preparations of APP_{WT} were analysed for CCO activity and spectrophotometric analysis showed significant changes in enzyme activity upon copper supplementation. Despite the level of significance in CCO activity, the results for replicates were conflicting with regards to observations of increased and decreased enzyme activity, thus no clear statement can be made whether excess copper is directed towards CCO. The second enzyme tested for copper-dependent changes in activity was the ubiquitously expressed cytoplasmic SOD1 antioxidant protein. In APP_{WT} cultures upon copper addition no changes were observed in SOD1 activity. Thus it can be concluded that increased cellular copper accumulation does not result in increased metallation of either CCO or SOD1.

There is evidence (Schmidt et al., 2000) that a reservoir of unmetallated apo-SOD1 exists in the cytosol in yeast, which upon copper availability becomes metallated and activated. However, such an increase was not observed in cultures supplemented with high amounts of copper, suggesting that either copper is directed to cellular copper stores rather than being available for SOD1 incorporation or the cytoplasmic pool of SOD1 was fully metallated, thus only increased protein production could lead to increased enzyme activity. Elevated cellular copper may ultimately lead to the production of ROS, indicating that the decrease in survival in APP_{WT} cultures might be due to increased oxidative insult that is not matched with an adequate response in oxidative stress defence. Determination of cellular adjustments to excess copper by increasing the abundance of transcripts encoding copper-binding proteins using the RT-PCR approach was unsuccessful. No clear conclusions can be drawn from the gene expression data for SOD1 and its copper chaperone CCS (figures 5.14 and 5.15). If SOD1 was one of the major targets of copper distribution and detoxification in excess copper conditions, an increase in

gene expression of both SOD1 and CCS might be expected to protect the cell from oxidative stress and possibly provide a transient buffering mechanism.

Additionally monitoring metallothionein gene expression and protein abundance would elucidate the localisation of intracellular excess copper. To conclusively establish whether increased protein production of SOD1, CCS or metallothionein is a governing factor in copper buffering, Western blot analysis and monitoring of RNA accumulation in conjunction with the use of ribosomal translation inhibitors in both APP_{WT} and APP_{swe} cell lines in deplete and high copper concentrations could be used.

Contrary to phenotypes observed in APP_{WT} cells, the APP_{swe} cell line displayed many characteristics of intracellular copper deficiency. Enzyme activities for both CCO and SOD1 were increased by and directly linked to increases in copper concentrations (figure 3.23 and 3.20, respectively). These data indicate that under normal culture conditions there may be a deficit in mitochondrial respiration and production of ATP required for cell survival. If the cell's requirements for ATP and thus copper are not met, vital functions such as energy dependent molecular transport and gene expression are impeded resulting in delay or abortion in the cell's response to extracellular and intracellular stimuli and likely cell death. It has not been established through experimental procedures whether this phenotype was the effect of the APP_{swe} mutation or simply its overexpression in this cell line.

The copper-deficient phenotypes of APP_{swe} cultures are rescued by supplementation with high concentrations of copper (300-500 μ M), as demonstrated in figure 3.25, to the point at which cell survival is restored to almost APP_{WT} survival rates. Further it was observed that under normal culture conditions the APP_{swe} cell line displays 50% less CCO activity than APP_{WT} (figure 3.22), which explains the decreased survival of control cultures relative to the wild type cell line. The apparent copper resistant phenotype of APP_{swe} cells is supported by increased activity in SOD1 in high copper. Although cellular copper accumulation (figure 3.28) similar to that in APP_{WT} is detected the oxidative stress posed on the cell is likely to be at lower levels than that in APP_{WT} due to copper incorporation into CCO and SOD1, thus lower levels of intracellularly available copper remains to facilitate oxidative damage. Further oxidative stress is opposed by increased levels of SOD1

contributing to enhanced cell survival. Although APP_{swe} cultures grow more readily in low copper concentrations compared with APP_{WT} culture (figure 3.26), copper supplemented cultures do not attain the same growth rate as control cultures indicating that there is a slight copper sensitivity at concentrations including and exceeding 50µM. These data are contradictory to the high copper concentrations required to initiate increases in CCO and SOD1 enzyme activity indicating that although exposure to high copper concentrations can restore cellular survival for a short period, copper exposure over a longer time period might still lead to detrimental effects on cell survival. APP_{swe} is cleaved to form Aβ more readily than APP_{WT} and produces around 2-8 fold more of this soluble copper-binding amyloid species (Citron et al., 1992), thus one could conclude that cell lines carrying the APP_{swe} mutation are less susceptible to copper toxicity due to an enhanced export function, which is supported by data from figure 3.28 showing reduced intracellular copper content compared to APP_{WT} cell lines. Although APP_{swe} cultures demonstrate increased copper resistance in a 24 hour period, the increased cleavage of APP_{swe} might result in increased extracellular Aβ that binds to secreted copper and accumulates locally thus increasing the potential of localised oxidative damage that can not be counteracted by the cell over a longer period of time. The failure of APP_{swe} growth recovery in low copper concentrations to the levels of the control culture (figure 3.26) might be representative of this scenario with Aβ fibrilisation being mediated by the 50µM copper supplement.

2D-LC was applied to whole cell protein extracts of both APP_{WT} and APP_{swe} cell lines. This method was developed to study differences in major cellular metal pools and their associated proteins in response to extracellular stimuli or cellular metal responses to genetic mutation. Thus 2D-LC provides an ideal tool to determine which possible role APP holds with regards to cellular copper homeostasis by comparing changes in copper distribution throughout the cell or alterations in copper concentrations within particular copper pools. Further identification of proteins associated with specific metal pools can be achieved by resolution of fractions containing the metal on SDS-PAGE and subsequent analysis using Principal Component Analysis.

Soluble extracts of APP_{WT} and APP_{swe} were separated by anion exchange and size exclusion chromatography and fractions analysed for manganese, iron, zinc, cobalt and copper content simultaneously (figures 3.4 and 3.5). One particular copper pool in the 100mM NaCl fraction at a size exclusion volume of 11ml displayed co-migration with a zinc pool in the same fractions in both cell lines indicating the presence of a putative copper and zinc binding species. Glutathione activity assays across the same copper and zinc containing fractions in a whole cell extract obtained from *Saccharomyces cerevisiae* show co-migration of the copper peak with a protein peak (figure 3.6). Copper did not co-migrate with glutathione, thus it is not the copper-binding species in yeast and unlikely to represent the copper binding species in APP_{WT} and APP_{swe} extracts. To identify the proteinaceous ligand associated with copper and zinc, fractions containing the metals were resolved on SDS-PAGE and subjected to PCA analysis (figures 3.17 and 3.18). Although one particular protein, designated pSOD1_{S5Y} (figure 3.16), displayed strong correlation patterns to the metal distribution and metal concentration across the analysed fractions final identification of the protein by MALDI-TOF mass spectrometry was unsuccessful. However, previous experiments on soluble rat liver mitochondria extracts using the same method displayed the same copper and zinc pools (figure 3.7). SDS-PAGE (figure 3.7), PCA (figure 3.8) and MALDI-TOF-MS analysis (figure 3.9) identified the copper and zinc binding species as SOD1, thus it was assumed that the same metal pools in APP_{WT} and APP_{swe} were associated with the same protein, SOD1. This assumption was confirmed by in-gel SOD1 activity assays performed on the copper and zinc containing fractions (figure 3.19). Direct comparison of triplicate metal analysis experiments confirmed SOD1 copper:zinc stoichiometry of 1:1 (Tainer et al., 1982) in APP_{WT}, however the copper and partially zinc content in the APP_{swe} SOD1 pool was decreased (figure 3.16) suggesting that the Swedish mutation or in APP or its overexpression modifies cellular copper content to the degree of functional copper deficiency. To assess whether decreased copper and zinc levels might be due to variation in the amounts of protein extract used for 2D-LC, aliquots of the 100mM NaCl fractions of post anion exchange separation were resolved on SDS-PAGE with a control of pure SOD1. No difference in protein abundance for SOD1 was observed in the two extracts (figure 3.16), thus the alteration in SOD1 metallation is most likely due to effects of the Swedish mutation.

Metallation status of CCO could not be assessed in this way due to CCO localisation to the membrane and its elimination from the protein extract early in the extraction process. Anion exchange and size exclusion chromatography were performed using an adjusted extraction protocol containing the non-ionic zwitter-detergent Chaps to generate a membraneous extract of APP_{WT}. However, metal content analysis of CCO by ICP-MS was not possible due to large amounts of suspended solids in the samples that interfere with ICP-MS. Additional difficulties arose with the resolution of Chaps-containing membraneous extract on HPLC columns, thus singular fractions usually subjected to ICP-MS for their metal-content characteristics could not be obtained. Analysis of membraneous samples by ICP-MS without resolution on the HPLC columns would result in metal content analysis of all membraneous proteins and not be specific for CCO. Further resolution of membraneous samples on Chaps containing SDS-PAGE was also unsuccessful (data not shown) and resulted in smeared gels that were inadequate for further analysis.

To test the effects of, and cellular responses to, copper deficiency both the APP_{WT} and APP_{swe} cell lines were treated with the copper chelator BCS. Since previous results indicate a copper-deficient phenotype in APP_{swe} cultures, treatment with BCS is expected to affect this cell line more severely than the APP_{WT} cell line. CCO and SOD1 activity assays demonstrate significant decreases in enzyme activities (figures 3.21 and 3.24) most likely due to inadequate metallation of both enzymes. This view is supported by analysis of cellular metal content (figure 5.12) which represents intracellular iron, copper and zinc concentrations after four generations of cell culture grown in BCS at levels that are in the low μM range and hardly detectable by ICP-MS. Especially high concentrations of BCS seem to affect growth of APP_{swe} cells more than the growth of APP_{WT} cells (figure 3.27). No growth was recorded for APP_{swe} cultures in BCS concentrations of 50-100 μM , whereas APP_{WT} cultures recovered from treatment with 50 μM BCS. At 5 μM BCS concentration both cell lines display 60% growth, however the discrepancy in the cell's ability to adjust to low intracellular copper becomes apparent at 10 μM BCS. At this concentration APP_{WT} growth remains at a level of 60%, whereas APP_{swe} growth drops to 25%. This trend continues with increasing BCS concentrations. It must be noted that at concentrations of 10-25 μM BCS the APP_{swe} cell line recovers from

impaired growth and reaches cell numbers comparable to those of APP_{WT} in a time-dependent manner (after 20 day rather than 9 days), which suggests rescue mechanisms that could potentially alter CCO and SOD1 enzyme activities and increase cell survival. Survival studies could not be performed on BCS treated cell lines to test for cell line-specific and BCS-mediated rates in survival due to the loss of cells and thus the means of standardisation between treatments during the cell culture process. As previously observed in copper-supplemented cultures, in which exposure to high copper concentrations initially increases CCO and SOD1 activity, but when monitored for a longer period results in cell death, the treatment with BCS might result in an initial decrease in CCO and SOD1 activity, which might be reversed after a certain time due to the cell adjusting to the environmental changes by mechanisms such as increased gene expression of copper importers, re-routing of copper chaperones or copper release from dispensable places namely the mitochondrial matrix or metallothioneins. However, due to a lack of extracellular copper and no indication of intracellular copper accumulation in metallothioneins or alternative storage it is not clear in what way the APP_{swe} cell line could adjust to severe copper deficiency and restore growth.

The maintenance of cellular copper levels and correct distribution to target proteins in accordance with cellular requirements is one of the main focuses in finding new therapeutics for neurodegenerative diseases, many of which show symptoms of metal deregulation and imbalance. However, before chelation or supplementation therapies can be devised a clear understanding of cellular pathways and their alterations due to changes in copper availability is paramount. Two of the most prevalent copper-enzymes in the cell are mitochondrial CCO and cytosolic SOD1. However, recently SOD1 localisation to the mitochondrial intermembrane space in *Saccharomyces cerevisiae* (Sturtz et al., 2001) and SOD1 accumulation in the mitochondrial matrix in the human brain (Vijayvergiya et al., 2005) has been detected. It was shown that translocation of SOD1 was dependent on a high intra-mitochondrial concentration of CCS (Sturtz et al., 2001) and also the non-metallated immature state of SOD1 (Field et al., 2003). Active mitochondrial SOD1 has further been detected in mammalian neuronal tissue (Stadtman and Levine, 2000), indicating that activation occurs within the mitochondria. It has further been demonstrated that the SOD1 pool in the cytosol and the mitochondria are freely

interchangeable when SOD1 is not metallated or the disulfide bond established, thus changes in exogenous copper could alter the SOD1 distribution equilibrium to the cytosol since CCS is present in the cytosol in large quantities and contributes to extra-mitochondrial maturation of the protein. It was suggested that SOD1 as well as CCO might obtain their copper co-factor from the mitochondrial matrix low molecular weight copper pool, which was reported by Cobine et. al. in yeast (Cobine et al., 2004). Studies showed that this CuL complex is present in the cytoplasm in an unmetallated state and translocates to the mitochondrial matrix upon Cu(I) binding (Cobine et al., 2006). Exogenous copper supplementation in yeast increased the mitochondrial CuL pool giving rise to the hypothesis that with regards to increased CCO activity in copper supplemented cultures, the CuL complex might be involved in the provision of copper to CCO in *SH-SY5Y* cells also. In this thesis a putative CuL complex was identified in rat liver mitochondria, however, it was not possible to perform comparative studies of CuL concentrations between APP_{WT} and APP_{swe} by 2D-LC and ICP-MS metal analysis. Metal analysis of 2D-LC samples in APP_{WT} whole cell extracts revealed very low amounts of putative CuL (figure 3.16) with the result that analysis was not further pursued, whereas mitochondrial extracts of APP_{WT} (figure 3.14) yielded amounts of protein too low for 2D-LC analysis.

For SOD1 activity assays whole cell extracts were prepared, thus it is impossible to determine the contribution of mitochondrial SOD1 or cytosolic SOD1 to the overall activity measured. Copper supplementation of APP_{swe} cultures resulted in increased enzyme activity indicating that SOD1 is partially unmetallated under normal culture conditions, which provides the conditions required for mitochondrial import of the enzyme. Upon increasing copper concentrations it is possible that not only the metallated state of cytosolic SOD1 increased, but also that of mitochondrial SOD1, thus preventing oxidative stress produced by increased copper concentrations in the cytosol and increased ROS being produced by newly metallated CCO. The increased survival and growth rate of APP_{swe} cells in high copper compared to the APP_{swe} control may be a direct result of activating both enzymes and increased copper efflux via A β . This finding is supported by studies in *SH-SY5Y* cells lacking both alleles for SOD1, which identified that although the decrease in SOD1 was less in mitochondria with respect to its cytosolic counterpart, the effects of SOD1

deficiency were highly noticeable in mitochondria rather than cytosolic proteins (Aquilano et al., 2006). It needs to be mentioned that liquid analysis of SOD1 activity by spectrophotometry represents all SOD activity and is not so specific for SOD1. Although SOD1 activity can be inactivated by the addition of KCN with residual activity originating from alternative SOD proteins, the decision was made not to use the chemical to perform these controls due to concerns for Health and Safety. Since SOD1 is the most abundant SOD isoform in mammalian cells activity was recorded as originating from SOD1. This might attribute to the variation in SOD1 activity measured between various experiments.

The increase in CCO activity in copper supplemented APP_{swe} cultures indicates a further symptom of early neurodegeneration in FAD patients carrying this mutation. Permanent reduction in oxidative phosphorylation creates cellular ATP deficits and dissipation in mitochondrial transmembrane potentials which result in release of cytochrome c and initiation of the apoptotic cascade (Krysko et al., 2001). The reduced level of CCO activity in APP_{swe} compared to APP_{WT} might be caused by a number of factors since the maturation of this protein complex requires a multitude of accessory proteins. Studies show that in copper-deficient *SH-SY5Y* cultures the CCO subunit COX2, which contains copper as a co-factor, is present at much lower levels (Rossi et al., 2001). This observation is not likely due to deficient copper-dependent mitochondrial import mechanisms, since this subunit is expressed within the mitochondrion. Furthermore, in copper-deficient cells the CuL complex suggested to metallate CCO, would remain in the cytoplasm, thus the mitochondrial matrix copper pool is reduced in its ability to mediate CCO assembly.

However, mitochondrial dysfunction is not only caused by reduced levels of CCO and SOD1 following copper depletion. Copper supplementation of APP_{WT} cultures resulted in decreased survival depending on copper concentration (figure 3.25) and attenuation of growth in high copper (figure 3.26). Although APP_{swe} cells show copper resistance and recovery of copper-dependent enzyme activity, growth is attenuated in high concentrations of copper (figure 3.26) indicating that copper-deficient phenotypes can not be rescued by metal supplementation alone. Anandatheerthavarada et. al. (Anandatheerthavarada et al., 2003) previously demonstrated full length APP insertion into the outer mitochondrial membrane in

cortical neurons of transgenic AD mice, and A β co-localisation with mitochondria has been reported in human AD affected brains (Lustbader et al., 2004) and Tg2576 mouse brain carrying the Swedish mutation of APP (Crouch et al., 2005). One important observation was that the decrease in CCO activity, which is thought to be caused by the presence of A β in the mitochondrion, is specific to brain regions normally affected by neurodegeneration in AD (Anandatheerthavarada et al., 2003). It was reported by Casley et. al. (Casley et al., 2002) that A β ₁₋₄₂ mediates the reduction in CCO activity directly and not through oxidative changes of the surrounding membrane environment. It is suggested that A β ₁₋₄₂ directly interacts with CCO and possibly through structural rearrangement upon binding prevents the association of reduced cytochrome c with CCO. Inhibition of CCO is thought to increase the production of ROS by the previous complexes of the electron transport chain (Casley et al., 2002). A β -mediated inhibition of CCO was dependent on the presence of Cu(II) and chelation of the metal reduced CCO inhibition (Crouch et al., 2005), therefore it was suggested that copper might aid the process either by A β oligomerisation, formation of dityrosine crosslinks (as described in section 1.6.1) or directly in A β -CCO interaction. An additional factor contributing to increased ROS production in mitochondria is the ability of A β to facilitate the reduction of Cu(II) to Cu(I). This in turn could result in the oxidation and carbonylation of membrane and proteins and ultimately the activation of apoptosis via cytochrome c release. These findings support the observation that in high copper concentrations cell growth is drastically alleviated in both APP_{WT} and APP_{swe} cell cultures. The mechanisms behind A β import into the mitochondrion are still unknown. It is possible that during increased APP cleavage and A β generation, which was observed in many FAD patients, combined with axonal transport inhibition through hyperphosphorylated tau protein the secretory pathway becomes congested and vesicles are redirected to organelles not normally targeted. This might account for the accumulation of intracellular copper which was not mirrored in increased CCO and SOD1 activity, but being bound to vesicular and mitochondrial A β . However, further studies need to be performed to validate this hypothesis.

Recent research has established links between the oxidative stress response and APP processing. Angeletti et. al. (Angeletti et al., 2005) demonstrated that the APP cleavage enzyme BACE1 and CCS stably interact via their C-terminal cytoplasmic

domain and domain I, respectively, and it was shown that overexpression of BACE1 directly competes for CCS with SOD1 resulting in decreased enzyme activity. This phenotype was rescued by CCS overexpression. The neuronal adaptor protein X11 α was shown to have a similar effect on SOD1 activity due to it binding to CCS domain III (McLoughlin et al., 2001). Despite the co-localisation of BACE1 and APP via X11 α , the adaptor protein inhibits the production of A β from APP in the presence of CCS, a process that is interrupted and results in increased A β generation in *SH-SY5Y* deletion mutants of CCS (Gray et al., 2010). Thus these data suggests that X11 α -mediated CCS interaction with BACE1 and Cu(I) transfer may contribute to cellular copper homeostasis by altering APP metabolism and thus preventing APP participation in copper homeostasis. Moreover, the interaction of APP, BACE1, CCS and X11 α could determine BACE1 activity or BACE1 association with APP in a copper-regulated manner.

The localisation of CCS also needs further consideration. CCS localisation in the mitochondrion additionally decreases the amount of CCS available to cytosolic SOD1 and BACE1, thus increased cellular copper might cause increased CCS concentrations in the mitochondrion due to increased oxidative stress as mentioned previously. This would ultimately result in increased APP cleavage, since less CCS is available to bind BACE1, and possible export of copper due to extracellular A β release. The fact that the APP gene contains a copper responsive element in its promoter region emphasises the role of APP in copper homeostasis (Bellingham et al., 2004b). It was shown that upon copper depletion in fibroblasts APP gene expression was down-regulated suggesting a role in copper export for APP. This view is supported by findings of this project that in APP_{swe} cultures copper-dependent enzyme activities are decreased compared to APP_{WT}. APP expression analysis in APP_{WT} and APP_{swe} neurons from AD patients needs to be performed to confirm that the down-regulation of APP is not cell-type specific or an artefact of experimental procedures. APP quantification could not be performed in APP_{WT} and APP_{swe} cell lines, since the APP_{swe} cell line was designed to overexpress the mutant APP gene. However, there is a line of evidence that APP might not be involved in copper efflux, but rather copper import. The ability of APP and A β to bind copper has led to the hypothesis that APP might be involved in plasmamembrane reduction of Cu(II) to Cu(I) prior to Ctr1-mediated import analogous to the role Fre1 plays in

copper import in yeast (Hassett and Kosman, 1995). The increase in intracellular copper monitored in both APP_{WT} and APP_{swe} cell lines (figure 3.28) supports this assumption. Although APP_{swe} cells produce up to eight times more A β (Citron et al., 1992) than APP_{WT} cells, both cell lines displayed increased concentrations of intracellular copper when treated with high exogenous concentrations of copper. If APP was involved in the cell's protection against excess copper, elevated intracellular copper levels would have been counteracted.

One factor of APP metabolism that has not been studied in very much detail is the APP AICD. AICD is produced by intramembraneous γ -secretase cleavage in both non-amyloidogenic and amyloidogenic pathways (figure 1.2). AICD is either restricted to cytosolic membranes by the adaptor protein X11 α or interacts with the adaptor proteins Jip1b and Fe65, which aid AICD transport into the nucleus and subsequent interaction with the nuclear histone acetylase Tip60 (von Rotz et al., 2004), where it indirectly regulates the gene expression of APP, BACE1 and Tip60 among others (Cao and Sudhof, 2001). The AICD-mediated gene expression for both APP and BACE1 ensures that full-length APP levels are at a constant steady-state. However, during increased APP metabolism as was detected for most FAD mutations, this feedback mechanism becomes imbalanced. Although gene expression of APP and BACE1 are linked and constant, additional cellular changes such as increased or decreased copper levels can influence APP processing and/or trafficking and possibly BACE1 activity, thus shifting the delicate balance towards pathways that could accelerate symptoms observed in AD patients.

The importance of oxidative stress in the progression of AD pathology is compelling. Due to its high metabolic rate, the brain is an organ rich in molecular oxygen and consumes large amounts of glucose. Energy production depends on the electron transport chain, which is renowned for its production of oxidative stress inducing by-products. Mitochondrial oxidative stress was shown to be involved in hyperphosphorylation of cytoplasmic tau (Melov et al., 2007), thus deregulating axonal transport of mitochondria and exocytic vesicles destined to participate in neuronal transmission. Two independent research groups (Tong et al., 2005, Borghi et al., 2007) identified oxidative stress as a factor contributing to increased BACE1 activity, but not gene expression or protein translation. This increased activity

facilitates the accumulation of extracellular A β and amyloid which exerts copper-catalysed oxidative insults to the surrounding membranes and proteins. In FAD mutations, such as the Swedish mutation of the APP gene, which already display symptoms of cellular oxidative stress either through reduced activity of cellular antioxidant defence or increased production of mitochondrial ROS, oxidative insult is likely to exacerbate disease progression. Studies in a PC12 APP_{swe} cell line demonstrated elevated activity of caspase 3 after treatment with hydrogen peroxide indicating that early onset AD in this particular FAD mutation might result from increased neuronal vulnerability to extracellular oxidative stress (Marques et al., 2003).

In the past decade particular emphasis has been placed on neurodegenerative diseases as pathologies involving alterations in metal homeostasis, oxidative stress and mitochondrial dysfunction. Special attention has been paid to the possible role of mitochondria in the early stages of disease development. However, there are no conclusions with regards to mitochondrial dysfunction being a consequence or the cause of neurodegeneration.

One hallmark to characterise the degree of AD progression in patients is the amount of deposited A β . Soluble A β is produced at low levels under physiological conditions and present in all biological fluids implying that under pathological conditions either the natural balance of A β metabolism is perturbed or a rogue form of the peptide exists in AD individuals (Bush, 2002). Association of A β with aberrant metal homeostasis was inferred from distribution patterns of amyloid deposits in the brain, which occurred particularly localised to synapses thus there is a possibility that reagents participant in synaptic transmission might contribute to amyloid pathology. A β was localised intra-mitochondrially and extracellularly, destinations characteristic for generation of ROS and high content of metal ions, in particular zinc and copper. Synaptic elevation of ROS production is correlated with the ability of A β to bind copper and participate in redox-cycling mediated reactions. Direct neuronal damage and a contribution of ROS to AD pathology was demonstrated by the reversal of age-related learning deficits and brain oxidative stress in mice during chronic systemic administration of synthetic catalytic scavengers of ROS (Liu et al., 2003). Although it is not yet established whether

ROS generation is a cause or consequence of neurodegeneration and A β toxicity it is likely that intracellular ROS production is an event early in disease progression. Studies have shown that intraneuronal A β accumulation precedes plaque formation in APP and PS double transgenic mice (Wirhth et al., 2001) and that hippocampal neuron loss exceeds amyloid plaque load in a transgenic mouse model of AD (Schmitz et al., 2004). These findings emphasise the importance of elucidating early cellular events in order to develop therapeutic agents for the prevention of the disease and to slow or abolish disease progression.

It was demonstrated that under physiological concentrations of copper and zinc synthetic A β added to CSF was readily degraded by metal requiring IDE and MMP (Saido and Iwata, 2006). Increased concentrations of copper and zinc seem to increase A β accumulation and oxidative stress suggesting that not only A β generation, but also metal availability, is increased in AD. The normal ageing brain displays increased copper concentrations, a feature which might lead to altered metal homeostasis and the onset of AD. However, to detect changes between normal and AD brains, it is insufficient to assess whole brain copper. Detailed post-mortem analyses are necessary to test the copper concentrations in different brain regions and also distinguish between extracellular and intracellular copper concentrations. General statements about brain copper concentrations with regards to AD do not hold true since specific regions in the brain are affected and although overall copper concentrations might be increased, local or indeed intracellular copper concentration might be reduced. It is therefore important to assess copper homeostasis in both a physiological model such as transgenic mice and cell culture. Only in a combined study, can the flux of copper be assessed and a thorough understanding of the interplay between organellar, cellular and systemic copper concentrations be gained.

Before discussing the effect of APP on cellular copper homeostasis, a critical appraisal of current models in the study of copper homeostasis in AD provides a useful context. There are several cell culture models using fibroblasts, *HEK296*, *PC12*, *SH-SY5Y* cells and many more harbouring APP mutations relevant to the respective studies. However, these models can only assess intracellular copper distribution, influx and efflux. The interplay between extracellular amyloid beta

deposits and their possible effect on cell survival through ROS production is not readily performed due to cell culture procedure and constant change of culture media resulting in the removal of extracellular factors contributing to the pathology. Additionally it is a challenge to recreate physiological concentrations of metals, serum constituents and nutrients in cell culture medium in a consistently stable and reliable manner, since physiological CSF represents an ultrafiltrate of blood (Saunders et al., 1999) supplemented with components that are actively transported into the CSF depending on cellular demands. Thus the results obtained in this study reflect rather the effect of exogenous copper and the APP_{swe} mutation on intracellular copper distribution and neuronal damage that is potentially caused by mitochondrial A β . Another model for the determination of the role of APP in copper homeostasis are transgenic mouse models harbouring relevant APP mutations, such as the Tg2976 mouse model overexpressing the human version of APP_{swe}. Mice possess a version of the APP protein in which a three amino acid change compared to the human protein results in reduced aggregation of A β and a higher affinity to Cu(II) with less observable ROS production. Deploying transgenic mice carrying the human APP additionally to the mouse counterpart in metal homeostasis studies carries the risk of data being obscured by the impact native APP has on the biochemical behaviour of human APP. The copper scavenging ability of mouse A β prevents human A β , at least in part, in participating in Cu(II) binding events and the reduction of Cu(II) to Cu(I), thus impairing analysis of ROS generation and the degree of amyloid deposition. However, both model systems in conjunction with *in vitro* studies to understand the biochemical dynamics of copper-binding to proteins allow an insight into cellular mechanisms contributing to neurodegeneration in the context of AD.

The APP protein plays a central role in the brain and might have functions beyond the participation in metal homeostasis. It was established that its AICD is involved in transcriptional activation (Cao and Sudhof, 2001) and the sAPP α domain in neurite outgrowth (Mattson et al., 1993) and it was speculated that APP participates in G-coupled protein signalling (Nishimoto et al., 1993) or even act as a metallochaperone. Despite the possibility of APP possessing diverse biological functions the presence of two copper-binding sites is prevalent and strongly

suggests a role in metal homeostasis. However, the exact role of APP has not been determined.

In the scope of this project the results obtained by biochemical analysis of cellular metal distribution, copper-dependent enzymatic activity assays and phenotypic analysis of cell growth and survival suggest that APP presents a means to facilitate copper efflux from the cell. Previously reported elevation of APP_{swe} cleavage by BACE1 results in increased production of A β species (Citron et al., 1992). At the same time cellular copper deficiency was demonstrated via increased copper-dependent enzyme activity upon copper supplementation. The relationship between A β production and copper efflux is partly assessed within this thesis. Whether these A β species are secreted or remain intracellular in mitochondria or microtubule associated secretory vesicles remains unknown and further research employing cellular fractionation techniques coupled with immunohistochemistry and ICP-MS analysis would aid in the identification of A β localisation.

Mitochondrial ROS production which is implicated in cytosolic tau hyperphosphorylation (Melov et al., 2007) might prevent the release of vesicular A β due to inhibition of APP-mediated axonal trafficking. The increase observed in intracellular copper concentration in APP_{WT} cultures might be a direct result of mitochondrial induced inhibition of vesicular transport, since copper-dependent enzyme activity did not change upon copper supplementation in this cell line. Accumulation of intracellular A β contributing to intracellular oxidative stress due to redox-cycling of bound copper contributes to the degeneration of neurons as well as vesicular lesions during A β membrane pore formation.

Deficiencies in axonal transport affect mitochondrial transport to the synapse, where large amounts of ATP are needed for active transport of extracellular zinc into vesicles following neurotransmission. Failure of zinc endocytosis results in constitutive neurotransmission and excitotoxicity. Further free synaptic zinc is scavenged by A β to form extracellular plaques (Lovell et al., 1999). These plaques constitute β -sheet fibrils inaccessible to IDE and MMP, thus a reduction of A β levels by its natural clearance mechanism is prevented. With zinc acting as catalytic co-factor of IDE and MMP, both enzyme activities are depleted when zinc that is readily available under normal physiological conditions is scavenged by A β

plaques. Since A β is produced under physiological conditions (Bush, 2003) potential treatments of AD need to be assessed carefully. Simple inhibition of BACE1 is impossible with regards to other physiological functions both BACE1 and A β may hold. BACE1 may be important in copper homeostasis, not just by processing APP, but the high affinity Cu(I) binding site in BACE1 might be directly involved in copper export, import or shuttling. BACE1 involvement in APP-mediated metal homeostasis suggests that treatment of AD with BACE1 inhibitors in the early stages might result in disruption of the physiological role that BACE1 plays and contribute to rather than prevent pathology. It was shown that copper binding to APP greatly reduces APP processing in vitro (Barnham et al., 2003b) via structural changes in the APP dimer, thus BACE1 together with CCS might be involved in regulating APP processing via metallation or dematallation of the protein.

The role of CCS in cellular copper distribution and possible implications in neuronal pathology also need to be clarified. Cellular CCS expression and localisation patterns in conditions of copper deficiency and copper surplus need to be established to determine the impact of CCS on copper trafficking and mediation of copper transport. Specifically the interactions of CCS with BACE1 and APP via X11 α hold potential explanations with regards to CCS-dependent copper-mediated BACE1 processing of APP. Although many of the aspects of copper transport remain to be identified results in this study suggest a contribution of APP to copper efflux. Whether this is due to APP regulation of efflux or direct involvement of APP in copper excretion remains unknown. The evidence supporting this hypothesis is briefly recapitulated below and summarised in figures 4.1 and 4.2.

The increased CCO and SOD1 activity in copper-supplemented APP_{swe} cultures is indicative of a copper deficient phenotype contributing to early onset neuronal degradation and reduction in survival compared to APP_{WT} cultures due to reduced CCO and SOD1 activity under normal culture conditions. Survival was restored almost to APP_{WT} levels upon copper supplementation, however, the growth of APP_{swe} cultures was inhibited in high copper indicating toxicity of prolonged copper exposure even at low dosage. Intracellular copper accumulation in both cell lines is most likely due to increased copper trafficking to CCO and SOD1 in APP_{swe}

and increased vesicular efflux of copper in APP_{WT} which was potentially prevented by failure of vesicular axonal trafficking. APP_{WT} displayed a high degree of vulnerability towards high and low copper concentrations suggesting deficiencies in detoxification of surplus copper. Additionally exogenous copper probably exerted a greater detrimental effect on APP_{WT} culture than APP_{swe}, since APP_{swe} provided more intracellular ligands for excess copper, thus shifting the equilibrium towards increasing copper import and in the process reducing the concentrations of extracellular copper.

The evidence for APP contribution in copper homeostasis obtained during this project highlights that especially in FAD early stages of AD might be caused by alterations in cellular metal homeostasis, however, advanced neurodegeneration is potentiated by both metal-dependent and metal-independent processes that fundamentally alter cellular metabolism and the cell's ability to tolerate a whole host of different stress insults.

Figure 4.1: Summary of processes involved in copper homeostasis in *SH-SY5Y* APP_{WT} cell lines supplemented with copper

Copper is imported into the cell by Ctr1 and distributed to three distinct pathways. Copper is bound by the copper chaperone for superoxide dismutase (CCS) for metal delivery to SOD1, to Cox17 for insertion into mitochondrial cytochrome c oxidase and to Hah1 for incorporation into proteins in the Golgi and exocytosis. Upon trafficking to the cell surface APP is cleaved either by α -secretase (APP_{WT}) or β -secretase (APP_{swe}). It was shown by McLoughlin et. al. (McLoughlin et al., 2001) that CCS binds BACE1 through the adapter protein X11- α . It was demonstrated that *SH-SY5Y* APP_{WT} cell lines supplemented with copper do not display increased SOD1 and CCO enzyme activity, thus it is hypothesised that the increased cellular copper content is likely to be distributed to the secretory pathway for excretion. However, this process might be affected by hyperphosphorylated tau-mediated retention of APP-containing vesicles. This could impact not only on the physiological functions of soluble APP fragments, but also interfere with secretion of other extracellular proteins and alter cellular copper homeostasis.

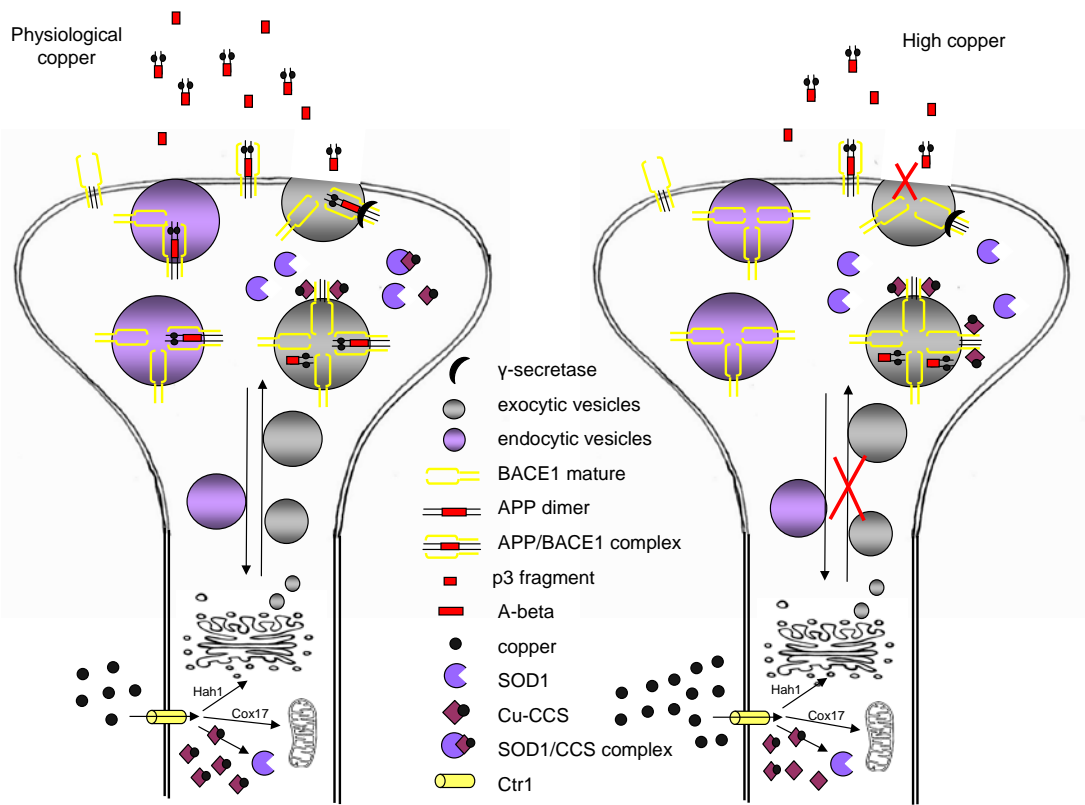
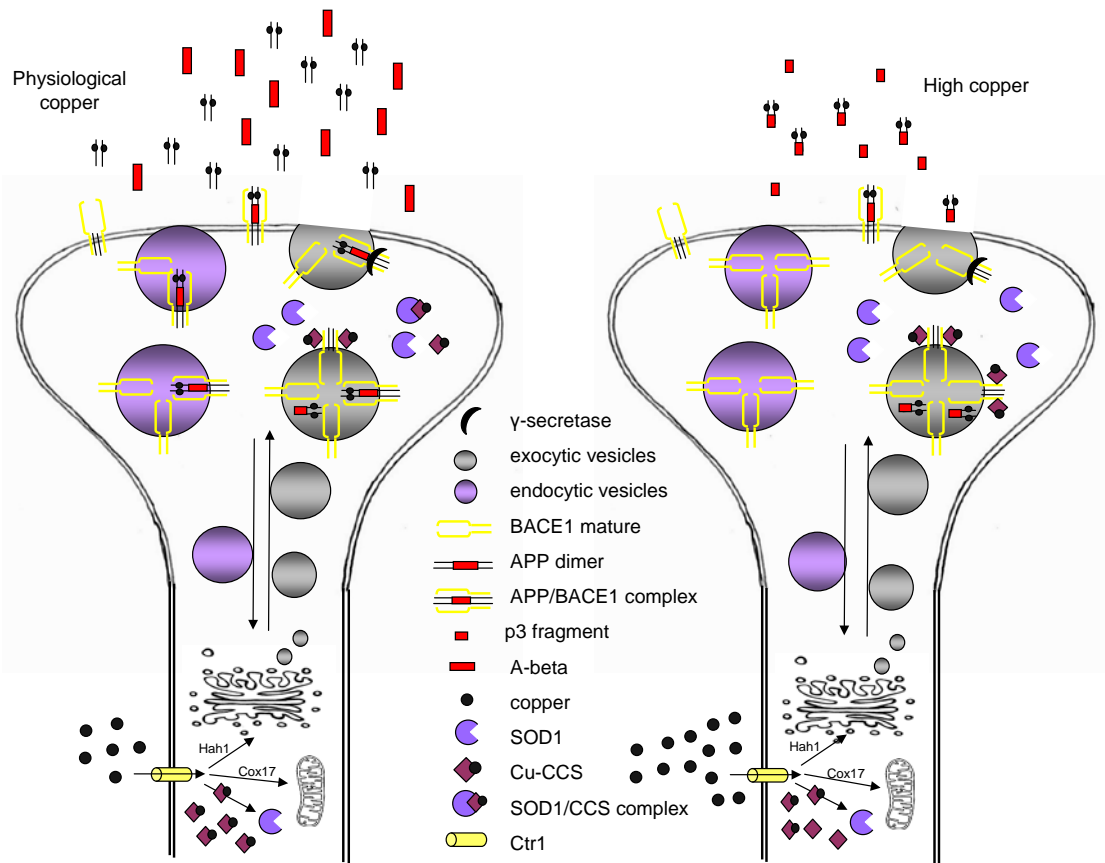


Figure 4.2: Evidence for alteration in cellular copper homeostasis by the Swedish mutation in *SH-SY5Y* cells and the implications for copper-dependent enzymes

Copper is imported into the cell by Ctr1 and distributed to three distinct pathways. Copper is bound by the copper chaperone for superoxide dismutase (CCS) for metal delivery to SOD1, to Cox17 for insertion into mitochondrial cytochrome c oxidase and to Hah1 for incorporation into proteins in the Golgi and exocytosis. Upon trafficking to the cell surface APP is cleaved either by α -secretase (APP_{WT}) or β -secretase (APP_{swe}). It was shown by McLoughlin et. al. (McLoughlin et al., 2001) that CCS binds BACE1 through the adapter protein X11- α . Citron et. al. (Citron et al., 1992) demonstrated that the Swedish mutation causes a 6-8 fold increase in APP cleavage by BACE1. It is thus hypothesised that the ability of CCS to deliver copper to SOD1 and BACE1, or at least interact with both proteins, might lead to aberrant copper homeostasis in cells containing the Swedish mutation. It was observed that in physiological copper concentrations APP_{swe} cell cultures displayed a copper-deficient phenotype, which could be rescued by copper supplementation. SOD1 and CCO enzyme activities increased in copper supplemented cells and survival rates were increased compared to the control. It is hypothesised that the copper deficit was reversed through increased copper transport by enhanced chaperone delivery of copper to respective target proteins, possibly resulting in reduced interactions between BACE1 and CCS. Whether this interaction is of a physiologically relevant or pathological nature remains to be determined.



4.3 Future work

The data presented in this thesis raised several issues regarding copper distribution and cellular responses to metal stimulation or depletion. Specifically copper-dependent enzymatic activity contributed to the understanding of alterations in copper homeostasis with regards to the Swedish mutation and changes in copper levels.

As a start to future work it might be worth increasing the number of replicates for SOD1 activity assays, whole cell metal content analysis and also survival studies to achieve greater insight about significance of the data (some replicates hardly displayed any significant changes). Attempts to compare the metal content for APP_{WT} and APP_{swe} in the SOD1 protein pool after 2D-LC and ICP-MS analysis have been made and data suggest decreased copper levels in APP_{swe} compared to APP_{WT} bound to this particular copper pool. However, data only represents a non-statistically significant trend, which needs to be pursued further in order to draw conclusions concerning the SOD1 metallation status.

The Cu(I) specific chelator BCS, used for copper depletion in both cell cultures, could potentially be substituted or combined with additional copper chelators, such as EDTA. In biological fluids as well as cell culture medium there is a constant equilibrium between the two oxidation states of copper. BCS chelation of Cu(I) shifts this equilibrium resulting in increased presence of Cu(II). BCS combined with a non-specific copper chelator might result in greater copper chelation, thus reduce the amount of cell passaging needed to completely devoid the cell of copper. A reduction in passaging would reduce the stress cells endure during the culturing process, which might lead to increased basal SOD1 activity and as a result might flaw data.

With regards to differences in copper trafficking between the two cell lines, it is of interest to establish the presence of the CuL complex in *SH-SY5Y* cells and subsequently compare its copper content in physiological and pathological copper concentrations.

One question that remains is the role of APP in copper homeostasis. Although results from this thesis point to APP mediating copper efflux, intense analysis of

APP cleavage fragments needs to be performed. Western blot analysis of secreted fragments and organellar fragments might identify further contributions of A β to neuronal degeneration or a possible physiological role during copper trafficking or detoxification. Analysis of the vesicular fraction for A β and APP content is of particular interest since data from intracellular copper content determination indicates that in copper supplemented APP_{WT} cells copper might accumulate in vesicles destined for synaptic excretion. Intracellular accumulation of such vesicles probably by hyperphosphorylated tau-mediated inhibition of axonal transport could contribute to cerebral metal imbalance.

Another question to be answered is the effect copper binding exerts on APP. It was reported that copper-binding to APP prevents APP processing by BACE1 due to inducing conformational changes in the APP dimer. A logical consequence would be that copper normally bound to A β resides in full-length APP and undergoes reinternalisation, rather than excretion. This changes not only physiological copper distribution, but also increases intracellular copper concentrations. However, increased APP cleavage in APP_{swe} indicates decreased basal levels of copper binding to APP, an effect which might be potentiated by increased A β generation. Western blot analysis of soluble A β and sAPP β in conjunction with full-length APP would identify cleavage preferences of BACE1 in APP_{WT} and APP_{swe} cultures in high and deplete copper concentrations depending on APP copper binding state.

The creation of an APP knock-out mutant in *SH-SY5Y* cultures and subsequent phenotypic analysis as performed in this work might provide further insight into the relevance of APP in copper homeostasis. However, it is possible that these mutants are not viable due to loss of neurite outgrowth and metal imbalance.

A bioinformatic based approach to elucidating the roles of BACE1 and APP copper-binding is the comparison of their copper-binding sites to copper-binding sites in other metalloproteins. APP is an evolutionarily conserved protein and comparison of its metal-binding site might be of use in the deduction of a function as chaperone, importer, exporter or even regulator of the above.

To determine which role CCS plays in copper distribution in elevated or depleted copper conditions, it is important to establish organellar CCS location. CCS-

mediated copper delivery can affect SOD1 activity, SOD1 import into mitochondria and function in an unknown capacity during BACE1 binding. It is not yet understood how copper depletion or supplementation influences CCS trafficking and variation in copper delivery to target proteins in either APP_{WT} and APP_{swe} culture, thus comparative studies of CCS localisation can be achieved by cell fractionation techniques coupled with copper content analysis by ICP-MS of respective cellular fractions and possible quantitative Western blot analysis to confirm protein presence. Results would further need to be verified by comparative analysis of CCS gene expression to establish whether changes in CCS localisation under varying copper concentration or genetic background is due to gene expression or variation in protein translation patterns. Studies employing ribosomal inhibitory agents would clarify the degree of translation-dependent changes in CCS activity. Another possibility is the expression of GFP-CCS in both cell lines to observe CCS trafficking and localisation under the microscope. However, this could potentially flaw results of cellular metal distribution and CCS localisation, since GFP may prevent trafficking of CCS into the mitochondrion or interfere with copper binding to the protein. Further, overexpressing CCS impedes direct comparison of cell lines carrying the modified gene and the amount of copper delivered to target proteins might vary due to varying expression levels.

Additionally to CCS gene expression analysis, studies of MT-3, CTR1, HAH1, ATP7A, COX17, BACE1, SOD1 and APP gene expression could be useful to assess the routes of distribution of excess exogenous copper throughout the cell. Admittedly, the gene expression analysis for APP might prove difficult in these two cell lines, since the APP_{swe} cell line was designed to overexpress the protein. Thus methods of standardisation need to be identified first.

References

- Aftab, A., Ann, P. W., Keyoumars, A., James, S. D. & Michael, L. S. (2007) Wilson's disease. *LANCET*, 369, 397-408.
- Alder, N. N. & Johnson, A. E. (2004) Cotranslational Membrane Protein Biogenesis at the Endoplasmic Reticulum. *Journal of Biological Chemistry*, 279, 22787-22790.
- Allen, R. G. & Tresini, M. (2000) Oxidative stress and gene regulation. *Free Radical Biology and Medicine*, 28, 463-499.
- Aller, S. G. & Unger, V. M. (2006) Projection structure of the human copper transporter CTR1 at 6-Å resolution reveals a compact trimer with a novel channel-like architecture. *Proceedings of the National Academy of Sciences of the United States of America*, 103, 3627-3632.
- Anandatheerthavarada, H. K., Biswas, G., Robin, M.-A. & Avadhani, N. G. (2003) Mitochondrial targeting and a novel transmembrane arrest of Alzheimer's amyloid precursor protein impairs mitochondrial function in neuronal cells. *The Journal of Cell Biology*, 161, 41-54.
- Anders, A., Gilbert, S., Garten, W., Postina, R. & Fahrenholz, F. (2001) Regulation of the {alpha}-secretase ADAM10 by its prodomain and proprotein convertases. *FASEB J.*, 15, 1837-1839.
- Andreini, C., Banci, L., Bertini, I. & Rosato, A. (2006) Zinc through the Three Domains of Life. *Journal of Proteome Research*, 5, 3173-3178.
- Andreini, C., Bertini, I., Cavallaro, G., Holliday, G. & Thornton, J. (2008) Metal ions in biological catalysis: from enzyme databases to general principles. *Journal of Biological Inorganic Chemistry*, 13, 1205-1218.
- Angeletti, B., Waldron, K. J., Freeman, K. B., Bawagan, H., Hussain, I., Miller, C. C. J., Lau, K.-F., Tennant, M. E., Dennison, C., Robinson, N. J. & Dingwall, C. (2005) BACE1 Cytoplasmic Domain Interacts with the Copper Chaperone for Superoxide Dismutase-1 and Binds Copper. *Journal of Biological Chemistry*, 280, 17930-17937.
- Annaert, W. G., Esselens, C., Baert, V., Boeve, C., Snellings, G., Cupers, P., Craessaerts, K. & De Strooper, B. (2001) Interaction with Telencephalin and the Amyloid Precursor Protein Predicts a Ring Structure for Presenilins. *Neuron*, 32, 579-589.
- Aquilano, K., Vigilanza, P., Rotilio, G. & Ciriolo, M. R. (2006) Mitochondrial damage due to SOD1 deficiency in SH-SY5Y neuroblastoma cells: a rationale for the redundancy of SOD1. *FASEB J.*, 20, 1683-1685.

- Araki, Y., Tomita, S., Yamaguchi, H., Miyagi, N., Sumioka, A., Kirino, Y. & Suzuki, T. (2003) Novel Cadherin-related Membrane Proteins, Alcadeins, Enhance the X11-like Protein-mediated Stabilization of Amyloid β -Protein Precursor Metabolism. *Journal of Biological Chemistry*, 278, 49448-49458.
- Arciello, M., Rotilio, G. & Rossi, L. (2005) Copper-dependent toxicity in SH-SY5Y neuroblastoma cells involves mitochondrial damage. *Biochemical and Biophysical Research Communications*, 327, 454-459.
- Arispe, N. (2004) Architecture of the Alzheimer's A β Ion Channel Pore. *Journal of Membrane Biology*, 197, 33-48.
- Armogida, M., Petit, A., Vincent, B., Scarzello, S., Da Costa, C. A. & Checler, F. (2001) Endogenous [beta]-amyloid production in presenilin-deficient embryonic mouse fibroblasts. *Nat Cell Biol*, 3, 1030-1033.
- Arnesano, F., Banci, L., Bertini, I., Martinelli, M., Furukawa, Y. & O'Halloran, T. V. (2004) The Unusually Stable Quaternary Structure of Human Cu,Zn-Superoxide Dismutase 1 Is Controlled by Both Metal Occupancy and Disulfide Status. *Journal of Biological Chemistry*, 279, 47998-48003.
- Assaf, S. Y. & Chung, S.-H. (1984) Release of endogenous Zn²⁺ from brain tissue during activity. *Nature*, 308, 734-736.
- Atwood, C. S., Scarpa, R. C., Huang, X., Moir, R. D., Jones, W. D., Fairlie, D. P., Tanzi, R. E. & Bush, A. I. (2000) Characterization of Copper Interactions with Alzheimer Amyloid β Peptides. *Journal of Neurochemistry*, 75, 1219-1233.
- Barnham, K. J., Ciccotosto, G. D., Tickler, A. K., Ali, F. E., Smith, D. G., Williamson, N. A., Lam, Y.-H., Carrington, D., Tew, D., Kocak, G., Volitakis, I., Separovic, F., Barrow, C. J., Wade, J. D., Masters, C. L., Cherny, R. A., Curtain, C. C., Bush, A. I. & Cappai, R. (2003a) Neurotoxic, Redox-competent Alzheimer's β -Amyloid Is Released from Lipid Membrane by Methionine Oxidation. *Journal of Biological Chemistry*, 278, 42959-42965.
- Barnham, K. J., McKinstry, W. J., Multhaup, G., Galatis, D., Morton, C. J., Curtain, C. C., Williamson, N. A., White, A. R., Hinds, M. G., Norton, R. S., Beyreuther, K., Masters, C. L., Parker, M. W. & Cappai, R. (2003b) Structure of the Alzheimer's Disease Amyloid Precursor Protein Copper Binding Domain. *Journal of Biological Chemistry*, 278, 17401-17407.
- Bartnikas, T. B. & Gitlin, J. D. (2003) Mechanisms of Biosynthesis of Mammalian Copper/Zinc Superoxide Dismutase. *Journal of Biological Chemistry*, 278, 33602-33608.
- Beauchamp, C. & Fridovich, I. (1971) Superoxide dismutase: Improved assays and an assay applicable to acrylamide gels. *Analytical Biochemistry*, 44, 276-287.

Beers, J., Glerum, D. M. & Tzagoloff, A. (1997) Purification, Characterization, and Localization of Yeast Cox17p, a Mitochondrial Copper Shuttle. *Journal of Biological Chemistry*, 272, 33191-33196.

Behr, D., Hesse, L., Masters, C. L. & Multhaup, G. (1996) Regulation of Amyloid Protein Precursor (APP) Binding to Collagen and Mapping of the Binding Sites on APP and Collagen Type I. *Journal of Biological Chemistry*, 271, 1613-1620.

Bellingham, S. A., Ciccotosto, G. D., Needham, B. E., Fodero, L. R., White, A. R., Masters, C. L., Cappai, R. & Camakaris, J. (2004a) Gene knockout of amyloid precursor protein and amyloid precursor-like protein-2 increases cellular copper levels in primary mouse cortical neurons and embryonic fibroblasts. *Journal of Neurochemistry*, 91, 423-428.

Bellingham, S. A., Lahiri, D. K., Maloney, B., La Fontaine, S., Multhaup, G. & Camakaris, J. (2004b) Copper Depletion Down-regulates Expression of the Alzheimer's Disease Amyloid- β Precursor Protein Gene. *Journal of Biological Chemistry*, 279, 20378-20386.

Bennett, B. D., Babu-Khan, S., Loeloff, R., Louis, J.-C., Curran, E., Citron, M. & Vassar, R. (2000a) Expression Analysis of BACE2 in Brain and Peripheral Tissues. *Journal of Biological Chemistry*, 275, 20647-20651.

Bennett, R. G., Duckworth, W. C. & Hamel, F. G. (2000b) Degradation of Amylin by Insulin-degrading Enzyme. *Journal of Biological Chemistry*, 275, 36621-36625.

Besser, L., Chorin, E., Sekler, I., Silverman, W. F., Atkin, S., Russell, J. T. & Hershfinkel, M. (2009) Synaptically Released Zinc Triggers Metabotropic Signaling via a Zinc-Sensing Receptor in the Hippocampus. *J. Neurosci.*, 29, 2890-2901.

Bitan, G., Kirkitadze, M. D., Lomakin, A., Vollers, S. S., Benedek, G. B. & Teplow, D. B. (2003) Amyloid β -protein (A β) assembly: A β ₄₀ and A β ₄₂ oligomerize through distinct pathways. *Proceedings of the National Academy of Sciences of the United States of America*, 100, 330-335.

Borchardt, T., Camakaris, J., Cappai, R., Masters, C. L., Beyreuther, K. & Multhaup, G. (1999) Copper inhibits beta-amyloid production and stimulates the non-amyloidogenic pathway of amyloid-precursor-protein secretion. *Biochem. J.*, 344, 461-467.

Borg, J.-P., Yang, Y., De Taddéo-Borg, M. N., Margolis, B. & Turner, R. S. (1998) The X11 α Protein Slows Cellular Amyloid Precursor Protein Processing and Reduces A β ₄₀ and A β ₄₂ Secretion. *Journal of Biological Chemistry*, 273, 14761-14766.

Borghini, R., Patriarca, S., Traverso, N., Piccini, A., Storage, D., Garuti, A., Cirmena, G., Odetti, P. & Tabaton, M. (2007) The increased activity of BACE1 correlates with oxidative stress in Alzheimer's disease. *Neurobiology of Aging*, 28, 1009-1014.

- Botelho, M. G., Gralle, M., Oliveira, C. L. P., Torriani, I. & Ferreira, S. R. T. (2003) Folding and Stability of the Extracellular Domain of the Human Amyloid Precursor Protein. *Journal of Biological Chemistry*, 278, 34259-34267.
- Bozym, R. A., Thompson, R. B., Stoddard, A. K. & Fierke, C. A. (2006) Measuring Picomolar Intracellular Exchangeable Zinc in PC-12 Cells Using a Ratiometric Fluorescence Biosensor *ACS Chemical Biology*, 1, 103-111.
- Brookmeyer, R., Ziegler-Graham, K., Johnson, E. & Arrighi, H. M. (2007) Forecasting the Global Burden of Alzheimer's Disease. John Hopkins University.
- Brou, C., Logeat, F., Gupta, N., Bessia, C., Lebail, O., Doedens, J. R., Cumano, A., Roux, P., Black, R. A. & Israël, A. (2000) A Novel Proteolytic Cleavage Involved in Notch Signaling: The Role of the Disintegrin-Metalloprotease TACE. *Molecular Cell*, 5, 207-216.
- Brown, N. M., Torres, A. S., Doan, P. E. & O'Halloran, T. V. (2004) Oxygen and the copper chaperone CCS regulate posttranslational activation of Cu,Zn superoxide dismutase. *Proceedings of the National Academy of Sciences of the United States of America*, 101, 5518-5523.
- Bull, P. C., Thomas, G. R., Rommens, J. M., Forbes, J. R. & Cox, D. W. (1993) The Wilson disease gene is a putative copper transporting P-type ATPase similar to the Menkes gene. *Nat Genet*, 5, 327-337.
- Burgos, P. V., Mardones, G. A., Rojas, A. L., DaSilva, L. L. P., Prabhu, Y., Hurley, J. H. & Bonifacino, J. S. (2010) Sorting of the Alzheimer's Disease Amyloid Precursor Protein Mediated by the AP-4 Complex. *Developmental Cell*, 18, 425-436.
- Busiglio, J., Gabuzda, D. H., Matsudaira, P. & Yankner, B. A. (1993) Generation of beta-amyloid in the secretory pathway in neuronal and nonneuronal cells. *Proceedings of the National Academy of Sciences of the United States of America*, 90, 2092-2096.
- Bush, A. I. (2002) Metal complexing agents as therapies for Alzheimer's disease. *Neurobiology of Aging*, 23, 1031-1038.
- Bush, A. I. (2003) The metallobiology of Alzheimer's disease. *Trends in Neurosciences*, 26, 207-214.
- Bush, A. I., Martins, R. N., Rumble, B., Moir, R., Fuller, S., Milward, E., Currie, J., Ames, D., Weidemann, A. & Fischer, P. (1990) The amyloid precursor protein of Alzheimer's disease is released by human platelets. *Journal of Biological Chemistry*, 265, 15977-15983.
- Bush, A. I., Masters, C. L. & Tanzi, R. E. (2003) Copper, β -amyloid, and Alzheimer's disease: Tapping a sensitive connection. *Proceedings of the National Academy of Sciences of the United States of America*, 100, 11193-11194.

Bush, A. I., Pettingell, W. H., Multhaup, G., D Paradis, M., Vonsattel, J. P., Gusella, J. F., Beyreuther, K., Masters, C. L. & Tanzi, R. E. (1994) Rapid induction of Alzheimer A beta amyloid formation by zinc. *Science*, 265, 1464-1467.

Buxbaum, J. D., Liu, K.-N., Luo, Y., Slack, J. L., Stocking, K. L., Peschon, J. J., Johnson, R. S., Castner, B. J., Cerretti, D. P. & Black, R. A. (1998a) Evidence That Tumor Necrosis Factor α Converting Enzyme Is Involved in Regulated α -Secretase Cleavage of the Alzheimer Amyloid Protein Precursor. *Journal of Biological Chemistry*, 273, 27765-27767.

Buxbaum, J. D., Thinakaran, G., Koliatsos, V., O'Callahan, J., Slunt, H. H., Price, D. L. & Sisoda, S. S. (1998b) Alzheimer Amyloid Protein Precursor in the Rat Hippocampus: Transport and Processing through the Perforant Path. *J. Neurosci.*, 18, 9629-9637.

Cai, D., Leem, J. Y., Greenfield, J. P., Wang, P., Kim, B. S., Wang, R., Lopes, K. O., Kim, S.-H., Zheng, H., Greengard, P., Sisoda, S. S., Thinakaran, G. & Xu, H. (2003) Presenilin-1 Regulates Intracellular Trafficking and Cell Surface Delivery of β -Amyloid Precursor Protein. *Journal of Biological Chemistry*, 278, 3446-3454.

Cai, H., Wang, Y., McCarthy, D., Wen, H., Borchelt, D. R., Price, D. L. & Wong, P. C. (2001) BACE1 is the major [beta]-secretase for generation of A[beta] peptides by neurons. *Nat Neurosci*, 4, 233-234.

Cai, X. D., Golde, T. E. & Younkin, S. G. (1993) Release of excess amyloid beta protein from a mutant amyloid beta protein precursor. *Science*, 259, 514-516.

Cao, X. & Sudhof, T. C. (2001) A Transcriptionally Active Complex of APP with Fe65 and Histone Acetyltransferase Tip60. *Science*, 293, 115-120.

Capell, A., Grünberg, J. R., Pesold, B., Diehlmann, A., Citron, M., Nixon, R., Beyreuther, K., Selkoe, D. J. & Haass, C. (1998) The Proteolytic Fragments of the Alzheimer's Disease-associated Presenilin-1 Form Heterodimers and Occur as a 100-150-kDa Molecular Mass Complex. *Journal of Biological Chemistry*, 273, 3205-3211.

Caporaso, G. L., Gandy, S. E., Buxbaum, J. D., Ramabhadran, T. V. & Greengard, P. (1992) Protein phosphorylation regulates secretion of Alzheimer beta/A4 amyloid precursor protein. *Proceedings of the National Academy of Sciences of the United States of America*, 89, 3055-3059.

Caporaso, G. L., Takei, K., Gandy, S. E., Matteoli, M., Mundigl, O., Greengard, P. & De Camilli, P. (1994) Morphologic and biochemical analysis of the intracellular trafficking of the Alzheimer beta/A4 amyloid precursor protein. *J. Neurosci.*, 14, 3122-3138.

Carr, H. S., George, G. N. & Winge, D. R. (2002) Yeast Cox11, a Protein Essential for Cytochrome cOxidase Assembly, Is a Cu(I)-binding Protein. *Journal of Biological Chemistry*, 277, 31237-31242.

- Carr, H. S. & Winge, D. R. (2003) Assembly of Cytochrome c Oxidase within the Mitochondrion. *Accounts of Chemical Research*, 36, 309-316.
- Carroll, M. C., Girouard, J. B., Ulloa, J. L., Subramaniam, J. R., Wong, P. C., Valentine, J. S. & Culotta, V. C. (2004) Mechanisms for activating Cu- and Zn-containing superoxide dismutase in the absence of the CCS Cu chaperone. *Proceedings of the National Academy of Sciences of the United States of America*, 101, 5964-5969.
- Casareno, R. L. B., Waggoner, D. & Gitlin, J. D. (1998) The Copper Chaperone CCS Directly Interacts with Copper/Zinc Superoxide Dismutase. *Journal of Biological Chemistry*, 273, 23625-23628.
- Casley, C. S., Canevari, L., Land, J. M., Clark, J. B. & Sharpe, M. A. (2002) β -Amyloid inhibits integrated mitochondrial respiration and key enzyme activities. *Journal of Neurochemistry*, 80, 91-100.
- Cater, M. A., McInnes, K. T., Li, Q.-X., Volitakis, I., La Fontaine, S., Mercer, J. F. B. & Bush, A. I. (2008) Intracellular copper deficiency increases amyloid- β secretion by diverse mechanisms. *Biochem J*, 412, 141-152.
- Chandrasekaran, K., Giordano, T., Brady, D. R., Stoll, J., Martin, L. J. & Rapoport, S. I. (1994) Impairment in mitochondrial cytochrome oxidase gene expression in Alzheimer disease. *Molecular Brain Research*, 24, 336-340.
- Cherny, R. A., Atwood, C. S., Xilinas, M. E., Gray, D. N., Jones, W. D., McLean, C. A., Barnham, K. J., Volitakis, I., Fraser, F. W., Kim, Y.-S., Huang, X., Goldstein, L. E., Moir, R. D., Lim, J. T., Beyreuther, K., Zheng, H., Tanzi, R. E., Masters, C. L. & Bush, A. I. (2001) Treatment with a Copper-Zinc Chelator Markedly and Rapidly Inhibits [beta]-Amyloid Accumulation in Alzheimer's Disease Transgenic Mice. *Neuron*, 30, 665-676.
- Cherny, R. A., Legg, J. T., McLean, C. A., Fairlie, D. P., Huang, X., Atwood, C. S., Beyreuther, K., Tanzi, R. E., Masters, C. L. & Bush, A. I. (1999) Aqueous Dissolution of Alzheimer's Disease A β Amyloid Deposits by Biometal Depletion. *Journal of Biological Chemistry*, 274, 23223-23228.
- Ciriolo, M. R., Desideri, A., Paci, M. & Rotilio, G. (1990) Reconstitution of Cu,Zn-superoxide dismutase by the Cu(I).glutathione complex. *Journal of Biological Chemistry*, 265, 11030-11034.
- Citron, M., Oltersdorf, T., Haass, C., McConlogue, L., Hung, A. Y., Seubert, P., Vigo-Pelfrey, C., Lieberburg, I. & Selkoe, D. J. (1992) Mutation of the [beta]-amyloid precursor protein in familial Alzheimer's disease increases [beta]-protein production. *Nature*, 360, 672-674.

Citron, M., Vigo-Pelfrey, C., Teplow, D. B., Miller, C., Schenk, D., Johnston, J., Winblad, B., Venizelos, N., Lannfelt, L. & Selkoe, D. J. (1994) Excessive production of amyloid beta-protein by peripheral cells of symptomatic and presymptomatic patients carrying the Swedish familial Alzheimer disease mutation. *Proceedings of the National Academy of Sciences of the United States of America*, 91, 11993-11997.

Cleary, J. P., Walsh, D. M., Hofmeister, J. J., Shankar, G. M., Kuskowski, M. A., Selkoe, D. J. & Ashe, K. H. (2005) Natural oligomers of the amyloid- β protein specifically disrupt cognitive function. *Nat Neurosci*, 8, 79-84.

Cobine, P. A., Ojeda, L. D., Rigby, K. M. & Winge, D. R. (2004) Yeast Contain a Non-proteinaceous Pool of Copper in the Mitochondrial Matrix. *Journal of Biological Chemistry*, 279, 14447-14455.

Cobine, P. A., Pierrel, F., Bestwick, M. L. & Winge, D. R. (2006) Mitochondrial Matrix Copper Complex Used in Metallation of Cytochrome Oxidase and Superoxide Dismutase. *Journal of Biological Chemistry*, 281, 36552-36559.

Cook, D. G., Forman, M. S., Sung, J. C., Leight, S., Kolson, D. L., Iwatsubo, T., Lee, V. M. Y. & Doms, R. W. (1997) Alzheimer's A β (1-42) is generated in the endoplasmic reticulum/intermediate compartment of NT2N cells. *Nat Med*, 3, 1021-1023.

Coulson, E. J., Paliga, K., Beyreuther, K. & Masters, C. L. (2000) What the evolution of the amyloid protein precursor supergene family tells us about its function. *Neurochemistry International*, 36, 175-184.

Crichton, R. R. & Pierre, J. L. (2001) Old Iron, Young Copper: from Mars to Venus. *BioMetals*, 14, 99-112.

Crouch, P. J., Blake, R., Duce, J. A., Ciccotosto, G. D., Li, Q.-X., Barnham, K. J., Curtain, C. C., Cherny, R. A., Cappai, R., Dyrks, T., Masters, C. L. & Trounce, I. A. (2005) Copper-Dependent Inhibition of Human Cytochrome c Oxidase by a Dimeric Conformer of Amyloid- β 1-42. *J. Neurosci.*, 25, 672-679.

Crouch, P. J., Harding, S.-M. E., White, A. R., Camakaris, J., Bush, A. I. & Masters, C. L. (2008) Mechanisms of A β mediated neurodegeneration in Alzheimer's disease. *The International Journal of Biochemistry & Cell Biology*, 40, 181-198.

Crouch, P. J., Tew, D. J., Du, T., Nguyen, D. N., Caragounis, A., Filiz, G., Blake, R. E., Trounce, I. A., Soon, C. P. W., Laughton, K., Perez, K. A., Li, Q. X., Cherny, R. A., Masters, C. L., Barnham, K. J. & White, A. R. (2009) Restored degradation of the Alzheimer's amyloid- β peptide by targeting amyloid formation. *Journal of Neurochemistry*, 108, 1198-1207.

- Culotta, V. C., Joh, H.-D., Lin, S.-J., Hudak Slekar, K. & Strain, J. (1995) A Physiological Role for *Saccharomyces cerevisiae* Copper/Zinc Superoxide Dismutase in Copper Buffering. *Journal of Biological Chemistry*, 270, 29991-29997.
- Culotta, V. C., Klomp, L. W. J., Strain, J., Casareno, R. L. B., Krems, B. & Gitlin, J. D. (1997) The Copper Chaperone for Superoxide Dismutase. *Journal of Biological Chemistry*, 272, 23469-23472.
- Curtain, C. C., Ali, F., Volitakis, I., Cherny, R. A., Norton, R. S., Beyreuther, K., Barrow, C. J., Masters, C. L., Bush, A. I. & Barnham, K. J. (2001) Alzheimer's Disease Amyloid- β Binds Copper and Zinc to Generate an Allosterically Ordered Membrane-penetrating Structure Containing Superoxide Dismutase-like Subunits. *Journal of Biological Chemistry*, 276, 20466-20473.
- Cvetkovic, A., Menon, A. L., Thorgersen, M. P., Scott, J. W., Poole II, F. L., Jenney JR, F. E., Lancaster, W. A., Praissman, J. L., Shanmukh, S., Vaccaro, B. J., Trauger, S. A., Kalisiak, E., Apon, J. V., Siuzdak, G., Yannone, S. M., Tainer, J. A. & Adams, M. W. W. (2010) Microbial metalloproteomes are largely uncharacterized. *Nature*, 466, 779-782.
- Da Silva, G. & Ming, L. J. (2007) Metallo-ROS in Alzheimer's Disease: Oxidation of Neurotransmitters by CuII- β -Amyloid and Neuropathology of the Disease. *Angewandte Chemie International Edition*, 46, 3337-3341.
- Dameron, C. T., Winge, D. R., George, G. N., Sansone, M., Hu, S. & Hamer, D. (1991) A copper-thiolate polynuclear cluster in the ACE1 transcription factor. *Proceedings of the National Academy of Sciences of the United States of America*, 88, 6127-6131.
- Danks, D. M., Campbell, P. E., Stevens, B. J., Mayne, V. & Cartwright, E. (1972) Menke's Kinky Hair Syndrome: An Inherited Defect in Copper Absorption With Widespread Effects. *Pediatrics*, 50, 188-201.
- De Strooper, B., Annaert, W., Cupers, P., Saftig, P., Craessaerts, K., Mumm, J. S., Schroeter, E. H., Schrijvers, V., Wolfe, M. S., Ray, W. J., Goate, A. & Kopan, R. (1999) A presenilin-1-dependent [γ]-secretase-like protease mediates release of Notch intracellular domain. *Nature*, 398, 518-522.
- De Strooper, B., Saftig, P., Craessaerts, K., Vanderstichele, H., Guhde, G., Annaert, W., Von Figura, K. & Van Leuven, F. (1998) Deficiency of presenilin-1 inhibits the normal cleavage of amyloid precursor protein. *Nature*, 391, 387-390.
- Dingwall, C. (2007) A copper-binding site in the cytoplasmic domain of BACE1 identifies a possible link to metal homeostasis and oxidative stress in Alzheimer's disease. *Biochemical Society Transactions*, 035, 571-573.
- Dizdaroglu, M. (1992) Oxidative damage to DNA in mammalian chromatin. *Mutation Research/DNAging*, 275, 331-342.

- Duce, J. A., Tsatsanis, A., Cater, M. A., James, S. A., Robb, E., Wikke, K., Leong, S. L., Perez, K., Johanssen, T., Greenough, M. A., Cho, H. H., Galatis, D., Moir, R. D., Masters, C. L., McLean, C., Tanzi, R. E., Cappai, R., Barnham, K. J., Ciccotosto, G. D., Rogers, J. T. & Bush, A.I. (2010) Iron-export ferroxidase activity of β -amyloid precursor protein is inhibited by zinc in Alzheimer's disease. *Cell*, 142, 857-867.
- Eehalt, R., Keller, P., Haass, C., Thiele, C. & Simons, K. (2003) Amyloidogenic processing of the Alzheimer β -amyloid precursor protein depends on lipid rafts. *The Journal of Cell Biology*, 160, 113-123.
- Esch, F. S., Keim, P. S., Beattie, E. C., Blacher, R. W., Culwell, A. R., Oltersdorf, T., McClure, D. & Ward, P. J. (1990) Cleavage of amyloid beta peptide during constitutive processing of its precursor. *Science*, 248, 1122-1124.
- Esler, W. P., Kimberly, W. T., Ostaszewski, B. L., Ye, W., Diehl, T. S., Selkoe, D. J. & Wolfe, M. S. (2002) Activity-dependent isolation of the presenilin-1 β -secretase complex reveals nicastrin and a β substrate. *Proceedings of the National Academy of Sciences of the United States of America*, 99, 2720-2725.
- Falzone, T. L., Stokin, G. B., Lillo, C., Rodrigues, E. M., Westerman, E. L., Williams, D. S. & Goldstein, L. S. B. (2009) Axonal Stress Kinase Activation and Tau Misbehavior Induced by Kinesin-1 Transport Defects. *J. Neurosci.*, 29, 5758-5767.
- Farzan, M., Schnitzler, C. E., Vasilieva, N., Leung, D. & Choe, H. (2000) BACE2, a β -secretase homolog, cleaves at the β site and within the amyloid- β region of the amyloid- β precursor protein. *Proceedings of the National Academy of Sciences of the United States of America*, 97, 9712-9717.
- Ferrer, M., Golyshina, O. V., Beloqui, A., Golyshin, P. N. & Timmis, K. N. (2007) The cellular machinery of *Ferroplasma acidiphilum* is iron-protein-dominated. *Nature*, 445, 91-94.
- Field, L. S., Furukawa, Y., O'Halloran, T. V. & Culotta, V. C. (2003) Factors Controlling the Uptake of Yeast Copper/Zinc Superoxide Dismutase into Mitochondria. *Journal of Biological Chemistry*, 278, 28052-28059.
- Folkesson, R., Malkiewicz, K., Kloskowska, E., Nilsson, T., Popova, E., Bogdanovic, N., Ganten, U., Ganten, D., Bader, M., Winblad, B. & Benedikz, E. (2007) A transgenic rat expressing human APP with the Swedish Alzheimer's disease mutation. *Biochemical and Biophysical Research Communications*, 358, 777-782.
- Förstl, H. & Kurz, A. (1999) Clinical features of Alzheimer's disease. *European Archives of Psychiatry and Clinical Neuroscience*, 249, 288-290.
- Frausto Da Silva, J. J. R. & Williams, R. J. P. (2001) *The Biological Chemistry of the Elements: The Inorganic Chemistry of Life*, Oxford, Oxford University Press.

- Frederickson, C. J., Klitenick, M. A., Manton, W. I. & Kirkpatrick, J. B. (1983) Cytoarchitectonic distribution of zinc in the hippocampus of man and the rat. *Brain Research*, 273, 335-339.
- Friedman, S. & Kaufman, S. (1965) 3,4-Dihydroxyphenylethylamine β -Hydroxylase. *Journal of Biological Chemistry*, 240, 4763-4773.
- Furukawa, Y. & O'Halloran, T. V. (2005) Amyotrophic Lateral Sclerosis Mutations Have the Greatest Destabilizing Effect on the Apo- and Reduced Form of SOD1, Leading to Unfolding and Oxidative Aggregation. *Journal of Biological Chemistry*, 280, 17266-17274.
- Furukawa, Y., Torres, A. S. & O'Halloran, T. V. (2004) Oxygen-induced maturation of SOD1: a key role for disulfide formation by the copper chaperone CCS. *EMBO J*, 23, 2872-2881.
- Gabbita, S. P., Lovell, M. A. & Markesbery, W. R. (1998) Increased Nuclear DNA Oxidation in the Brain in Alzheimer's Disease. *Journal of Neurochemistry*, 71, 2034-2040.
- Glerum, D. M., Shtanko, A. & Tzagoloff, A. (1996a) Characterization of COX17, a Yeast Gene Involved in Copper Metabolism and Assembly of Cytochrome Oxidase. *Journal of Biological Chemistry*, 271, 14504-14509.
- Glerum, D. M., Shtanko, A. & Tzagoloff, A. (1996b) SCO1 and SCO2 Act as High Copy Suppressors of a Mitochondrial Copper Recruitment Defect in *Saccharomyces cerevisiae*. *Journal of Biological Chemistry*, 271, 20531-20535.
- Goldgaber, D., Lerman, M. I., McBride, O. W., Saffiotti, U. & Gajdusek, D. C. (1987) Characterization and chromosomal localization of a cDNA encoding brain amyloid of Alzheimer's disease. *Science*, 235, 877-880.
- Gong, Y., Chang, L., Viola, K. L., Lacor, P. N., Lambert, M. P., Finch, C. E., Krafft, G. A. & Klein, W. L. (2003) Alzheimer's disease-affected brain: Presence of oligomeric A β ligands (ADDLs) suggests a molecular basis for reversible memory loss. *Proceedings of the National Academy of Sciences of the United States of America*, 100, 10417-10422.
- Gouras, G. K., Tsai, J., Naslund, J., Vincent, B., Edgar, M., Checler, F., Greenfield, J. P., Haroutunian, V., Buxbaum, J. D., Xu, H., Greengard, P. & Relkin, N. R. (2000a) Intraneuronal A β 42 Accumulation in Human Brain. *Am J Pathol*, 156, 15-20.
- Gouras, G. K., Xu, H., Gross, R. S., Greenfield, J. P., Hai, B., Wang, R. & Greengard, P. (2000b) Testosterone reduces neuronal secretion of Alzheimer's β -amyloid peptides. *Proceedings of the National Academy of Sciences of the United States of America*, 97, 1202-1205.

- Gralla, E. B., Thiele, D. J., Silar, P. & Valentine, J. S. (1991) ACE1, a copper-dependent transcription factor, activates expression of the yeast copper, zinc superoxide dismutase gene. *Proceedings of the National Academy of Sciences of the United States of America*, 88, 8558-8562.
- Gralle, M., Oliveira, C. L. P., Guerreiro, L. H., McKinstry, W. J., Galatis, D., Masters, C. L., Cappai, R., Parker, M. W., Ramos, C. H. I., Torriani, I. & Ferreira, S. T. (2006) Solution Conformation and Heparin-induced Dimerization of the Full-length Extracellular Domain of the Human Amyloid Precursor Protein. *Journal of Molecular Biology*, 357, 493-508.
- Gray, E. H., De Vos, K. J., Dingwall, C., Perkinson, M. S. & Miller, C. C. (2010) Deficiency of the Copper Chaperone for Superoxide Dismutase Increases Amyloid-beta Production. *J. Alzheimers Dis.*
- Grbovic, O. M., Mathews, P. M., Jiang, Y., Schmidt, S. D., Dinakar, R., Summers-Terio, N. B., Ceresa, B. P., Nixon, R. A. & Cataldo, A. M. (2003) Rab5-stimulated Up-regulation of the Endocytic Pathway Increases Intracellular β -Cleaved Amyloid Precursor Protein Carboxyl-terminal Fragment Levels and A β Production. *Journal of Biological Chemistry*, 278, 31261-31268.
- Greenfield, J. P., Tsai, J., Gouras, G. K., Hai, B., Thinakaran, G., Checler, F., Sisodia, S. S., Greengard, P. & Xu, H. (1999) Endoplasmic reticulum and trans-Golgi network generate distinct populations of Alzheimer β -amyloid peptides. *Proceedings of the National Academy of Sciences of the United States of America*, 96, 742-747.
- Griffith, L. S., Mathes, M. & Schmitz, B. (1995) β -Amyloid precursor protein is modified with O-linked N-acetylglucosamine. *Journal of Neuroscience Research*, 41, 270-278.
- Gunawardena, S. & Goldstein, L. S. B. (2001) Disruption of Axonal Transport and Neuronal Viability by Amyloid Precursor Protein Mutations in *Drosophila*. *Neuron*, 32, 389-401.
- Haass, C., Hung, A. Y., Schlossmacher, M. G., Teplow, D. B. & Selkoe, D. J. (1993) beta-Amyloid peptide and a 3-kDa fragment are derived by distinct cellular mechanisms. *Journal of Biological Chemistry*, 268, 3021-3024.
- Haass, C., Koo, E. H., Capell, A., Teplow, D. B. & Selkoe, D. J. (1995) Polarized sorting of beta-amyloid precursor protein and its proteolytic products in MDCK cells is regulated by two independent signals. *The Journal of Cell Biology*, 128, 537-547.
- Haass, C., Koo, E. H., Mellon, A., Hung, A. Y. & Selkoe, D. J. (1992a) Targeting of cell-surface [beta]-amyloid precursor protein to lysosomes: alternative processing into amyloid-bearing fragments. *Nature*, 357, 500-503.

Haass, C., Schlossmacher, M. G., Hung, A. Y., Vigo-Pelfrey, C., Mellon, A., Ostaszewski, B. L., Lieberburg, I., Koo, E. H., Schenk, D., Teplow, D. B. & Selkoe, D. J. (1992b) Amyloid [beta]-peptide is produced by cultured cells during normal metabolism. *Nature*, 359, 322-325.

Haass, C. & Selkoe, D. J. (2007) Soluble protein oligomers in neurodegeneration: lessons from the Alzheimer's amyloid [beta]-peptide. *Nat Rev Mol Cell Biol*, 8, 101-112.

Hardy, J. A. & Higgins, G. A. (1992) Alzheimer's disease: the amyloid cascade hypothesis. *Science*, 256, 184-185.

Harris, M. E., Hensley, K., Butterfield, D. A., Leedle, R. A. & Carney, J. M. (1995) Direct Evidence of oxidative Injury Produced by the Alzheimer's beta-Amyloid Peptide (1-40) in Cultured Hippocampal Neurons. *Experimental Neurology*, 131, 193-202.

Hartley, D. M., Walsh, D. M., Ye, C. P., Diehl, T., Vasquez, S., Vassilev, P. M., Teplow, D. B. & Selkoe, D. J. (1999) Protofibrillar Intermediates of Amyloid beta - Protein Induce Acute Electrophysiological Changes and Progressive Neurotoxicity in Cortical Neurons. *J. Neurosci.*, 19, 8876-8884.

Hartmann, D., De Strooper, B., Serneels, L., Craessaerts, K., Herreman, A., Annaert, W., Umans, L., Lübke, T., Lena Illert, A., Von Figura, K. & Saftig, P. (2002) The disintegrin/metalloprotease ADAM 10 is essential for Notch signalling but not for α -secretase activity in fibroblasts. *Human Molecular Genetics*, 11, 2615-2624.

Hartmann, T., Bieger, S. C., Bruhl, B., Tienari, P. J., Ida, N., Allsop, D., Roberts, G. W., Masters, C. L., Dotti, C. G., Unsicker, K. & Beyreuther, K. (1997) Distinct sites of intracellular production for Alzheimer's disease A[beta]40/42 amyloid peptides. *Nat Med*, 3, 1016-1020.

Hassett, R. & Kosman, D. J. (1995) Evidence for Cu(II) Reduction as a Component of Copper Uptake by *Saccharomyces cerevisiae*. *Journal of Biological Chemistry*, 270, 128-134.

Hayashi, H., Mizuno, T., Michikawa, M., Haass, C. & Yanagisawa, K. (2000) Amyloid precursor protein in unique cholesterol-rich microdomains different from caveolae-like domains. *Biochimica et Biophysica Acta (BBA) - Molecular and Cell Biology of Lipids*, 1483, 81-90.

Heaton, D. N., George, G. N., Garrison, G. & Winge, D. R. (2000) The Mitochondrial Copper Metallochaperone Cox17 Exists as an Oligomeric, Polycopper Complex. *Biochemistry*, 40, 743-751.

Heber, S., Herms, J., Gajic, V., Hainfellner, J., Aguzzi, A., Rulicke, T., Kretschmar, H., Von Koch, C., Sisodia, S., Tremml, P., Lipp, H.-P., Wolfner, D. P. & Muller, U. (2000) Mice with Combined Gene Knock-Outs Reveal Essential and Partially Redundant Functions of Amyloid Precursor Protein Family Members. *J. Neurosci.*, 20, 7951-7963.

Hellman, N. E., Kono, S., Mancini, G. M., Hoogeboom, A. J., De Jong, G. J. & Gitlin, J. D. (2002) Mechanisms of Copper Incorporation into Human Ceruloplasmin. *Journal of Biological Chemistry*, 277, 46632-46638.

Helson, L., Das, S. K. & Hajdu, S. I. (1975) Human Neuroblastoma in Nude Mice. *Cancer Research*, 35, 2594-2599.

Hensley, K., Carney, J. M., Mattson, M. P., Aksenova, M., Harris, M., Wu, J. F., Floyd, R. A. & Butterfield, D. A. (1994) A model for beta-amyloid aggregation and neurotoxicity based on free radical generation by the peptide: relevance to Alzheimer disease. *Proceedings of the National Academy of Sciences of the United States of America*, 91, 3270-3274.

Herms, J., Anliker, B., Heber, S., Ring, S., Fuhrmann, M., Kretschmar, H., Sisodia, S. & Muller, U. (2004) Cortical dysplasia resembling human type 2 lissencephaly in mice lacking all three APP family members. *EMBO J*, 23, 4106-4115.

Hersh, L. B. & Rodgers, D. W. (2008) Neprilysin and Amyloid Beta Peptide Degradation. *Current Alzheimer Research*, 5, 225-231.

Horecker, B. L. & Heppel, L. A. (1949) The reduction of cytochrome c by xanthine oxidase. *The Journal of Biological Chemistry*.

Hornig, Y.-C., Cobine, P. A., Maxfield, A. B., Carr, H. S. & Winge, D. R. (2004) Specific Copper Transfer from the Cox17 Metallochaperone to Both Sco1 and Cox11 in the Assembly of Yeast Cytochrome c Oxidase. *Journal of Biological Chemistry*, 279, 35334-35340.

Howell, G. A. & Frederickson, C. J. (1990) A retrograde transport method for mapping zinc-containing fiber systems in the brain. *Brain Research*, 515, 277-286.

Howell, G. A., Welch, M. G. & Frederickson, C. J. (1984) Stimulation-induced uptake and release of zinc in hippocampal slices. *Nature*, 308, 736-738.

<http://www.alzforum.org>

[http://www.bio.davidson.edu/people/kabern/berndcv/lab/website\(summer2009\)/lshomepage/glutathione-skeletal.png](http://www.bio.davidson.edu/people/kabern/berndcv/lab/website(summer2009)/lshomepage/glutathione-skeletal.png)

<http://www.chemicalbook.com>

http://www.comberservice.ie/foto/_optional_glovebox_clip_image002.jpg

http://www.epa.gov/oppbppd1/biopesticides/ingredients/tech_docs/tech_116900.htm.

http://www.invitrogen.com/etc/medialib/en/images/ics_organized/brands/molecular-probes.par.49619.image.-1.0.1.gif.

[http://www.liv.ac.uk/physiology/ncs/catalogue/cloning/pcdna3.1\(-\).htm](http://www.liv.ac.uk/physiology/ncs/catalogue/cloning/pcdna3.1(-).htm).

<http://www.metallo.scripps.edu/promise/cox.html>.

<http://www.natureprotocols.com/2008/11/12/metalloprotein.php>.

<http://www.themedicalbiochemistrypage.org/vitamins.html>.

Huang, X., Atwood, C. S., Hartshorn, M. A., Multhaup, G., Goldstein, L. E., Scarpa, R. C., Cuajungco, M. P., Gray, D. N., Lim, J., Moir, R. D., Tanzi, R. E. & Bush, A. I. (1999) The A β Peptide of Alzheimer's Disease Directly Produces Hydrogen Peroxide through Metal Ion Reduction *Biochemistry*, 38, 7609-7616.

Hung, A. Y., Koo, E. H., Haass, C. & Selkoe, D. J. (1992) Increased expression of beta-amyloid precursor protein during neuronal differentiation is not accompanied by secretory cleavage. *Proceedings of the National Academy of Sciences of the United States of America*, 89, 9439-9443.

Hung, I. H., Casareno, R. L. B., Labesse, G., Mathews, F. S. & Gitlin, J. D. (1998) HAH1 Is a Copper-binding Protein with Distinct Amino Acid Residues Mediating Copper Homeostasis and Antioxidant Defense. *Journal of Biological Chemistry*, 273, 1749-1754.

Hung, Y. H., Robb, E. L., Volitakis, I., Ho, M., Evin, G., Li, Q.-X., Culvenor, J. G., Masters, C. L., Cherny, R. A. & Bush, A. I. (2009) Paradoxical Condensation of Copper with Elevated β -Amyloid in Lipid Rafts under Cellular Copper Deficiency Conditions. *Journal of Biological Chemistry*, 284, 21899-21907.

Hussain, I., Powell, D., Howlett, D. R., Tew, D. G., Meek, T. D., Chapman, C., Gloger, I. S., Murphy, K. E., Southan, C. D., Ryan, D. M., Smith, T. S., Simmons, D. L., Walsh, F. S., Dingwall, C. & CHRISTIE, G. (1999) Identification of a Novel Aspartic Protease (Asp 2) as [beta]-Secretase. *Molecular and Cellular Neuroscience*, 14, 419-427.

Huttunen, H. J., Guenette, S. Y., Peach, C., Greco, C., Xia, W., Kim, D. Y., Barren, C., Tanzi, R. E. & Kovacs, D. M. (2007) HtrA2 Regulates β -Amyloid Precursor Protein (APP) Metabolism through Endoplasmic Reticulum-associated Degradation. *Journal of Biological Chemistry*, 282, 28285-28295.

Ittner, L. M., Ke, Y. D. & Goetz, J. R. (2009) Phosphorylated Tau Interacts with c-Jun N-terminal Kinase-interacting Protein 1 (JIP1) in Alzheimer Disease. *Journal of Biological Chemistry*, 284, 20909-20916.

Iwata, N., Tsubuki, S., Takaki, Y., Shirotani, K., Lu, B., Gerard, N. P., Gerard, C., Hama, E., Lee, H.-J. & Saido, T. C. (2001) Metabolic Regulation of Brain Abeta by Neprilysin. *Science*, 292, 1550-1552.

Jensen, L. T. & Winge, D. R. (1998) Identification of a copper-induced intramolecular interaction in the transcription factor Mac1 from *Saccharomyces cerevisiae*. *EMBO J*, 17, 5400-5408.

Jiang, Q., Lee, C. Y. D., Mandrekar, S., Wilkinson, B., Cramer, P., Zelcer, N., Mann, K., Lamb, B., Willson, T. M., Collins, J. L., Richardson, J. C., Smith, J. D., Comery, T. A., Riddell, D., Holtzman, D. M., Tontonoz, P. & Landreth, G. E. (2008) ApoE Promotes the Proteolytic Degradation of A[beta]. *Neuron*, 58, 681-693.

Jobling, M. F., Huang, X., Stewart, L. R., Barnham, K. J., Curtain, C., Volitakis, I., Perugini, M., White, A. R., Cherny, R. A., Masters, C. L., Barrow, C. J., Collins, S. J., Bush, A. I. & Cappai, R. (2001) Copper and Zinc Binding Modulates the Aggregation and Neurotoxic Properties of the Prion Peptide PrP106-126 *Biochemistry*, 40, 8073-8084.

Kaler, S. G., Holmes, C. S., Goldstein, D. S., Tang, J., Godwin, S. C., Donsante, A., Liew, C. J., Sato, S. & Patronas, N. (2008) Neonatal Diagnosis and Treatment of Menkes Disease. *New England Journal of Medicine*, 358, 605-614.

Kamal, A., Stokin, G. B., Yang, Z., Xia, C.-H. & Goldstein, L. S. B. (2000) Axonal Transport of Amyloid Precursor Protein Is Mediated by Direct Binding to the Kinesin Light Chain Subunit of Kinesin-I. *Neuron*, 28, 449-459.

Kang, J., Lemaire, H.-G., Unterbeck, A., Salbaum, J. M., Masters, C. L., Grzeschik, K.-H., Multhaup, G., Beyreuther, K. & Mueller-Hill, B. (1987) The precursor of Alzheimer's disease amyloid A4 protein resembles a cell-surface receptor. *Nature*, 325, 733-736.

Kang, J. & Mueller-Hill, B. (1990) Differential splicing of Alzheimer's disease amyloid A4 precursor RNA in rat tissues: PreA4695 mRNA is predominantly produced in rat and human brain. *Biochemical and Biophysical Research Communications*, 166, 1192-1200.

Kayed, R., Head, E., Thompson, J. L., McIntire, T. M., Milton, S. C., Cotman, C. W. & Glabe, C. G. (2003) Common Structure of Soluble Amyloid Oligomers Implies Common Mechanism of Pathogenesis. *Science*, 300, 486-489.

Keller, J. N., Mark, R. J., Bruce, A. J., Blanc, E., Rothstein, J. D., Uchida, K., Waeg, G. & Mattson, M. P. (1997a) 4-Hydroxynonenal, an aldehydic product of membrane lipid peroxidation, impairs glutamate transport and mitochondrial function in synaptosomes. *Neuroscience*, 80, 685-696.

- Keller, J. N., Pang, Z., Geddes, J. W., Begley, J. G., Germeyer, A., Waeg, G. & Mattson, M. P. (1997b) Impairment of Glucose and Glutamate Transport and Induction of Mitochondrial Oxidative Stress and Dysfunction in Synaptosomes by Amyloid β -Peptide: Role of the Lipid Peroxidation Product 4-Hydroxynonenal. *Journal of Neurochemistry*, 69, 273-284.
- Kibbey, M. C., Jucker, M., Weeks, B. S., Neve, R. L., Van Nostrand, W. E. & Kleinman, H. K. (1993) beta-Amyloid precursor protein binds to the neurite-promoting IKVAV site of laminin. *Proceedings of the National Academy of Sciences of the United States of America*, 90, 10150-10153.
- Kim, B.-E., Nevitt, T. & Thiele, D. J. (2008) Mechanisms for copper acquisition, distribution and regulation. *Nat Chem Biol*, 4, 176-185.
- Kirazov, E., Kirazov, L., Bigl, V. & Schliebs, R. (2001) Ontogenetic changes in protein level of amyloid precursor protein (APP) in growth cones and synaptosomes from rat brain and prenatal expression pattern of APP mRNA isoforms in developing rat embryo. *International Journal of Developmental Neuroscience*, 19, 287-296.
- Kitaguchi, N., Takahashi, Y., Tokushima, Y., Shiojiri, S. & Ito H. (1988) Novel precursor of Alzheimer's disease amyloid protein shows protease inhibitory activity. *Nature*, 331, 530-532.
- Klomp, L. W. J., Lin, S.-J., S.Yuan, D., Klausner, R. D., Culotta, V. C. & Gitlin, J. D. (1997) Identification and Functional Expression of HAH1, a Novel Human Gene Involved in Copper Homeostasis. *Journal of Biological Chemistry*, 272, 9221-9226.
- Kolhekar, A. S., Roberts, M. S., Jiang, N., Johnson, R. C., Mains, R. E., Eipper, B. A. & Taghert, P. H. (1997) Neuropeptide Amidation in Drosophila: Separate Genes Encode the Two Enzymes Catalyzing Amidation. *J. Neurosci.*, 17, 1363-1376.
- Kong, G., Miles, L., Crespi, G., Morton, C., NG, H., Barnham, K., McKinstry, W., Cappai, R. & Parker, M. (2008) Copper binding to the Alzheimer's disease amyloid precursor protein. *European Biophysics Journal*, 37, 269-279.
- Koo, E. H., Sisodia, S. S., Archer, D. R., Martin, L. J., Weidemann, A., Beyreuther, K., Fischer, P., Masters, C. L. & Price, D. L. (1990) Precursor of amyloid protein in Alzheimer disease undergoes fast anterograde axonal transport. *Proceedings of the National Academy of Sciences of the United States of America*, 87, 1561-1565.
- Krysko, D. V., Roels, F., Leybaert, L. & D'Herde, K. (2001) Mitochondrial Transmembrane Potential Changes Support the Concept of Mitochondrial Heterogeneity During Apoptosis. *J. Histochem. Cytochem.*, 49, 1277-1284.
- Kulathila, R., A. Merkler, K. & J. Merkler, D. (1999) Enzymatic formation of C-terminal amides. *Natural Product Reports*, 16, 145-154.

- Lacor, P. N., Buniel, M. C., Furlow, P. W., Sanz Clemente, A., Velasco, P. T., Wood, M., Viola, K. L. & Klein, W. L. (2007) A β Oligomer-Induced Aberrations in Synapse Composition, Shape, and Density Provide a Molecular Basis for Loss of Connectivity in Alzheimer's Disease. *J. Neurosci.*, 27, 796-807.
- Lamb, A. L., Torres, A. S., O'Halloran, T. V. & Rosenzweig, A. C. (2001) Heterodimeric structure of superoxide dismutase in complex with its metallochaperone. *Nat Struct Mol Biol*, 8, 751-755.
- Lambert, M. P., Barlow, A. K., Chromy, B. A., Edwards, C., Freed, R., Liosatos, M., Morgan, T. E., Rozovsky, I., Trommer, B., Viola, K. L., Wals, P., Zhang, C., Finch, C. E., Krafft, G. A. & Klein, W. L. (1998) Diffusible, nonfibrillar ligands derived from A β 1-42 are potent central nervous system neurotoxins. *Proceedings of the National Academy of Sciences of the United States of America*, 95, 6448-6453.
- Lambert, M. P., Viola, K. L., Chromy, B. A., Chang, L., Morgan, T. E., YU, J., Venton, D. L., Krafft, G. A., Finch, C. E. & Klein, W. L. (2001) Vaccination with soluble A β oligomers generates toxicity-neutralizing antibodies. *Journal of Neurochemistry*, 79, 595-605.
- Lammich, S., Kojro, E., Postina, R., Gilbert, S., Pfeiffer, R., Jasionowski, M., Haass, C. & Fahrenholz, F. (1999) Constitutive and regulated α -secretase cleavage of Alzheimer's amyloid precursor protein by a disintegrin metalloprotease. *Proceedings of the National Academy of Sciences of the United States of America*, 96, 3922-3927.
- Larin, D., Mekios, C., Das, K., Ross, B., Yang, A.-S. & Gilliam, T. C. (1999) Characterization of the Interaction between the Wilson and Menkes Disease Proteins and the Cytoplasmic Copper Chaperone, HAH1p. *Journal of Biological Chemistry*, 274, 28497-28504.
- Lauren, J., Gimbel, D. A., Nygaard, H. B., Gilbert, J. W. & Strittmatter, S. M. (2009) Cellular prion protein mediates impairment of synaptic plasticity by amyloid-[bgr] oligomers. *Nature*, 457, 1128-1132.
- Lee, J.-H., Lau, K.-F., Perkinson, M. S., Standen, C. L., Shemilt, S. J. A., Mercken, L., Cooper, J. D., McLoughlin, D. M. & Miller, C. C. J. (2003) The Neuronal Adaptor Protein X11 α Reduces A β Levels in the Brains of Alzheimer's APP^{swe} Tg2576 Transgenic Mice. *Journal of Biological Chemistry*, 278, 47025-47029.
- Lee, R. K., Wurtman, R. J., Cox, A. J. & Nitsch, R. M. (1995) Amyloid precursor protein processing is stimulated by metabotropic glutamate receptors. *Proceedings of the National Academy of Sciences of the United States of America*, 92, 8083-8087.
- Leem, J. Y., Vijayan, S., Han, P., Cai, D., Machura, M., Lopes, K. O., Veselits, M. L., Xu, H. & Thinakaran, G. (2002) Presenilin 1 Is Required for Maturation and Cell Surface Accumulation of Nicastrin. *Journal of Biological Chemistry*, 277, 19236-19240.

- Lewen, A., Matz, P. & Chan, P. H. (2000) Free radical pathways in CNS injury. *Journal of Neurotrauma*, 17, 871-890.
- Li, Y., Hough, C. J., Suh, S. W., Sarvey, J. M. & Frederickson, C. J. (2001) Rapid Translocation of Zn²⁺ From Presynaptic Terminals Into Postsynaptic Hippocampal Neurons After Physiological Stimulation. *J Neurophysiol*, 86, 2597-2604.
- Liu, R., Liu, I. Y., Bi, X., Thompson, R. F., Doctrow, S. R., Malfroy, B. & Baudry, M. (2003) Reversal of age-related learning deficits and brain oxidative stress in mice with superoxide dismutase/catalase mimetics. *Proceedings of the National Academy of Sciences of the United States of America*, 100, 8526-8531.
- Llanos, R. M. & Mercer, J. F. B. (2002) The Molecular Basis of Copper Homeostasis Copper-Related Disorders. *DNA and Cell Biology*, 21, 259-270.
- Lovell, M. A., Robertson, J. D., Teesdale, W. J., Campbell, J. L. & Markesbery, W. R. (1998) Copper, iron and zinc in Alzheimer's disease senile plaques. *Journal of the Neurological Sciences*, 158, 47-52.
- Lovell, M. A., Xie, C. & Markesbery, W. R. (1999) Protection against amyloid beta peptide toxicity by zinc. *Brain Research*, 823, 88-95.
- Luk, E., Yang, M., Jensen, L. T., Bourbonnais, Y. & Culotta, V. C. (2005) Manganese Activation of Superoxide Dismutase 2 in the Mitochondria of *Saccharomyces cerevisiae*. *Journal of Biological Chemistry*, 280, 22715-22720.
- Luo, Y., Bolon, B., Kahn, S., Bennett, B. D., Babu-Khan, S., Denis, P., Fan, W., Kha, H., Zhang, J., Gong, Y., Martin, L., Louis, J.-C., Yan, Q., Richards, W. G., Citron, M. & Vassar, R. (2001) Mice deficient in BACE1, the Alzheimer's [beta]-secretase, have normal phenotype and abolished [beta]-amyloid generation. *Nat Neurosci*, 4, 231-232.
- Lustbader, J. W., Cirilli, M., Lin, C., Xu, H. W., Takuma, K., Wang, N., Caspersen, C., Chen, X., Pollak, S., Chaney, M., Trinchese, F., Liu, S., Gunn-Moore, F., Lue, L.-F., Walker, D. G., Kuppusamy, P., Zewier, Z. L., Arancio, O., Stern, D., Yan, S. S. & Wu, H. (2004) Aβ Directly Links A{beta} to Mitochondrial Toxicity in Alzheimer's Disease. *Science*, 304, 448-452.
- Makarova, A., Williams, S. & Strickland, D. (2004) Proteases and lipoprotein receptors in Alzheimer's disease. *Cell Biochemistry and Biophysics*, 41, 139-178.
- Maret, W. & Vallee, B. L. (1998) Thiolate ligands in metallothionein confer redox activity on zinc clusters. *PNAS*, 95, 3478-3482.
- Mark, R. J., Hensley, K., Butterfield, D. A. & Mattson, M. P. (1995) Amyloid beta-peptide impairs ion-motive ATPase activities: evidence for a role in loss of neuronal Ca²⁺ homeostasis and cell death. *J. Neurosci.*, 15, 6239-6249.

- Mark, R. J., Pang, Z., Geddes, J. W., Uchida, K. & Mattson, M. P. (1997) Amyloid beta -Peptide Impairs Glucose Transport in Hippocampal and Cortical Neurons: Involvement of Membrane Lipid Peroxidation. *J. Neurosci.*, 17, 1046-1054.
- Marlow, L., Cain, M., Pappolla, M. & Sambamurti, K. (2003) β -secretase processing of the Alzheimer's amyloid protein precursor (APP). *Journal of Molecular Neuroscience*, 20, 233-239.
- Marques, C. A., Keil, U., Bonert, A., Steiner, B., Haass, C., Müller, W. E. & Eckert, A. (2003) Neurotoxic Mechanisms Caused by the Alzheimer's Disease-linked Swedish Amyloid Precursor Protein Mutation. *Journal of Biological Chemistry*, 278, 28294-28302.
- Masters, B. A., Quaipe, C. J., Erickson, J. C., Kelly, E. J., Froelick, G. J., Zambrowicz, B. P., Brinster, R. L. & Palmiter, R. D. (1994) Metallothionein III is expressed in neurons that sequester zinc in synaptic vesicles. *J. Neurosci.*, 14, 5844-5857.
- Matsuoka, Y., Picciano, M., La Francois, J. & Duff, K. (2001) Fibrillar [beta]-amyloid evokes oxidative damage in a transgenic mouse model of Alzheimer's disease. *Neuroscience*, 104, 609-613.
- Mattiazzi, M., D'Aurelio, M., Gajewski, C. D., Martushova, K., Kiaei, M., Beal, M. F. & Manfredi, G. (2002) Mutated Human SOD1 Causes Dysfunction of Oxidative Phosphorylation in Mitochondria of Transgenic Mice. *Journal of Biological Chemistry*, 277, 29626-29633.
- Mattson, M. P. (1994) Secreted forms of β -amyloid precursor protein modulate dendrite outgrowth and calcium responses to glutamate in cultured embryonic hippocampal neurons. *Journal of Neurobiology*, 25, 439-450.
- Mattson, M. P., Cheng, B., Culwell, A. R., Esch, F. S., Lieberburg, I. & Rydel, R. E. (1993) Evidence for excitoprotective and intraneuronal calcium-regulating roles for secreted forms of the [beta]-amyloid precursor protein. *Neuron*, 10, 243-254.
- Mattson, M. P. & Goodman, Y. (1995) Different amyloidogenic peptides share a similar mechanism of neurotoxicity involving reactive oxygen species and calcium. *Brain Research*, 676, 219-224.
- Maxfield, A. B., Heaton, D. N. & Winge, D. R. (2004) Cox17 Is Functional When Tethered to the Mitochondrial Inner Membrane. *Journal of Biological Chemistry*, 279, 5072-5080.
- Maynard, C. J., Cappai, R., Volitakis, I., Cherny, R. A., White, A. R., Beyreuther, K., Masters, C. L., Bush, A. I. & Li, Q.-X. (2002) Overexpression of Alzheimer's Disease Amyloid- β Opposes the Age-dependent Elevations of Brain Copper and Iron. *Journal of Biological Chemistry*, 277, 44670-44676.
- McCord, J. M. & Fridovich, I. (1969) Superoxide Dismutase. *Journal of Biological Chemistry*, 244, 6049-6055.

- McLean, C. A., Cherny, R. A., Fraser, F. W., Fuller, S. J., Smith, M. J., Beyreuther, K., Bush, A. I. & Masters, C. L. (1999) Soluble Pool of Abeta Amyloid as a Determinant of Severity of Neurodegeneration in Alzheimer's Disease. *Ann. Neurol.*, 46, 860-866.
- McLoughlin, D. M. & Miller, C. C. J. (1996) The intracellular cytoplasmic domain of the Alzheimer's disease amyloid precursor protein interacts with phosphotyrosine-binding domain proteins in the yeast two-hybrid system. *FEBS Letters*, 397, 197-200.
- McLoughlin, D. M., Standen, C. L., Lau, K. F., Ackerley, S., Bartnikas, T. B., Gitlin, J. D. & Miller, C. C. J. (2001) The Neuronal Adaptor Protein X11alpha Interacts with the Copper Chaperone for SOD1 and Regulates SOD1 Activity. *J. Biol. Chem.*, 276, 9303-9307.
- Mecocci, P., MacGarvey, U. & Beal, M. F. (1994) Oxidative damage to mitochondrial DNA is increased in Alzheimer's disease. *Annals of Neurology*, 36, 747-751.
- Meloni, G., Polanski, T., Braun, O. & Vasak, K. M. (2009) Effects of Zn²⁺, Ca²⁺, and Mg²⁺ on the Structure of Zn7Metallothionein-3: Evidence for an Additional Zinc Binding Site. *Biochemistry*, 48, 5700-5707.
- Melov, S., Adlard, P. A., Morten, K., Johnson, F., Golden, T. R., Hinerfeld, D., Schilling, B., Mavros, C., Masters, C. L., Volitakis, I., Li, Q.-X., Loughton, K., Hubbard, A., Cherny, R. A., Gibson, B. & Bush, A. I. (2007) Mitochondrial Oxidative Stress Causes Hyperphosphorylation of Tau. *PLoS ONE*, 2, e536.
- Mendoza-Naranjo, A., Gonzalez-Billault, C. & Maccioni, R. B. (2007) Abeta1-42 stimulates actin polymerization in hippocampal neurons through Rac1 and Cdc42 Rho GTPases. *J Cell Sci*, 120, 279-288.
- Mercer, J. F. B., Barnes, N., Stevenson, J., Strausak, D. & Llanos, R. M. (2003) Copper-induced trafficking of the Cu-ATPases: A key mechanism for copper homeostasis. *BioMetals*, 16, 175-184.
- Mercer, J. F. B. & Llanos, R. M. (2003) Molecular and Cellular Aspects of Copper Transport in Developing Mammals. *J. Nutr.*, 133, 1481-1484.
- Milward, E. A., Papadopoulos, R., Fuller, S. J., Moir, R. D., Small, D., Beyreuther, K. & Masters, C. L. (1992) The amyloid protein precursor of Alzheimer's disease is a mediator of the effects of nerve growth factor on neurite outgrowth. *Neuron*, 9, 129-137.
- Mok, S. S., Sberna, G., Heffernan, D., Cappai, R., Galatis, D., Clarris, H. J., Sawyer, W. H., Beyreuther, K., Masters, C. L. & Small, D. H. (1997) Expression and analysis of heparin-binding regions of the amyloid precursor protein of Alzheimer's disease. *FEBS Letters*, 415, 303-307.

- Mullan, M., Crawford, F., Axelman, K., Houlden, H., Lilius, L., Winblad, B. & Lannfelt, L. (1992) A pathogenic mutation for probable Alzheimer's disease in the APP gene at the N-terminus of [beta]-amyloid. *Nat Genet*, 1, 345-347.
- Müller, U., Cristina, N., Li, Z.-W., Wolfer, D. P., Lipp, H.-P., Rüllicke, T., Brandner, S., Aguzzi, A. & Weissmann, C. (1994) Behavioral and anatomical deficits in mice homozygous for a modified [beta]-amyloid precursor protein gene. *Cell*, 79, 755-765.
- Multhaup, G., Schlicksupp, A., Hesse, L., Beher, D., Ruppert, T., Masters, C. L. & Beyreuther, K. (1996) The Amyloid Precursor Protein of Alzheimer's Disease in the Reduction of Copper(II) to Copper(I). *Science*, 271, 1406-1409.
- Munter, L.-M., Voigt, P., Harmeier, A., Kaden, D., Gottschalk, K. E., Weise, C., Pipkorn, R., Schaefer, M., Langosch, D. & Multhaup, G. (2007) GxxxG motifs within the amyloid precursor protein transmembrane sequence are critical for the etiology of A[beta]₄₂. *EMBO J*, 26, 1702-1712.
- Nelson, K. T. & Prohaska, J. R. (2008) Copper deficiency in rodents alters dopamine beta-mono-oxygenase activity, mRNA and protein level. *British Journal of Nutrition*, 1-11.
- Nishimoto, I., Okamoto, T., Matsuura, Y., Takahashi, S., Okamoto, T., Murayama, Y. & Ogata, E. (1993) Alzheimer amyloid protein precursor complexes with brain GTP-binding protein Go. *Nature*, 362, 75-79.
- Nitsch, R. M., Deng, A., Wurtman, R. J. & Growdon, J. H. (1997) Metabotropic Glutamate Receptor Subtype mGluR1 α Stimulates the Secretion of the Amyloid β -Protein Precursor Ectodomain. *Journal of Neurochemistry*, 69, 704-712.
- Nittis, T., George, G. N. & Winge, D. R. (2001) Yeast Sco1, a Protein Essential for Cytochrome c Oxidase Function Is a Cu(I)-binding Protein. *Journal of Biological Chemistry*, 276, 42520-42526.
- Nose, Y., Kim, B.-E. & Thiele, D. J. (2006) Ctr1 drives intestinal copper absorption and is essential for growth, iron metabolism, and neonatal cardiac function. *Cell Metabolism*, 4, 235-244.
- O'Halloran, T. V. (1993) Transition metals in control of gene expression. *Science*, 261, 715-725.
- Oddo, S., Caccamo, A., Smith, I. F., Green, K. N. & Laferla, F. M. (2006) A Dynamic Relationship between Intracellular and Extracellular Pools of A{beta}. *Am J Pathol*, 168, 184-194.
- Opazo, C., Huang, X., Cherny, R. A., Moir, R. D., Roher, A. E., White, A. R., Cappai, R., Masters, C. L., Tanzi, R. E., Inestrosa, N. C. & BUSH, A. I. (2002) Metalloenzyme-like Activity of Alzheimer's Disease β -Amyloid. *Journal of Biological Chemistry*, 277, 40302-40308.

- Palmiter, R. D., Cole, T. B., Quaife, C. J. & Findley, S. D. (1996) ZnT-3, a putative transporter of zinc into synaptic vesicles. *Proceedings of the National Academy of Sciences of the United States of America*, 93, 14934-14939.
- Palmiter, R. D., Findley, S. D., Whitmore, T. E. & Durnam, D. M. (1992) MT-III, a brain-specific member of the metallothionein gene family. *Proceedings of the National Academy of Sciences of the United States of America*, 89, 6333-6337.
- Parker, W. D., JR. & Parks, J. K. (1995) Cytochrome C Oxidase in Alzheimer's Disease Brain: Purification and Characterization. *Neurology*, 45, 482-486.
- Parks, J. K., Smith, T. S., Trimmer, P. A., Bennett, J. P. & Parker, W. D. (2001) Neurotoxic A β peptides increase oxidative stress in vivo through NMDA-receptor and nitric-oxide-synthase mechanisms, and inhibit complex IV activity and induce a mitochondrial permeability transition in vitro. *Journal of Neurochemistry*, 76, 1050-1056.
- Pennanen, C., Kivipelto, M., Tuomainen, S., Hartikainen, P., Hänninen, T., Laakso, M. P., Hallikainen, M., Vanhanen, M., Nissinen, A., Helkala, E.-L., Vainio, P., Vanninen, R., Partanen, K. & Soininen, H. (2004) Hippocampus and entorhinal cortex in mild cognitive impairment and early AD. *Neurobiology of Aging*, 25, 303-310.
- Perez, R. G., Squazzo, S. L. & Koo, E. H. (1996) Enhanced Release of Amyloid - Protein from Codon 670/671 Swedish Mutant -Amyloid Precursor Protein Occurs in Both Secretory and Endocytic Pathways. *Journal of Biological Chemistry*, 271, 9100-9107.
- Peschon, J. J., Slack, J. L., Reddy, P., Stocking, K. L., Sunnarborg, S. W., Lee, D. C., Russell, W. E., Castner, B. J., Johnson, R. S., Fitzner, J. N., Boyce, R. W., Nelson, N., Kozlosky, C. J., Wolfson, M. F., Rauch, C. T., Cerretti, D. P., Paxton, R. J., March, C. J. & Black, R. A. (1998) An Essential Role for Ectodomain Shedding in Mammalian Development. *Science*, 282, 1281-1284.
- Petris, M. J., Mercer, J. F. B., Culvenor, J. G., Lockhart, P. J., Gleeson, P. A. & Camakaris, J. (1996) Ligand-regulated transport of the Menkes copper P-type ATPase efflux pump from the Golgi apparatus to the plasma membrane: a novel mechanism of regulated trafficking. *EMBO J*, 15, 6084-6095.
- Petris, M. J., Smith, K., Lee, J. & Thiele, D. J. (2003) Copper-stimulated Endocytosis and Degradation of the Human Copper Transporter, hCtr1. *Journal of Biological Chemistry*, 278, 9639-9646.
- Plant, L. D., Webster, N. J., Boyle, J. P., Ramsden, M., Freir, D. B., Peers, C. & Pearson, H. A. (2006) Amyloid [beta] peptide as a physiological modulator of neuronal [math>\bar{A}-type K⁺ current. *Neurobiology of Aging*, 27, 1673-1683.
- Ponting, C. P., Hutton, M., Nyborg, A., Baker, M., Jansen, K. & Golde, T. E. (2002) Identification of a novel family of presenilin homologues. *Human Molecular Genetics*, 11, 1037-1044.

- Prohaska, J. R. (2008) Role of copper transporters in copper homeostasis. *Am J Clin Nutr*, 88, 826S-829.
- Prohaska, J. R. & Gybina, A. A. (2004) Intracellular Copper Transport in Mammals. *J. Nutr.*, 134, 1003-1006.
- Pufahl, R. A., Singer, C. P., Peariso, K. L., Lin, S. J., Schmidt, P. J., Fahrni, C. J., Culotta, V. C., Penner-Hahn, J. E. & O'Halloran, T. V. (1997) Metal Ion Chaperone Function of the Soluble Cu(I) Receptor Atx1. *Science*, 278, 853-856.
- Qin, W. & Jia, J. (2008) Down-regulation of insulin-degrading enzyme by presenilin 1 V97L mutant potentially underlies increased levels of amyloid beta 42. *European Journal of Neuroscience*, 27, 2425-2432.
- Qiu, W. Q., Walsh, D. M., Ye, Z., Vekrellis, K., Zhang, J., Podlisny, M. B., Rosner, M. R., Safavi, A., Hersh, L. B. & Selkoe, D. J. (1998) Insulin-degrading Enzyme Regulates Extracellular Levels of Amyloid β -Protein by Degradation. *Journal of Biological Chemistry*, 273, 32730-32738.
- Rae, T. D., Schmidt, P. J., Pufahl, R. A., Culotta, V. C. & O'Halloran, T. V. (1999) Undetectable Intracellular Free Copper: The Requirement of a Copper Chaperone for Superoxide Dismutase. *Science*, 284, 805-808.
- Rae, T. D., Torres, A. S., Pufahl, R. A. & O'Halloran, T. V. (2001) Mechanism of Cu,Zn-Superoxide Dismutase Activation by the Human Metallochaperone hCCS. *Journal of Biological Chemistry*, 276, 5166-5176.
- Raichle, M. E. (1982) The Pathophysiology of Brain Ischaemia. *Ann. Neurol.*, 13, 2-10.
- Rink, L. & Haase, H. (2009) Zinc as an Alternative Signal to Calcium. *FASEB J.*, 23, LB408-.
- Rockenstein, E. M., McConlogue, L., Tan, H., Power, M., Masliah, E. & Mucke, L. (1995) Levels and Alternative Splicing of Amyloid Protein Precursor (APP) Transcripts in Brains of APP Transgenic Mice and Humans with Alzheimers Disease. *Journal of Biological Chemistry*, 270, 28257-28267.
- Rogers, J. T., Randall, J. D., Cahill, C. M., Eder, P. S., Huang, X., Gunshin, H., Leiter, L., McPhee, J., Sarang, S. S., Utsuki, T., Greig, N. H., Lahiri, D. K., Tanzi, R. E., Bush, A. I., Giordano, T. & Gullans, S. R. (2002) An Iron-responsive Element Type II in the 5'-Untranslated Region of the Alzheimer's Amyloid Precursor Protein Transcript. *Journal of Biological Chemistry*, 277, 45518-45528.
- Roher, A. E., Kasunic, T. C., Woods, A. S., Cotter, R. J., Ball, M. J. & Fridman, R. (1994) Proteolysis of A[beta] Peptide from Alzheimer Disease Brain by Gelatinase A. *Biochemical and Biophysical Research Communications*, 205, 1755-1761.

Rosen, D. R., Siddique, T., Patterson, D., Figlewicz, D. A., Sapp, P., Hentati, A., Donaldson, D., Goto, J., O'Regan, J. P., Deng, H.-X., Rahmani, Z., Krizus, A., McKenna-Yasek, D., Cayabyab, A., Gaston, S. M., Berger, R., Tanzi, R. E., Halperin, J. J., Herzfeldt, B., Van Den Bergh, R., Hung, W.-Y., Bird, T., Deng, G., Mulder, D. W., Smyth, C., Laing, N. G., Soriano, E., Pericak-Vance, M. A., Haines, J., Rouleau, G. A., Gusella, J. S., Horvitz, H. R. & Brown, R. H. (1993) Mutations in Cu/Zn superoxide dismutase gene are associated with familial amyotrophic lateral sclerosis. *Nature*, 362, 59-62.

Rossi, L., Marchese, E., Lombardo, M. F., Rotilio, G. & Ciriolo, M. R. (2001) Increased susceptibility of copper-deficient neuroblastoma cells to oxidative stress-mediated apoptosis. *Free Radical Biology and Medicine*, 30, 1177-1187.

Rossjohn, J., Cappai, R., Feil, S. C., Henry, A., McKinstry, W. J., Galatis, D., Hesse, L., Multhaup, G., Beyreuther, K., Masters, C. L. & Parker, M. W. (1999) Crystal structure of the N-terminal, growth factor-like domain of Alzheimer amyloid precursor protein. *Nat Struct Mol Biol*, 6, 327-331.

Rutherford, J. C. & Bird, A. J. (2004) Metal-Responsive Transcription Factors That Regulate Iron, Zinc, and Copper Homeostasis in Eukaryotic Cells. *Eukaryotic Cell*, 3, 1-13.

Sabo, S. L., Ikin, A. F., Buxbaum, J. D. & Greengard, P. (2001) The Alzheimer Amyloid Precursor Protein (APP) and Fe65, an APP-Binding Protein, Regulate Cell Movement. *The Journal of Cell Biology*, 153, 1403-1414.

Saido, T. C. (1998) Alzheimer's disease as proteolytic disorders: anabolism and catabolism of beta-amyloid. *Neurobiology of Aging*, 19, S69-75.

Saido, T. C. & Iwata, N. (2006) Metabolism of amyloid [beta] peptide and pathogenesis of Alzheimer's disease: Towards presymptomatic diagnosis, prevention and therapy. *Neuroscience Research*, 54, 235-253.

Saladin, K. (2007) *Physiology and Anatomy: The unity of Form and Function*.

Sambrook, J. & Russell, D. W. (2001) *Molecular Cloning: A Laboratory Manual*, New York, Cold Spring Harbour Laboratory Press.

Saunders, N., Habgood, M. & Dziegielewska, K. (1999) Barrier Mechanisms In The Brain, I. Adult Brain. *Clinical and Experimental Pharmacology and Physiology*, 26, 11-19.

Schäfer, S., Wirths, O., Multhaup, G. & Bayer, T. A. (2007) Gender dependent APP processing in a transgenic mouse model of Alzheimer's disease. *Journal of Neural Transmission*, 114, 387-394.

Scheuermann, S., Hamsch, B., Hesse, L., Stumm, J., Schmidt, C., Beher, D., Bayer, T. A., Beyreuther, K. & Multhaup, G. (2001) Homodimerization of Amyloid Precursor Protein and Its Implication in the Amyloidogenic Pathway of Alzheimer's Disease. *Journal of Biological Chemistry*, 276, 33923-33929.

Scheuner, D., Eckman, C., Jensen, M., Song, X., Citron, M., Suzuki, N., Bird, T. D., Hardy, J., Hutton, M., Kukull, W., Larson, E., Levy-Lahad, L., Viitanen, M., Peskind, E., Poorkaj, P., Schellenberg, G., Tanzi, R., Wasco, W., Lannfelt, L., Selkoe, D. & Younkin, S. (1996) Secreted amyloid [beta]-protein similar to that in the senile plaques of Alzheimer's disease is increased in vivo by the presenilin 1 and 2 and APP mutations linked to familial Alzheimer's disease. *Nat Med*, 2, 864-870.

Schippling, S., Kontush, A., Arlt, S., Buhmann, C., Stürenburg, H.-J., Mann, U., Müller-Thomsen, T. & Beisiegel, U. (2000) Increased lipoprotein oxidation in Alzheimer's disease. *Free Radical Biology and Medicine*, 28, 351-360.

Schlondorff, J., Becherer, J. D. & Blobel, C. P. (2000) Intracellular maturation and localization of the tumour necrosis factor alpha convertase (TACE). *Biochem. J.*, 347, 131-138.

Schmidt, P. J., Kunst, C. & Culotta, V. C. (2000) Copper Activation of Superoxide Dismutase 1 (SOD1) in Vivo. *Journal of Biological Chemistry*, 275, 33771-33776.

Schmidt, P. J., Rae, T. D., Pufahl, R. A., Hamma, T., Strain, J., O'Halloran, T. V. & Culotta, V. C. (1999) Multiple Protein Domains Contribute to the Action of the Copper Chaperone for Superoxide Dismutase. *Journal of Biological Chemistry*, 274, 23719-23725.

Schmitz, C., Rutten, B. P. F., Pielen, A., Schafer, S., Wirths, O., Tremp, G., Czech, C., Blanchard, V., Multhaup, G., Rezaie, P., Korr, H., Steinbusch, H. W. M., Pradier, L. & Bayer, T. A. (2004) Hippocampal Neuron Loss Exceeds Amyloid Plaque Load in a Transgenic Mouse Model of Alzheimer's Disease. *Am J Pathol*, 164, 1495-1502.

Schubert, W., Prior, R., Weidemann, A., Dirksen, H., Multhaup, G., Masters, C. L. & Beyreuther, K. (1991) Localization of Alzheimer [beta]A4 amyloid precursor protein at central and peripheral synaptic sites. *Brain Research*, 563, 184-194.

Sekler, I., Sensi, S. I., Hershfinkel, M. & Silverman, W. F. (2007) Mechanism and Regulation of Cellular Zinc Transport. *Molecular Medicine*, 13, 337-343.

Selkoe, D. J., Podlisny, M. B., Joachim, C. L., Vickers, E. A., Lee, G., Fritz, L. C. & Oltersdorf, T. (1988) Beta-amyloid precursor protein of Alzheimer disease occurs as 110- to 135-kilodalton membrane-associated proteins in neural and nonneural tissues. *Proceedings of the National Academy of Sciences of the United States of America*, 85, 7341-7345.

Sevcenco, A.-M., Krijger, G., Pinkse, M., Verhaert, P., Hagen, W. & Hagedoorn, P.-L. (2009) Development of a generic approach to native metalloproteomics: application to the quantitative identification of soluble copper proteins in *Escherichia coli*. *Journal of Biological Inorganic Chemistry*, 14, 631-640.

Shigematsu, K., McGeer, P. L. & McGeer, E. G. (1992) Localization of amyloid precursor protein in selective postsynaptic densities of rat cortical neurons. *Brain Research*, 592, 353-357.

- Shoji, M., Golde, T. E., Ghiso, J., Cheung, T. T., Estus, S., Shaffer, L. M., Cai, X. D., McKay, D. M., Tintner, R., Frangione, B. & ET, A. (1992) Production of the Alzheimer amyloid beta protein by normal proteolytic processing. *Science*, 258, 126-129.
- Siegel, S. J., Bieschke, J., Powers, E. T. & Kelly, J. W. (2007) The Oxidative Stress Metabolite 4-Hydroxynonenal Promotes Alzheimer Protofibril Formation *Biochemistry*, 46, 1503-1510.
- Sisodia, S. S. (2002) BIOMEDICINE: A Cargo Receptor Mystery APParently Solved? *Science*, 295, 805-807.
- Sisodia, S. S., Annaert, W., Kim, S.-H. & De Strooper, B. (2001) [gamma]-Secretase: never more enigmatic. *Trends in Neurosciences*, 24, 2-6.
- Skovronsky, D. M., Doms, R. W. & Lee, V. M. Y. (1998) Detection of a Novel Intraneuronal Pool of Insoluble Amyloid β Protein that Accumulates with Time in Culture. *The Journal of Cell Biology*, 141, 1031-1039.
- Smart, T. G., Xie, X. & Krishek, B. J. (1994) Modulation of inhibitory and excitatory amino acid receptor ion channels by zinc. *Progress in Neurobiology*, 42, 393-441.
- Smith, D. G., Cappai, R. & Barnham, K. J. (2007) The redox chemistry of the Alzheimer's disease amyloid [beta] peptide. *Biochimica et Biophysica Acta (BBA) - Biomembranes*, 1768, 1976-1990.
- Snyder, E. M., Nong, Y., Almeida, C. G., Paul, S., Moran, T., Choi, E. Y., Nairn, A. C., Salter, M. W., Lombroso, P. J., Gouras, G. K. & Greengard, P. (2005) Regulation of NMDA receptor trafficking by amyloid-[beta]. *Nat Neurosci*, 8, 1051-1058.
- Soba, P., Eggert, S., Wagner, K., Zentgraf, H., Siehl, K., Kreger, S., Lower, A., Langer, A., Merdes, G., Paro, R., Masters, C. L., Muller, U., Kins, S. & Beyreuther, K. (2005) Homo- and heterodimerization of APP family members promotes intercellular adhesion. *EMBO J*, 24, 3624-3634.
- Stadtman, E. R. & Levine, R. L. (2000) Protein Oxidation. *Annals of the New York Academy of Sciences*, 899, 191-208.
- Stamer, K., Vogel, R., Thies, E., Mandelkow, E. & Mandelkow, E. M. (2002) Tau blocks traffic of organelles, neurofilaments, and APP vesicles in neurons and enhances oxidative stress. *The Journal of Cell Biology*, 156, 1051-1063.
- Stokin, G. B., Lillo, C., Falzone, T. L., Brusch, R. G., Rockenstein, E., Mount, S. L., Raman, R., Davies, P., Masliah, E., Williams, D. S. & Goldstein, L. S. B. (2005) Axonopathy and Transport Deficits Early in the Pathogenesis of Alzheimer's Disease. *Science*, 307, 1282-1288.

Storey, E., Beyreuther, K. & Masters, C. L. (1996) Alzheimer's disease amyloid precursor protein on the surface of cortical neurons in primary culture co-localizes with adhesion patch components. *Brain Research*, 735, 217-231.

Strange, P. G. (1996) *Brain Biochemistry and Brain Disorders*, Oxford University Press.

Strausak, D., Fontaine, S. L., Hill, J., Firth, S. D., Lockhart, P. J. & Mercer, J. F. B. (1999) The Role of GMXCXXC Metal Binding Sites in the Copper-induced Redistribution of the Menkes Protein. *Journal of Biological Chemistry*, 274, 11170-11177.

Strausak, D., Mercer, J. F. B., Dieter, H. H., Stremmel, W. & Multhaup, G. (2001) Copper in disorders with neurological symptoms: Alzheimer's, Menkes, and Wilson diseases. *Brain Research Bulletin*, 55, 175-185.

Strozyk, D., Launer, L. J., Adlard, P. A., Cherny, R. A., Tsatsanis, A., Volitakis, I., Blennow, K., Petrovitch, H., White, L. R. & Bush, A. I. (2009) Zinc and copper modulate Alzheimer A[β] levels in human cerebrospinal fluid. *Neurobiology of Aging*, 30, 1069-1077.

Sturtz, L. A., Diekert, K., Jensen, L. T., Lill, R. & Culotta, V. C. (2001) A Fraction of Yeast Cu,Zn-Superoxide Dismutase and Its Metallochaperone, CCS, Localize to the Intermembrane Space of Mitochondria. *Journal of Biological Chemistry*, 276, 38084-38089.

Suazo, M., Hodar, C., Morgan, C., Cerpa, W., Cambiazo, V., Inestrosa, N. C. & Gonzalez, M. (2009) Overexpression of amyloid precursor protein increases copper content in HEK293 cells. *Biochemical and Biophysical Research Communications*, 382, 740-744.

Suh, Y.-H. & Checler, F. (2002) Amyloid Precursor Protein, Presenilins, and α -Synuclein: Molecular Pathogenesis and Pharmacological Applications in Alzheimer's Disease. *Pharmacological Reviews*, 54, 469-525.

Sun, X., He, G., Qing, H., Zhou, W., Dobie, F., Cai, F., Staufenbiel, M., Huang, L. E. & Song, W. (2006) Hypoxia facilitates Alzheimer's disease pathogenesis by up-regulating BACE1 gene expression. *Proceedings of the National Academy of Sciences*, 103, 18727-18732.

Suzuki, N., Cheung, T. T., Cai, X. D., Odaka, A., Otvos, L., JR., Eckman, C., Golde, T. E. & Younkin, S. G. (1994) An increased percentage of long amyloid beta protein secreted by familial amyloid beta protein precursor (beta APP717) mutants. *Science*, 264, 1336-1340.

Tainer, J. A., Getzoff, E. D., Beem, K. M., Richardson, J. S. & Richardson, D. C. (1982) Determination and analysis of the 2 Å structure of copper, zinc superoxide dismutase. *Journal of Molecular Biology*, 160, 181-217.

- Tamagno, E., Robino, G., Obbili, A., Bardini, P., Aragno, M., Parola, M. & Danni, O. (2003) H₂O₂ and 4-hydroxynonenal mediate amyloid [beta]-induced neuronal apoptosis by activating jnks and p38mapk. *Experimental Neurology*, 180, 144-155.
- Tanaka, S., Shiojiri, S., Takahashi, Y., Kitaguchi, N., Ito, H., Kameyama, M., Kimura, J., Nakamura, S. & Ueda, K. (1989) Tissue-specific expression of three types of [beta]-protein precursor mRNA: Enhancement of protease inhibitor-harboring types in Alzheimer's disease brain. *Biochemical and Biophysical Research Communications*, 165, 1406-1414.
- Thiele, D. J. (1988) ACE1 regulates expression of the *Saccharomyces cerevisiae* metallothionein gene. *Mol. Cell. Biol.*, 8, 2745-2752.
- Thompsett, A. R., Abdelraheim, S. R., Daniels, M. & Brown, D. R. (2005) High Affinity Binding between Copper and Full-length Prion Protein Identified by Two Different Techniques. *Journal of Biological Chemistry*, 280, 42750-42758.
- Tomimoto, H., Akiguchi, I., Wakita, H., Nakamura, S. & Kimura, J. (1995) Ultrastructural localization of amyloid protein precursor in the normal and postischemic gerbil brain. *Brain Research*, 672, 187-195.
- Tong, Y., Zhou, W., Fung, V., Christensen, M. A., Qing, H., Sun, X. & Song, W. (2005) Oxidative stress potentiates BACE1 gene expression and A β generation. *Journal of Neural Transmission*, 112, 455-469.
- Tonnesen, T., Kleijer, W. J. & Horn, N. (1991) Incidence of Menkes disease. *Human Genetics*, 86, 408-410.
- Tottey, S., Waldron, K. J., Firbank, S. J., Reale, B., Bessant, C., Sato, K., Cheek, T. R., Gray, J., Banfield, M. J., DENNISON, C. & ROBINSON, N. J. (2008) Protein-folding location can regulate manganese-binding versus copper- or zinc-binding. *Nature*, 455, 1138-1142.
- Treiber, C., Simons, A., Strauss, M., Hafner, M., Cappai, R., Bayer, T. A. & Multhaup, G. (2004) Clioquinol Mediates Copper Uptake and Counteracts Copper Efflux Activities of the Amyloid Precursor Protein of Alzheimer's Disease. *Journal of Biological Chemistry*, 279, 51958-51964.
- Uchida, Y., Takio, K., Titani, K., Ihara, Y. & Tomonaga, M. (1991) The growth inhibitory factor that is deficient in the Alzheimer's disease brain is a 68 amino acid metallothionein-like protein. *Neuron*, 7, 337-347.
- Van Nostrand, W. E., Wagner, S. L., Shankle, W. R., Farrow, J. S., Dick, M., Rozemuller, J. M., Kuiper, M. A., Wolters, E. C., Zimmerman, J. & Cotman, C. W. (1992) Decreased levels of soluble amyloid beta-protein precursor in cerebrospinal fluid of live Alzheimer disease patients. *Proceedings of the National Academy of Sciences of the United States of America*, 89, 2551-2555.
- Vassar, R. (2005) Beta-Secretase, APP and Abeta in Alzheimer's disease. *Subcell. Biochem.*, 38, 79-103.

Vassar, R., Bennett, B. D., Babu-Khan, S., Kahn, S., Mendiaz, E. A., Denis, P., Teplow, D. B., Ross, S., Amarante, P., Loeloff, R., Luo, Y., Fisher, S., Fuller, J., Edenson, S., Lile, J., Jarosinski, M. A., Biere, A. L., Curran, E., Burgess, T., Louis, J.-C., Collins, F., Treanor, J., Rogers, G. & Citron, M. (1999) β -Secretase Cleavage of Alzheimer's Amyloid Precursor Protein by the Transmembrane Aspartic Protease BACE. *Science*, 286, 735-741.

Vieira, S., Rebelo, S., Domingues, S., Da Cruz E Silva, E. & Da Cruz E Silva, O. (2009) S655 phosphorylation enhances APP secretory traffic. *Molecular and Cellular Biochemistry*, 328, 145-154.

Vijayvergiya, C., Beal, M. F., Buck, J. & Manfredi, G. (2005) Mutant Superoxide Dismutase 1 Forms Aggregates in the Brain Mitochondrial Matrix of Amyotrophic Lateral Sclerosis Mice. *J. Neurosci.*, 25, 2463-2470.

Vitek, M. P., Bhattacharya, K., Glendening, J. M., Stopa, E., Vlassara, H., Bucala, R., Manogue, K. & Cerami, A. (1994) Advanced glycation end products contribute to amyloidosis in Alzheimer disease. *Proceedings of the National Academy of Sciences of the United States of America*, 91, 4766-4770.

Von Rotz, R. C., Kohli, B. M., Bosset, J., Meier, M., Suzuki, T., Nitsch, R. M. & Konietzko, U. (2004) The APP intracellular domain forms nuclear multiprotein complexes and regulates the transcription of its own precursor. *J Cell Sci*, 117, 4435-4448.

Vulpe, C., Levinson, B., Whitney, S., Packman, S. & Gitschier, J. (1993) Isolation of a candidate gene for Menkes disease and evidence that it encodes a copper-transporting ATPase. *Nat Genet*, 3, 7-13.

Waldron, K. J., Tottey, S., Yanagisawa, S., Dennison, C. & Robinson, N. J. (2007) A Periplasmic Iron-binding Protein Contributes toward Inward Copper Supply. *Journal of Biological Chemistry*, 282, 3837-3846.

Walsh, D. M., Klyubin, I., Fadeeva, J. V., Cullen, W. K., Anwyl, R., Wolfe, M. S., Rowan, M. J. & Selkoe, D. J. (2002) Naturally secreted oligomers of amyloid β protein potently inhibit hippocampal long-term potentiation in vivo. *Nature*, 416, 535-539.

Walter, J., Capell, A., Hung, A. Y., Langen, H., Schnölzer, M., Thinakaran, G., Sisodia, S. S., Selkoe, D. J. & Haass, C. (1997) Ectodomain Phosphorylation of β -Amyloid Precursor Protein at Two Distinct Cellular Locations. *Journal of Biological Chemistry*, 272, 1896-1903.

Walter, J., Fluhrer, R., Hartung, B., Willem, M., Kaether, C., Capell, A., Lammich, S., Multhaup, G. & Haass, C. (2001) Phosphorylation Regulates Intracellular Trafficking of β -Secretase. *Journal of Biological Chemistry*, 276, 14634-14641.

Wang, X., Moualla, D., Wright, J. A. & Brown, D. R. (2010) Copper binding regulates intracellular alpha-synuclein localisation, aggregation and toxicity. *Journal of Neurochemistry*, 113, 704-714.

- Weidemann, A., König, G., Bunke, D., Fischer, P., Salbaum, J. M., Masters, C. L. & Beyreuther, K. (1989) Identification, biogenesis, and localization of precursors of Alzheimer's disease A4 amyloid protein. *Cell*, 57, 115-126.
- White, A. R., Du, T., Laughton, K. M., Volitakis, I., Sharples, R. A., Xilinas, M. E., Hoke, D. E., Holsinger, R. M. D., Evin, G. V., Cherny, R. A., Hill, A. F., Barnham, K. J., Li, Q.-X., Bush, A. I. & Masters, C. L. (2006) Degradation of the Alzheimer Disease Amyloid β -Peptide by Metal-dependent Up-regulation of Metalloprotease Activity. *Journal of Biological Chemistry*, 281, 17670-17680.
- White, A. R., Multhaup, G., Maher, F., Bellingham, S., Camakaris, J., Zheng, H., Bush, A. I., Beyreuther, K., Masters, C. L. & Cappai, R. (1999a) The Alzheimer's Disease Amyloid Precursor Protein Modulates Copper-Induced Toxicity and Oxidative Stress in Primary Neuronal Cultures. *J. Neurosci.*, 19, 9170-9179.
- White, A. R., Reyes, R., Mercer, J. F. B., Camakaris, J., Zheng, H., Bush, A. I., Multhaup, G., Beyreuther, K., Masters, C. L. & Cappai, R. (1999b) Copper levels are increased in the cerebral cortex and liver of APP and APLP2 knockout mice. *Brain Research*, 842, 439-444.
- Wilson, C. A., Doms, R. W., Zheng, H. & Lee, V. M. Y. (2002) Presenilins are not required for A β 42 production in the early secretory pathway. *Nat Neurosci*, 5, 849-855.
- Wilson, C. M. & High, S. (2007) Ribophorin I acts as a substrate-specific facilitator of N-glycosylation. *J Cell Sci*, 120, 648-657.
- Wilson, C. M., Kraft, C., Duggan, C., Ismail, N., Crawshaw, S. G. & High, S. (2005) Ribophorin I Associates with a Subset of Membrane Proteins after Their Integration at the Sec61 Translocon. *Journal of Biological Chemistry*, 280, 4195-4206.
- Wirh's, O., Multhaup, G. & Bayer, T. A. (2004) A modified β -amyloid hypothesis: intraneuronal accumulation of the β -amyloid peptide – the first step of a fatal cascade. *Journal of Neurochemistry*, 91, 513-520.
- Wirh's, O., Multhaup, G., Czech, C., Blanchard, V., Moussaoui, S., Tremp, G., Pradier, L., Beyreuther, K. & Bayer, T. A. (2001) Intraneuronal A β accumulation precedes plaque formation in β -amyloid precursor protein and presenilin-1 double-transgenic mice. *Neuroscience Letters*, 306, 116-120.
- Wolfe, M. S., Xia, W., Ostaszewski, B. L., Diehl, T. S., Kimberly, W. T. & Selkoe, D. J. (1999) Two transmembrane aspartates in presenilin-1 required for presenilin endoproteolysis and γ -secretase activity. *Nature*, 398, 513-517.
- Wu, X., Sinani, D., Kim, H. & Lee, J. (2009) Copper Transport Activity of Yeast Ctr1 Is Down-regulated via Its C Terminus in Response to Excess Copper. *Journal of Biological Chemistry*, 284, 4112-4122.

Xia, W., Ray, W. J., Ostaszewski, B. L., Rahmati, T., Kimberly, W. T., Wolfe, M. S., Zhang, J., Goate, A. M. & Selkoe, D. J. (2000) Presenilin complexes with the C-terminal fragments of amyloid precursor protein at the sites of amyloid β -protein generation. *Proceedings of the National Academy of Sciences of the United States of America*, 97, 9299-9304.

Xie, Z., Romano, D. M. & Tanzi, R. E. (2005) RNA Interference-mediated Silencing of X11 α and X11 β Attenuates Amyloid β -Protein Levels via Differential Effects on β -Amyloid Precursor Protein Processing. *Journal of Biological Chemistry*, 280, 15413-15421.

Yamaguchi-Iwai, Y., Serpe, M., Haile, D., Yang, W., Kosman, D. J., Klausner, R. D. & Dancis, A. (1997) Homeostatic Regulation of Copper Uptake in Yeast via Direct Binding of MAC1 Protein to Upstream Regulatory Sequences of FRE1 and CTR1. *Journal of Biological Chemistry*, 272, 17711-17718.

Yamamoto, M., Kawanishi, T., Kiuchi, T., Ohta, M., Yokota, I., Ohata, H., Momose, K., Inoue, K. & Hayakawa, T. (1998) Discrepant intracellular pH changes following intracellular Ca²⁺ increases induced by glutamate and Ca²⁺ ionophores in rat hippocampal neurons. *Life Sciences*, 63, 55-63.

Yamazaki, T., Koo, E. H. & Selkoe, D. J. (1996) Trafficking of cell-surface amyloid beta-protein precursor. II. Endocytosis, recycling and lysosomal targeting detected by immunolocalization. *J Cell Sci*, 109, 999-1008.

Yamazaki, T., Koo, E. H. & Selkoe, D. J. (1997) Cell Surface Amyloid beta - Protein Precursor Colocalizes with beta 1 Integrins at Substrate Contact Sites in Neural Cells. *J. Neurosci.*, 17, 1004-1010.

Yan, R., Bienkowski, M. J., Shuck, M. E., Miao, H., Tory, M. C., Pauley, A. M., Brashler, J. R., Stratman, N. C., Mathews, W. R., Buhl, A. E., Carter, D. B., Tomasselli, A. G., Parodi, L. A., Heinrikson, R. L. & Gurney, M. E. (1999) Membrane-anchored aspartyl protease with Alzheimer's disease [beta]-secretase activity. *Nature*, 402, 533-537.

Yan, R., Han, P., Miao, H., Greengard, P. & Xu, H. (2001) The Transmembrane Domain of the Alzheimer's β -Secretase (BACE1) Determines Its Late Golgi Localization and Access to β -Amyloid Precursor Protein (APP) Substrate. *Journal of Biological Chemistry*, 276, 36788-36796.

Young-Pearse, T. L., Bai, J., Chang, R., Zheng, J. B., Loturco, J. J. & Selkoe, D. J. (2007) A Critical Function for β -Amyloid Precursor Protein in Neuronal Migration Revealed by In Utero RNA Interference. *J. Neurosci.*, 27, 14459-14469.

Yu, G., Nishimura, M., Arawaka, S., Levitan, D., Zhang, L., Tandon, A., Song, Y.-Q., Rogava, E., Chen, F., Kawarai, T., Supala, A., Levesque, L., Yu, H., Yang, D.-S., Holmes, E., Milman, P., Liang, Y., Zhang, D. M., Xu, D. H., Sato, C., Rogava, E., Smith, M., Janus, C., Zhang, Y., Aebbersold, R., Farrer, L., Sorbi, S., Bruni, A., Fraser, P. & St George-Hyslop, P. (2000) Nicastrin modulates presenilin-mediated notch/glp-1 signal transduction and [beta]APP processing. *Nature*, 407, 48-54.

Zelko, I. N., Mariani, T. J. & FOLZ, R. J. (2002) Superoxide dismutase multigene family: a comparison of the CuZn-SOD (SOD1), Mn-SOD (SOD2), and EC-SOD (SOD3) gene structures, evolution, and expression. *Free Radical Biology and Medicine*, 33, 337-349.

Zheng, H., Jiang, M., Trumbauer, M. E., Sirinathsinghji, D. J. S., Hopkins, R., Smith, D. W., Heavens, R. P., Dawson, G. R., Boyce, S., Conner, M. W., Stevens, K. A., Slunt, H. H., Sisodia, S. S., Chen, H. Y. & Van Der Ploeg, L. H. T. (1995) [beta]-amyloid precursor protein-deficient mice show reactive gliosis and decreased locomotor activity. *Cell*, 81, 525-531.

Zou, K., Yamaguchi, H., Akatsu, H., Sakamoto, T., Ko, M., Mizoguchi, K., Gong, J.-S., Yu, W., Yamamoto, T., Kosaka, K., Yanagisawa, K. & Michikawa, M. (2007) Angiotensin-Converting Enzyme Converts Amyloid {beta}-Protein 1 42 (A{beta}1 42) to A{beta}1 40, and Its Inhibition Enhances Brain A{beta} Deposition. *J. Neurosci.*, 27, 8628-8635.

Chapter 5: Appendix

5.1 Spectrophotometric analysis of SOD1 activity

Liquid SOD1 activity assays were performed to obtain absolute data for comparison of SOD1 activity between APP_{WT} and APP_{swe} cell lines in copper supplemented or depleted conditions. The assay was performed using the xanthine/xanthine oxidase system which is outlined in section 2.4.7.2.4. Oxidation of xanthine to uric acid by xanthine oxidase under aerobic conditions releases anionic superoxide, which reduces oxidised cytochrome c triggering an increase in absorbance intensity when measured at a wavelength of 550nm. SOD1 prevents the reduction of cytochrome c by sequestration and dismutation of the superoxide to hydrogen peroxide. The measured increase in absorbance intensity due to free superoxide is quenched and directly relates to SOD1 activity.

Whole cell soluble protein extracts of APP_{WT} and APP_{swe} were prepared as outlined in section 2.4.7.2.3. Cultures were supplemented with increasing concentrations of copper and grown to 80% confluence for another 24 hours or supplemented with BCS and grown for four generations before being subjected to further analysis. Supplement concentrations are specified in figures 5.1 through 5.4.

Cell pellets were obtained from one 150cm² flask per sample and resuspended in 420µl of 50mM phosphate buffer, pH 7.8 and 120µl of 10% (w/v) SDS. Following incubation at 37°C for 30 minutes the sample was cooled and 60µl of 3M KCl added. After further incubation intact cells were pelleted and the supernatant analysed for protein content by BSA-calibrated Coomassie assay. A fresh SOD1 standard curve was prepared on the day of experiment to control for mechanical or experimental variation. Pure SOD1 extracted from human erythrocytes was titrated to the working solution in 0.5 unit increments up to 3 units of SOD1 activity. Reactions for the standard curve were supplemented with 60µl of the 300mM KCl, 2% (w/v) SDS, 35mM phosphate buffer mixture which was used for sample extraction to control for differences in absorbance arising from reaction components other than cytochrome c. Spectra for both cell lines in either supplementation conditions were taken for 30 minutes using 100µg of protein per measurement with the reaction being initiated by titration of 50µM xanthine to the cuvette.

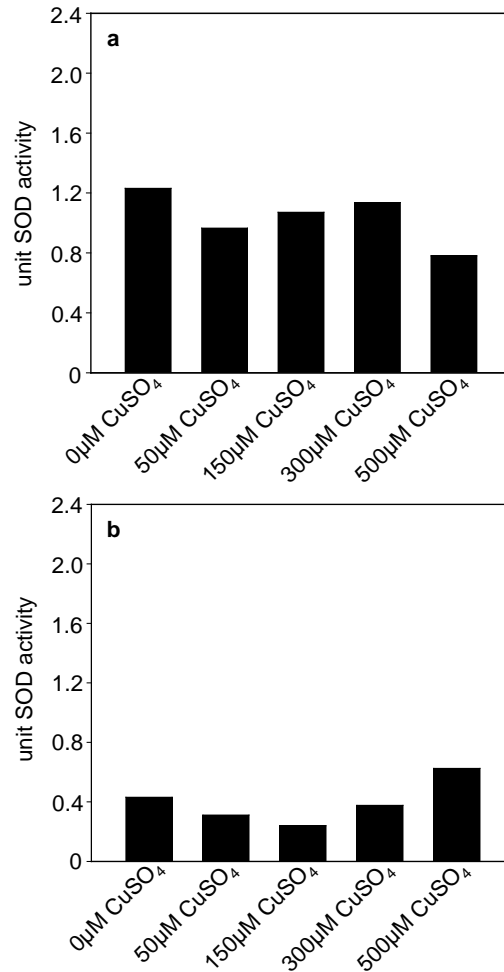


Figure 5.1: SOD1 activity in *SH-SY5Y* APP_{WT} under copper supplementation

Whole cell protein extracts were prepared from 1x150cm² flask per sample of 80% confluent monolayer culture as described in section 2.4.7.2.3. Three independent extracts were produced. The protein content was estimated by BSA-calibrated Coomassie assay and all three extracts diluted to the same protein concentration to minimise experimental variation. On the day of experiment a fresh standard curve using pure SOD1 was prepared. Samples could not be analysed in triplicate due to the duration of individual analyses. SOD1 activity was measured spectrophotometrically at a wavelength of 550nm as described in section 2.4.7.2.4. Histograms represent enzyme activity in units SOD for APP_{WT} replicate 2 (a) and replicate 3 (b). The first replicate is shown in figure 3.20.

Data displayed in figure 5.1 shows two independent replicates of SOD1 activity measurements in APP_{WT} whole cell protein extracts. Due to the long time period each of each of the experiments triplicate measurements could not be obtained, thus it is difficult to determine, whether changes in enzyme activity are statistically significant. Direct comparison between both replicates is not possible due to the use of different SOD1 standard curves. This results in different SOD1 activity values for the controls. Although there seems to be a threefold difference between the two replicates, it must be noted, that there is no major change in enzyme activity across increasing copper treatments. This data is consistent with the replicate shown in figure 3.20. The results of measuring SOD1 activity in cells grown under copper deplete conditions indicate a decrease in enzyme activity with increasing BCS concentration, although a decrease in activity reduction can be observed in higher BCS concentrations in both replicates shown in figure 5.2 and in figure 3.21. This might be caused by the cell adjusting to low copper levels redirecting endogenous copper from copper stores to essential copper-binding enzymes such as SOD1 or alterations in protein expression as the cell prepares for apoptosis. Another option for base level SOD1 activity in high BCS concentrations is the exhaustion of enzyme assay sensitivity, thus the plateau might represent zero base levels of SOD1 activity.

SOD1 activity of copper supplemented APP_{swe} cells is shown in figure 5.3. It must be noted that, although there is no increasing or decreasing trend in SOD1 activity, enzyme activity is increased at 50 μ M copper in each replicate. This data is consistent with data shown in figure 3.20 where a general increase in SOD1 activity is observed. Although no definite statements about copper-dependent alterations in enzyme activity can be made, the increase of enzyme activity at 50 μ M copper seems to be cell line specific. This feature was not observed in APP_{WT} supplemented with copper, thus a copper-dependent mechanism for increased SOD1 metallation or altered metabolism might be responsible for this observation. As previously observed for BCS-supplemented APP_{WT} cultures, SOD1 enzyme activity decreased in BCS-supplemented APP_{swe} cells with even small amounts of BCS accounting for most of the decrease in enzyme activity.

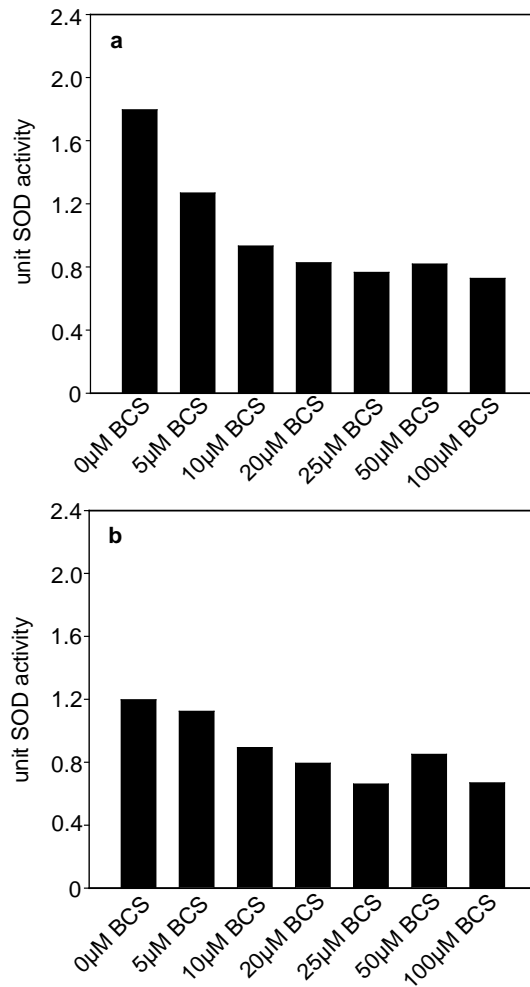


Figure 5.2: SOD1 activity in *SH-SY5Y* APP_{WT} under copper depletion

Whole cell protein extracts were prepared and the SOD activity assay performed as previously described. Histograms represent replicate 2 (a) and replicate 3 (b) of three independent replicates. Replicate 1 is shown in figure 3.21.

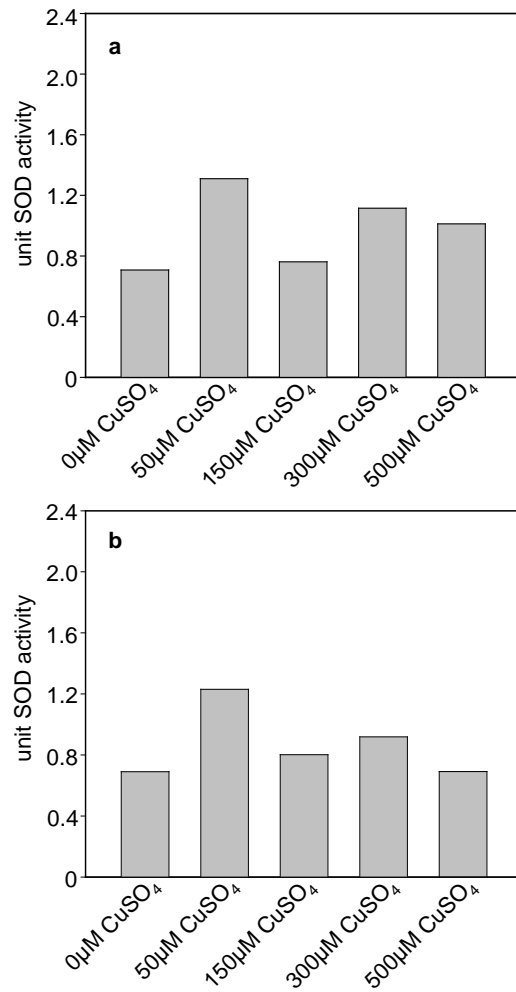


Figure 5.3: SOD1 activity in *SH-SY5Y* APP_{swe} under copper supplementation

Whole cell protein extracts were prepared and the SOD1 activity assay performed as previously described. Histograms show replicate 2 (a) and replicate 3 (b) of three independent experiments. Replicate 1 is shown in figure 3.20.

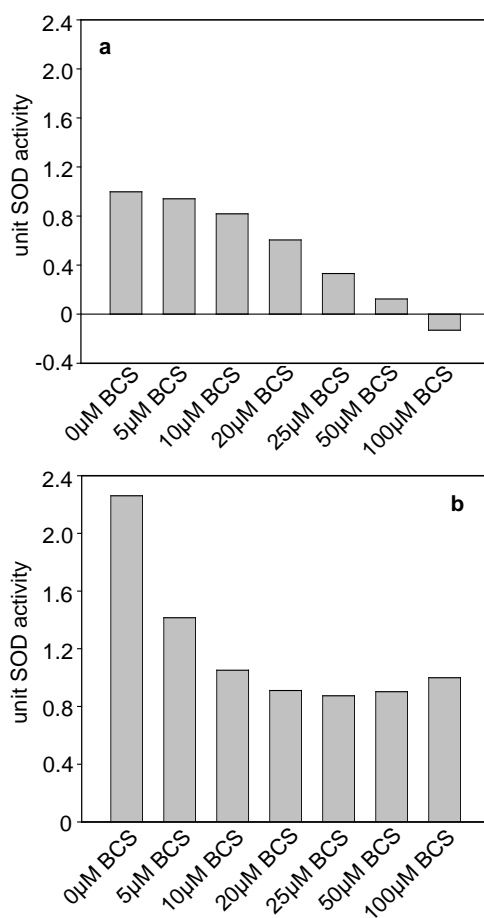


Figure 5.4: SOD1 activity in *SH-SY5Y APP_{swe}* under copper depletion

Whole cell protein extracts were prepared and SOD1 activity assay performed as previously described. Histograms depict replicate 2 (a) and replicate 3 (b) from three independent experiments. Replicate 1 is shown in figure 3.21.

5.2 Analysis of CCO activity

The CCO activity assay is based on the same principles as the SOD1 activity assay. The rate of oxidation of reduced cytochrome c is measured spectrophotometrically at a wavelength of 550nm. Upon oxidation of cytochrome c quenching of the absorbance spectrum is expected which relates directly to enzyme activity. Full reduction of cytochrome c is essential prior to the experiment, thus titration of the reducing agent ascorbic acid to the final working solution was performed to determine the concentration of reducing agent needed to fully reduce cytochrome c. Figure 5.5 shows spectra obtained during titration of 50 μ M increments of ascorbic acid to the assay working solution and increased absorbance of cytochrome c at 550nm was observed. Absorbance plateaus at concentrations of 350-400 μ M of ascorbic acid indicating that cytochrome c reduction is complete. It was calculated that a minimum of 64mM ascorbic acid were required to fully reduce the 50 μ M cytochrome c stock solution. Addition of 100mM ascorbic acid to the stock solution resulted in a colour change from red to pink indicating reduction of cytochrome c. Excess reducing agent was removed by dialysis in 20mM phosphate buffer, pH 7.8 using dialysis membrane with a molecular weight cut-off of 3,500 Da.

Whole cell membrane extracts were prepared from one 150cm² flask per sample for both cell lines and pellets resuspended in 1ml of 20mM phosphate buffer, pH 7.8. Lysis was performed in a sonication waterbath in three intervals of three minutes with five minute intervals on ice. Intact cells were removed by low spin and the supernatant subjected to ultracentrifugation to collect the membraneous fraction of the extract. The pellet was resuspended in 0.5ml of 20mM phosphate buffer and protein content determined by BSA-calibrated BCA protein assay. Samples for both cell lines and various copper or BCS treatments were adjusted to the same protein concentration to control for sample variation. To control for full cytochrome c reduction for each individual measurement, aliquots (0.9ml) of fully reduced 3 μ M working solution were scanned between wavelengths 200nm and 800nm to compare absorbance at 550nm. The CCO assay reaction was initiated by addition of 8 μ g protein extract and the rate of cytochrome c oxidation determined using $\epsilon_{550\text{nm}} = 29,500 \text{ M}^{-1} \text{ cm}^{-1}$.

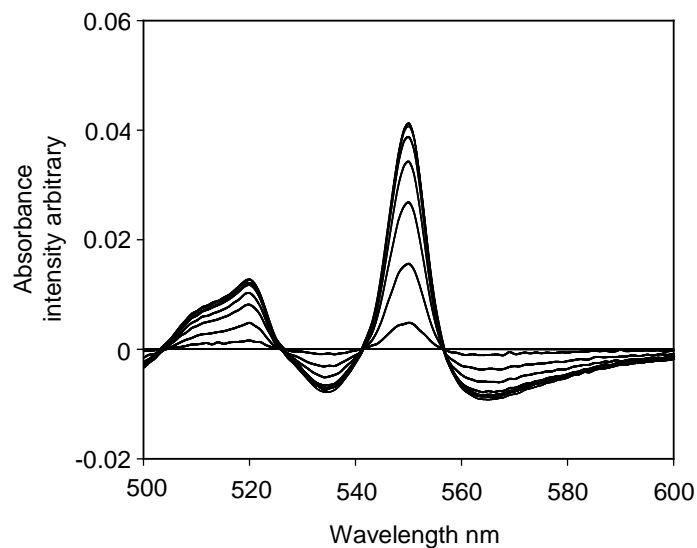


Figure 5.5: Reduction assay of cytochrome c for cytochrome oxidase activity assay

The CCO activity assay measures the oxidation of cytochrome c by CCO. Thus, it is required for the cytochrome c to be fully reduced before the activity assay to detect the best possible absorbance signal. An aliquot (0.9ml) of $3\mu\text{M}$ cytochrome c in 20mM KPO_4 buffer has been treated with increasing concentrations ($50\mu\text{M}$ increments) of 2.5M ascorbic acid and absorbance spectra were taken at a wavelength of 550nm . Saturation was observed at $350\mu\text{M}$ with an arbitrary absorbance of 0.04 . It was calculated that 64.8mM ascorbic acid were needed to fully reduce the $50\mu\text{M}$ cytochrome c stock, however an excess of this concentration was used and the surplus reductant removed by dialysis.

Triplicate measurements of three individual replicates for both cell lines and all copper or BCS treatments were taken. Figure 5.6 shows two additional replicates of copper supplemented APP_{WT} to that shown in figure 3.23. Whereas no significant changes in enzyme activity were observed in the latter replicate, the replicates shown here contradict with statistically significant increases and decreases in CCO activity. Therefore no definite statement about copper-dependent changes of CCO activity in APP_{WT} cultures can be made. BCS treated APP_{WT} cells as shown in figure 5.7 display a clear and significant reduction in CCO activity, a feature which is highly replicable.

CCO activity assayed in copper supplemented APP_{swe} cultures as shown in figure 5.8 indicates significant increases in CCO activity in higher concentrations of copper. Although one replicate does not show any significance (figure 5.8 panel a) the additional replicate in figure 3.23 clearly indicates increased enzyme activity. As for APP_{WT}, the APP_{swe} cell line displays significant decreases in enzyme activity due to BCS treatment as shown in figure 5.9 and 3.24.

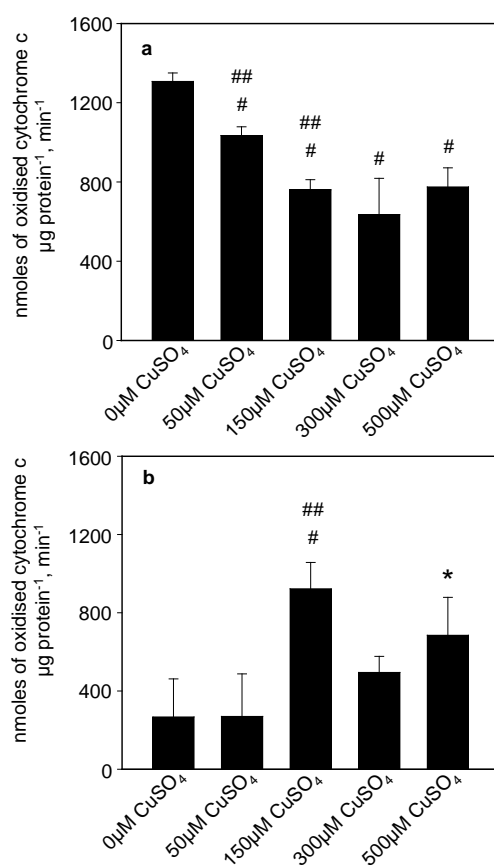


Figure 5.6: Cytochrome c oxidase activity in *SH-SY5Y* APP_{WT} under copper supplementation

Whole cell protein extracts were prepared from 1x150cm² flask per sample of 80% confluent monolayer culture as described in section 2.4.7.3.1. The protein content of three independent extracts was estimated using the BCA assay for membraneous protein and all three extracts diluted to the same protein concentration to minimise experimental variation. Prior to the activity assay cytochrome c was fully reduced with molar excess of ascorbic acid, which was subsequently removed by dialysis. Cytochrome oxidase activity was measured spectrophotometrically at a wavelength of 550nm as described in section 2.4.7.3.6. Histograms show enzyme activity as calculated using $\epsilon_{550\text{nm}} = 29,500 \text{ M}^{-1}\text{cm}^{-1}$ for APP_{WT} replicate 2 (a) and replicate 3 (b). Replicate 1 is shown in figure 3.28. Error bars represent standard deviation for triplicate measurements. Symbols represent statistical significance as follows: *: p<0.05 compared to the control, #: p<0.01 compared to the control, **: p<0.05 compared to previous treatment, ##: p< 0.01 compared to previous treatment.

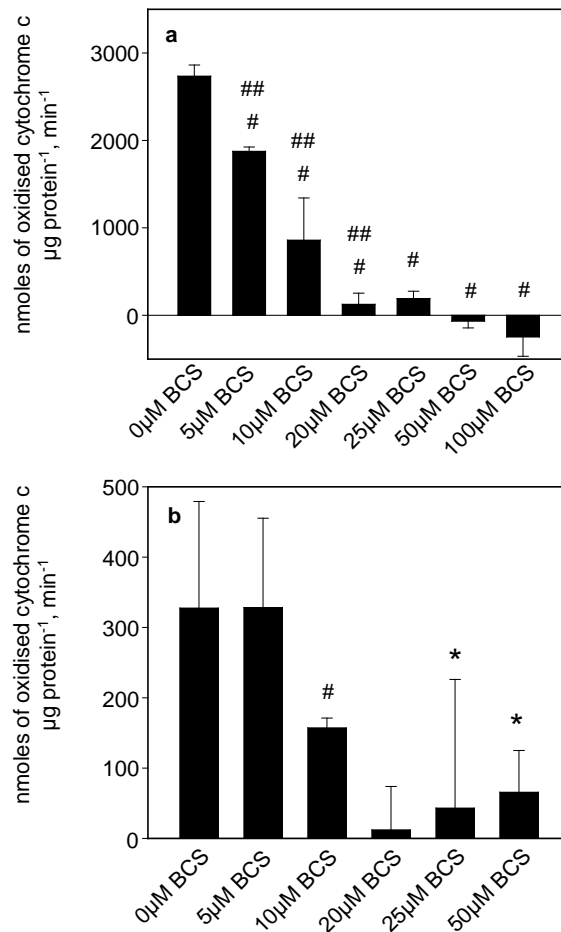


Figure 5.7: Cytochrome c oxidase activity in *SH-SY5Y* APP_{WT} and APP_{Swe} under copper depletion

Whole cell protein extracts of three independent experiments were prepared and the cytochrome c oxidase assay performed as described previously. Cytochrome oxidase activity was measured spectrophotometrically at a wavelength of 550nm as described in section 2.4.7.3.6. Histograms show enzyme activity as calculated using $\epsilon_{550\text{nm}} = 29,500 \text{ M}^{-1}\text{cm}^{-1}$ for APP_{WT} replicate 2 (a) and replicate 3 (b). Replicate 1 is shown in figure 3.29. Error bars represent standard deviation for triplicate measurements. Results indicate a decrease in cytochrome oxidase activity. Symbols represent statistical significance as follows: *: $p < 0.05$ compared to the control, #: $p < 0.05$ compared to the control, **: $p < 0.05$ compared to previous treatment, ##: $p < 0.01$ compared to previous treatment.

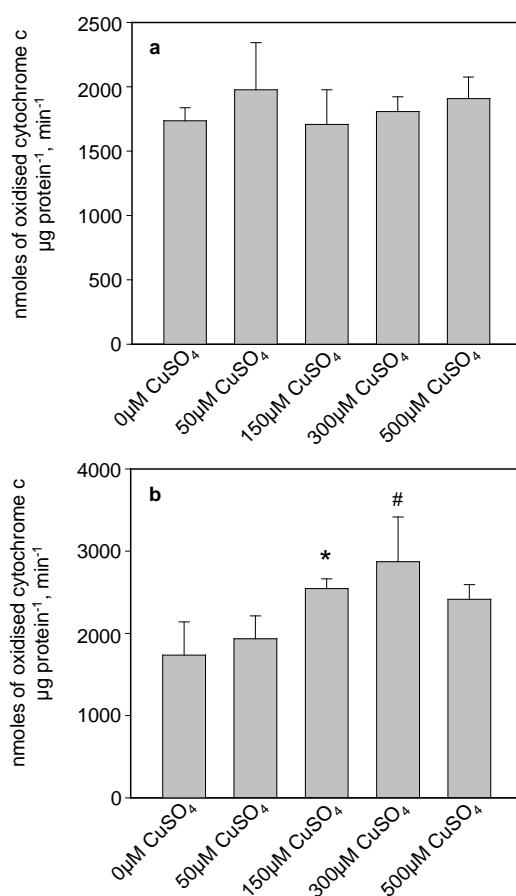


Figure 5.8: Cytochrome c oxidase activity in *SH-SY5Y* APP_{swe} under copper supplementation

Whole cell protein extracts of three independent experiments were prepared and cytochrome oxidase activity assay performed as previously described. Cytochrome oxidase activity was measured spectrophotometrically at a wavelength of 550nm as described in section 2.4.7.3.6. Histograms show enzyme activity as calculated using $\epsilon_{550\text{nm}} = 29,500 \text{ M}^{-1}\text{cm}^{-1}$ for APP_{swe} replicate 2 (a) and replicate 3 (b). Replicate 1 is shown in figure 3.28. Error bars represent standard deviation for triplicate measurements. Results indicate increased cytochrome oxidase activity in the APP_{swe} cell line. Symbols represent statistical significance as follows: *: $p < 0.05$ compared to the control, #: $p < 0.01$ compared to the control, **: $p < 0.05$ compared to previous treatment, ##: $p < 0.01$ compared to previous treatment.

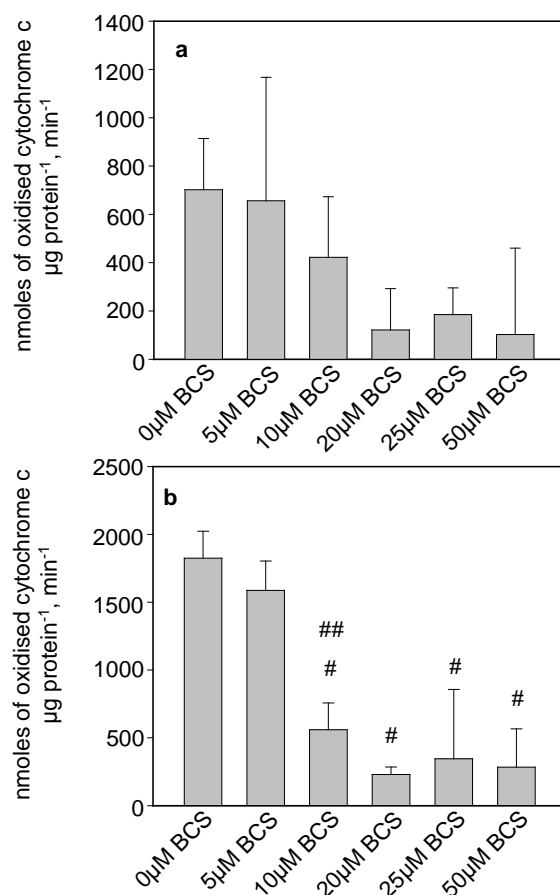


Figure 5.9: Cytochrome c oxidase activity in *SH-SY5Y* APP_{swe} under copper depletion

Whole cell protein extracts of three independent experiments were prepared and cytochrome oxidase activity assay performed as described previously. Cytochrome oxidase activity was measured spectrophotometrically at a wavelength of 550nm as described in section 2.4.7.3.6. Histograms show enzyme activity as calculated using $\epsilon_{550\text{nm}} = 29,500 \text{ M}^{-1} \text{ cm}^{-1}$ for APP_{swe} replicate 2 (a) and replicate 3 (b). Replicate 1 is shown in figure 3.29. Error bars represent standard deviation for triplicate measurements. Results indicate a decrease in cytochrome oxidase activity in this cell line. Symbols represent statistical significance as follows: *: $p < 0.05$ compared to the control, #: $p < 0.01$ compared to the control, **: $p < 0.05$ compared to previous treatment, ###: $p < 0.01$ compared to previous treatment.

5.3 Survival studies under copper supplementation

Survival rates were monitored in copper supplemented APP_{WT} and APP_{swe} cell lines. Appropriate concentrations of copper were added to cultures and grown to 80% confluence for another 24 hours. Ratios of life to dead cells were established by manually counting cells in a hemocytometer following trypan blue staining with cells excluding the stain counted as life and those penetrated by the stain counted as dead. Figures 5.10 and 5.11 show survival data for APP_{WT} and APP_{swe}, respectively. As previously observed in figure 3.25 panel a, a significant decrease in survival was detected in APP_{WT} cultures directly linked to the amount of copper added to the culture. Although the replicate shown in figure 5.10 panel b does not display significant changes, a slight reduction is observed which follows the trend of the more prominent phenotypes in replicates shown in figures 5.10 and 3.25 panels a.

APP_{swe} cultures supplemented with copper as shown in figure 5.11 do not display any significant change in survival. The survival between control groups is comparable between the two cell lines, indicating that the overexpression of APP_{swe} does not affect survival under culture conditions. However, the replicates presented in figure 5.10 differ from the replicate shown in figure 3.25, where a statistically significant increase in survival was detected in high copper concentrations. The APP_{swe} control culture shows reduced survival rates compared with the APP_{WT} control culture, suggesting that there might be a survival difference in both cell lines under culture conditions with APP_{swe} displaying resistance to high copper that is higher compared to that of APP_{WT}.

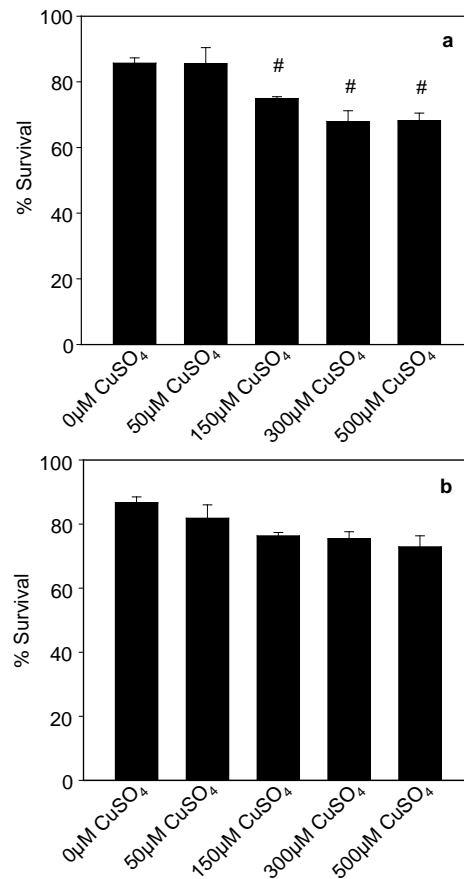


Figure 5.10: Survival of *SH-SY5Y* APP_{WT} under increasing copper concentrations

Cell cultures of 1×10^6 cells were prepared for the *SH-SY5Y* APP_{WT} cell line and grown for several days before being supplemented with the appropriate concentration of copper and grown for another 24 hours. Cultures were harvested as described in section 2.2.3.2 and analysed for life and dead cells by the trypan blue exclusion method using a hemocytometer. Survival rates are shown for APP_{WT} replicate 2 (a) and replicate 3 (b). Replicate 1 is shown in figure 3.25. Error bars represent standard deviation of triplicate measurements. Results indicate a slight but statistically significant decrease in survival when extracellular copper levels are increased. Symbols represent statistical significance as follows: *: $p < 0.05$ compared to the control, #: $p < 0.01$ compared to the control, **: $p < 0.05$ compared to previous treatment, ##: $p < 0.01$ compared to previous treatment.

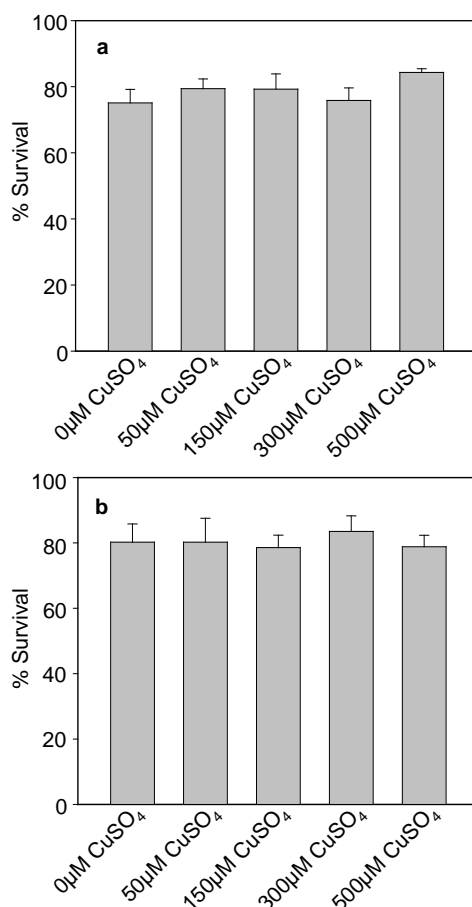


Figure 5.11: Survival of *SH-SY5Y* APP_{swe} under increasing copper concentrations

Cell cultures of 1×10^6 cells were prepared for the *SH-SY5Y* APP_{swe} cell line and grown for several days before being supplemented with the appropriate concentration of copper and grown for another 24 hours. Cultures were harvested as described in section 2.2.3.2 and analysed for life and dead cells by the trypan blue exclusion method using a hemocytometer. Survival rates are shown for APP_{swe} replicate 2 (a) and replicate 3 (b). Replicate 1 is shown in figure 3.25. Error bars represent standard deviation of triplicate measurements. Symbols represent statistical significance as follows: *: $p < 0.05$ compared to the control, #: $p < 0.01$ compared to the control, **: $p < 0.05$ compared to previous treatment, ###: $p < 0.01$ compared to previous treatment.

5.4 Metal content of APP_{WT} and APP_{swe} under copper depletion

Cellular metal content was previously determined in copper supplemented cultures of APP_{WT} and APP_{swe} as shown in figures 3.28 and 3.29 detecting significant increases in copper but not zinc and iron content in both cell lines. Whole cell metal content was determined in both cell lines that were treated with increasing concentrations of BCS. Cultures were grown in independent triplicates for four generations in the appropriate concentrations of BCS and following harvest were resuspended in 65% ultrapure (v/v) HNO₃ at a cell count of 1.5x10⁶ per sample. Cells were left to lyse for at least one week at room temperature and samples analysed for metal content by ICP-MS subsequent to two high spin centrifugation steps to remove unlysed cells and cell debris. ICP-MS measurements were performed in triplicate and data is shown in figure 5.12. There is no evidence of significant changes in metal content for copper, zinc and iron in BCS treated cultures in both cell lines. This might be due to complete cellular metal depletion during the four generations of cell culture with metal trafficking processes continuously transporting metals to the cell surface and ultimately shifting the cellular metal equilibrium to the cell surface where metals were sequestered from the culture system by BCS. Changes in cellular metal content at this stage could be minimal and below detection levels of the ICP-MS or influenced by external contaminations which would hardly influence data with high metal content, but may interfere with data showing minimal amounts of metal. Another complication in determining exact changes in metal content in BCS treated cells is that BCS could be occupied by metal originating from lysed cells in culture, which would be more prevalent in higher BCS concentrations compared to lower BCS concentrations which a cell could survive. With several changes of BCS containing growth medium between cell culture generations it is possible that more metal was extracted from culture subjected to higher BCS concentrations and that data obtained would be flawed as a result. This issue is not prevalent in copper supplemented cultures as they are only grown for another 24 hours and do not require growth medium change. Thus, if supplementations are performed carefully the same amount of copper is added to all cells, which renders the data more comparable between triplicate measurements and samples within one replicate.

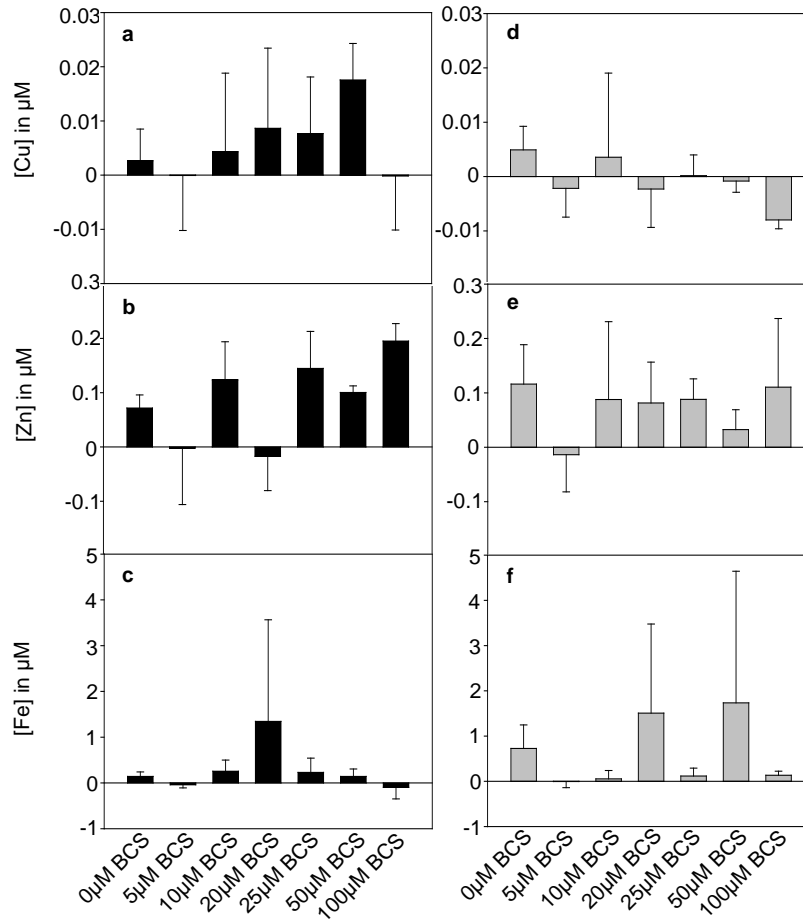


Figure 5.12: Total metal analysis in whole cell *SH-SY5Y* APP_{WT} and APP_{swe} under copper depletion

APP_{WT} and APP_{swe} cells were cultured in increasing concentrations of BCS for four generations and seeded for the final analysis. Cultures were harvested at 80% confluency and cell numbers determined as described in section 2.4.6.1 using a Coulter Cell Counter system. Aliquots of 1.5×10^6 cells for each cell line and copper depletion status were resuspended in 1ml of ultrapure 65% (v/v) HNO₃. Samples were incubated at room temperature for at least one week and repeatedly centrifuged to remove cells and cell debris, before being analysed by ICP-MS for copper, zinc and iron content. Whole cell metal content is shown for APP_{WT} copper (a), zinc (b) and iron (c) concentrations and for APP_{swe} copper (d), zinc (e) and iron (f) concentrations. Error bars represent standard deviation of triplicate measurements.

5.5 Comparison of expression levels of *hsod1* and *hccs* genes in *SH-SY5Y* APP_{WT} and APP_{swe} under copper supplementation and depletion

The copper chaperone CCS and its target protein SOD1 are both soluble proteins and closely linked to cellular copper status and homeostasis, thus should provide ideal candidate genes to monitor changes in one particular cellular copper trafficking pathway. Cell line specific patterns of gene expression of both *hsod1* and *hccs* could give an indication about differences in copper handling between APP_{WT} and APP_{swe} and possibly provide an insight in copper-dependent alterations in gene expression. Although a multitude of genes coding for copper-binding proteins or copper transporting/trafficking proteins could be studied in this manner, the focus was based on these two genes, especially since there was evidence of CCS and BACE1 interactions and possible redirection of copper away from SOD1 (Angeletti et al., 2005). It has previously been shown that in yeast high copper concentrations lead to an increase in *sod1* gene expression as one of the cellular copper buffering mechanisms (Culotta et al., 1995). Gene expression was tested on the neuroblastoma cell lines in high copper concentrations and copper depletion conditions.

APP_{WT} and APP_{swe} cells were cultured in increasing BCS concentrations for four generations before being seeded for the final analysis. Copper supplementations were performed 24 hours before cells were harvested. Whole cell RNA extracts were prepared from one 150cm² flask per sample of 80% confluent monolayer culture using the phenol extraction protocol adapted from Sambrook and Russell (Sambrook and Russell, 2001) and described in section 2.3.1.1.

Cell pellets were resuspended in 10 volumes of pre-warmed RNA lysis buffer (50mM Tris-Cl, pH 8.0, 100mM NaCl, 20mM EDTA, pH 8.0, 2% (w/v) SDS, 60mM β-mercaptoethanol, 10µg/ml proteinase K) and incubated at 37°C for 30 minutes. A 5x phenol extraction was performed by adding an equal volume of 5:1 phenol:lysis buffer to the sample, which was centrifuged at 4,000rpm for 10 minutes and the aqueous top layer collected into a new tube. An equal volume of 1:1:1 phenol:chloroform:lysis buffer added and the centrifugation step repeated. The aqueous top layer was collected into corex ultracentrifuge tubes and adjusted to 0.5M ammonium acetate using a 10M stock. RNA was subsequently precipitated by

adding 2.5 volumes of 100% ethanol (-20°C) and sample incubation at -20°C for 2 hours. Following the incubation the nucleic acid was pelleted by ultracentrifugation at 12,000 rpm for 30 minutes at 4°C. The supernatant was discarded, the pellet resuspended in a small volume (2ml) of 70% (v/v) ethanol and the centrifugation step repeated. The pellet was then allowed to air-dry over night, resuspended in 50µl DEPC-treated water and the amount of RNA per sample was estimated. Following DNaseI treatment reverse transcription was performed using the Im-PromII reverse transcription kit and 1µg of RNA per sample. Preliminary studies shown in figure 5.13 show that the reverse transcription step was more successful using oligo(dT)₁₅ primers rather than gene specific primers. For all steps in the RT-PCR reaction a master-mix solution was prepared and aliquots added to each sample RNA to control for experimental variation. Reverse transcription was performed as specified in section 2.3.1.2.3 with reaction components and volumes as shown in table 2.2. The PCR reaction step was performed as outlined in section 2.3.1.3 and 1.5µl of cDNA were used per sample. The PCR reaction was run for 30 cycles and gene products visualised on a 2% (w/v) agarose gel using 100kb ladder as size marker. To test whether the *hccs* and *hsod1* primers generated the expected product, preliminary studies were performed as shown in figure 5.13. RT-PCR products obtained from whole cell APP_{WT} RNA extracts were run on a 2% (w/v) agarose gel and single products visualised at 210bp and 230bp for *hsod1* and *hccs*, respectively. The observed products were of the same length as was expected. In the following RT-PCR reactions the house keeping gene *β-actin* was used as loading control. Standardisation of *hβ-actin* between samples was achieved by adjusting loading volumes until a homogenous signal intensity from all samples was detected. PCR products of *hccs* and *hsod1* were loaded onto the gel as multiple volumes of the volumes determined for *hβ-actin* as their expression was less prominent. Due to loss of RNA during sample preparation or RNA estimation errors due to low concentration in the sample, certain individual copper or BCS treatments did not show any PCR products and were thus excluded from the analysis.

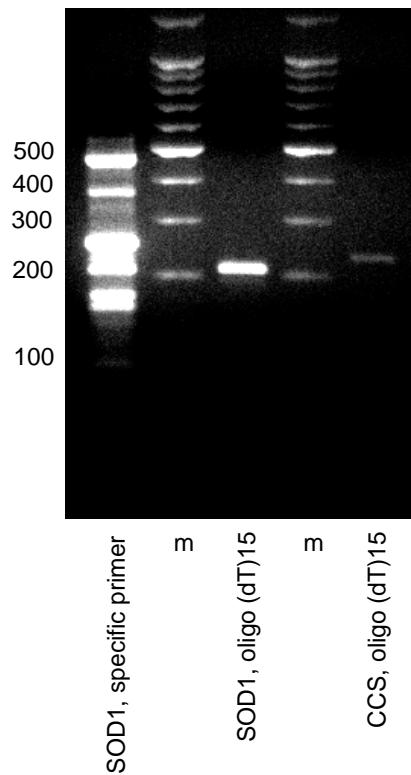


Figure 5.13: Verification of primers for RT-PCR

Whole cell RNA extracts of *SH-SY5Y* APP_{WT} have been subjected to reverse transcriptase polymerase chain reaction to test primer for generation of correct product size. Expected product sizes for human *sod1* and human *ccs* are 210 and 230 bp, respectively. The gel shows products of RT-PCR reactions using *sod1* specific primers and oligo(dT)₁₅ primers being use for the reverse transcription step. Single products at 210 and 230 bp can be detected for *hsod1* and *hccs*, whereas the use of specific primers during the reverse transcription step results in multiple products of varying sizes. For all RT reactions oligo(dT)₁₅ primers will be used with gene specific primer being used in the PCR reaction.

Results of RT-PCR experiments are shown in figures 5.14 and in duplicate experiments in figure 5.15. All gene products were subjected to the same gel to prevent false data due to minimal differences in gel composition such as ethidium bromide or agarose content and to control for differences in UV exposure and photography. However, most of the *hccs* and *hsod1* gene products do not show any trend in gene expression depending on cellular copper status. This might in part be due to signal saturation of the house keeping gene. Although sometimes fractions of a μl were loaded onto the gel to prevent signal saturation due to large amounts of PCR product, the signal might still be saturated which prevents the accurate evaluation of correct sample volumes to be loaded onto the gel. Further it must be noted that when working with such small volumes, pipetting errors or slight volume changes are clearly visible and might be mistaken as a genuine result. Experiments with varying amounts of cDNA and RNA were performed (data not shown), but yielded no improvement to the gel loading optimisation process.

Although most of the data does not reveal copper-dependent alterations in gene expression, two interesting observations need to be mentioned. Firstly, in both replicates the BCS supplemented APP_{WT} cell line displays a decrease in *hsod1* expression which is accompanied by a slight increase in *hccs* gene expression. This has physiological implications since it is detrimental for the cell to use energy on the production of proteins that can not be metallated due to co-factor deprivation. At the same time gene expression switches to cellular mechanisms that could rescue this deficient phenotype by providing more copies of copper-trafficking proteins. It would be interesting to perform gene expression studies on copper importers such as Ctr1 and Dmt1 to test whether the compensatory mechanisms for copper deficiency include increased gene expression of copper importers or copper exporters. With a presumed role of APP in copper export it might be worth testing APP gene expression in copper depleted cell lines. Secondly, figure 3.14 panel b shows an interesting expression pattern of *hccs* and *hsod1* whose PCR products signals seem to be inverted. No copper-dependent trend of increased or decreased gene expression can be observed, however in 50 μM copper *hsod1* expression is high, whereas it is low in *hccs* at 50 μM of copper. At a copper concentration of 150 μM , however, *hsod1* gene expression signals are low as compared with *hccs* which shows a large amount of PCR product. This is an unusual scenario, one which is

unlikely to be due to experimental error. Results suggest that there is an intricate interplay between the expression levels of *hccs* and *hsod1*, with the reduction in one causing an increase in the other. From a homeostatic point of view, in high copper the cell needs to adjust to either excrete excess copper or generate more ligands for the excess metal. Thus an increase in gene expression of copper exporters and certain copper chaperones such as HAH1 and a decrease in gene expression of copper importers would be expected. Increases in extracellular and intracellular copper increases the risk of ROS generation, thus one would expect the gene expression of the antioxidant SOD1 and its chaperone to increase. However, copper might be directed to other compartments for excretion rather than storage in intracellular ligands, thus there is no need for increased expression of SOD1. Further, one would expect that CCS and SOD1 are co-expressed since their physiological roles are co-dependent. However, with the suggestion that CCS also binds to other cellular targets, its expression might be governed by additional factors depending on its role in other pathways and the expression of the proteins CCS interacts with.

Figure 5.14: Comparison of expression levels of *hsod1* and *hccs* in SH-SY5Y APP_{WT} and APP_{swe} under copper supplementation and depletion

APP_{WT} and APP_{swe} cells were cultured in increasing concentrations of BCS (0 μ M, 5 μ M, 10 μ M, 20 μ M, 25 μ M, 50 μ M and 100 μ M) for four generations before being seeded for the final analysis. Copper supplementations were performed 24 hours before cells were harvested for RNA extraction. Whole cell RNA extracts were prepared from 1x150cm² flask per sample of 80% confluent monolayer culture using the phenol extraction protocol as described in section 2.3.1.1. Briefly, cell pellets were lysed in lysis buffer (50mM Tris-Cl, pH 8.0, 100mM NaCl, 20mM EDTA, pH 8.0, 2% (w/v) SDS, 60mM β -Mercaptoethanol, 10 μ g/ml proteinase K) and incubated at 37 $^{\circ}$ C for 30 minutes. Subsequent extractions using a 5:1 phenol:lysis buffer and 1:1:1 phenol:lysis buffer:chloroform were performed and protein and RNA precipitated by the addition of 0.5M ammonium acetate and 100% ethanol. RNA was pelleted, resuspended in 50 μ l DEPC-treated water and analysed for RNA content using a NanoDrop ND-1000 Spectrophotometer. Aliquots of each sample (5 μ g of RNA) were subjected to DNaseI treatment before reverse transcription was performed with 1 μ g RNA of each sample (see sections 2.3.1.2.1 and 2.3.1.2.2). Reverse transcription using oligo(dT)₁₅ primers for *hsod1*, *hccs* and *h β -actin* was followed by polymerase chain reaction (1.5 μ l of cDNA per 100 μ l reaction volume) using gene specific primers with product sizes of 210bp, 230bp and 612bp, respectively. *H β -actin* was used as control and standardised by adjusting the volume loaded onto a 2% (w/v) agarose gel across the samples. Multiple volumes of *hsod1* and *hccs* were loaded in comparison to *h β -actin*. Gels show expression of *h β -actin*, *hsod1* and *hccs* for APP_{WT} in increasing copper (a), APP_{WT} in increasing BCS (b), APP_{swe} in increasing copper (c) and APP_{swe} in increasing BCS (d). Depending on the success of the RNA extract only a few copper and BCS concentrations are shown on the gels.

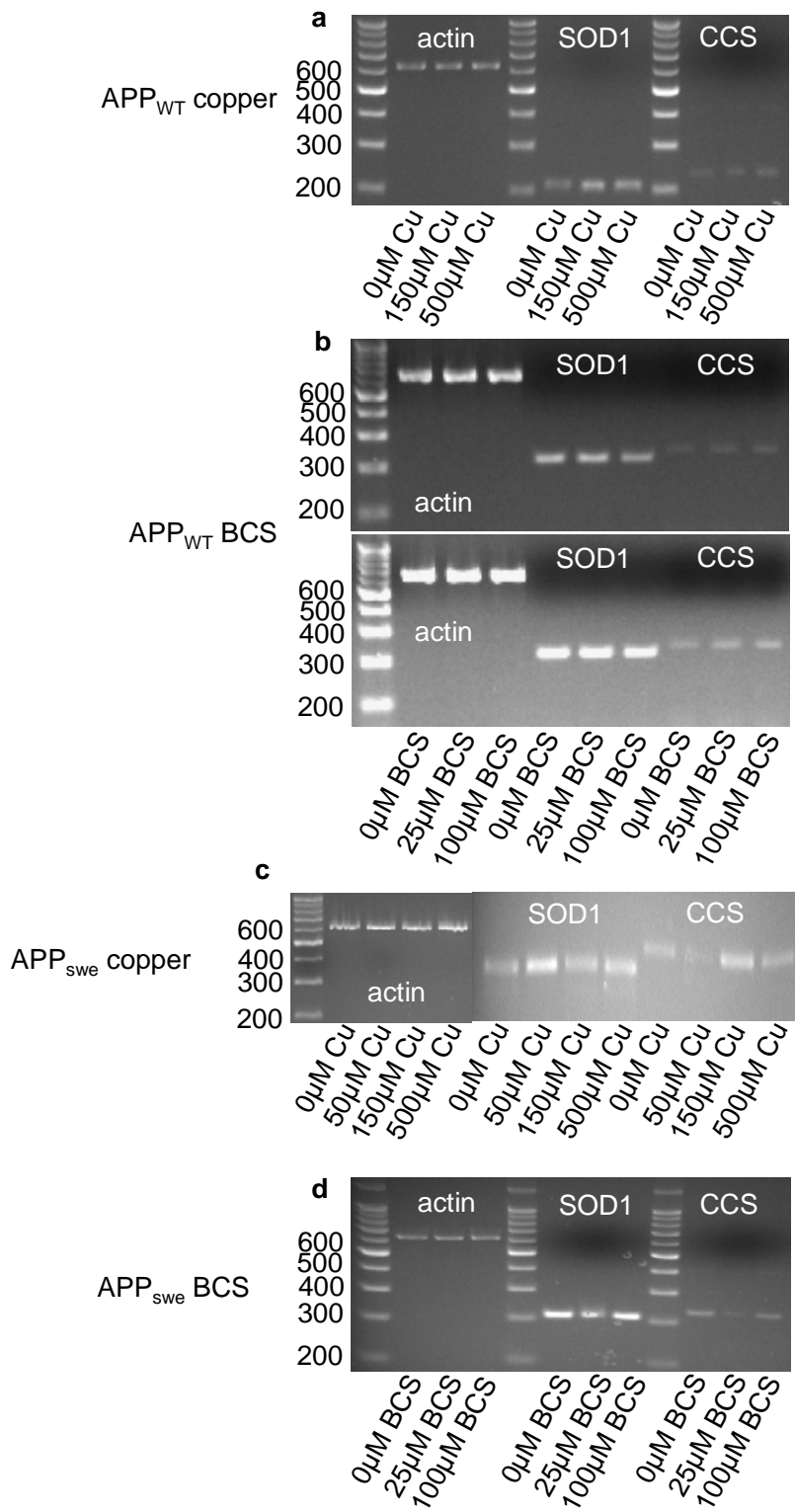


Figure 5.15: Comparison of expression levels of *hsod1* and *hccs* in SH-SY5Y APP_{WT} and APP_{swe} under copper supplementation and depletion duplicate

RNA extraction and RT-PCR were performed as previously described for copper supplemented and depleted APP_{WT} and APP_{swe} cell lines. The same concentrations of reagents and volumes of RNA/cDNA were used in this RT-PCR. *Hβ-actin* was used as control and standardised by adjusting the volume loaded onto a 2% (w/v) agarose gel across the samples. Multiple volumes of *hsod1* and *hccs* were loaded in comparison to *hβ-actin*. Gels show expression of *hβ-actin*, *hsod1* and *hccs* for APP_{WT} in increasing copper (a), APP_{WT} in increasing BCS (b), APP_{swe} in increasing copper (c) and APP_{swe} in increasing BCS (d). Depending on the success of the RNA extract only a few copper and BCS concentrations are shown on the gels.

